ABSTRACT

Title of Dissertation:	CO_2 TRANSCRITICAL REFRIGERATION WITH MECHANICAL SUBCOOLING: ENERGY EFFICIENCY, DEMAND RESPONSE AND THERMAL STORAGE
	John Dennis Bush, Doctor of Philosophy, 2018
Dissertation directed by:	Professor Reinhard Radermacher, Department of Mechanical Engineering

This dissertation examines two important concepts: improvements to transcritical carbon dioxide (CO_2) refrigeration systems being deployed in supermarkets, and their potential use for demand response and load shifting in a utility-connected application. As regulatory pressure increases to reduce the use of ozone depleting and greenhouse gases as refrigerants, the heating, ventilation, air conditioning and refrigeration (HVAC&R) industry is moving towards alternative refrigerants including natural substances such as carbon dioxide. CO_2 has already gained traction as the refrigerant of choice for supermarket applications in some countries, but deployment in warmer climates has been slower due to concerns over efficiency when the cycle operates in transcritical mode. Among the cycle enhancements considered to overcome these concerns is the use of dedicated mechanical subcooling. Laboratory testing was performed on a transcritical booster system with mechanical subcooling to quantify

the system performance with and without the subcooler. Data was used to develop and validate transient models, which in turn were used to study the system-wide effects of demand response, particularly short-term shedding of medium or low temperature load. Systems can provide value to the electric grid if they can be responsive to changes in electric utility generation, as indicated by direct calls to shed load or price signals. To further expand the potential usefulness of the refrigeration cycle in grid-interactive operation, the integration of thermal storage is considered. In particular, the integration of thermal storage into the subcooling system is investigated. The mechanical subcooler is used to "charge" a storage media (such as water or another phase change material) overnight, and the storage media allows the subcooler to turn off during peak hours. This allows the system to shift load and allow temporary reduction in electric power usage without a reduction in delivered refrigerating capacity. These two paths are potentially complementary: the load shifting of the integrated thermal storage provides long-term load reduction, while direct load shedding in evaporators allows more agile, short-term reductions. The models developed and validated with laboratory data and expanded upon with thermal energy storage and demand response approaches provide new learnings into enhanced load shifting and demand response capability. The findings of this work show that particularly in time-of-use rate structures with a high ratio of on-peak to off-peak pricing, the thermal storage and load shedding strategies here can provide a reduction in total refrigerating energy cost, even though the changes proposed introduce a slight increase in daily energy under the simulated conditions. In a simulated hot day for Baltimore, Maryland, the energy consumption was 2.6% higher

using the thermal storage system than without. In the most extreme case, comparing an aggressive real-world Time-of-Use rate with thermal storage and load shedding against a flat-rate case from the same utility and no controls or storage, a cost savings reduction of 21% was calculated. Comparing baseline operation against a controlled load-shifting strategy under the same time-of-use rate plan, the cost reduction was in the range of 2.8-8.7% depending upon the specific plan.

CO_2 TRANSCRITICAL REFRIGERATION WITH MECHANICAL SUBCOOLING: ENERGY EFFICIENCY, DEMAND RESPONSE AND THERMAL STORAGE

by

John Dennis Bush

Dissertation submitted to the Faculty of the Graduate School of the
University of Maryland, College Park, in partial fulfillment
of the requirements for the degree of
Doctor of Philosophy
2018

Advisory Committee:
Professor Reinhard Radermacher, Chair
Professor Michael Ohadi
Professor Jelena Srebric
Professor Bao Yang
Associate Research Scientist Vikrant Aute
Professor Peter Sunderland, Dean's Representative

Dedication

For Lauren

Acknowledgements

I would like to express my sincere gratitude to my advisor, Dr. Reinhard Radermacher, for his support, encouragement and guidance throughout my time as a graduate student. I have learned a great deal about how to be a researcher and a professional under Dr. Radermacher's guidance. I would also like to thank my dissertation committee, Dr. Jelena Srebric, Dr. Michael Ohadi, Dr. Bao Yang, Dr. Vikrant Aute, and Dr. Peter Sunderland, for their service and contribution to this dissertation. I owe a particular gratitude to Dr. Vikrant Aute and Dr. Jiazhen Ling, who have provided generous advice and mentorship throughout my effort.

I have now done two stints in the Center for Environmental Energy Engineering (CEEE) and want to express my thanks to the many great friends and colleagues, too many to list here, who have helped me along the way. In my academic and professional lives, I have found the students and alumni of CEEE to be a constant source of inspiration and motivation. I am also thankful to the Electric Power Research Institute, who have funded my studies and allowed me the freedom to pursue this degree. To Dr. Ron Domitrovic, my mentor and friend, thank you.

Of course, I am grateful to my family. My mother Marielle and step-father Joe, and my brothers, Joe and Geoff, and their beautiful families have been a constant source of support and love. My father, Timothy, remains with me for every step.

Most importantly to my beautiful wife Lauren, I am forever grateful for your support and love. I could not have done this without you.

Table of Contents

List of Tables

List of Figures

Chapter 1: Introduction

Motivation

This research effort will focus on a combination of two related motivations. The first is understanding and evaluating the transcritical CO_2 booster refrigeration cycle for commercial refrigeration applications, and particularly the potential to improve efficiency and capacity by the use of dedicated mechanical subcooling. The second is to develop and improve methods of implementing thermal storage to this cycle to enable participation in demand response and load-shifting applications. Each of these motivations is described in more detail below.

Motivation: CO_2 Refrigeration

Legislative pressures to eliminate the usage of ozone depleting and global warming gases are pushing the research, development and application of natural refrigerants such as carbon dioxide (CO_2 or R744) for heating, cooling, refrigeration and water heating applications. Recently the Kigali Amendment to the Montreal Protocol (Kigali 2016) formalized a global agreement to phase down greenhouse gas production and use. In the U.S., the Environmental Protection Agency is expected to implement the agreement pending legal obstacles (EPA 2016). States are also taking steps including notable proposed actions by California to limit refrigerant use across nearly all applications (California Air Resources Board 2016) One of the oldest refrigerants, R744 has recently received renewed attention, particularly for commercial refrigeration as well as water heating applications. It has several advantages as a refrigerant: it has

zero ozone depletion potential (ODP), 1.0 global warming potential (GWP), low-cost, is commonly available, and is listed as an ASHRAE A1 refrigerant, considered non-toxic and non-flammable. Also, due to its high volumetric heat capacity, R744 systems generally require smaller components for comparable capacity than conventional refrigerants. However, there are a number of challenges which have to date prevented widespread adoption of R744. High operating pressure, efficiency issues in transcritical operation, and low familiarity and availability of equipment are among just a few barriers. R744 operates at a very high pressure: low-temperature (LT) and medium-temperature (MT) evaporator pressures of 1.4 to 3.5 MPa are typical, and compressor discharge pressure of 8.0-10.0 MPa are also common. CO_2 has a low critical point (7.38 MPa and 304.13 K), meaning that these systems are often in transcritical operation in many climates.

Supermarket refrigeration systems are one of the areas where this usage of CO_2 as a refrigerant is increasing, because of the environmental and safety traits of the refrigerant. Since supermarket refrigerating equipment is traditionally distributed across a machine room, throughout the store, and outdoors for heat rejection, the charge requirement is often quite large, and the system's extensive piping network is prone to leakage. In fact, supermarket refrigerant leak rates are estimated to be on average 25% with a typical charge quantity of 4,000 pounds (1,814 kg) (EPA 2016), meaning a typical store may lose 1,000 pounds (454 kg) per year. With a high-GWP refrigerant, this results in a direct greenhouse gas emissions rate which may equal or exceed the indirect emissions from power production to run the equipment. The requirement for a

non-flammable, non-toxic refrigerant, with minimal GWP and zero ODP, which can provide refrigerating and freezing capability through the use of a familiar central refrigerating rack configuration points to CO_2. However, CO_2 refrigerating systems can have lower efficiency than the conventional HFC systems they are intended to replace, particularly in hot climates. Therefore, improvements to the cycle must be implemented in order to allow CO_2 to be best applied.

Motivation: Demand Response with CO_2 Refrigeration Systems

A definition of Demand Response (DR) is provided by Motegi (2007) as follows:

> *Demand Response (DR) is a set of time-dependent program activities and tariffs that seek to reduce electricity use or shift usage to another time period. DR provides control systems that encourage load shedding or load shifting during times when the electric grid is near its capacity or electricity prices are high. DR helps to manage building electricity costs and to improve electric grid reliability.*

Demand response has long been of interest to some electric utility companies, particularly those whose peak demand periods approach the limits of their generating capacity: reducing the peak can allow them to avoid using expensive generating resources, as well as reducing stress on transmission infrastructure and potentially delaying investment and maintenance. In regions of the country with an independent system operator (ISO), the variation of price can be seen in publicly-available

locational marginal pricing (LMP) data, which shows the time-dependent variation of the price of production and delivery of electricity. An example is shown in Figure 1.

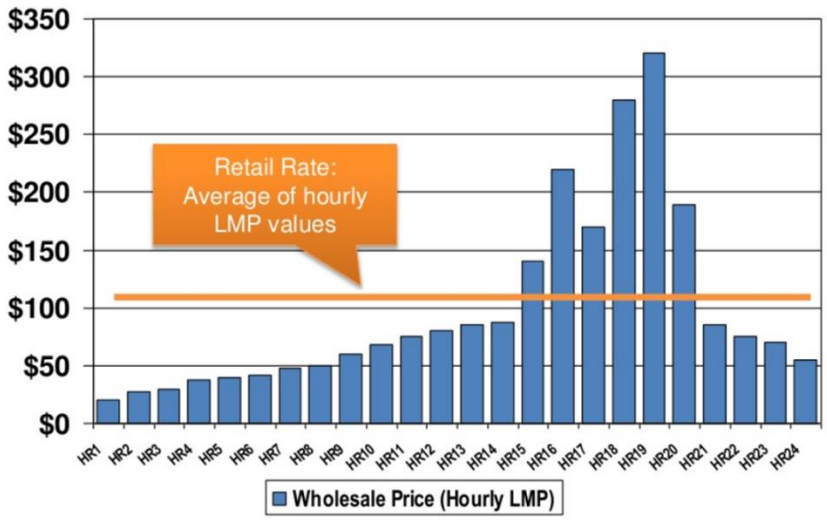

Figure 1 Example Locational Marginal Price (LMP) (Ulmer 2015)

The price of electricity generally follows demand, itself a function of outdoor temperature. An example of electric load as it varies with outdoor temperature is shown in Figure 2.

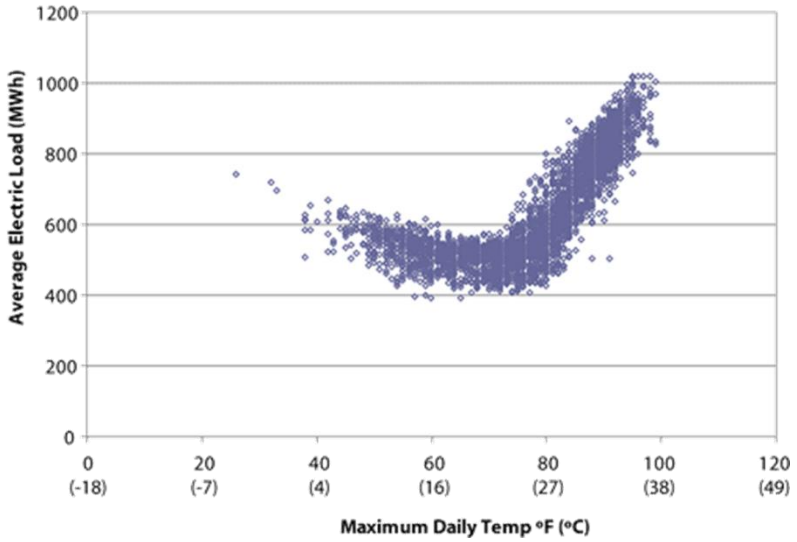

Figure 2 Total Utility Load vs. Daily High Temperature for New Orleans, LA (EPA 2018)

In addition to the peak reduction capabilities described by Motegi, DR is also becoming of more interest as society moves to incorporate more renewable electricity technologies. As renewable generation increases, flexible end-uses become more important, as renewable generation tends to be intermittent. Developing end-use equipment with the ability to respond to a changing power supply, store energy, and shift energy usage in time will be an important part of the transition to a more distributed and renewable-heavy electric grid.

Among end-use devices, some are more attractive for demand response than others. It is desirable for these devices to be large loads which are predictable and tolerant to interruption. Large power consumers are of interest to maximize the amount of response per transaction; scheduling an interruption from a single 50-kilowatt device is more desirable than from 500 individual 100-watt devices. Predictability is similarly important: it is preferable to request interruption of a device whose operating state is reasonably known such as an air conditioner during the hottest part of the day, rather than a device whose power is intermittent and hard to predict such as a simple electric resistance water heater, which only runs briefly for standby loss much of the day. Tolerance to interruption is also critical: turning off residential lights in the evening is likely to lead to customer complaints; a brief pause to the re-charge of an electric vehicle overnight may not be noticed at all.

Considering these factors, large-scale commercial and industrial refrigeration systems are an area with good potential for demand response. This research effort will focus

in particular on supermarket refrigeration. Supermarket refrigeration is a large load: about 50% of store energy consumption is for refrigerating equipment, totaling over 2.5 million kWh per year for a typical store (ENERGY STAR 2016). It also has a higher base load than most other application types, with refrigerating equipment running around the clock (Hart et al. 2014). Also, supermarkets contain a large thermal mass of refrigerated and frozen product, some of which is also tolerant to some interruption of service (Hirsch et al. 2015). And finally, as regulatory changes require the adoption of new technology such as CO_2 booster systems, there may be opportunity to implement new storage and control strategies with these new systems.

Literature Review

CO_2 Refrigeration

The modern resurgence of CO_2 as a refrigerant is often credited to the work of Gustav Lorentzen (Lorentzen 1993; Lorentzen 1994). Lorentzen and his colleagues first investigated CO_2 for the application of mobile air conditioning, later also identifying it's potential for applications such as heat pump water heaters. There are a number of ways in which CO_2 is commonly used as a refrigerant, each with merits and disadvantages. One of the most common is in water heating, where high-temperature heat rejection allows high-temperature water heating with attractive efficiency (Nekså 1998). This application, first deployed in mass in Japan, is today fairly common, with 400,000-500,000 units deployed per year and total deployment estimated at around 5 million systems (Shecco 2016). CO_2 is also being used with increasing frequency in commercial refrigeration, one configuration of which is the subject of this work.

Generally, CO_2 is used in refrigeration as a stand-alone refrigerant, as the low stage of cascade cycles, or as a pumped secondary fluid with another fluid as the primary refrigerant. Deployment of transcritical systems discussed in this work are still small in North America. As of early 2017, there were more than 150 known CO_2 transcritical grocery stores in Canada and more than 260 in the United States, compared with over 9,000 in Europe (Shecco 2017).

A review of the various configurations of refrigeration systems implementing CO_2 was performed by Sharma (2014). The researchers reviewed transcritical booster systems along with cascade systems and secondary loop systems in order to compare the configurations, their merits and drawbacks, and identified the best option for different climate zones. This included comparison with a typical baseline R404A system. In a secondary loop system, a high-side refrigerant operates in a DX cycle, cooling a secondary fluid which is pumped. This can be single-phase (such as water/glycol mixture) or two-phase (such as CO_2). In a cascade system, the low-stage refrigerant is also part of a vapor compression cycle; the evaporator of the high stage and the condenser of the low stage are coupled in a heat exchanger called the cascade condenser. Some configurations combine traits of these cycles, such as the combined secondary/cascade (CSC) system, where the low-temperature working fluid provides DX cooling to LT refrigeration loads, and pumped liquid refrigerant is supplied to the MT loads. The work of Sharma suggested that the best configuration depends on climate zone; they found transcritical cycles with bypass compressors to be the most efficient configuration in northern climates, and R404A DX systems (followed closely

by CSC cascade) to be the best in southern climates, with cross over in moderate climates. In an assessment by Purohit et al. (2017), a study of several modern low-GWP refrigerating options was considered. This included booster cycles using parallel compression or dedicated mechanical subcooling, and combined CO_2/R1234ze(E) arrangements in secondary or cascade configurations. A baseline R404A multiplex was considered as well. The researchers found that among CO_2-only options, the dedicated subcooler had a greater benefit than the parallel compression approach (both together could be better still); each of the alternative approaches was similar or better than the R404A plant in terms of energy. The CO_2-only options were also found to be better in terms of energy than either of the CO_2/R1234ze(E) hybrid systems.

Booster systems are two-stage R744 refrigeration systems, so named because a low-temperature (LT), sub-critical compressor stage "boosts" refrigerant from the LT pressure to the medium-temperature (MT) pressure range, where MT compressors then increase pressure to the gas cooler/condenser. Laboratory tests of a booster system without subcooling were performed by Sharma et al. (2015), and compared with cycle models (Sharma et al., 2014). These results showed test conditions in the range of approximately 283-308K ambient air temperature, which includes both subcritical and transcritical operation. In their study, the evaporator loads were held constant. It was observed that the LT compressor operated at a constant power and mass flow across outdoor temperature ranges, as it discharges to a roughly fixed intermediate condition and is in a way isolated from the outdoor conditions. However, the MT compressor, which also compresses flash tank bypass vapor, required higher power and mass flow

with higher outdoor temperatures to provide the same capacity to the MT evaporator. In some configurations, the bypass gas is circulated with dedicated compressors. Stated differently, the proportion of bypass gas being moved by the MT compressor or bypass compressor increases with increasing outdoor temperature.

During operation in transcritical mode (where the refrigerant is above and below the critical point at different stages of the cycle), the behavior is different than a typical subcritical cycle. Unlike a typical subcritical cycle, where efficiency decreases as high-side pressure increases, in transcritical operation efficiency may increase with increasing pressure to an optimum point, before decreasing (Kim 2004). This is illustrated in Figure 1, which shows ideal transcritical cooling cycles with isentropic compression and an assumed gas cooler leaving temperature of 310K. Three high-side pressure values are plotted: 8.0 MPa, 9.0 MPa and 10.0 MPa. The reader may note the slope of the 310K isotherm as it varies with pressure, compared with the slope of the isentropic line at the same pressures. Increasing pressure from the 8.0 MPa case to 9.0 MPa leads to a large increase in heat rejection for a comparably small increase in work. Increasing from 9.0 MPa to 10.0 MPa also increases heat rejection and work, but with a much smaller heat rejection benefit relative to the work increase. Among these three options, the highest COP is realized in case 2, the 9.0 MPa gas cooler pressure. Modeling and laboratory studies have been performed to examine this behavior in greater detail. For instance, Wang et al. (2013) showed an optimal pressure for R744 heat pumps with varying inlet water temperatures, a result supported by Hou et al. (2014) in a study of the effect of EEV position on a refrigeration cycle. A number of

simulation efforts have also addressed this point, including Ge and Tassou (2011) who modeled steady-state performance of a supermarket-style transcritical refrigeration rack, and identified high-side pressure control as a means of optimizing performance in transcritical operation. Work by Cecchinato et al. (2007) demonstrates a control strategy for transcritical systems in which control switches from an optimized pressure control to minimize gas cooler leaving temperature in the transcritical zone and the transition to subcritical, switching to a target subcooling set-point in the subcritical zone.

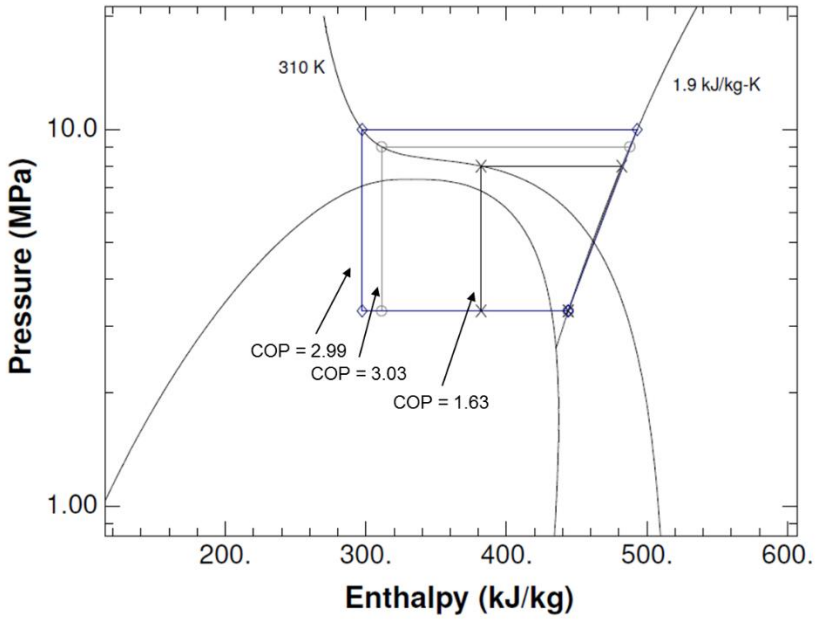

Figure 3: Simple Transcritical Cycle with Varied Gas Cooler Pressure

Another important consideration for the booster cycle is that the configuration couples the low-temperature and medium-temperature stages together; the LT stage is in a sense isolated from the outdoor condition, as the liquid refrigerant entering the expansion valve and the discharge of the LT compressor are both at essentially fixed conditions. The impact of load ratio and bypass flow are discussed in Sharma et al

(2015) and Sawalha et al. (2015). Sharma et al performed laboratory tests of a booster system without subcooling and compared them with cycle models. The results showed test conditions in the range of approximately 283-308K ambient air temperature, which includes both subcritical and transcritical operation. In their study, the evaporator loads were held constant. It was observed that the LT compressor operated at a constant power and mass flow across outdoor temperature ranges, as it discharges to a roughly fixed intermediate condition and is in a way isolated from the outdoor conditions. However, the MT compressor, which also compresses flash tank bypass vapor, required higher power and mass flow with higher outdoor temperatures to provide the same capacity to the MT evaporator. In some configurations, the bypass gas is circulated with dedicated compressors. This configuration is referred to as a parallel compression cycle, and the auxiliary compressor has a slightly lower pressure ratio because the suction gas is at the flash tank pressure rather than the evaporator pressure. Several researchers have demonstrated an efficiency improvement with the parallel compression cycle (e.g. Chesi et al 2014, Gullo et al 2016). CO_2 transcritical booster systems are becoming more common, particularly in colder climates, but more slowly emerging in warmer regions.

There are a few approaches to improving efficiency that receive a fair amount of attention in the literature. Two in particular focus on reducing the impact of throttling losses on the transcritical cycle. One such method is ejectors. Ejectors are considered particularly attractive for CO_2 refrigeration cycles because of the large pressure

reduction in the expansion process. Simulations by Deng et al. (2007) for example showed an 18-22% efficiency improvement is possible in transcritical refrigeration. Haida et al. (2016) recently performed laboratory evaluation of a transcritical R744 rack with and without ejectors, and found COP improvements up to 7% using the ejectors. The improvement was most significant with gas cooler pressures near the critical pressure. Further research by Gullo et al. (2017) suggests that combining ejectors, over-fed evaporators and parallel compression can produce significant savings compared with the baseline. Laboratory tests by Boccardi et al. (2017) on CO_2 transcritical heat pumps show an optimal ejector configuration exists, and COP improvements in the range of 13-20% were observed using the ejector in the laboratory. Another proposed method is expanders, which use a mechanical energy recovery device to recovery energy in the expansion process. Zheng et al. (2013) described a variety of approaches and evaluations showing strong potential for efficiency improvements. However, due to cost and complexity there are not currently commercial systems with expanders.

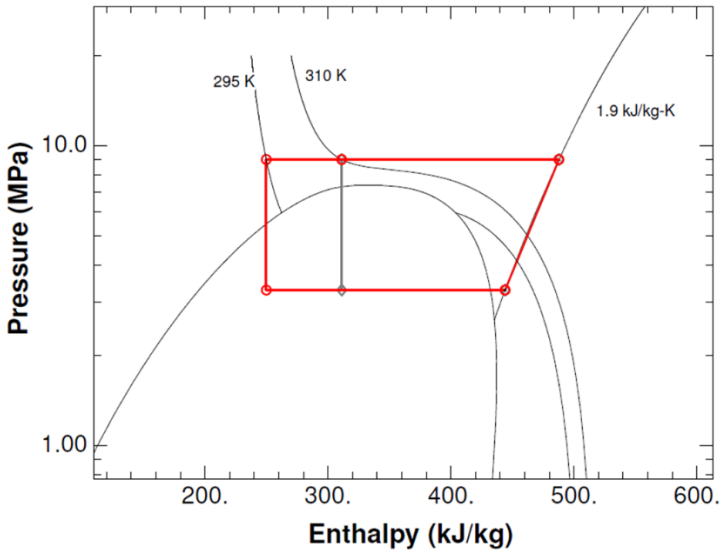

Figure 4: Simple Transcritical Cycle with Subcooling

Another way to improve efficiency is through the use of subcooling. Figure 2 shows the same idealized cycle, with 9.0 MPa high-side pressure. In this case, two gas cooler leaving temperatures are shown: 310K and 295K. The COP with the 295K discharge temperature is 46% higher than with the 310K discharge temperature; a much lower-quality two-phase refrigerant is sent to the evaporator in the diagrammed cycle, and capacity is significantly improved for the same compressor work. Llopis et al. (2015) analyzed the CO_2 transcritical cycle with mechanical subcooling, using simplified cycle models. The model had a single evaporator stage, and compressor models with both single-stage and two-stage with intercooling; detailed component models were not included. The results showed COP improvements of about 20%, as well as a lower optimal gas cooler pressure using the subcooler, both benefits. No experimental validation was provided. A study by Sarkar (2013) similarly evaluated subcoolers with the transcritical CO_2 refrigeration cycle, in this case modeling the cycle with a thermoelectric subcooler. Similar to Llopis et al. (2015), the base refrigeration cycle

was simplified, with focus on the high level effect of the subcooler, but again significant COP improvement (25.6%) and reduced gas cooler pressure were shown. Recently, several authors published work evaluating mechanical subcooling for laboratory prototype systems. A single-stage transcritical system was tested with a dedicated mechanical subcooler using R600a refrigerant by Sanchez et al. (2016). In that study, the mechanical subcooler was found to both improve capacity and allow for a lower gas cooler pressure, with capacity and COP improvements of up to 42% and 17% respectively. Testing was in transcritical operation only. The system also had a dedicated internal heat exchanger for subcooling which improved capacity and COP by 12% and 3% respectively. Nebot-Andres et al. (2016) studied the same mechanical subcooling system at additional operating conditions, with similar efficiency and capacity improvements reported. Shoenfeld (2013) performed laboratory testing on a single-stage transcritical CO_2 refrigeration system using thermoelectric subcooling, similarly finding improvements to COP and capacity. More recently Dai et al. (2017) presented a novel concept of combining an expander with a thermoelectric subcooler, where the expander can power the subcooler. The researchers calculate for a single-stage transcritical cycle a COP up to 38% higher than the baseline. Experimental validation has not yet been performed. In a study with a similar concept, Jamali et al. (2017) propose using a thermoelectric generator, heated by the waste heat of the gas cooler, to provide some of the power for a thermoelectric cooler, which provides subcooling. The calculations suggest 19% COP improvement; again laboratory evaluation has not been performed. However, none of these efforts look at two-stage evaporating system such as boosters, and therefore do not capture the effect of

subcooling on such a cycle. Mazzola et al. (2016) reported on system-level energy analysis from several supermarkets, including high-side pressure measurements, and compared stores without subcooling to those with different kinds of subcooling (dedicated mechanical subcooling, coupling with other A/C equipment, and groundwater). This effort identified significant peak reduction and energy savings particularly at peak load periods for all methods. This study did not evaluate cycle performance in detail, though. Another recent effort (Eikevik et al. 2016) examined a single-evaporator transcritical system with a dedicated mechanical subcooler using R290. Nebot-Andres et al. (2017) evaluated approaches in which a single-stage CO_2 transcritical cycle has a mechanical subcooler using R1234yf, or alternatively is in a cascade configuration with R1234yf as the high-side fluid. The researchers concluded that there are times when each configuration is better (and at the highest temperatures, the cascade configuration is preferable); but if one approach must be selected, the mechanical subcooling approach provides better average efficiency across a typical operating range, with considerably higher COP compared with the cascade configuration in lower ambient temperatures, versus only slightly higher COP for the cascade configuration in hot conditions. Internal heat exchangers, which provide a subcooling effect via internal heat exchange, are an important component to improve capacity and efficiency of CO_2 cycles as was demonstrated by Torella et al. (2011) through experimental work; internal heat exchangers can be paired with other efficiency enhancements as part of overall system design. The subcooling system needs to be accounted for in engineering design of the system: the overall refrigerant mass

flow requried to balance operation is less because of reduced flash gas, meaning total compressor displacement can be less.

A number of other simulation efforts have been undertaken for R744 refrigeration systems, though generally these studies do not have laboratory data validation. Baek et al. (2004) modeled a two-stage compression and intercooling cycle; this study focused on finding optimal inter-stage pressure for a two-stage compression process. Ge and Tassou (2011) modeled a supermarket-style booster system to analyze opportunities for efficiency improvements. Citing the high nonlinearity of CO_2 at transcritical conditions, the researchers opted to use a sensitivity analysis to identify optimal operating pressure. This study showed that optimal high side pressure is only a function of outdoor temperature, and not the function of the intermediate pressure or MT and LT evaporator stage pressure. Sawalha (2008) performed a similar analysis using EES. More recently, Gullo et al. (2016) investigated several technologies for hot-climate operation via simulation, including mechanical subcooling and parallel compression, as well as investigating cascade systems with R134a/R744. Their findings suggest that each of these improvements (subcooling and parallel compression) can be deployed in a way that makes the R744 system roughly equal in terms of energy consumption to the cascade system. Gullo's findings showed that the mechanical subcooling system was the best option in terms of annual energy consumption among the considered systems. Ge and Tassou (2014) also modeled a CO_2 transcritical cascade system to study heat recovery performance in the U.K. Polzot et al. (2017) showed overall energy savings using extensive heat recovery, compared with a baseline of R134a-CO_2 cascade

with a separate dedicated HFC heat pump; the savings are dependent upon climate. Tsamos et al. (2017) modeled all-CO_2 configurations of a booster with parallel compression, and two all-CO_2 cascade configurations (with and without parallel compressor). The non-cascade booster with parallel compression was found to be best among these options. A recent effort by Fidorra et al. (2016) describes the booster system with cold thermal energy storage – this paper is discussed in greater detail in the "Demand Response with Refrigeration" section, below.

A study of five real-world installations of R744 transcritical supermarket systems in Sweden was performed by Sawalha et al. (2015). These systems were also modeled using Engineering Equation Solver (EES). Sawalha shows real-world performance is improved with the subcooler, and also importantly shows that the removal of flash gas from the intermediate vessel (the flash tank) has an important impact on efficiency. In an extension of this effort, Karampour and Sawalha (2017) used field measurements and whole-building energy simulation to model integrated systems, where heat recovery from the gas cooler/condenser is utilized for heating loads and the CO_2 system is also used for air conditioning loads; the modeling suggested better performance compared with stand-alone conventional HFC solutions, but emphasized that efficiency enhancements such as subcooling and ejectors are needed particularly in warm and hot climates.

An important factor in the real-world operation of transcritical CO_2 systems is the performance of the condenser/gas cooler as the system operates near the critical point.

Some research has been performed in this area recently, including work by Kondou and Hrnjak (2011) who performed tests on condensing properties of CO_2 at pressures approaching the critical point. They compared results with correlations developed by others such as Cavallini et al. (2006) and Dang and Hihara (2003). A finding of interest is the decrease in heat transfer coefficient at pressures approaching the critical pressure, an operating regime of key importance to transcritical R744 systems. A laboratory test by Tsamos et al. (2017) examined two-row and three-row heat exchanger designs for a booster system in laboratory testing, and found significant improvements to COP enabled by the three-row configuration due to lower refrigerant leaving temperatures.

Transient simulation is a valuable tool for understanding the dynamic behavior of vapor compression systems and can allow researchers to study their performance in changing conditions, and simulate control methods without having to do extensive and costly laboratory tests. A CO_2 refrigeration modeling library was developed in Modelica by Pfafferott (2004). In this work the researchers were focused on aircraft cooling equipment. The researchers found fair agreement with experimental results for heat exchangers, and noted increased error in modeling the gas cooler. The researchers observed that the discretization of the heat exchanger causes inaccuracy near the critical point, a problem which can be reduced by higher discretization. Similar was observed by Sanchez et al. (2012) who studied the effect of degree of discretization on accuracy and calculation time.

Shi (2010) developed a transient model using Dymola, showing a limited validation with results recorded from a real store installation. They studied the difference between using a one-dimensional (1-D) and 2-D gas cooler model as compared with a 3-D model to reduce simulation time, noting that 1-D worked well with all gas cooler fans running, but in part-load operation, the results of the 2-D and 1-D models deviated too much to be acceptable; the authors recommended not using the one-dimensional model for this reason. They also studied the effect of natural convection on the gas cooler model, noting that it is important to consider natural convection to accurately portray performance in conditions where the fan(s) are off. Abdelaziz et al. (2006) demonstrated developments to their enthalpy-based solver for transient simulations by modeling a transcritical CO_2 model. A heat exchanger model was proposed which could simulate evaporators, condensers or gas coolers with the same method; the proposed component used the moving boundary layer approach, handling supercritical fluid as a vapor region. Zheng (2015) developed transient models of a CO_2 ejector expansion refrigeration cycle (EERC), also applying a moving boundary approach for the heat exchanger. This cycle was again a single-stage system, in this case studying the performance of ejectors. Salazar (2014), noting few works in the literature addressing transient controls of transcritical systems, developed a lumped energy balance model for simulating a single-stage CO_2 transcritical system. They used this model, which relies on physical correlations and empirical coefficients derived from other studies, to simulate PID control methods. In a paper describing transient modeling of small stand-alone refrigeration systems using CO_2, Mastrullo et al. (2015) summarized the literature regarding CO_2 refrigeration modeling by noting that, at that

time, the validated, transient models of CO_2 refrigeration systems were few. Hafner et al. (2014) presented a transient model using Modelica of a booster cycle which was used to simulate a multi-ejector approach. However, the laboratory system used for data validation was a single-stage (not booster) configuration with ejectors; the baseline booster system was not tested in the laboratory. Therefore, the researchers also developed a simulated booster cycle, also neglecting the low stage.

Demand Response with Refrigeration

In practice there are many ways of providing demand response. Albadi and El-Saadany (2007) described programs using the classification structure shown in Figure 5:

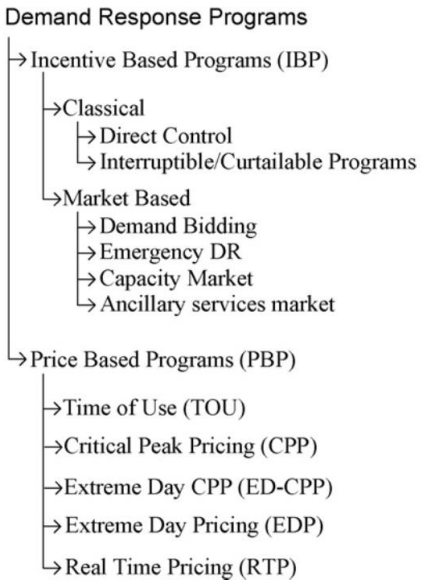

Figure 5: Demand Response Program Classifications (Albadi and El-Saadany (2007))

Each of these has potential benefits and draw backs, and target applications. For instance, direct load control is more common for residential usage and may be used with load control switches for air conditioners and water heaters. For large commercial applications it may be more common to participate in demand bidding, bidding on load reduction targets in the electricity wholesale market. Price-based programs like time of use rates are attractive to end-users who can reasonably schedule usage; storage and load shifting may help customers move their consumption to low-cost hours. HVAC and refrigeration equipment can be implemented directly or indirectly into any of these programs, with the control and implementation differing by program type. In the simplest case in direct or interruptible control, an on-off signal or even direct relay interruption may be the method. On the other extreme, in Real Time Pricing scenarios the control may be part of a more sophisticated scheme such as a building supervisory control, or even controlled by an external aggregator who sends control signals to a distributed network of connected equipment.

Motegi (2007) describes some of the various DR implementations in commercial buildings. Among their observations is that HVAC (and by extension, refrigeration) is an excellent resource for demand response because HVAC&R load is substantial and a large contributor to peak loads; the “thermal flywheel” of conditioned spaces allows temporary reduction in capacity without immediate comfort impacts; and finally commercial HVAC&R equipment is often at least partially connected to existing

building energy management systems. All of the above factors mean that HVAC&R loads offer a valuable opportunity for DR.

Load shifting may be done on a regular or even daily basis. A state-of-the-art study by Arteconi et al. (2012) describes thermal storage opportunities and points out that ice and water storage are the methods with most of the market share (ice being the largest). Refrigerant subcooling using thermal storage is one approach that has been studied (e.g. Huang et al. 2007, Chieh et al. 2004) and in conventional-refrigerant applications the COP benefits are in the range of 8% using an ice storage subcooler.

Many studies have evaluated the options for thermal storage media for various thermal storage applications. For instance, review of cold storage materials for air conditioning (Li et al. 2012) and for subzero applications (Li et al. 2013) have been performed and describe dozens of potential blends and their phase change temperature and latent heat of phase change. Li's work also describes the key criteria in material selection, which include cycling stability, conductivity, chemical stability and cost. Oró et al. (2012) also summarized an extensive list of phase change materials with melting temperatures from -86°C to +20°C. Oró et al. also described some commercially-available cold storage equipment. Cost is always a critical consideration, and thermal storage could be financially attractive in the right conditions: Hasnain (1998) described thermal storage using chilled water, ice or eutectic salt, and provided a comparison of cost for a chiller system with and without

ice storage. The analysis stated that ice storage integration could result in a lower total system cost because of the opportunity to use a smaller-capacity chiller.

Supermarket refrigeration equipment can be considered for demand response and load shifting, having inherent storage in the store because of refrigerated and frozen products. The use of refrigerated and frozen goods in grocery stores as a thermal storage medium has been studied in limited cases. In such an approach, the refrigeration capacity to a particular zone – for instance, a walk-in freezer – can be reduced or interrupted for a period of time to reduce power without damaging the product in the store. Hirsch (2015) performed pilot type testing in supermarket stores to evaluate and quantify this potential. One factor they identified as important was establishing the timescale for DR using different resources, such as walk-in or display case refrigerators and freezers; however, the store owner in their pilot was particularly sensitive to using the refrigerated cases for DR and therefore they were considered off-limits. This highlights one issue: food retailers are likely to be sensitive to participating in programs that will affect (or be perceived to affect) their product. Hirsch also looked at different methods for DR: pre-cooling or not, changing the discharge air temperature in critical cases or non-critical cases, and controlling the compressors based on measured "product simulator" temperatures rather than controlling discharge air temperature. Using these methods they were able to shed up to 10 kW of load on average during DR events in a real, operating supermarket. One suggestion from this study was that the ability to switch between control points – the discharge air temperature or the temperature of a product simulator inside the case –

might be best for control, as the case air temperature responds to DR changes much more rapidly than product simulator temperature. They also identified a research need in the area of DR control to increase the system's power consumption, for times when excess grid power is available such as renewable integration.

Others have looked at the methods for planning and controlling the shifting of loads using foodstuff as the storage medium. Vinther et al. (2015) examined a learning-based pre-cooling algorithm for this. The goal of the algorithm is to determine the appropriate timing and duration of pre-cooling for refrigerated or frozen goods. Their initial interest was avoiding a capacity shortfall on the hottest day of the year, rather than capitalizing on a demand response price signal or similar, but the concept is similar. Hovgaard et al. (2011) examined the use of model predictive control with adjustments to display case storage temperatures to provide a flexible load in response to pricing, including the ability to regulate power up or down; they found their predictive control method could save 9-32% by considering predictions of load profile and electricity prices. Prediction of the load itself is important for this approach; Rasmussen (2016) studied models for forecasting the electrical load of supermarkets. The researchers found that using store data, local weather observations, weather forecasting, and knowledge of open/closed hours for the store, they could accurately model electrical load. However, this approach takes a store-level view rather than considering individual refrigerated or freezer loads and the temperatures within. Shafiei (2013) modeled a CO_2 Booster cycle, like that discussed in this work, for supervisory control under DR loads. Shafiei's work is to produce a modular

simulation method, with parametric models of the condenser, suction manifold (including estimate of a bulk compressor power) and the display cases; these components can be tuned with real data and used to estimate power and predict the system response under DR loading. A similar modeling approach was described by O'Connell et al. (2014) and also implemented in the work of Hirsch (2015), who used it to model display cases supported with empirical data from stores. Hirsch considered simplified refrigeration cycle models based on an empirical multiplier applied to Carnot efficiency, but found the gray-box display case models to agree well with measured data from the display cases.

While much of the research focuses on storage within the end-use or load shifting by adjusting temperature set-points, the concept of applying thermal storage within the CO_2 booster cycle has been explored only recently. Fidorra et al. (2016) provided an overview of four possible configurations, shown in Figure 6 below. The configurations included are briefly descried here. In Layout #1, a dedicated medium-temperature evaporator can be used to cool a storage medium, which may later be used for subcooling. This has the advantage of being internal to the cycle. A TRNSYS model of such a concept was explored by Polzot et al. (2015), who considered a water tank as the storage medium. Layout #2 shows storage integrated in the MT level load such as by a phase change material inside display cabinets; a similar concept was explored by Waschull et al. (2014). In Layout #3, storage is used to cool the receiver liquid outlet to the evaporators, to reduce the required mass flow for a given cooling capacity. In Layout #4, a storage medium upstream of the receiver

inlet can be charged or discharged by adjusting the refrigerant pressure passing through the storage medium. Lowering the pressure boils some refrigerant to charge the storage media; increasing the pressure to a point where the saturation temperature is warmer than the storage temperature in turn allows the refrigerant to be cooled by the storage medium.

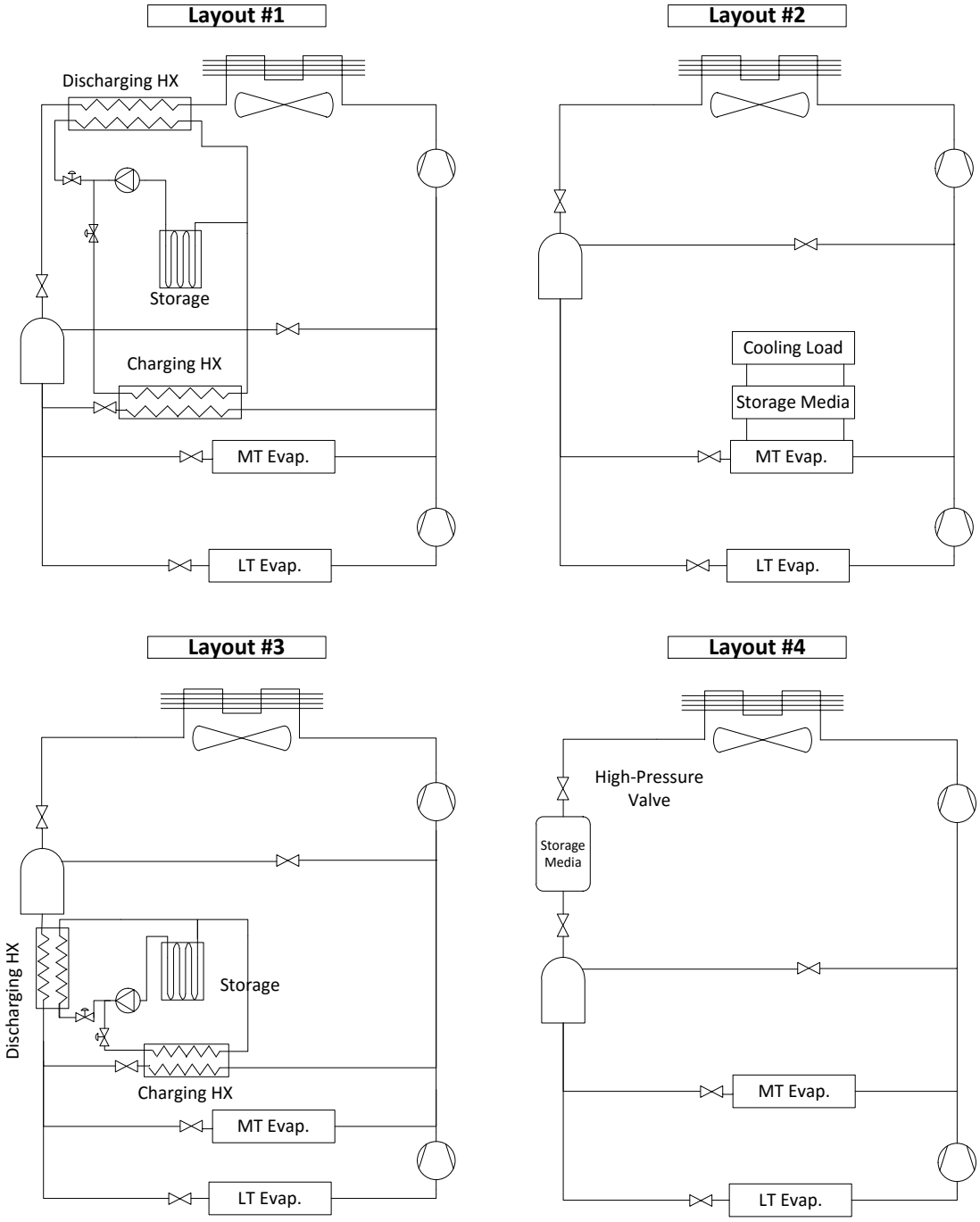

Figure 6 Thermal Storage Integration Configurations Proposed by Fidorra et al. (2016)

Fidorra et al. identified the above storage approaches and evaluated them through steady-state thermodynamic analysis. The researchers found Layout #1 to have high

demand reduction potential, with relatively small hardware required; a large temperature difference leads to relatively low efficiency though. Layout #2 was also assessed to have high potential for peak reduction, but sizing and deployment of the storage material is challenging. In Layout #3, small temperature differences mean that large heat exchangers are needed and the total reduction potential is comparatively small. In Layout #4, there are no new heat exchangers required other than the storage itself; however, the temperature difference between charging and discharging is small which may present heat transfer challenges. Research gaps in the areas of detailed simulation models and transient simulations were identified. In addition, the work of Fidorra does not examine the opportunity to use external sources (such as a dedicated cooling unit) for storage; there may be an opportunity for improved efficiency from dedicated cooling equipment.

Summary of Literature Review

CO_2 refrigeration systems including transcritical booster systems have been a popular topic in the literature in recent years. This is driven by surging interest in low-GWP refrigerant solutions for refrigeration applications. The challenge that may be most frequently identified in the literature is efficiency at high outdoor temperature conditions, and researchers have investigated a variety of paths to improving efficiency. The primary relevant paths of research are:

- Examining possible system architectures for using CO_2, either as the only refrigerant or as part of a multi-refrigerant system;

- Optimizing performance of the transcritical cycle (including booster cycle) through optimal control of pressure levels;
- Reducing the penalty of throttling losses through devices like ejectors and expanders;
- Reducing the flash gas, particularly in transcritical operation, through the use of subcooling.

In laboratory evaluations, researchers have mostly studied single-stage systems or subsystems of the booster cycle, with few data sets of full-fledged two-stage booster systems found in the literature. Much of the recent focus of current laboratory efforts is on ejectors and parallel compression. A laboratory evaluation of the booster cycle using dedicated mechanical subcooling was not found in the literature review for this effort. Many steady-state models have been developed, but fewer transient models of the full booster cycle have been published as yet. In particular, no transient model validated with laboratory data was found studying the booster system with mechanical subcooling.

Demand response as it relates to refrigeration is an area that has seen a recent increase in interest, as utilities move towards an "integrated grid" concept. Many of the studies in this area consider store-level controls: adjusting set-points and using load prediction strategies. Research has also examined the concept of shedding load by interrupting cooling capacity to display cases or other loads, often from the perspective of quantifying the behavior of the case itself (rather than the detailed impact on the larger system). Conventional thermal storage, using ice or another

material to provide direct cooling (applied to the load) and offset mechanical cooling is well represented in the literature. Alternative concepts of thermal storage integration into the refrigeration cycle are emerging in parallel to this work, and Fidorra et al. (2016) have explored several versions of this concept with the booster cycle. The concept of thermal storage applied to subcooling using dedicated mechanical subcooling was not found in the literature. The combined application of thermal storage as applied to the cycle along with load shedding has also not been explored.

Objectives

The objectives of this work are focused on improved energy efficiency and improved ability to operate effectively and flexibly in demand response applications using the CO_2 booster cycle. The objectives are:

1. Perform experiments to quantify the performance of the booster cycle with and without dedicated mechanical subcooling as it varies with outdoor temperature. Capture transient behavior of the booster cycle, measuring cycle response to shedding medium temperature or low temperatures loads in particular. Develop insight into the benefit of the subcooling as it varies with size of the subcooler
2. Develop transient models to expand understanding of cycle response to load shedding. Quantify the response of the system to varying degrees of load shedding at each evaporating stage. Develop the ability to simulate load shedding scenarios in a simulated supermarket refrigeration system, and quantify the potential operating cost reduction of demand response in these applications.

3. Develop the concept of a thermal storage subcooler, charged by and offsetting the dedicated mechanical subcooling system. Study the impact of the thermal storage subcooler on whole-system behavior and efficiency. Verify that the storage subcooler can provide load-shifting that does not affect refrigerating capacity. Evaluate demand response scenarios incorporating the storage system to provide added benefit.

Chapter 2: Refrigeration Systems and Subcooling

This section discusses the major system configurations in commercial refrigeration applications, and types of subcoolers and their potential applicability. The chapter first categorizes the major configurations of refrigeration systems and then describes the subcooling approaches that are used. The analysis includes commercial and some industrial refrigeration (particularly configurations that are related to, or potentially applicable in commercial refrigeration), but excludes residential refrigeration. The purpose of this chapter is to:

- Illustrate the relevant alternatives to the CO_2 booster cycle and highlight key differences
- Describe appropriate approaches to subcooling which may be applied to some or all of the system types described herein. Identify benefits, drawbacks and applicability of subcooling technologies using existing literature where possible.

System Configurations

This section broadly categorizes the configurations of refrigeration equipment that are used for commercial refrigeration applications.

Booster

The booster cycle is discussed at length in this effort, and will be treated only briefly here. The booster system integrates the low-temperature and medium-temperature stages of a refrigeration system into one cycle. The low-temperature stage compressor discharges to the suction level of the medium temperature stage; a flash tank/receiver is at an intermediate pressure above the MT stage pressure. In a typical application it

is common for the compressor rack to combine single-speed compressors with one variable-speed compressor per stage, to provide capacity matching. The compressors are controlled to maintain the pressure level of the suction manifold. A basic booster cycle schematic is shown in Figure 7.

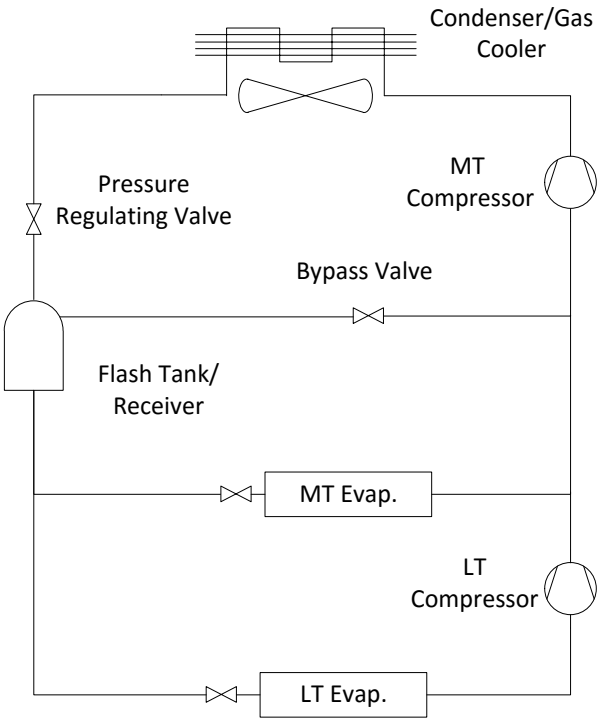

Figure 7 Basic Booster System Schematic

Remote/Packaged Condensing Units

Remote condensing units are very common for applications like small walk-in coolers and freezers, food retail and some smaller industrial applications. Remote condensing units are typically sold as pre-engineered systems with all of the components except for the expansion device and evaporator in a single package. The typical configuration includes a single compressor, receiver, condenser and fan, and suction

accumulator if appropriate. A remote condensing unit is specified to pair with the evaporator for the application; for instance, a condensing unit may be paired directly with a hung evaporator in a walk-in cooler or freezer.

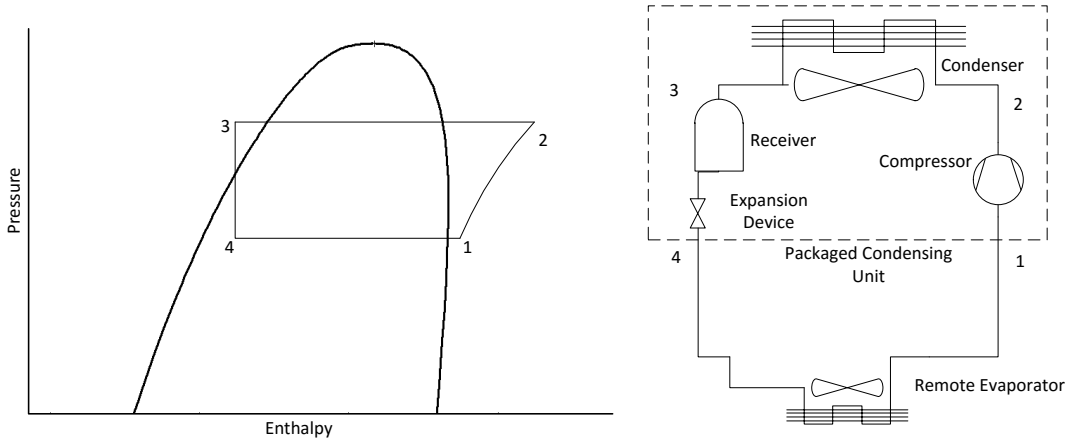

Figure 8 Typical Remote Packaged Condensing Unit Pressure-Enthalpy Diagram and Schematic

Packaged condensing units are common because they are inexpensive and easily accessible, and readily integrate with a variety of evaporator types for small applications. They are designed and sold by many major manufacturers, using a wide range of refrigerants, and generally have performance characteristics that are known and tabulated by the manufacturer. Most are fixed-speed, though variable-speed compressors are also available.

The efficiency of remote condensing unit systems has been calculated in several studies, summarized in the table below.

Table 1 Results of Packaged Condensing Unit Laboratory Tests (: COP visually interpreted from graph)*

Study	Equipment	Conditions	COP
Hwang et al. (2007)	Condensing unit, R290 refrigerant	35C cond. air in, -23.3C evap. air in	0.88
		18.3C cond. air in, -23.3C evap. air in	1.31
		35C cond. air in, 1.7C evap. air in	1.79
		18.3C cond. air in, 1.7C evap. air in	2.66
	Condensing unit, R410A refrigerant	35C cond. air in, -23.3C evap. air in	0.8
		18.3C cond. air in, -23.3C evap. air in	1.27
		35C cond. air in, 1.7C evap. air in	1.71
		18.3C cond. air in, 1.7C evap. air in	2.64
	Condensing unit, R404A refrigerant	35C cond. air in, -23.3C evap. air in	0.78
		18.3C cond. air in, -23.3C evap. air in	1.24
		35C cond. air in, 1.7C evap. air in	1.57
		18.3C cond. air in, 1.7C evap. air in	2.39
Kabeel et al. (2016)	Condensing unit, R134a refrigerant	26C cond. air in, -6C evap. air in	2.175
	Condensing unit, R1234ze refrigerant	24C cond. air in, -5C evap. air in	2.292
Aprea et al. (2011)	Condensing unit, R22 refrigerant	35C cond. Air in, 2C evap. air in	2.8
		35C cond. Air in, -5C evap. air in	2.4*
		35C cond. Air in, 8C evap. air in	3.2
	Condensing unit, R422D refrigerant	35C cond. Air in, 2C evap. air in	2.1*
		35C cond. Air in, -5C evap. air in	1.8*
		35C cond. Air in, 8C evap. air in	2.3*

For packaged condensing units, unlike the other systems described here, the COPs in the literature can be readily corroborated with manufacturer specification. Tecumseh,

a U.S.-based manufacturer of refrigeration equipment, provides efficiency data for their off-the-shelf condensing units. A selection of systems are described here for comparison with the above (Tecumseh 2014, Tecumseh 2014a, Tecumseh 2016).

Table 2 Manufacturer Performance Data for Condensing Units (Tecumseh 2014, Tecumseh 2014a, Tecumseh 2016).

Model	Refrigerant	Test Condition	Capacity	Power	COP
AJA7494ZXDXC	R404A	37.8C cond. inlet air, -17.8C evap. inlet air:	1612	1459	1.10
		37.8C cond. inlet air, -3.6C evap. inlet air:	2881	2142	1.35
		26.7C cond. inlet air, -6.7C evap. inlet air:	3136	1842	1.70
AJA7565YXDEC	R134a	37.8C cond. inlet air, -17.8C evap. inlet air:	840	819	1.03
		37.8C cond. inlet air, -3.6C evap. inlet air:	1707	1245	1.37
		26.7C cond. inlet air, -6.7C evap. inlet air:	1869	1169	1.60
AE4430U-AA1ACK	R290 (Propane)	37.8C cond. inlet air, -15C evap. inlet air:	425	270	1.57
		37.8C cond. inlet air, -3.6C evap. inlet air:	645	320	2.01
		26.7C cond. inlet air, -6.7C evap. inlet air:	692	290	2.39

Multiplex DX

Multiplex systems are currently the most common configuration for the major loads within a supermarket, and there are some variations to the basic configuration. Multiplex systems consist of multiple compressors with a shared liquid, suction and discharge manifolds and condenser or condensers. Multiple evaporator loops are connected to the liquid and suction manifold and distributed throughout the store. An example of this configuration for a single suction group is shown in Figure 9 (Baxter, 2002).

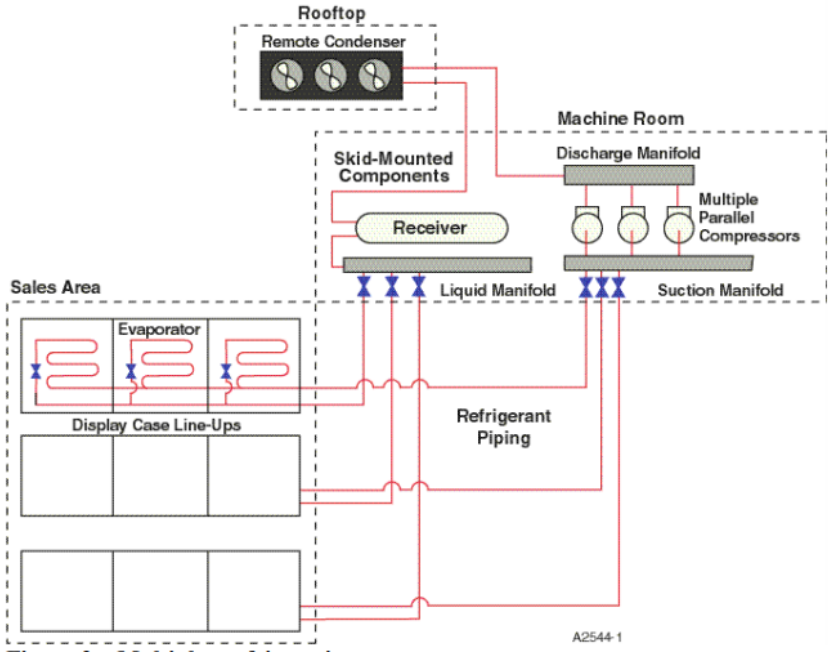

Figure 9 Typical Configuration of a Multiplex Refrigeration System (Showing One Suction Group) (Baxter, 2002)

Multiplex systems may be separate racks of compressors per temperature group, or may have a “split-suction” configuration, where the refrigerant charge, condenser, and liquid manifold are shared between the low-temperature and medium temperature compressor groups, but compressor groups each have a dedicated suction manifold at the appropriate pressure level. The refrigeration rack is installed in a machine room, rooftop mezzanine, or other remote location. A concern with multiplex systems is the requirement for a large volume of charge. Since the system is in a central location and distributes refrigerant all around the store, charge quantities are large and leak rates are high. An average store in the U.S. leaks approximately 30% of its’ charge, and total refrigerant quantity per store is typically in the range of 1400-2300 kg (Faramarzi and Walker 2004). To reduce charge and the length of refrigerant piping, some stores are engineered with multiple distributed systems each located as close as possible to the appropriated group of loads.

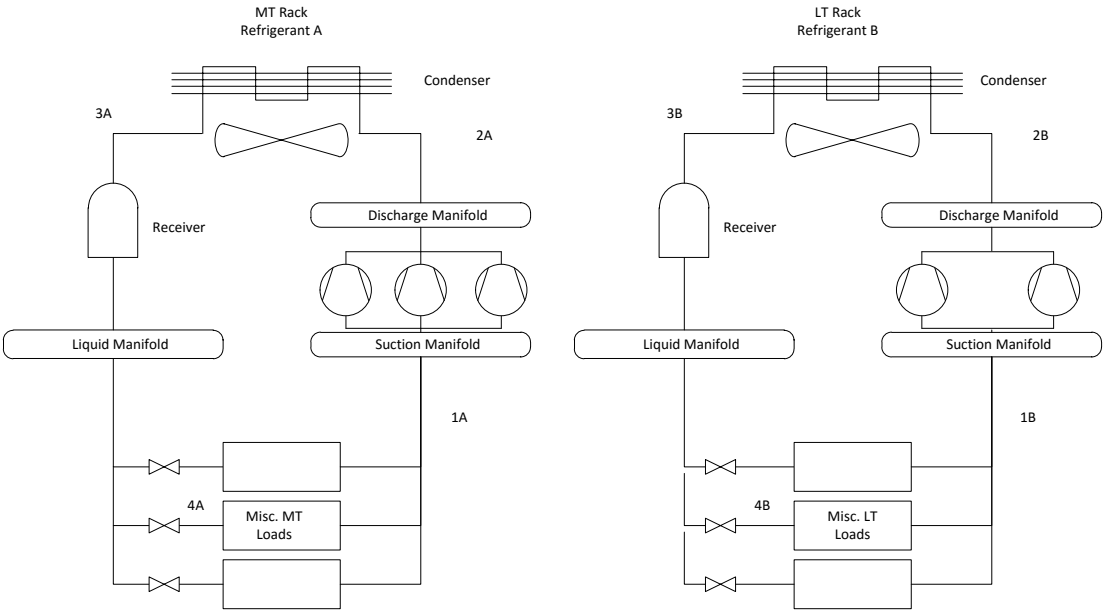

Figure 10 Schematic of Multiplex Configurations for MT and LT Racks

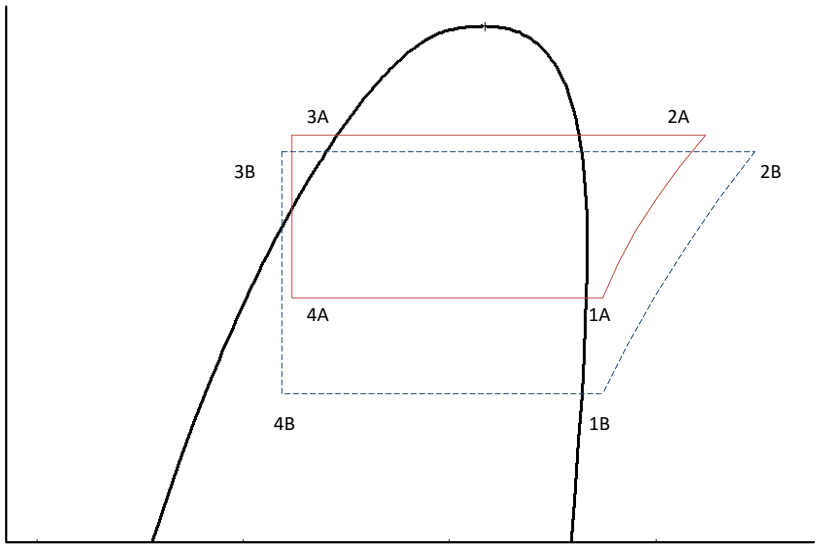

Figure 11 Pressure-Enthalpy Diagrams for MT and LT Multiplex Racks

Multiplex systems are highly customizable and may include features such as heat reclaim (where heat is recovered from compressor discharge vapor, for water heating, space heating or other useful application) or subcooling.

While multiplex systems are extremely common, they are generally site-built, and laboratory- or field-measured COP is uncommon in the literature. Baxter (2002) provides field-measured, seasonal-average COPs for multiplex refrigeration systems, as follows: for LT loads, the COP from May through August was 2.48 with an average saturated suction temperature of -28.4°C and saturated discharge temperature of 28.2°C. In November through February, the COP was 2.83 with -29°C SST and 21.7°C SDT. The MT system COP averaged 3.82 from May through August, with -5.1°C SST and 28.5°C SDT, and 4.90 from November through February, with -6.6

SST and 19.4°C SDT. The store used R404A for low temperature loads and R22 for medium temperature loads.

Indirect/Pumped Secondary

In recent years efforts to reduce refrigerant charge and leakage have led to more systems using indirect or pumped secondary systems to reduce the charge of a higher-GWP or toxic or flammable refrigerant. Pumped secondary systems use a primary refrigeration circuit to cool a secondary fluid, which is pumped to the end use. The secondary fluid may be a volatile fluid such as carbon dioxide or a non-volatile fluid such as water or brine. Pumped secondary systems are much like chillers, and the secondary working fluid is selected depending on the needs of the application. Application of the pumped secondary configuration can help to reduce the charge of the primary working fluid or to keep that working fluid contained to a single location. For example, in ammonia/carbon dioxide systems, a relatively small charge of ammonia may be contained in a machine room or similar while a safe, secondary working fluid such as carbon dioxide is circulated to the evaporators (Bush and Mitchell 2017). Pumped secondary systems introduce additional power consumption from pumps. The also require an intermediate heat exchanger between the primary and secondary fluids.

A review by Wang et al. (2010) described a range of secondary-loop systems including volatile secondary and single-phase secondary fluids, with different primary

working fluids, and found that the energy consumption was similar to conventional DX systems, varying higher or lower depending on system design, climate, and other site-specific considerations. The main motivation for this configuration in supermarket applications is reduction of high-GWP or hazardous refrigerant charge, rather than energy savings.

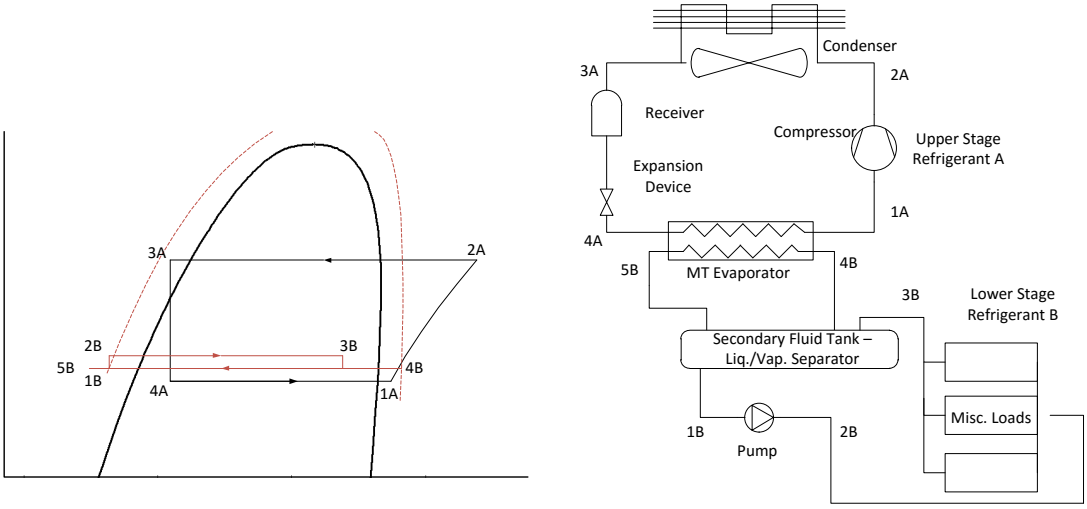

Figure 12 Schematic and Pressure-Enthalpy Diagram for Secondary Loop System

A study by Faramarzi and Walker (2004) details a field trial of a secondary-loop refrigeration system, compared with a then state-of-the-art DX multiplex system. The secondary loop system had some enhancements such as evaporative cooled condensers which explain some of the efficiency improvement over the baseline; nonetheless, efficiency was reported and is shown here in Figure 13. The LT COP ranged from approximately 2.3-2.5, while the MT COP range from approximately 3.5-3.8 in most conditions.

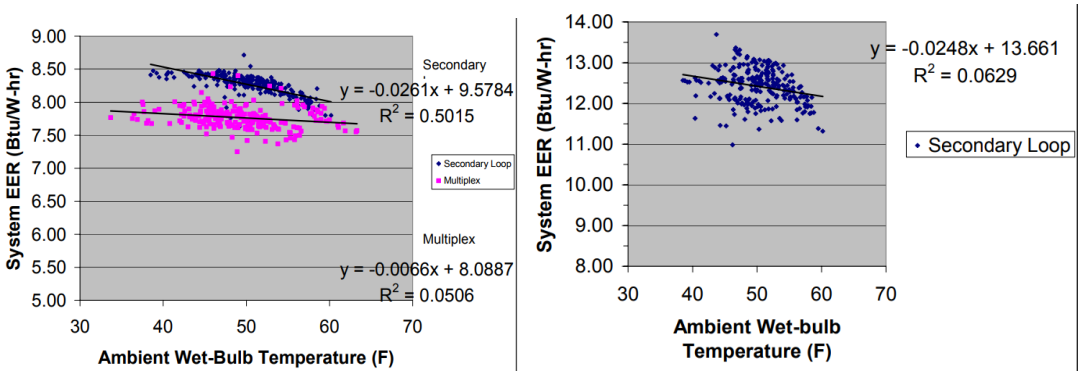

*Figure 13 Efficiency of Secondary-Loop System Using R507A and a Salt-Water Secondary Fluid, Showing Low-Temperature Efficiency (with Baseline Multiplex, left) and Medium-Temperature Efficiency (right). EER = COP * 3.412 (Faramarzi and Walker, 2004)*

The efficiency of a set of three Swedish HFC-based supermarket refrigeration racks was measured in the field in Sawalha et al. (2017). Each system uses a multiplex DX low-temperature and indirect medium-temperature configuration.. The relevant details of the systems are described in Table 3. The number of units refers to the separate rack systems in each store; in other words, 2 MT units means the store has two separate systems serving the MT loads through the store.

Table 3 Descriptions of HFC Multiplex Refrigeration Racks Studied in Sawalha et al. (2017)

	RS1	RS2	RS3
Refrigerant	MT: R404A; LT: R404A	MT: R407C; LT: R404A	MT1: R404A; MT2: R407C; LT: R404A
Cooling Capacity	MT: 87 kW; LT: 18 kW	MT: 175 kW; LT: 36 kW	MT: 410 kW; LT: 81 kW
Subcooler	Yes	Yes	Yes
Heat Recovery	No	No	Yes
Heat Transfer Fluid	MT: Prop. Glycol; LT: DX	MT: Eth. Glycol; LT: DX	MT: Prop. Glycol; LT: DX
Number of Units	MT: 1; LT: 1	MT: 2; LT: 2	MT: 2; LT: 2

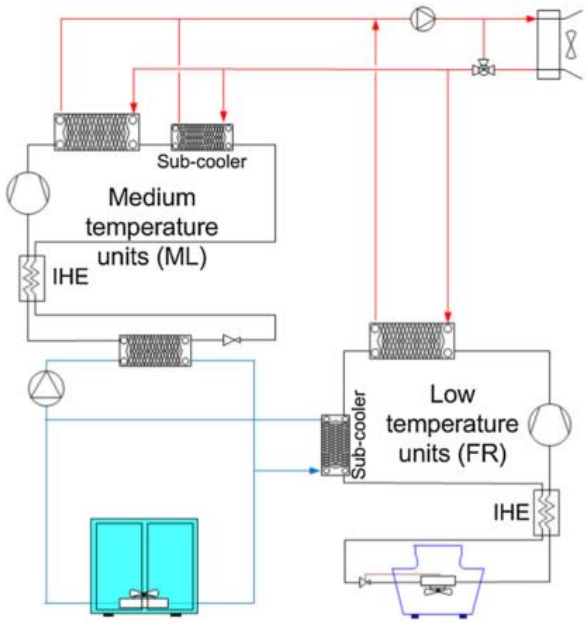

Figure 14: Schematic of the Reference Multiplex Refrigeration Systems for Sawalha et al. (2017)

The COP for each system is shown in Figure 15.

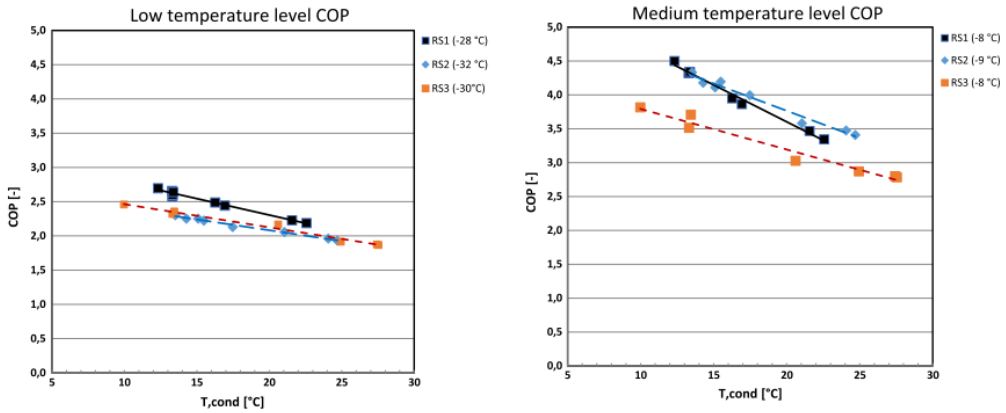

Figure 15 Measured COP vs. Condensing Temperature of HFC Multiplex Systems from Sawalha et al. (2017) with SST in Parentheses in Legend

Cascade

Cascade systems use two, interconnected vapor compression systems to provide refrigeration. One circuit, the “high-side”, rejects heat via the condenser to the

ambient, cooling water, or otherwise outside of the cycle. The “low-side” circuit provides refrigeration, and the condenser of the low-side fluid is the evaporator of the high-side fluid. The low-side fluid may be configured for one or multiple evaporators and suction pressure levels. Cascade systems are applied in a range of applications, including industrial and commercial. The most common use of cascade systems is in applications with a large temperature difference between the lowest evaporator and the condenser, such as low-temperature freezing. The cascade configuration allows two different refrigerants to be specified, each with the appropriate thermodynamic properties for the range of its operation. CO_2 is often used as the low-side refrigerant in cascade systems, while a refrigerant with more desirable traits for high-temperature operation is used as the high side refrigerant. Cascade systems have the efficiency benefits that come from two-stage compression, but this benefit is tempered by the need for the intermediate heat exchanger.

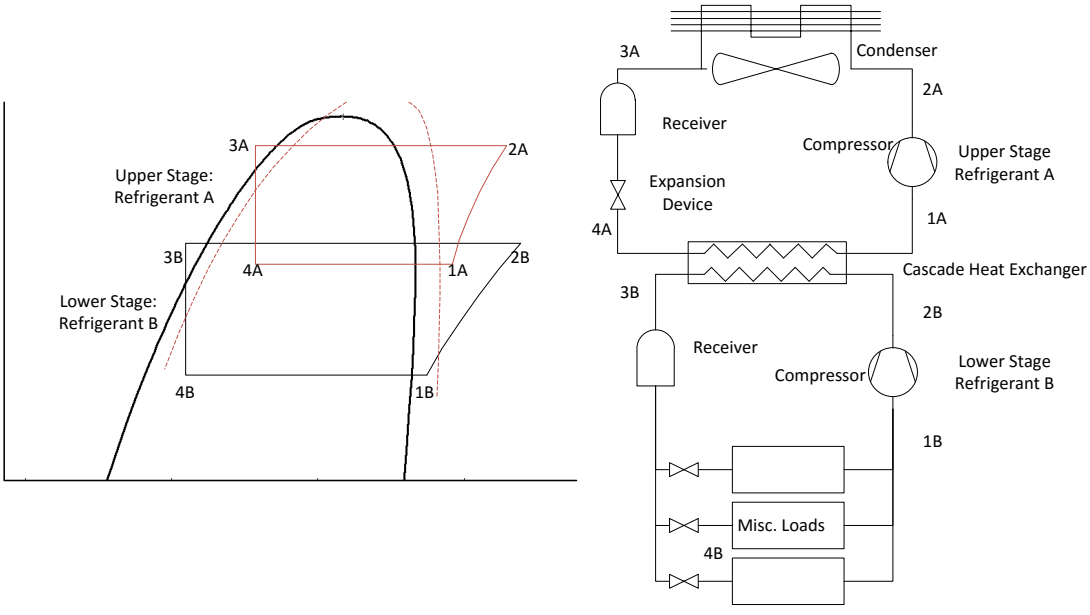

Figure 16 Configuration and Pressure-Enthalpy Diagram for Cascade System

Cascade systems have been modeled in many theoretical studies but there are fewer sources for laboratory- or field-measured COP values. Dapoza and Fernández-Seara (2011) tested a prototype of an ammonia-carbon dioxide cascade system for freezing processes. In this study, a range of evaporating temperatures between -50°C to -35°C were tested, with a range of CO_2 condensing (inter-stage) temperatures and a 30°C condensing temperature with 5°C of subcooling. These results are shown in Figure 17.

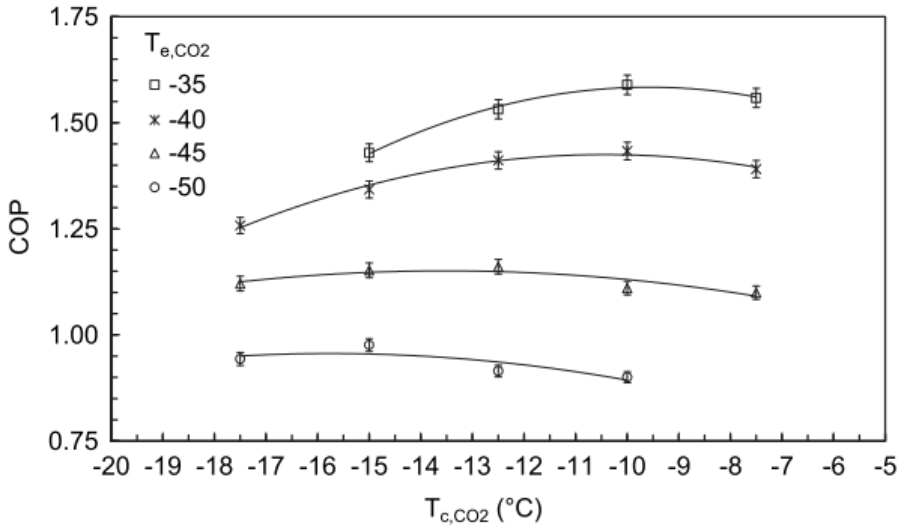

Figure 17 COP vs CO_2 Condensing Temperature for a Range of Evaporator Temperatures, at 30°C High-Side Condensing Temperature, for a NH_3/CO_2 Cascade System (Dapdoza and Fernández-Seara 2011)

Bingming et al. (2009) presented a laboratory test of a NH_3/CO_2 system and compared the results with experimental results for a two-stage, ammonia-only system, as well as a single-stage ammonia system and a single stage ammonia system with economizer. This result, shown in Figure 18, shows similar COP to the above results,

and supports the idea that cascade systems are a good solution particularly at very low evaporating temperatures; the cascade system has the best efficiency below about -40°C.

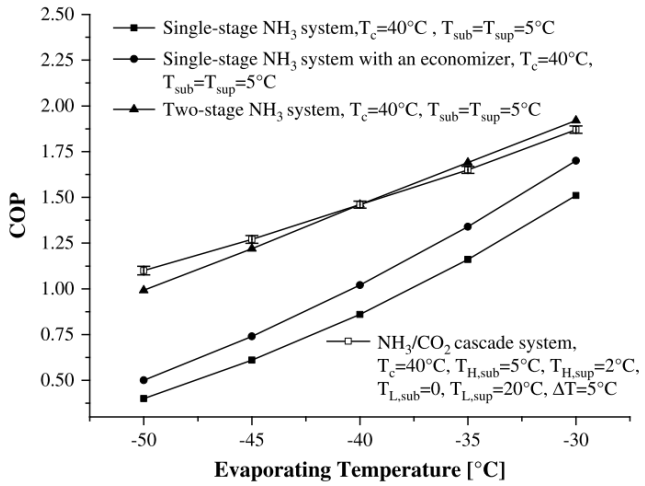

Figure 18 COP vs. Evaporating Temperature for NH_3/CO_2 Cascade System, Single Stage NH_3 System with and without Economizer, and Two-Stage NH_3 system (Bingming et al 2009)

Cascade Hybrid

A number of hybrid versions of cascade systems exist to achieve multiple evaporator levels as needed in supermarket systems. In each, the low-side refrigerant is used for low-temperature loads and has a dedicated compressor much like in a conventional cascade cycle. The medium-temperature loads may be met using the high stage fluid, the low stage fluid, or a third fluid. The first configuration shown in Figure 19 uses a pumped secondary fluid cooled by a MT evaporator in the high stage of the cascade system, where LT loads are cooled by the low stage of the cascade system. In this configuration, the high side fluid is contained to the machine room. The medium

temperature loads are cooled with a separate pumped fluid such as a brine, and the low temperature loads are cooled with the low stage of the cascade, such as subcritical CO_2. This configuration is adopted by at least one major supermarket chain in the U.S., with the primary motivation being charge reduction. The configuration is expected to have a similar or higher overall energy consumption than a simple DX system due to the lower saturated suction temperature required to cool the secondary fluid.

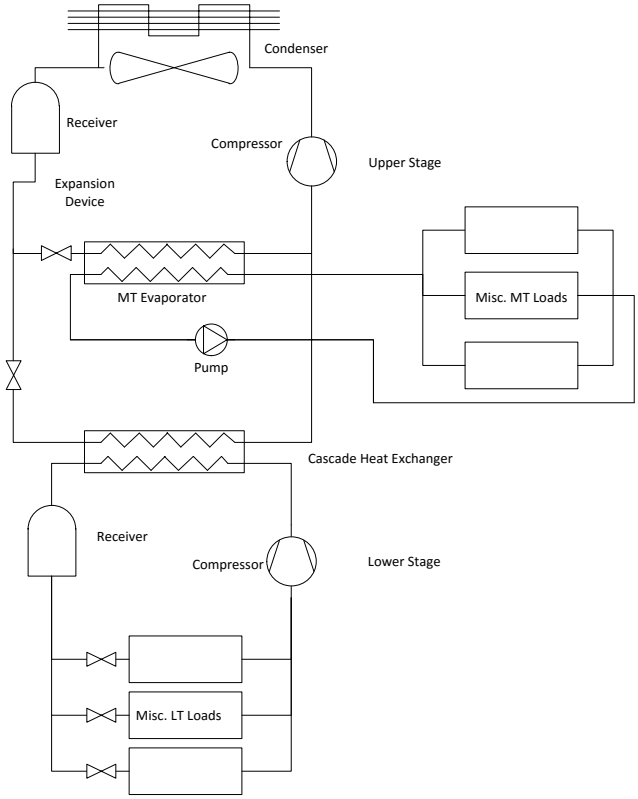

Figure 19 Hybrid Cascade with Pumped Secondary Fluid MT Loads, Cooled by High-Stage MT Evaporator, and Low-Stage Cascade LT Evaporators

Alternatively the MT loads can be satisfied using either the high-stage or low-stage refrigerant. The high-stage refrigerant may be used: in this configuration the high side

of the system resembles a multiplex configuration with the cascade heat exchanger as one of several loads in parallel. Tsamos (2016) illustrates this configurations, shown in Figure 20. This configuration is also sometimes referred to simply as a “cascade system” in the literature, particularly in the context of supermarket systems when comparing with other CO_2 refrigeration options.

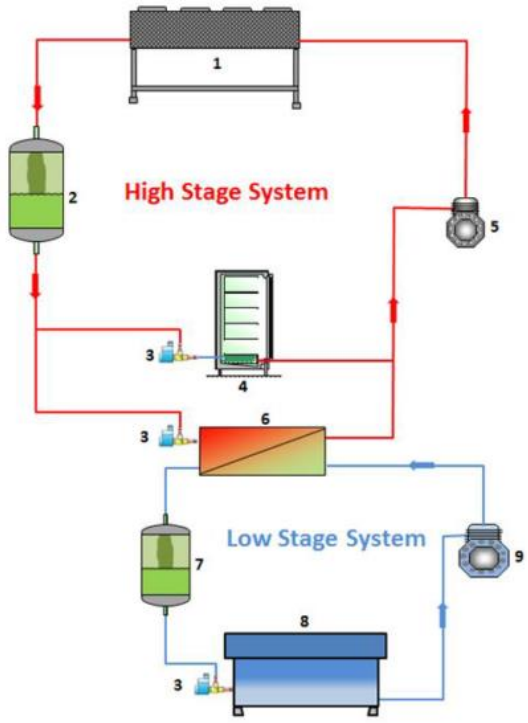

Figure 20 Hybrid Cascade with DX High-Stage MT Evaporators and Cascade Low-Stage LT Evaporators (Tsamos 2016)

In another configuration, the MT loads may be satisfied using the low-stage refrigerant. In this case, the MT loads are satisfied using pumped volatile refrigerant, and the LT loads are the evaporator of the low stage of the cascade system. Heat rejection for both stages takes place in the cascade heat exchanger. This configuration is shown in Figure 21.

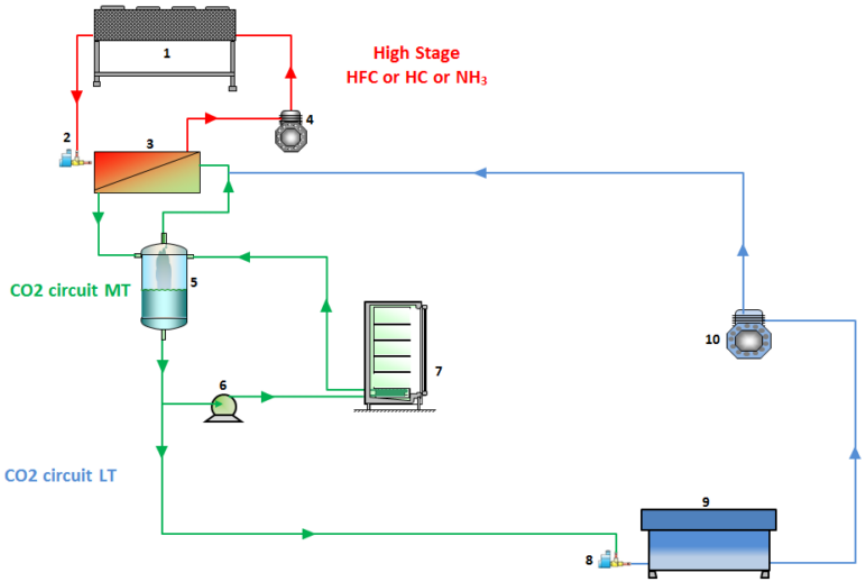

Figure 21 Hybrid Cascade with Pumped MT Evaporators Using Low-Stage Refrigerant and Cascade Low-Stage LT Evaporators (Tsamos 2016).

Laboratory and evaluation of a configuration similar to that shown in Figure 21 was performed by Cabrejas (2006). The system under test has a design load of up to 16.6 kW of MT load and 8.0 kW of LT load. The researchers report a COP of the entire system ranging from 1.4 to 2.8, under a range of load cases (from 10 kW load to 16.6 kW load on the MT stage, with full load on the LT stage – Load Ratio = 1.25 to 2.075). The test was performed with a 35°C condensing temperature, -9°C MT evaporating temperature and -36°C LT temperature.

In models comparing various CO_2 booster improvements with a baseline of a R134a-CO_2 cascade system, Gullo et al. (2016). The cascade system used as baseline uses high-stage refrigerant DX for the MT loads, like the configuration shown in Figure 20. The cascade system has a higher COP than the alternatives at high outdoor temperatures. The COP as modeled is approximately 2.05 below 15°C outdoor, 1.85

at 20°C outdoor and 1.45 at 35°C outdoor. The other configurations evaluated include a conventional booster (CB), an improved booster (IB), configurations of boosters with parallel compression (PC) and mechanical subcooling (MS) or both. The modeled load for all systems was 97 kW MT and 18 kW LT (Load Ratio = 5.39).

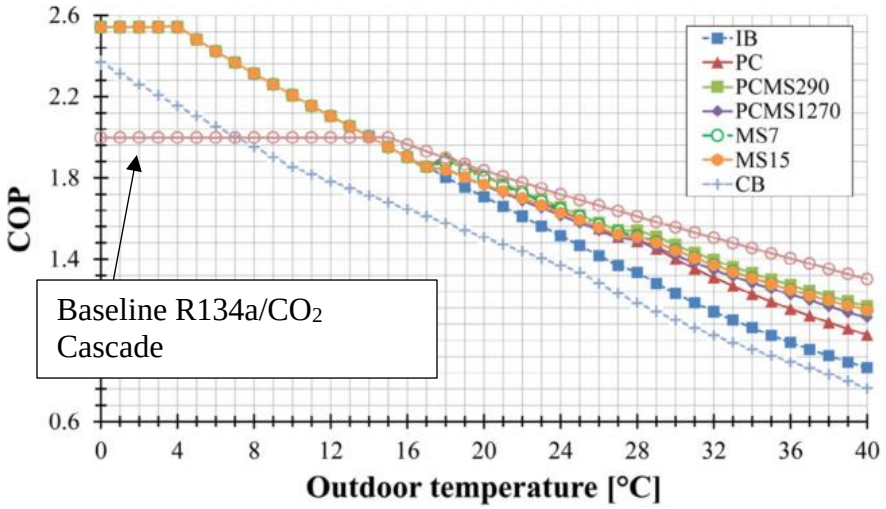

Figure 22 COP vs. Outdoor Temperature of a R134a-CO_2 Cascade Supermarket System Compared with Various CO_2-Only Refrigeration Configurations (-10°C MT and -35°C LT) (Gullo et al. 2016)

Summary

The systems described above are summarized here with a simple CO_2 booster system as a basis of comparison.

- Baseline CO_2 Booster
    - Summary Description: The booster cycle is a two-stage integrated supermarket refrigeration system providing MT and LT loads. The LT compressor stage discharges to the suction level of the MT compressors; a

flash tank is maintained at an intermediate pressure. The system operates as subcritical or transcritical depending on outdoor temperature.

  - Strengths: CO_2 is the only refrigerant, with GWP of 1.0, 0.0 ODP and an A1 safety designation.
  - Weaknesses: Efficiency is worse than alternatives in transcrtical operation unless cycle enhancements are included.

- Remote/Packaged Condensing Units
  - Summary Description: Very common packaged refrigeration systems applied in commercial and industrial refrigeration, packaged condensing units are generally applied with one or a small number of evaporators connected to each condensing unit. They are especially common in small food retail applications such as convenience stores.
  - Strengths: Simple and low cost, flexible, refrigerant charge may be kept relatively low with close proximity to load.
  - Weaknesses: Generally less efficient than alternatives; refrigerant rules may present challenges as A2, A2L, or A3 refrigerants would need to enter the occupied space.
- Multiplex DX and Multiplex with Pumped Secondary
  - Summary Description: Multiplex refrigeration systems are the most common supermarket refrigeration equipment configuration, comprising central machine-room systems with distributed, DX evaporators throughout the facility.
  - Strengths: Centralized design allows for integration of efficiency improvement measures such as subcooling.

    - Weaknesses: Large refrigerant charge, long distribution lines are prone to leaking; refrigerant rules present challenges with A2, A2L or A3 refrigerants. This problem is reduced in pumped secondary systems, but those have an associated efficiency penalty.

- Cascade
    - Summary Description: Uses two vapor compression systems connected via a common heat exchanger, acting as an evaporator in the high stage, and a condenser in the low stage.
    - Strengths: Offers improved efficiency in some cases, particularly with large temperature differences; charge of high-side refrigerant can be relatively small and contained enabling many options; if CO_2 is the low-stage refrigerant it may be maintained in subcritical operation.
    - Weaknesses: Added cost and complexity; efficiency can be lower than alternatives particularly in small temperature lift conditions. Does not provide multiple evaporator stages for supermarket style installations.
- Cascade Hybrid
    - Summary Description: Variants on cascade systems which add parallel evaporators, pumped refrigerant or pumped brine to cool additional end-use loads.
    - Strengths: Similar benefits to cascade, but able to provide multiple evaporating stages to fit supermarket or other configurations.
    - Weaknesses: Similar weaknesses to cascade, though overcomes the inability to provide multiple evaporating stages.

Subcooling Approaches

Subcooling in this context refers to an auxiliary cooling effect that is provided to the refrigerant on the liquid side of the cycle. Subcooling can be provided in a number of different ways and may be applied at different points of the cycle. The subcooling effect may be supplied from elsewhere within the same refrigeration cycle, from a separate cycle, from a dedicated piece of equipment, or from some other external source. Qureshi et al. (2013) discussed the following categories: ambient subcooling, subcooling with liquid-suction heat exchanger, subcooling with external heat exchanger, and mechanical subcooling. Ambient subcooling, which entails adding heat transfer area to achieve subcooled liquid temperatures lower than the typical "design" range, is not covered here. The term "mechanical subcooling" needs special consideration: it may refer to an integrated subcooling loop within the cycle, or a separate dedicated piece of equipment. An additional category should be considered, which is subcooling between systems, which is included in this section.

Liquid-Suction Heat Exchange

Liquid-suction heat exchangers, sometimes referred to as suction line heat exchangers or SLHX, transfer heat between the liquid leaving the condenser and the refrigerant leaving the evaporator. The heat exchanger can provide two benefits: first, providing superheat to the suction line, ensuring no liquid reaching the compressor; and second, subcooling the liquid line, reducing flash gas. In an idealized system this means lower-quality refrigerant entering the evaporator, and maximum evaporator surface exposed to two-phase refrigerant. The benefits of SLHXs have been documented, and vary with the refrigerant type as shown by Klein et al. (2000). Klein et al. showed

that, once the effects of pressure drop in the SLHX and minor changes to mass flow rate accompanying pressure drop are accounted for, the capacity of a simple cycle may improve by up to about 20% or drop by up to about 5% for different refrigerants. The researchers observed that the change in the suction conditions of the refrigerant (higher temperature and lower pressure) caused by the SLHX changes the suction density and, in a fixed-speed compressor, reduces mass flow rate. This change in mass flow reduces the COP below the value that would be calculated using ideal assumptions, and while there is still a benefit for most refrigerants, in a few cases it can lead to reduced COP. The benefit found in the study was greatest with R404A and R507A, and the penalty existed for R717 (ammonia), R32 and R22. The other refrigerants evaluated had smaller benefits. A simple schematic of a suction line heat exchanger configuration is shown in Figure 23.

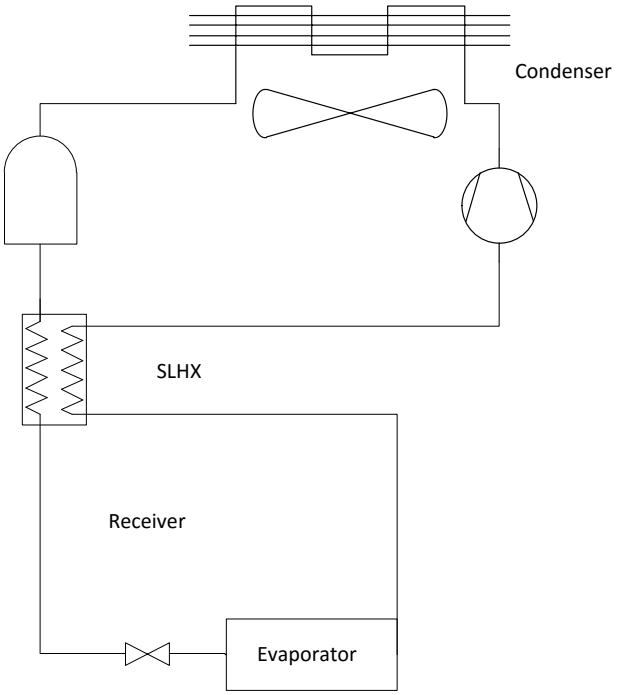

Figure 23 Shematic Showing Suction Line Heat Exchanger

Subcooling Between Systems

Subcooling may be provided between two pieces of equipment operating in parallel. In a refrigeration application, one common approach is using the MT refrigeration system to provide subcooling for the LT refrigeration system. An additional evaporator is added to the MT system, which is connected to the LT system's liquid line. The reason that the MT system is used to provide subcooling is that the MT system will have higher cycle COP, assuming both cycles operate with the same heat rejection temperature. The subcooler in effect adds capacity to the LT evaporators, by increasing the workload of the MT system. The added LT capacity is provided at the COP of the MT system. This improves the combined COP. Figure 24 is a schematic of two simple systems connected by a subcooler. The subcooler is essentially a

parallel evaporator in the MT rack, on the left. In the LT cycle, the subcooler produces lower-quality refrigerant at the inlet to the LT evaporators.

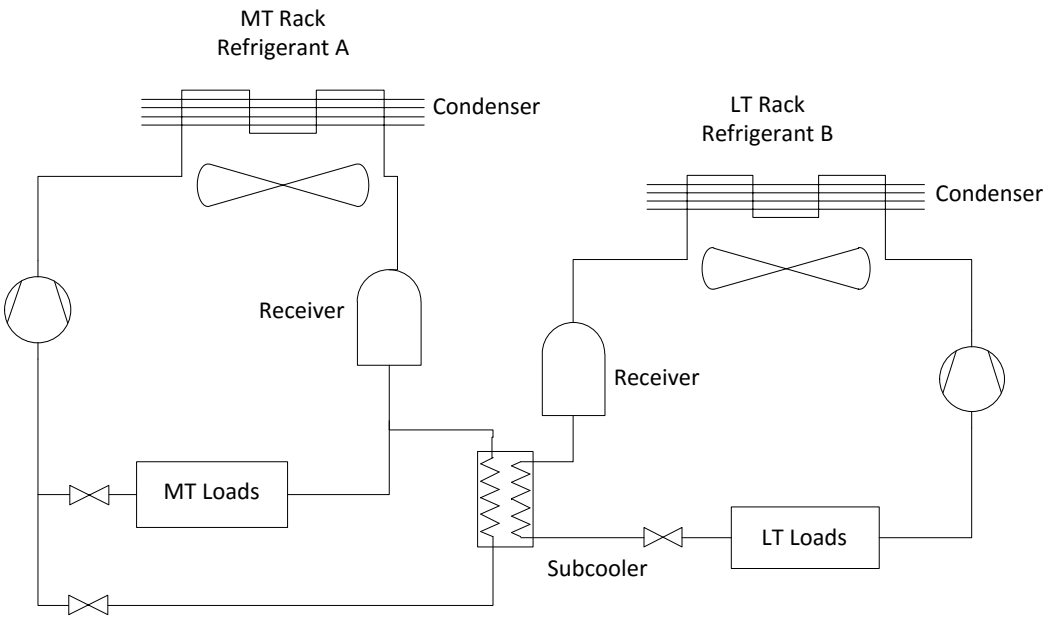

Figure 24 Schematic Showing Subcooling Between Systems

It is of interest to study the impact of subcooling on overall COP, as it varies with subcooling capacity, medium- and low-temperature loading, and weather changes. In general these terms can be defined as follows for a simple system without subcooling. For a given individual evaporator,

$$Q_{hx} = \dot{m}_{refrigerant} * (h_{refrig.out} - h_{refrig.in})$$

And for a given stage of refrigeration, for example the MT stage:

$$Q_{MT} = \sum_{MT\ Evaps.} Q_{hx}$$

With no subcooling, the total capacity of a two-stage supermarket system with LT and MT stages is described by:

$$Q_{tot} = Q_{LT} + Q_{MT}$$

And power is calculated as:

$$P_{tot} = P_{LT} + P_{MT} + P_{Anc.} = \frac{Q_{LT}}{COP_{LT}} + \frac{Q_{MT}}{COP_{MT}} + P_{Fans} + P_{Pumps} + P_{Electronics} + \cdots$$

Where $P_{Anc.}$ is the power of all the required ancillary power in the system: condenser and evaporator fans, pumps, electronics, heaters, and so on. Studies vary in whether or not ancillary power is captured in the calculated COP; often for modeling analysis, a cycle-only COP is calculated, while for field measurements the ancillary power is included in the review. COP is computed as:

$$COP_{tot} = \frac{Q_{tot}}{P_{tot}}$$

Liang and Zhang (2011) performed a study of subcooling between MT and LT refrigerating equipment, to evaluate the optimal sizing and operation of such a subcooler. This effort includes a discussion of the COP. When subcooling with a capacity Q_{SC} is added to a system, the MT system must provide both Q_{MT} and Q_{SC},

and the required work of the LT system is reduced. The total delivered capacity is the same, but may be expressed as:

$$Q_{tot} = (Q_{LT} - Q_{SC}) + (Q_{MT} + Q_{SC})$$

The new power $P_{tot,sc}$ may be re-calculated in terms of the adjusted power $P_{LT,sc}$ and $P_{MT,sc}$:

$$P_{tot,sc} = P_{LT,sc} + P_{MT,sc} = (\frac{Q_{LT} - Q_{SC}}{COP_{LT}}) + (\frac{(Q_{MT} + Q_{SC}}{COP_{MT}})$$

The COP with subcooling can then be re-written in terms of only capacity and efficiencies as:

$$COP_{tot,sc} = \frac{Q_{tot}}{P_{tot,sc}} = \frac{Q_{LT} + Q_{MT}}{\frac{Q_{LT}}{COP_{LT}} + \frac{Q_{MT}}{COP_{MT}} - \frac{Q_{SC}}{COP_{LT}} + \frac{Q_{SC}}{COP_{MT}}} \ (Liang\ and\ Zhang\ 2011)$$

The percentage of overall energy savings depends on the size ratio of the two systems and the outdoor operating temperature. Savings in the range of >20% were calculated for the best conditions. The maximum subcooling is limited by the temperature entering the MT side of the subcooler. The saving potential is greater when there is a lower ratio of MT-to-LT loads, which is shown in Figure 25.

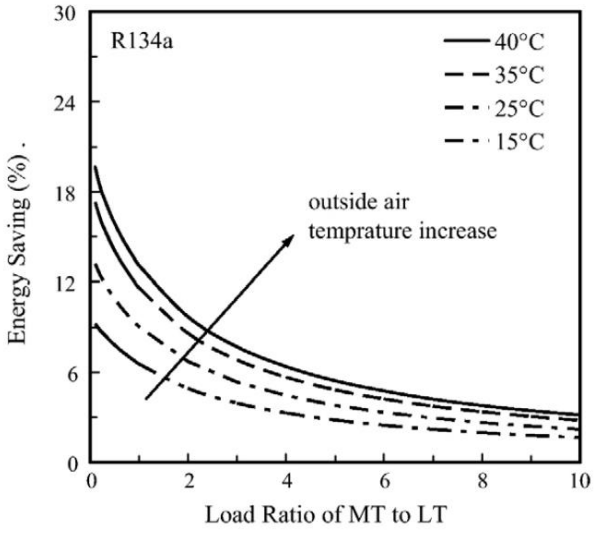

Figure 25: Energy Savings vs. Load Ratio at Varying Outdoor Air Temperature with the MT System Providing Subcooling to the LT System (Liang and Zhang 2011)

Integrated Mechanical Subcooling

Integrated mechanical subcooling refers to subcooling performed by refrigerant which is part of the same primary refrigerant circuit as the cycle being subcooled. An example configuration shown in Figure 26 has a two-stage compressor; refrigerant leaving the condenser splits into two streams, labeled A1 and A2.

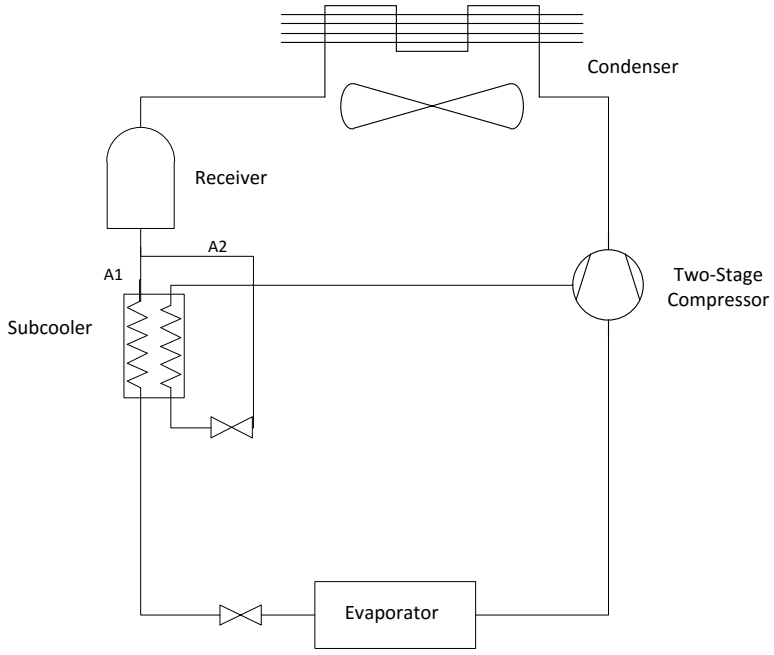

Figure 26 Integrated Mechanical Subcooler with Two-Stage Compressor

Liquid in A1 flows through the high-pressure side of the subcooler and then to the expansion valve and the evaporators as normal. Liquid in A2 is throttled to an intermediate pressure and flows to the low-pressure side of the subcooler, evaporating and providing subcooling to A1. The evaporated intermediate-pressure refrigerant then goes to the suction of the second stage of compression. In this way the subcooler acts as an intermediate stage of the cycle. This may have an added benefit of cooling the compressor inlet at the second stage.

The capacity of this cycle with internal subcooling may be defined as:

$$Q_{tot} = Q_{primary} + Q_{SC}$$

Where $Q_{primary}$ is the capacity that would be delivered if only ambient subcooling was present, and Q_{SC} is the additional capacity from subcooling. The total power includes

the power of the first stage is that required to compress the gas leaving the evaporator (stream A1 from Figure 26) to the intermediate stage; the second stage compresses both the first stage discharge and the subcooler leaving vapor (stream A2 from Figure 26) to the condensing pressure.

$$P_{tot} = P_{stage1} + P_{stage2}$$

This approach as studied by Torella et al. (2009) in the laboratory. The researchers found that COP increased by over 20% across a wide range of evaporating and condensing temperatures when compared with a two-stage system with no subcooling; the benefit was greatest at higher condensing temperatures.

Another approach may be taken in which the primary compressor is a single-stage compressor, and a dedicated second compressor circulates refrigerant for subcooling. This configuration is shown in Figure 27.

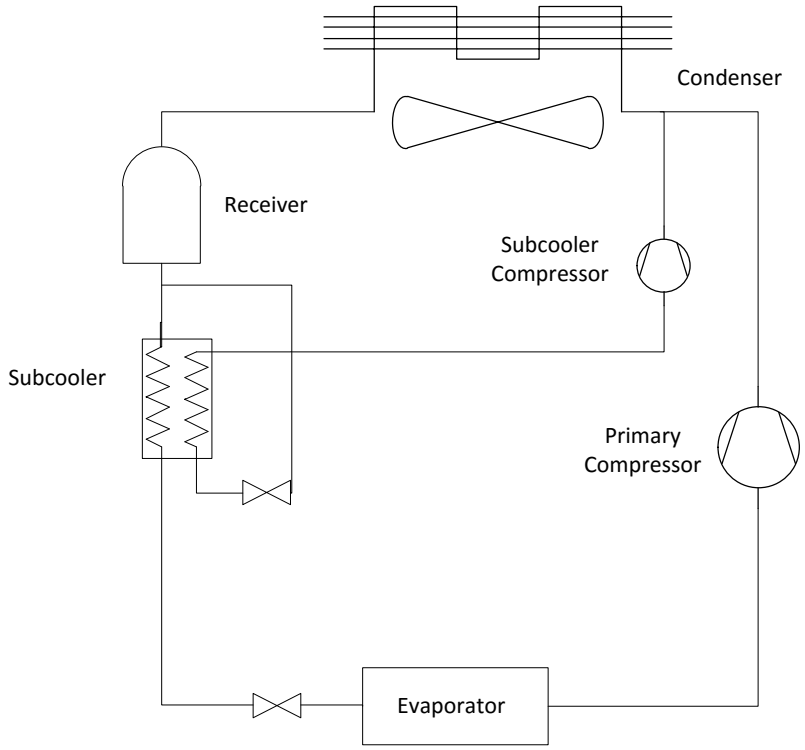

Figure 27 Integrated Mechanical Subcooler with Dedicated Subcooler Compressor

The work of Khan and Zubair (2000) analytically evaluated this configuration and showed an optimal configuration for improved COP. The optimum temperature for the subcooler evaporator to operate was found to be about halfway between the condensation and evaporation temperatures of the cycle for most conditions. The researchers analytically found an improved COP of approximately 25% at the best inter-stage pressure setting.

In this case the capacity is the same:

$$Q_{tot} = Q_{primary} + Q_{SC}$$

While the power is simply the sum of the power of the two compressors.

$$P_{tot} = P_{primary} + P_{SC}$$

The two approaches are shown on a pressure-enthalpy diagram in Figure 28.

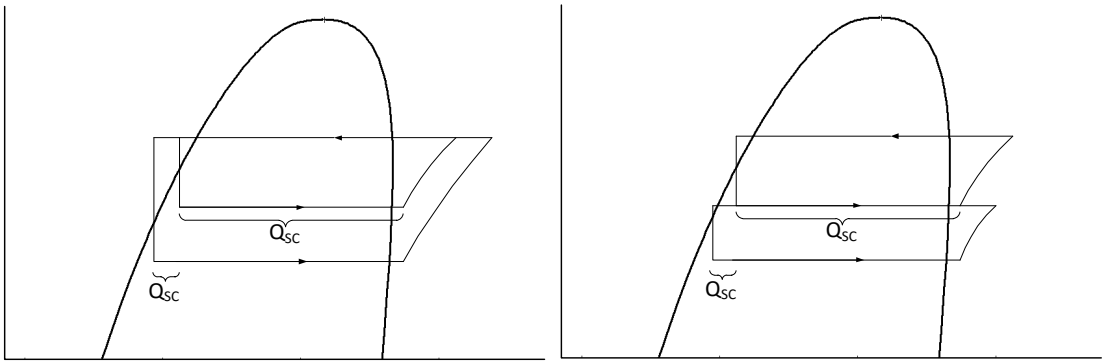

Figure 28 Pressure Enthalpy Diagrams of Integrated Mechanical Subcooling with Dedicated Compressor (left) and Two-Stage Compressor (right)

Dedicated Mechanical Subcooling

Dedicated mechanical subcooling is similar to subcooling between systems as described above, except that the subcooling is provided by a dedicated piece of equipment which does not perform another function. In the case of dedicated mechanical subcooling, a stand-alone system like a small chiller is applied to the liquid line of the larger refrigeration system.

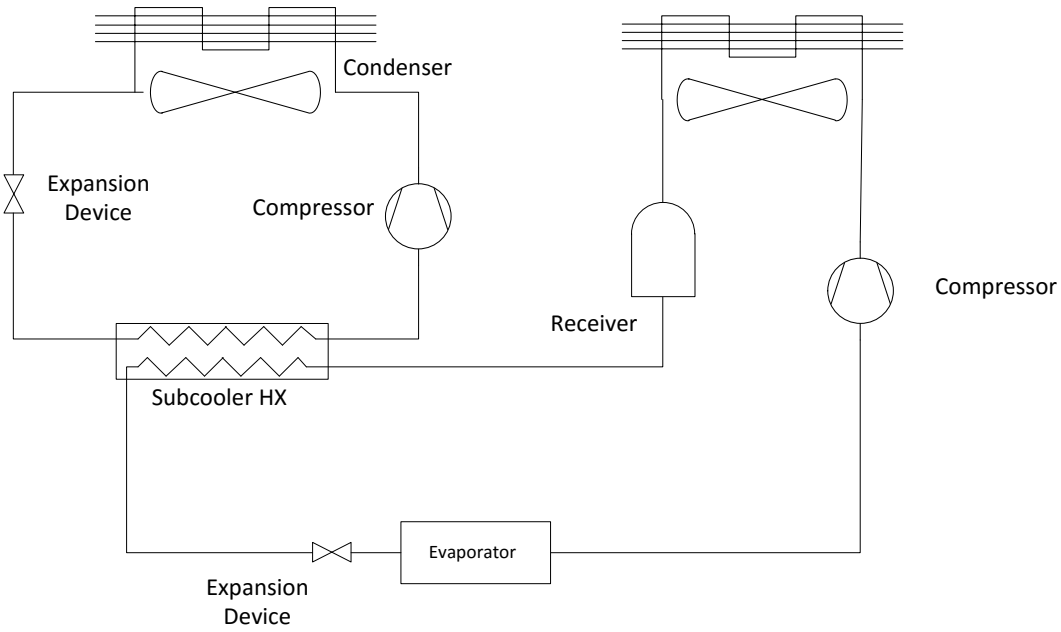

Figure 29 Schematic of Dedicated Mechanical Subcooler System

In the case of dedicated mechanical subcooling in a system with a single evaporator stage, the capacity of the total cycle is the capacity of the primary cycle without subcooling, plus the subcooling capacity:

$$Q_{tot} = Q_{primary} + Q_{SC}$$

The power of the total cycle is the sum of the primary system power plus the subcooler power:

$$P_{tot} = P_{primary} + P_{SC} = \frac{Q_{primary}}{COP_{primary}} + \frac{Q_{SC}}{COP_{SC}}$$

And the COP of the total system is

$$COP_{tot} = \frac{Q_{tot}}{P_{tot}} = \frac{Q_{primary} + Q_{SC}}{\frac{Q_{primary}}{COP_{primary}} + \frac{Q_{SC}}{COP_{SC}}}$$

Like the case of subcooling between systems, the dedicated mechanical subcooling provides an overall efficiency boost because the subcooler operates at a higher COP

than the primary cycle, adding capacity to the primary cycle at a higher efficiency. The benefits of the subcooler increase with increasing capacity, but with diminishing benefit: as the subcooler provides lower temperatures, its own COP decreases.

Subcooling with External Heat Exchanger

Subcooling may also be achieved using a heat exchanger to another external heat sink. This could be an evaporative-cooled coil, a groundwater loop, or as will be examined later in this effort, a thermal storage media. The concept is much the same as the dedicated mechanical subcooling approach and the performance may be described by:

$$Q_{tot} = Q_{primary} + Q_{SC}$$

$$P_{tot} = P_{primary} + P_{SC}$$

$$COP_{tot} = \frac{Q_{tot}}{P_{tot}} = \frac{Q_{primary} + Q_{SC}}{\frac{Q_{primary}}{COP_{primary}} + P_{SC}}$$

The power of the subcooling system depends on what is being used for subcooling. In the case of applying thermal storage, the energy consumption to provide the subcooling capacity may be offset in time from when the capacity is delivered to the primary cycle; in this case it is necessary to consider performance either in terms of cumulative energy or at relevant instantaneous times. The following discussion considers a storage media that is charged by a dedicated vapor compression system.

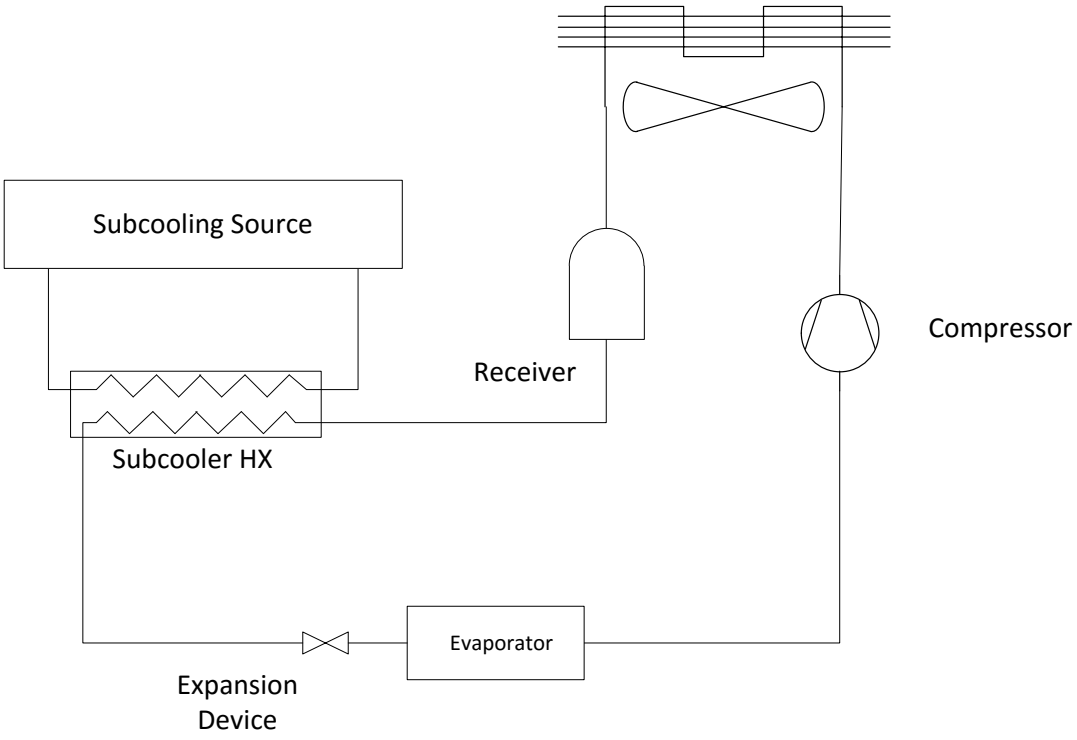

Figure 30 Schematic of Subcooling with an Unspecified Auxiliary Source of Subcooling

To consider the instantaneous COP, one must consider that the capacity during charging is the capacity of the primary cycle but the power includes the charging of the storage media:

$$Q_{tot,charging} = Q_{primary}$$

$$P_{tot,charging} = P_{primary} + P_{SC}$$

$$COP_{tot,charging} = \frac{Q_{tot,charging}}{P_{tot,charging}} = \frac{Q_{primary}}{P_{primary} + P_{SC}}$$

Clearly the COP is lower during this period than a baseline system alone. However during discharge the capacity is increased while the power is not.

$$Q_{tot,discharging} = Q_{primary} + Q_{sc}$$

$$P_{tot,discharging} = P_{primary}$$

$$COP_{tot,charging} = \frac{Q_{tot,discharging}}{P_{tot,discharging}} = \frac{Q_{primary} + Q_{sc}}{P_{primary}}$$

Here, the instantaneous efficiency is improved. Considering energy, additional factors must be considered. The efficiency of charging and discharging the storage media must be considered. Three factors are important. First is the approach temperature between the storage media and the charging/discharging refrigerants. If an approach temperature $\Delta T_{approach}$ is required between the storage media and the refrigerant in either charging or discharging operation, then the subcooler must provide charging at $2*\Delta T_{approach}$ below the eventual subcooling temperature. This reduces energy efficiency compared with providing instantaneous subcooling. The other factor to consider is the possible difference in efficiency of the subcooler between the time of charging and discharging. If charging of the subcooling media is performed at a time when the ambient temperature is significantly lower than the time when the subcooling is desired, the efficiency of the subcooler cycle will be greater and this improvement may overcome the reduced efficiency due to the reduced charging temperature. On the other hand if the ambient temperature is higher, the overall efficiency will suffer. Fortunately subcooling may be most desirable during hot outdoor temperature conditions, so charging during colder hours should often be feasible. A third consideration is the standby and parasitic losses in storage itself. The storage media may require pumps or other auxiliary power, and may be required to stand idle, incurring thermal losses between the time of charging and discharging. This must be considered as well.

Summary

The subcooling approaches detailed above are summarized here.

- Liquid-Suction Heat Exchange
    - Summary Description: Heat exchangers transferring heat between the refrigerant leaving the condenser and the refrigerant leaving the evaporator.
    - Strengths: Ensures superheat to the compressor; provides subcooling, reducing flash gas; in many cases, improves COP; simple and inexpensive compared to other measures; only requires added heat exchanger and valves
    - Weaknesses: In some cases, effects of added pressure drop can lower COP. Relatively small total benefit compared with some other approaches
    - Observed Efficiency: Improvements of up to 20% or reductions up to 5% depending on refrigerants and operating conditions
- Subcooling Between Systems
    - Summary Description: In systems operating in parallel, subcooling provided to one system with cooling provided by other system. In a supermarket, typically the MT system provides subcooling for the LT system.
    - Strengths: improves overall efficiency by shifting some work from less-efficient LT cycle to more-efficient MT cycle; only requires added heat exchanger and valves
    - Weaknesses: Diminishing benefit with higher MT-to-LT load ratio
    - Observed Efficiency: Energy savings range from up to approximately 20% in low MT-to-LT scenarios, to up to 3% in very high MT-to-LT scenarios
- Integrated Mechanical Subcooling

    - Summary Description: Using an internal circuit, some liquid refrigerant is evaporated to subcool the primary liquid-line refrigerant; secondary circuit is compressed in two-stage compression or dedicated subcooling compressor
    - Strengths: Improved efficiency; shared refrigerant circuit is less complex than dedicated mechanical subcooling with second circuit
    - Weaknesses: Added compressor or two-stage compressor needed; in the case of CO_2 in transcritical mode, subcooler circuit may have high flash gas
    - Observed Efficiency: 20-25% COP improvement
- Dedicated Mechanical Subcooling
    - Summary Description: A separate, dedicated cooling unit is used to provide subcooling to the primary refrigeration circuit
    - Strengths: Refrigerant selection or sizing not limited by primary system; improved efficiency
    - Weaknesses: More complex than other options, requires full vapor compression system aside from primary circuit
    - Observed Efficiency: 19-38% COP improvement
- Subcooling with External Heat Exchanger
    - Summary Description: A heat exchanger provides cooling via some other external heat sink
    - Strengths: Depending on heat sink, subcooling may be free, flexible, or otherwise convenient; can integrate storage
    - Weaknesses: Limited to available heat sink options
    - Observed Efficiency: Depends on external resource

Chapter Summary

This chapter summarizes the system configurations that may be considered in commercial refrigeration applications along with the CO_2 booster cycle, which is the primary focus of this dissertation. In some cases, such as with small, packaged remote condenser equipment, the restrictions of the application may dictate selection of one over the other. In other cases, such as hybrid cascade applications, energy analysis for a particular design and climate, along with equipment and utility costs, may be needed to determine the best option. Large multiplex systems face legislative challenges around usage of high-GWP refrigerants, and safety concerns associated with implementing low-GWP refrigerants into these systems may push declining use in new systems.

Subcooling options are also discussed in this chapter. Subcooling systems can be used to improve capacity and/or efficiency in many cases. The simplest approach, liquid-suction heat exchange, provides increased capacity and efficiency in many cases. In applications with separate MT and LT systems, an overall benefit can be seen by providing subcooling to the LT stage using the MT system. In more complex approaches, integrated or dedicated mechanical subcooling systems can provide large COP improvements, at the expense of added equipment and complexity. An intriguing possibility is the use of other external sources, such as cold thermal energy storage media, to provide subcooling with added flexibility.

Chapter 3: Laboratory Testing and Steady State Performance

This chapter describes laboratory testing of a CO_2 transcritical booster refrigeration system with and without dedicated mechanical subcooling. The system was constructed by a refrigeration system manufacturer, as a laboratory-scale version of a supermarket-style configuration. Steady-state testing was performed to map performance with and without the dedicated subcooler to quantify the performance improvement using the subcooler. Further, transient tests were performed to capture "load-shed" behavior of the transcritical booster system. The objectives of the work detailed in this chapter are to:

- Provide new, detailed, laboratory evaluation of a complete CO_2 booster system with and without subcooling
- Quantify the benefits of the dedicated mechanical subcooler and its impact on the overall cycle behavior
- Provide a basis for modeling systems under simulated, realistic loading and weather conditions

Overview

For the laboratory testing portion of this effort a transcritical booster refrigeration rack with dedicated mechanical subcooling was procured from a manufacturer, Systems LMP. The configuration of the test rack is shown in Figure 31. The system under test has a variable-speed MT compressor with a nominal capacity of 17.6 kW and a single-speed LT compressor with a nominal capacity of 6.8 kW. Two plate heat exchangers serve as the LT and MT evaporators. Water-glycol is used as the heat transfer fluid, and is pumped by

250-watt pumps. The mechanical subcooler, using R134a refrigerant, has a nominal compressor capacity of 8.1 kW and also has a plate heat exchanger evaporator. A condenser/gas cooler with a two-speed fan was installed in a psychrometric chamber to simulate the outdoor environment; the control of this condenser was to switch to low speed below approximately 290K outdoor temperature. The subcooler provides cooling to a water-glycol circuit which in turn cooled the R744 leaving the condenser/gas cooler; this configuration was selected by the manufacturer for stability with the relatively small laboratory test rack. The pump for this subcooling circuit was a 250-watt model.

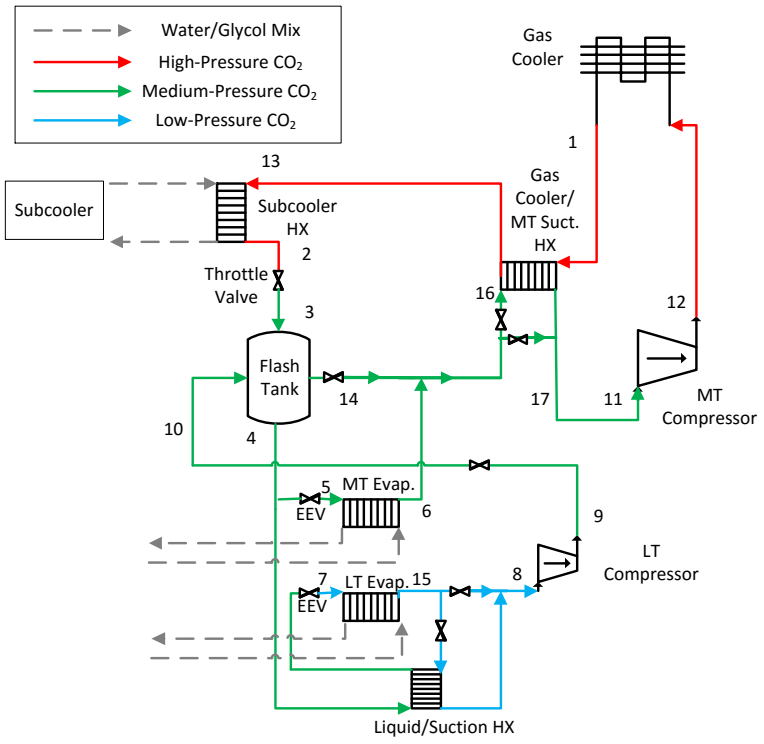

Figure 31: System Schematic

To characterize performance of the system, laboratory tests were performed with imposed load to capture capacity and efficiency. The gas cooler/condenser was installed in a psychrometric chamber and the water/glycol tanks were heated with electric resistance heaters

to provide load. The rack and the mechanical subcooler were located in a conditioned laboratory space which was typically 293K to 297K.

Figure 32 Transcritical Booster Rack During Installation

Figure 33 Transcritical Booster Rack During Installation

Figure 34 Refrigeration System and Glycol Tanks during System Installation Process

Figure 35 Condenser/Gas Cooler during Installation

The instrumentation for the laboratory test is described in Table 4. Discharge temperature from the MT compressor (point #12 on Figure 31) was not captured, so an isentropic efficiency estimate was used based on manufacturer software calculations for each condition. The uncertainty of the calculated test results was calculated for each test point using the uncertainty propogation methods in Engineering Equation Solver (EES), which uses the method described in a NIST technical note (Taylor and Kuyatt, 1994). The refrigerating capacity of each evaporator had uncertainty ≤0.6%; the uncertainty of the calculated LT compressor power was ≤2.7%, and for the MT compressor was 2.4-5.3%, with the larger uncertainty in the lower discharge pressure conditions. The uncertainty of the COP was 2.3-4.3% with a large portion of the uncertainty owing to the compressor power uncertainty.

Table 4 Instrumentation for the Laboratory Test			
Reading	Description	Location(s)	Accuracy
Pressure	Refrigerant Pressure - high pressure	Points 1, 12	+/- 0.11% FS – Nominal pressure range: 0-13.79 MPa
Pressure	Refrigerant Pressure - normal pressure	Points 4,5,7,9,11	+/- 0.11% FS - Nominal pressure range 3.45 MPa
Temperature	Thermocouples: Type T	(all indicated points)	+/- 1K
Flow	Refrigerant Mass Flow	Points 6 ,8,11	liquid +/- 0.10% reading; gas +/-0.25% reading
Flow	Water/Glycol Flow	(each glycol loop)	+/- 1% reading
Air Temperature/ Humidity	Air Temperature/Humidity	Gas cooler inlet, rack ambient	Temp.: +/- 0.2K at 293K Humidity: +/- 1 + 0.008*reading %RH
Power	Rack Power, Gas Cooler Power		Power: 0.2% reading
Power	Subcooler Power		Power: 0.5% reading

Using the data gathered above, key quantities are calculated. Refrigerant enthalpies are calculated using NIST's REFPROP version 9.1 (Lemmon et al. 2013). Refrigerant capacity in each evaporator is calculated using

$$Q = m * (h_{out} - h_{in}) \quad (1)$$

While compressor work is calculated similarly as

$$W = m * (h_{out} - h_{in}) \quad (2)$$

The COP of the system is the sum of capacities divided by the sum of work inputs, described below

$$COP = \sum Q / \sum W \quad (3)$$

The COP is presented here using refrigerant-side measurements.

Steady State Result Summary

Tests were done in both transcritical and subcritical operating modes, with and without the subcooler running. Eleven test points are examined and also simulated. Figure 36 shows the results of Test #1 on a pressure-enthalpy diagram, with the most relevant state points indicated using the number scheme from Figure 31. Table 5 shows the results for the tests, calculated from the refrigerant side. The subcooler power in Table 5 is estimated since full refrigerant-side capacity measurements were not taken on the subcooler cycle. Test #1 will be used as an example for describing the cycle behavior.

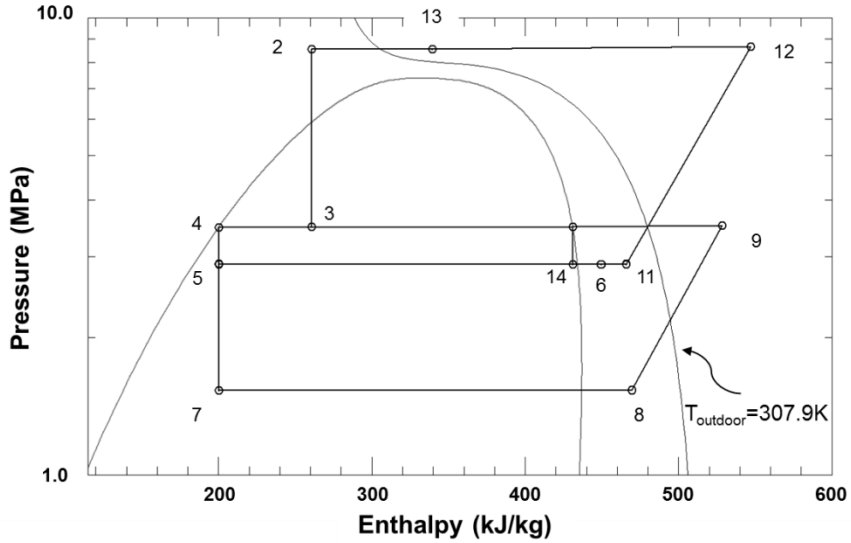

Figure 36: Pressure-Enthalpy Diagram for R744 Booster Cycle Laboratory Test Results with 307.9 K Outdoor, with Point Numbers from Figure 31 Indicated

For this test the ambient temperature of the outdoor chamber was 307.9 K. The effect of the subcooler can be seen on the high-pressure line here: the temperature entering the subcooler (Point 13) was 310.6K, 2.7K above ambient. The refrigerant temperature leaving the subcooler (Point 2) was 298.0 K. This significantly impacts the refrigerant quality entering the flash tank:

with isenthalpic expansion from the high pressure state at 310.6K to the flash tank pressure of 3.49 MPa, the refrigerant quality would have been 0.61. With the subcooler, the actual refrigerant quality to the flash tank was 0.27.

Table 5: Summary of Test Results Including Refrigerant-Side Capacity and Power and COP

Test	Outdoor Air Temp.	Discharge Pressure	MT Compressor Power	LT Compressor Power	Subcooler Power*	Total Power	MT Comp. Mass Flow
-	K	MPa	kW	kW	kW	kW	kg/s
1	307.9	8.66	6.66	1.54	1.17	9.37	0.0889
2	312.3	8.69	7.71	1.5	1.17	10.38	0.1058
3	302.1	8.43	5.92	1.54	1.17	8.63	0.0792
4	297	7.17	6.23	1.55	1.17	8.95	0.1056
5	280.9	5.12	2.99	1.54	1.17	5.7	0.0788
6	289.1	6.04	5.26	1.51	1.17	7.94	0.1143
7 (no sub)	296.2	7.00	7.13	1.54	0	8.67	0.1484
8 (no sub)	281.2	5.41	5.14	1.49	0	6.62	0.1424
9 (no sub)	308	8.75	8.68	1.51	0	10.19	0.1247
10 (no sub)	302.1	8.62	7.81	1.51	0	9.32	0.1091
11 (no sub)	289.3	6.14	6.12	1.45	0	7.58	0.1365
Test	MT Evap. Mass Flow	LT Evap. Mass Flow	MT Bypass	MT Capacity	LT Capacity	Total Capacity	COP
-	kg/s	kg/s	%	kW	kW	kW	-
1	0.0313	0.0263	65	7.81	7.03	14.84	1.58
2	0.0264	0.0228	75	6.56	6.15	12.72	1.23
3	0.0389	0.0279	51	9.72	7.42	17.14	1.99
4	0.0331	0.0294	69	8.18	7.67	15.84	1.77
5	0.0319	0.0238	60	7.97	6.43	14.4	2.53
6	0.0239	0.0237	79	5.93	6.39	12.32	1.55
7 (no sub)	0.0081	0.0269	95	1.97	7.07	9.04	1.04
8 (no sub)	0.0159	0.0234	89	3.91	6.25	10.16	1.53
9 (no sub)	0.0086	0.0269	93	2.13	7.09	9.22	0.9
10 (no sub)	0.0275	0.0265	75	6.8	7.06	13.85	1.49
11 (no sub)	0.0047	0.0229	97	1.16	6.15	7.30	0.96

This reduction in flash gas has significant implications for efficiency of the cycle. The flash tank requires sufficient liquid refrigerant returning from the condenser/gas cooler to balance the leaving liquid to the evaporators. Absent a subcooler, this balance would require additional flow to the condenser/gas cooler, requiring an increased flow through the MT compressor (and/or a reduction in the capacity delivered to the evaporators). Tests 1-7 in Table 5 are those with the mechanical subcooler active; Tests 7-11 are without subcooling.

Discussion of Results

Comparing test points with similar outdoor temperatures, the capacity and COP are both considerably higher in tests with the subcooler, and this is true in both the transcritical and subcritical test conditions. The COP improves in part because the subcooler itself operates at a comparatively efficient state: the subcooler removes heat from the gas cooler/condenser leaving refrigerant (which is a few degrees above outdoor temperature) and rejects heat to the laboratory space, in the range of 293K-297K. The most substantial difference may be seen in the MT capacity and the refrigerant bypass percentage, which will be addressed later. The bypass flow is also shown in Table 5, and is computed as:

$$m_{bypass} = m_{MT\ comp.} - m_{MT\ evap.} \quad (4)$$

$$\text{MTBypass}(\%) = \frac{\dot{m}_{\text{bypass}}}{\dot{m}_{\text{MTcomp.}}} * 100\% \quad MT\ Bypass\ (\%) = (m_{bypass} / m_{MT\ comp.}) * 100\% \quad (5)$$

Comparing two tests in which the outdoor temperature setting was the same, one with and one without the subcooler, helps clarify the impact the subcooler has on the overall performance. In particular, with transcritical tests the difference is pronounced and can be seen

since all high-side enthalpy points are known from measurement data. Figure 37 shows test results for the nominal 308K test point with and without subcooling. The blue cycle represents the without-subcooling test (Test #9), while the black cycle shows the with-subcooling test (Test #1). The outdoor temperature isothermal line is also plotted. The most important difference is the gas cooler leaving state. In Test #9, the temperature at the outlet of the gas cooler is 311.3K. In Test #1, the temperature leaving the gas cooler is 310.6K and leaving the subcooler, the temperature is 298.0K. This is particularly important considering the refrigerant quality entering the flash tank: at 3.50 MPa, the refrigerant quality entering the flash tank is 0.27 in Test #1 and 0.65 in Test #9. For the system to operate in a steady condition, the amount of liquid returning to the flash tank has to balance the liquid sent to the evaporators. The benefit of the subcooler is providing a higher percentage of liquid to the flash tank, allowing a lower overall flow-rate in the MT compressor and through the gas cooler/condenser, reducing compressor work and increasing efficiency.

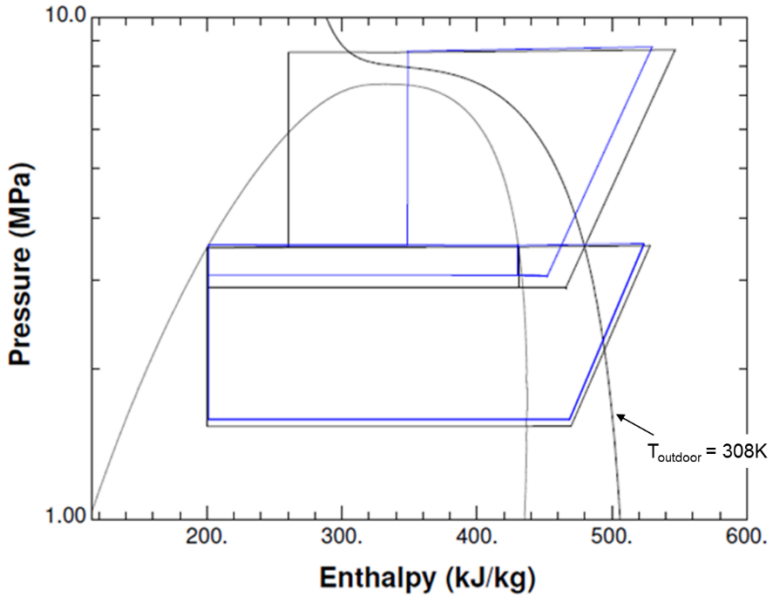

Figure 37 Test Results for Nominal 308K Test Condition with and without Mechanical Subcooler

Figure 38 shows the pressure at different stages of the cycle, plotted against outdoor temperature. The discharge pressure of the MT compressor (Point #12) increases roughly linearly with outdoor temperature until the 302K test points, where the pressure is held roughly constant.

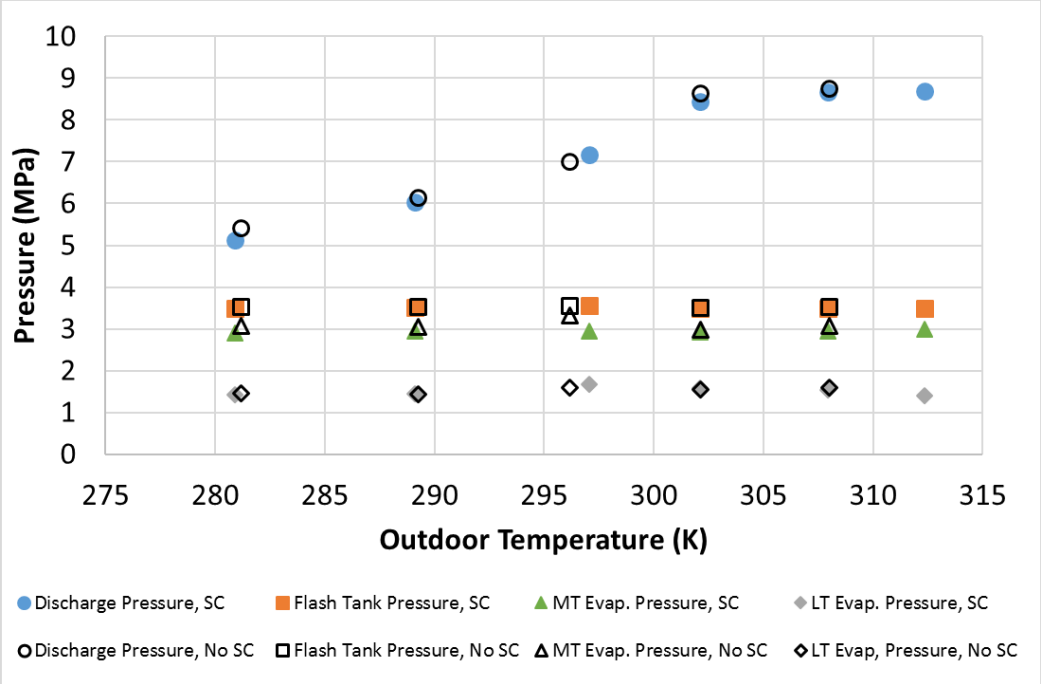

Figure 38 Pressure of Cycle Points vs. Outdoor Yemperature with and without Mechanical Subcooler

Table 6: Refrigerant Pressure at Different Cycle Points					
Test	Outdoor Air Temp.	Discharge Pressure	Flash Tank Pressure	MT Evap. Pressure	LT Evap. Pressure
-	K	MPa	MPa	MPa	MPa
1	307.94	8.66	3.49	2.94	1.54
2	312.34	8.69	3.50	2.98	1.40
3	302.13	8.43	3.48	2.92	1.59
4	297.04	7.17	3.56	2.94	1.68
5	280.88	5.12	3.48	2.90	1.42
6	289.09	6.04	3.50	2.95	1.44
7 (no sub)	296.16	7.00	3.55	3.31	1.59
8 (no sub)	281.20	5.41	3.53	3.06	1.46
9 (no sub)	308.00	8.75	3.52	3.08	1.58
10 (no sub)	302.12	8.62	3.50	2.98	1.56
11 (no sub)	289.28	6.14	3.52	3.04	1.44

Figure 39 shows the normalized flow rate in each evaporator and the medium temperature compressor, for the with-subcooler tests. Normalized flow is calculated for each point of interest as the ratio of the measured flow divided by the LT flow rate:

$$\dot{m}_{norm} = \dot{m} / \dot{m}_{LT} \qquad (6)$$

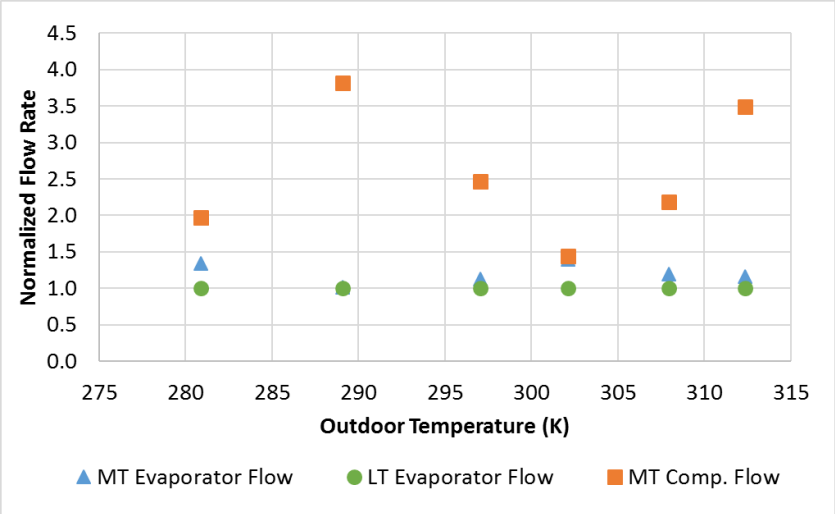

Figure 39 Normalized Mass Flow Rate for Each Evaporator and MT Compressor, with Subcooling

This graph shows bypass flow which is highest at 289K (Test #6 from Table 5) increasing from a lower bypass rate at the 281K test point (Test #5). The bypass flow then decreases with increasing outdoor temperature to the 302K test point (Test #3) and then increases again with increasing outdoor temperature. This agrees in general with the findings of Sharma et al. (2014a, 2014b), who showed a similar phenomenon through modeling; in the present testing the phenomenon is much more pronounced. However, in Sharma's model, the ratio of MT to LT loads was roughly 2:1. In the current laboratory set-up, the loading was closer to 1:1, meaning the LT loads were a substantially larger portion of the load. Since the LT load in this system is in essence isolated from the gas cooler (with the compressor discharging to the flash tank), it stands to reason that bypass flow requirements will be higher with a higher proportion of LT load than in a system with a lower LT proportion.

In order to understand the requirement for high bypass flow in some conditions, an analysis of the heat transfer within the gas cooler is considered. Since capacity of the gas cooler is not precisely measured in subcritical conditions in the experiment, the model may be used to assist in this understanding. Using the validated model calculations for heat transfer in the gas cooler, the phenomenon driving the required mass flow (and with it, overall COP) may be better observed.

Figure 40 shows the effectiveness of the GC/condenser. A finite volume HX model (Jiang et al. 2006) was used to calculate the refrigerant-side heat transfer coefficient (HTC) for the modeled gas cooler, using simplified assumptions: for each subcritical pressure, the refrigerant inlet condition was set at 27.8K superheat entering the condenser, and the air temperature set at 5.6K below the saturated refrigerant temperature. For supercritical conditions, the outdoor

temperature was set to 305.4K and the refrigerant inlet temperature set to 366.4K. Importantly, in these simplified calculations the mass flow rate was held constant, to isolate for the effect of pressure on HTC and allow for calculation of more pressures than were tested. The result is an average heat transfer coefficient for the gas cooler under conditions similar to the range of test conditions, which is also plotted in Figure 40.

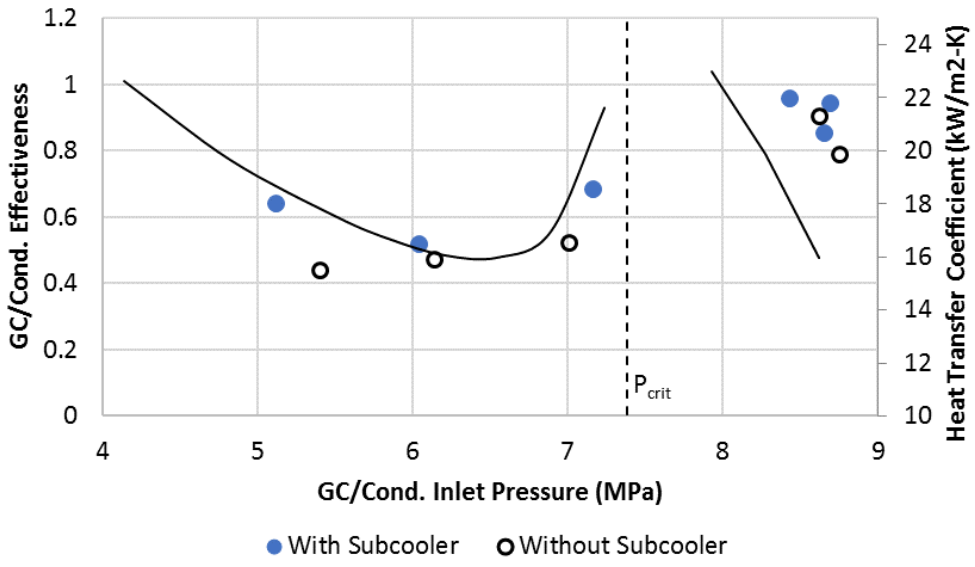

Figure 40 Gas Cooler/Condenser Effectiveness vs. Inlet Pressure; Also Shown is a Calculated Heat Transfer Coefficient for the Gas Cooler Using a Fixed Mass Flow Rate to Isolate the Effect of Pressure

The heat transfer coefficient in the gas cooler/condenser decreases with increasing pressure to a local minimum at approximately 6.5 MPa, before increasing to the critical point. This is supported by the work of Kondou and Hrnjak (2011) and Cavallini (2006) who studied heat transfer and condensation (albeit for horizontal, smooth tubes). Cavallini's correlation shows a local minimum at about 6.5 MPa for the conditions they considered, though Kondou's testing showed the minimum closer to the critical pressure. After the critical point the HTC again decreases with increasing pressure. The effectiveness of the gas cooler/condenser under test showed a corresponding trend.

Plotting COP vs. condensing pressure, the trend is also replicated as shown in Figure 41, along with COP vs. Outdoor Temperature for reference.

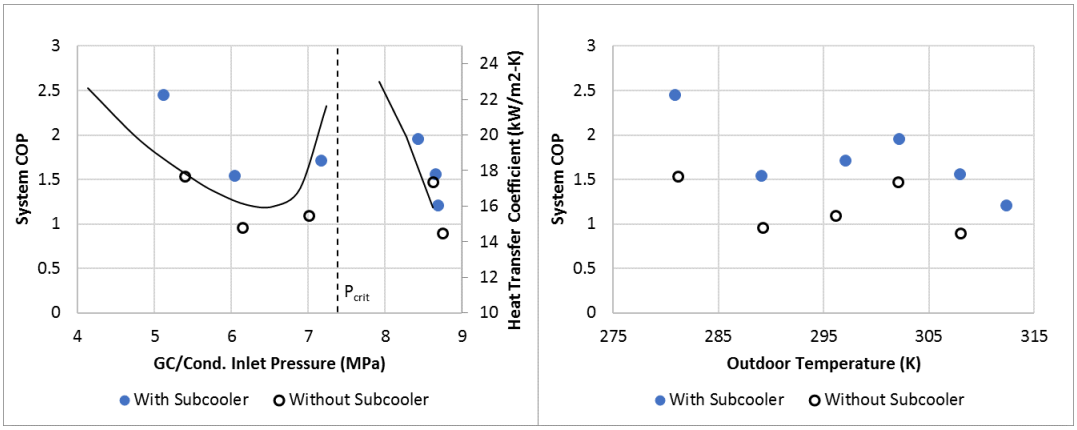

Figure 41 Gas COP vs. Inlet Pressure with Calculated Heat Transfer Coefficient for the Gas Cooler Using a Fixed Mass Flow Rate to Isolate the Effect of Pressure (left); COP vs. Outdoor Temperature (right)

This result, combined with the pressure vs. outdoor temperature shown in Figure 38 and the mass flow rate (particularly the bypass flow) in Figure 39 shows a challenge for systems operating near the critical point; the reduced condenser effectiveness combined with the booster cycle's requirement for bypass flow creates and necessitates a high proportion of bypass flow in this pressure range to satisfy the heat rejection requirements of the cycle.This phenomenon would be particularly prevalent in cycles with a high ratio of LT loading.

Considering the effect of the loading ratio, Sawalha et al. (2015) showed a method to calculate the COP of each stage, and the COP of systems with the same performance traits but different load ratios. This method calculates the efficiency of each stage by attributing some portion of the MT compressor work to removal of heat from the LT evaporators, and can be used to estimate how differently the system would perform if a larger fraction of the load were the efficient MT stage. It does not account for other system differences that would exist – for

instance, this system had a single, variable-capacity MT compressor, where in reality a larger system with a larger MT stage would most likely have multiple, staged fixed-speed MT compressors. This is also useful because in the present laboratory testing, at inefficient conditions the MT evaporator capacity decreased significantly and in the most extreme conditiosn, the load ratio was very low though though the COP of each individual stage was not particularly low; this had the effect of strongly biasing the overall COP towards the LT COP. The results of this anaylsis, shown in Table 7, show that for some of the lowest-efficiency tests, such as Tests 7, 9, and 11, the increase in efficiency if the LR had been 1.0 would have been 10-15%. Comparing the COP with LR = 3 (a more typical supermarket value) with the measured COPs, the improvement in total COP would be on the order of 13-29% depending on the test condition. Figure 42 shows the COP of each stage as measured, calculated using this method, along with the total COP. The theoretical bounds of total COP are in between the MT and LT COP, depending on the load ratio.

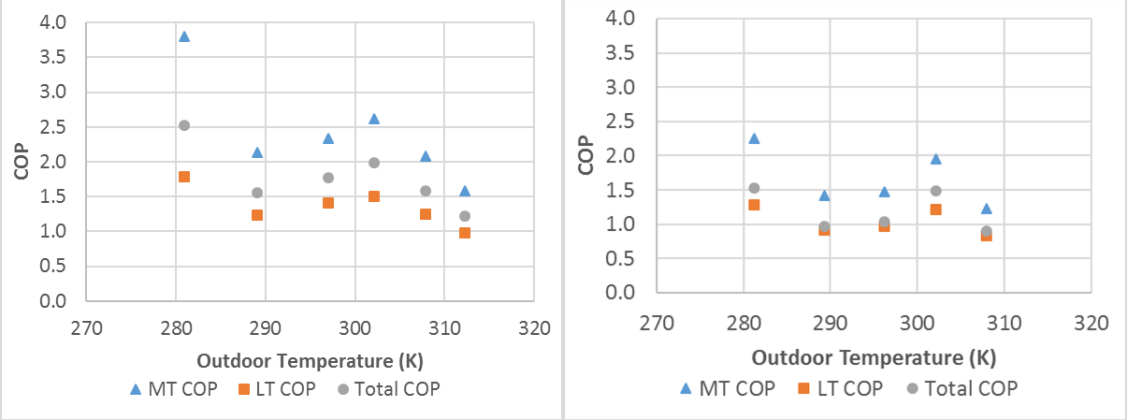

Figure 42: COP of Each Compressor Stage Calculated and Combined COP with (left) and without (right) Subcooling

Table 7: COP Calculated for Each Stage and for Different Load Ratios Using Method from Sawalha (2015)

Test	Outdoor Air Temp.	COP MT	COP LT	LR	COP Tot	COP, LR = 1	COP, LR = 2	COP, LR = 3	COP, LR = 4
-	K	-	-	-	-	-	-	-	-
1	307.9	2.08	1.25	1.11	1.58	1.56	1.70	1.78	1.84
2	312.3	1.59	0.98	1.07	1.22	1.22	1.32	1.38	1.41
3	302.1	2.62	1.51	1.31	1.99	1.91	2.10	2.21	2.28
4	297	2.34	1.41	1.07	1.77	1.76	1.92	2.01	2.06
5	280.9	3.81	1.78	1.24	2.53	2.43	2.76	2.97	3.10
6	289.1	2.13	1.24	0.93	1.55	1.57	1.72	1.81	1.86
7 (no sub)	296.2	1.47	0.96	0.28	1.04	1.16	1.25	1.30	1.33
8 (no sub)	281.2	2.25	1.28	0.63	1.53	1.63	1.79	1.89	1.95
9 (no sub)	308	1.22	0.84	0.30	0.90	1.00	1.06	1.10	1.12
10 (no sub)	302.1	1.95	1.21	0.96	1.49	1.49	1.62	1.69	1.74
11 (no sub)	289.3	1.41	0.91	0.19	0.97	1.11	1.19	1.24	1.27

Steady State Modeling

A system solver was developed to simulate the CO_2 refrigeration system (Beshr 2016). This new component based vapor compression system steady solver falls under the successive solution scheme category of solvers where a variable is solved before moving on to the next variable. This approach is fast and robust because the number of iterative variables for a certain system using this approach are less than the number of variables in the simultaneous approach (which uses a non-linear equation solver to solve all the unknown variables simultaneously). Also, this solver has many benefits and unique features compared to the existing solvers. Firstly, this solver overcomes the flexibility problem associated with successive solution scheme system solvers. This happens through using highly flexible data structures. Therefore, this solver is capable of simulating large number of different designs of

vapor compression systems including arbitrary system configurations, multiple air and refrigerant paths, and user defined refrigerants. Moreover, this solver implements a component-based solution scheme. This means that it treats the different component models as black box objects so that the equations or any other information used in any component model are not exposed to the solver. Therefore, detailed engineering models and solvers can be used to represent the different components without affecting the complexity, robustness, or computational speed of the system level solver. Figure 10 shows the solver outline. The solver is based on the enthalpy marching approach (Winkler et al. 2008) where the enthalpy (refrigerant state in general) is propagated from one component to the next (e.g. the pressure and enthalpy outlet of the compressor is the pressure and enthalpy inlet to the gas cooler).

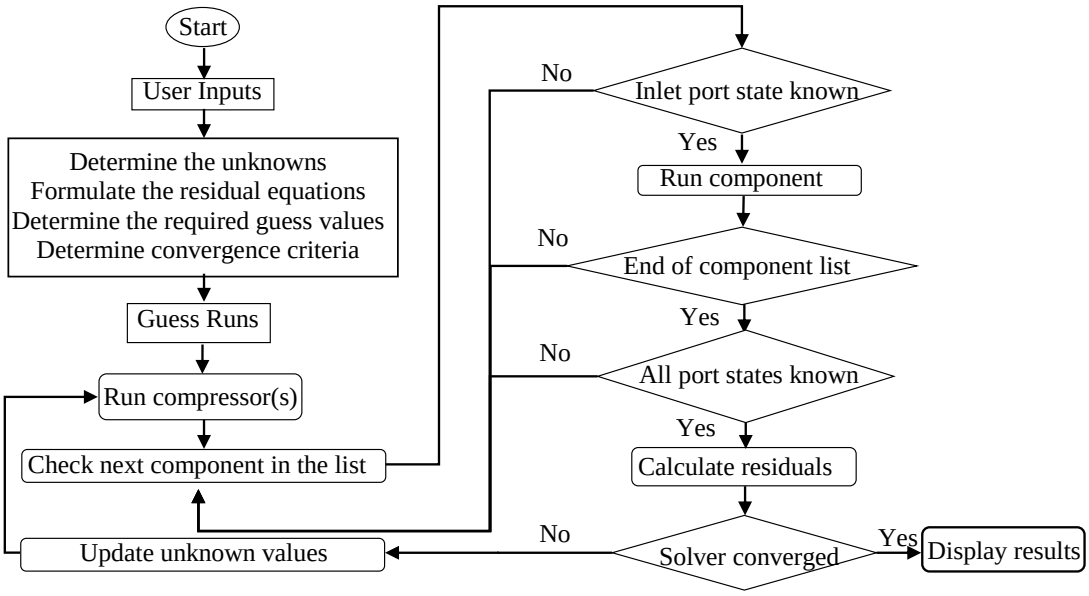

Figure 43. Solver Flowchart

The CO_2 gas cooler component model is based on a finite volume HX model (Jiang et al. 2006) while the subcooler HX, MT and LT evaporators use a finite volume plate HX model (Qiao et al. 2013). The R134a subcooler is not simulated in the system model and the inlet glycol operating condition is based on the experimental data. The LT compressor model is a ten-coefficient (AHRI-540-2015 Standard) model with a power adjustment factor of 0.87 while the MT compressor is defined using the volumetric and isentropic efficiencies, the displacement volume and RPM. The solution scheme requires setting 4 different convergence criteria in the system. The selected criteria are the discharge pressure for transcritical test points (outlet GC/condenser quality for subcritical test points), expansion valve outlet quality at point 14, and superheat at the outlet of each of the two evaporators. These convergence criteria values are set to be equal to the experimental values for the corresponding testing conditions.

The validation results for the COP, power consumption and total system capacity are shown in Figure 11. The predictions are within 3% of the experimental data.

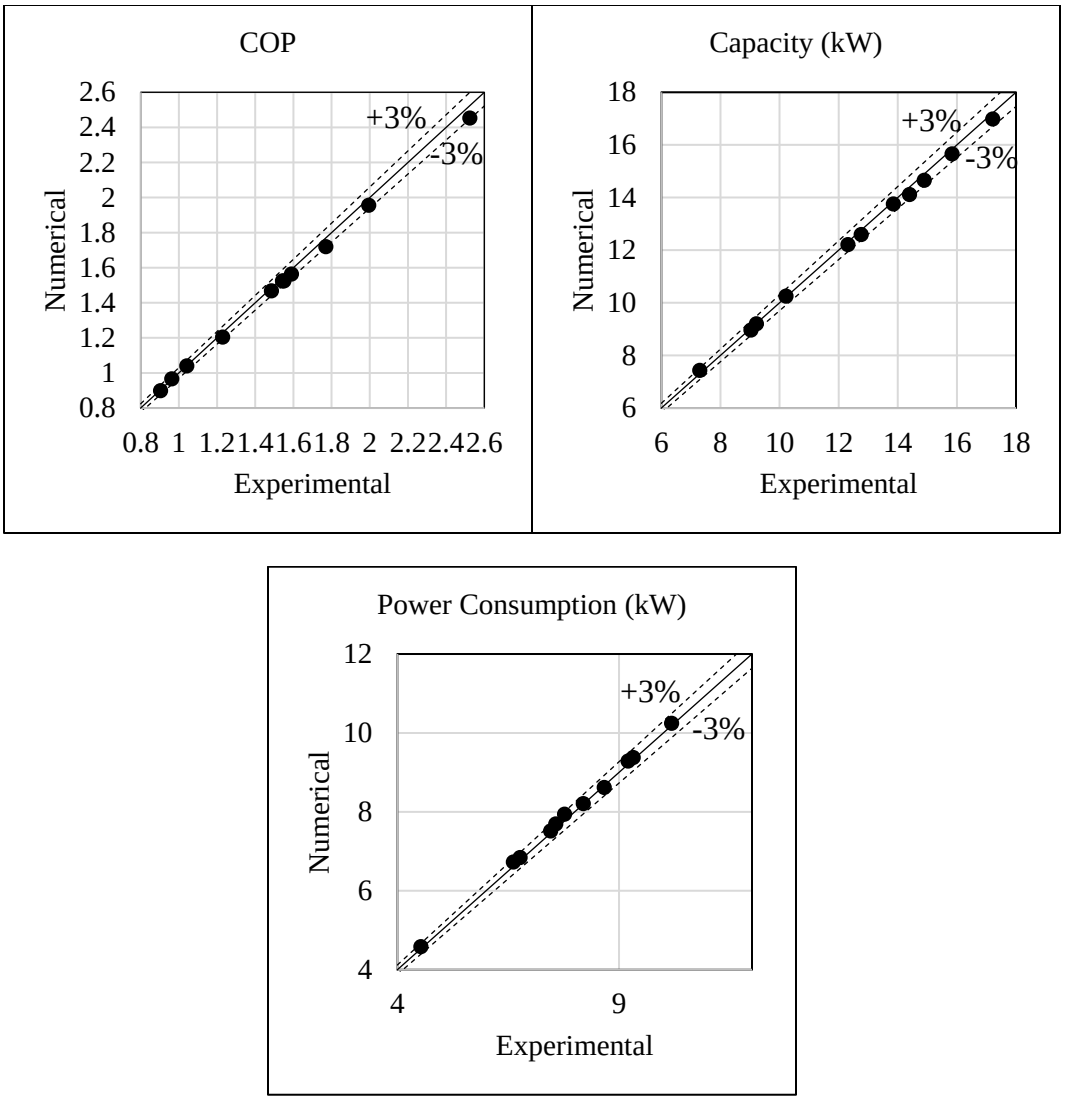

Figure 44. Validation Results

Parametric Analysis of Subcooler

The model was used to perform a parametric study on the effect of the subcooler, varying the capacity of the subcooler. Since laboratory results showed that the subcooler had a beneficial impact on overall system efficiency at all test conditions, it is of interest to understand to what extent additional subcooling capacity would improve overall efficiency. A simple modification was made to the simulation

settings to perform this simulation: the inlet glycol condition to the subcooling plate heat exchanger was adjusted and the simulation re-run to evaluate new steady state results. The constraints and inputs to the model were otherwise held constant. The power of the mechanical subcooler, which was not itself modeled, was calculated first assuming a constant COP, and then with COP adjusted by +/- 25% to show the effect of subcooler efficiency on the expected overall system COP. One important consideration for interpreting the results of this simulation is that the compressor RPM is a set input to the model. The results therefore show increased refrigerating capacity with increased subcooler capacity, when in real operation the result may instead be reduced compressor RPM and lower total power to provide equal refrigerating capacity.

The simulation was run for test points #2, #4 and #6. The results are shown in Figure 45, Figure 46, and Figure 47 respectively. COP increased with lower-temperature glycol in the subcooler, and bypass flow percentage decreased with lower-temperature glycol in the subcooler. The improvement in overall system COP depends on the efficiency of the subcooler, and the effect was most pronounced in the lowest outdoor temperature test, where the subcooler power makes up the largest percentage of overall system power. The graphs also show the COP of the CO_2 cycle only (meaning, with subcooling power excluded from the total power). This shows why the benefit of reducing subcooler temperature diminishes for the Test #4 and Test#6; as the COP of the CO_2 cycle itself improves, the efficiency benefit of subcooling gets marginally less. Though the actual cycle efficiency of the subcooler

was not modeled here, it is evident that a balance point exists at which adding subcooling capacity at relatively lower COP may reduce total cycle COP.

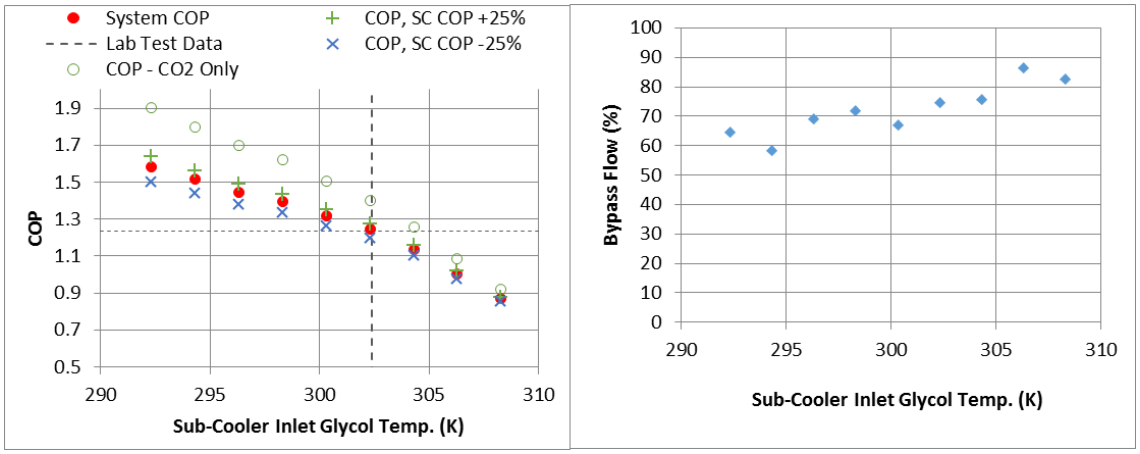

Figure 45 Parametric Analysis of Subcooler Results: COP vs. Subcooling Plate HX Glycol Inlet Temperature (left) and Bypass Flow Percentage vs. Subcooling Plate HX Glycol Inlet Temperature For Test #2 (312.3K Outdoor Temperature)

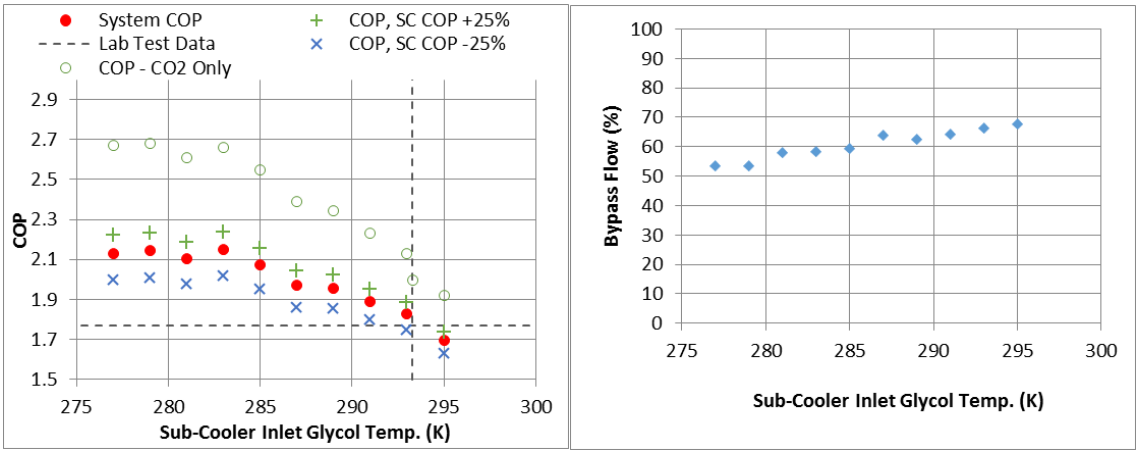

Figure 46 Parametric Analysis of Subcooler Results: COP vs. Subcooling Plate HX Glycol Inlet Temperature (left) and Bypass Flow Percentage vs. Subcooling Plate HX Glycol Inlet Temperature For Test #4 (297.0K Outdoor Temperature)

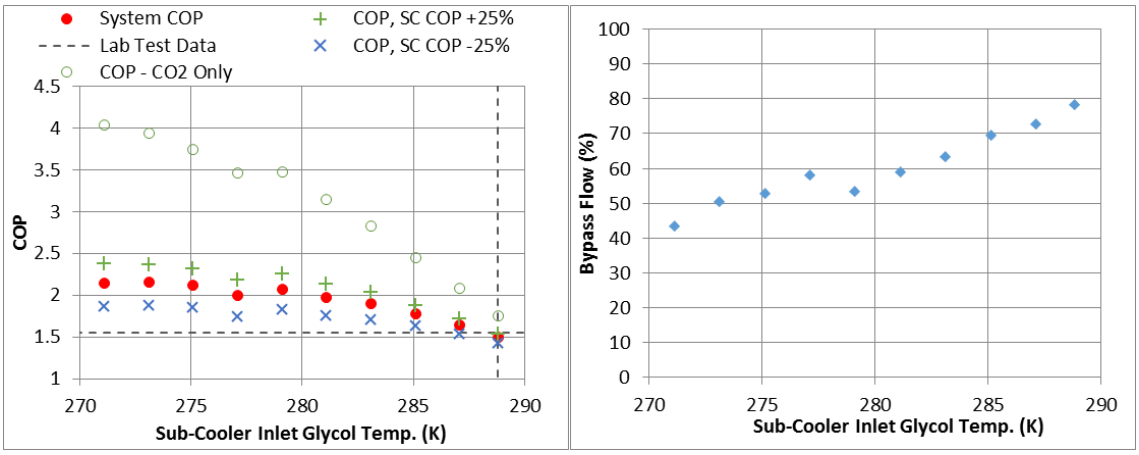

Figure 47 Parametric Analysis of Subcooler Results: COP vs. Subcooling Plate HX Glycol Inlet Temperature (left) and Bypass Flow Percentage vs. Subcooling Plate HX Glycol Inlet Temperature For Test #6 (289.1K Outdoor Temperature)

Chapter Summary

This chapter details laboratory testing of a transcritical booster system with dedicated mechanical subcooling. The system was tested in a range of condenser/gas cooler inlet air temperatures and with simulated load for the MT and LT evaporators. The system was tested with and without subcooling; the subcooler provides a substantial improvement to capacity and efficiency by reducing the flash gas and requirement for bypass flow. Because the system had a high proportion of LT loads, there is high bypass flow in the MT compressor, and in cases without subcooling the total system capacity is reduced at hot outdoor conditions without the subcooler. The efficiency of the cycle had a local minimum in the transitional region just below the critical point, as the effectiveness of the condenser is comparatively low in this region. In a steady-state modeling task, the effect of sizing of the subcooler was investigated. The COP of the CO_2 primary cycle excluding the subcooler increases with decreasing subcooler temperature, while the COP of the subcooler itself is less as leaving temperature decreases. As the primary CO_2 cycle efficiency gets higher, the benefit of additional subcooling diminishes.

Chapter 4: Transient Behavior

This chapter describes the development of transient models of the CO_2 booster refrigeration system that was tested in the laboratory. Laboratory tests of three transient scenarios were performed. Using transient laboratory test results, the model is validated for transcritical and subcritical operating modes. A preliminary study on the effects of demand response "shed" events at each stage of the cycle was also performed. The objectives of the work described in this chapter are:

- Develop transient model of full booster cycle with dedicated mechanical subcooler using the Modelica language and Dymola simulation environment.
- Using laboratory test results, validate model in transient operating conditions in transcritical and subcritical operating modes
- Using validated model, expand understanding of load shed behavior of booster cycle by modeling partial-load, per-stage load sheds

Model Description

The booster cycle was modeled using the object-oriented simulation language Modelica and the Dymola simulation environment, using many components from the University of Maryland CEEE Modelica Library. The Sdirk34hw solver, a 4th-order single-step/Runge-Kutta solver is the primary solver used. The cycle described in laboratory testing was replicated with the exception of the LT evaporator suction line heat exchanger: because of the large superheat from the LT evaporator related to the laboratory test set-up, the LT suction line heat exchanger did not engage during typical operation, so it was omitted from this simulation for simplicity. The schematic of the system as modeled is shown in Figure 48.

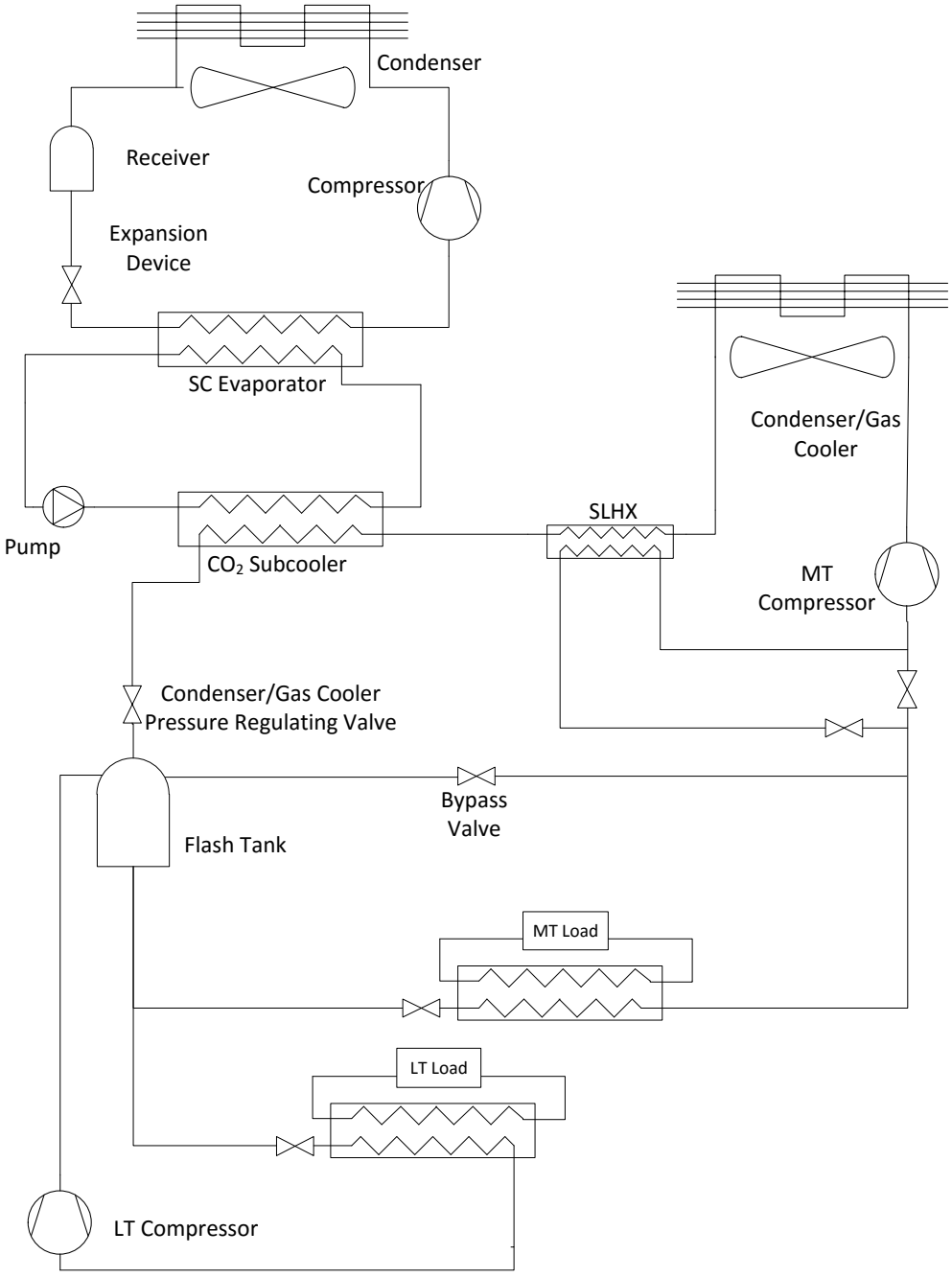

Figure 48 CO_2 Booster Cycle Schematic as Modeled for Validation

The following describes some of the key component models.

Heat Exchangers

The model contains a number of plate heat exchanger components. For these the CEEE Modelica Library plate heat exchanger component is used as a basis with modification as appropriate. The model includes refrigerant-to-refrigerant and refrigerant-to-brine plate heat exchangers, as well as subcritical and transcritical refrigerant behavior.

There are a total of 5 plate heat exchangers in the model. Each parallel flow channel is modeled using the finite volume method. The finite volume approach that was adopted here is described generally in Qiao (2014) using components from the CEEE Modelica Library. The heat exchanger geometries are described in Table 8. The MT evaporator, LT evaporator, and subcooler are CO_2-to-glycol components. The subcooler evaporator is a R134a-to-glycol heat exchanger. The suction line heat exchanger is CO_2-to-CO_2. The condenser/gas cooler is also modeled using the finite volume method. The flash tank is modeled as a lump control volume. There are three ports: an inlet port of refrigerant returning from the high side; a vapor outlet port of bypass refrigerant to the MT compressor, and a liquid otulet port to the MT and LT evaporators. The component model is the same as that described in Qiao et al (2015) modified to the geometry of the CO_2 system.

Table 8 Plate Heat Exchanger Geometries

Description	Dimensions (Length, Width, Hydraulic Diameter)	Number of Channels / Plates
MT Evaporator – CO_2 to Glycol	0.53 m, 0.11m, $8.75*10^{-4}$ m	26 Channels / 27 Plates
LT Evaporator – CO_2 to Glycol	0.21m, 0.073m, $1.06*10^{-3}$ m	16 Channels / 17 Plates
Suction Line Heat Exchanger – CO_2 to CO_2	0.32m, 0.11m, $8.75*10^{-4}$ m	6 Channels / 7 Plates
Subcooler – CO_2 to Glycol	0.32m, 0.11m, $8.75*10^{-4}$ m	12 Channels / 13 Plates
Subcooler – R134a to Glycol	0.32m, 0.11m, $8.75*10^{-4}$ m	12 Channels / 13 Plates

Each heat exchanger includes a *SingleNode* heat transfer component which is the interface between each fluid and the heat exchanger walls. The component includes heat exchanger geometry and materials, and computes an energy balance between the walls and the fluids for a heat exchanger with *n* nodes and connecting fluids A and B:

$$Cp_{wall} * \frac{m_{wall}}{n} * \frac{dT_{node}}{dt} = Q_{A,node} + Q_{B,node}$$

The *SingleNode* component connects to each fluid control volume and exchanges the node temperature T_{node} as well as heat transfer Q.

For each control volume node *i* the energy balance is computed as

$$Q_i = HTC_i * A_{surf.,i} * (T_{wall,i} - T_{fluid,i})$$

The heat transfer coefficient is calculated differently depending upon the fluid. For brine and air components the heat transfer coefficient is taken as a constant and

determined empirically within a range of reasonable bounds based on laboratory results.

For refrigerant components the *FiniteVolumeFluidCV* component from the CEEE Modelica Library is used. This component computes the properties and flows for a discretized heat exchanger of fixed control volumes. The HTC is calculated at each time step for each node. For each refrigerant component three values of α are taken as parameters for liquid, two-phase and vapor, α_{liq}, α_{tp} and α_{vap}. To ensure smooth transitions between phases, the three are spliced together in an intermediate step using the Modelica *spliceFunction* as proposed by Qiao (2014):

$$HTC_{int.,1} = splice(\alpha_{liq}, \alpha_{tp}, 0.1 - x, 0.1)$$

$$HTC_{int.,2} = splice(\alpha_{vap}, \alpha_{tp}, T_{wall} - T_{sat}, 1)$$

$$HTC_{int.,3} = \begin{cases} splice(HTC_{int,1}, HTC_{int,2}, 0.95 - x, 0.05) & condenser \\ splice\left(HTC_{int,1}, \alpha_{vap}, 0.9 - x, 0.1\right) & evaporator \end{cases}$$

Finally,

$$HTC = \left(\frac{\dot{m}_{avg}}{\dot{m}_0}\right)^{0.8} * HTC_{int.,3}$$

Where $\dot{m}_{avg}$ is the average of mass flow rate into and out of the node and $\dot{m}_0$ is a parameter for the nominal flow rate of the component. In the case of transcritical or near-critical flow, further modification is needed. Refrigerant quality is used in the

smoothing funtions above, but transcritical refrigerant has no “quality” value since there is no h_f or h_l. To retain the same equations and smooth transition, the values of h_f and h_l are retained from the point 7.2 MPa; therefore the interpolation of HTC values can still be performed across the range of enthalpy conditions while near or above the critical point. Further, since heat transfer coefficient varies greatly in the near-critical and transcritical regions, the values of α is modified as a function of refrigerant pressure, rather than input as a fixed parameter as in the components operating well below the critical point.

The energy balance in the control volume is calculated as,

$$\dot{m}_{in} + \dot{m}_{out} = V\left[\left.\frac{\partial\rho}{\partial p}\right|_h \frac{dP}{dt} + \left.\frac{\partial\rho}{\partial h}\right|_P \frac{dh}{dt}\right]$$

$$\dot{m}_{in}h_{in} + \dot{m}_{out}h_{out} + Q = V\left[\left(h\left.\frac{\partial\rho}{\partial p}\right|_h - 1\right)\frac{dP}{dt} + \left(h\left.\frac{\partial\rho}{\partial h}\right|_P - \rho\right)\frac{dh}{dt}\right]$$

Compressors

The model includes three compressors: the MT, LT and subcooler compressors. The model consists of a small control volume of refrigerant at the inlet to the compressor, and a base compressor component.

The compressor base component takes compressor speed in RPM as an input. The parameters include a fixed volumetric and isentropic efficiency, as well as displacement D. The following equations describe performance:

$$\dot{m} = (\eta_{vol} * \rho * D * \frac{RPM}{60})$$

$$h_{out} = h_{in} + \frac{h_{out,s} - h_{in}}{\eta_{isen}}$$

$$W = \dot{m}(h_{out} - h_{in})$$

The MT compressor was modeled with a displacement of 6.46*10-5 m3 and isentropic efficiency of 60%. Compressor speed was controlled in the range of 550 to 1,750 rpm. The LT compressor was modeled with displacement of 2.532*10-5 m3 and isentropic efficiency of 72%. The LT compressor was controlled with a fixed speed of 1,750 rpm. Both of the aforementioned compressors are modeled with CO_2 refrigerant. The subcooler compressor, using R134a, has a displacement of 8.09*10-5 m3 and was modeled with isentropic efficiency of 85%. Fixed efficiency was used, derived from experimental and manufacturers data.

Valves

The valves were modeled as ideal valves with diameter as an input from proportional-integral (P-I) control. The valve is assumed to be isenthalpic and the equation governing the relationship of flow and pressure is

$$\dot{m} = Cv * {D_i}^2 * \rho^{0.5} * (dp)^{0.5}$$

The Modelica function *regroot* is used for the pressure drop, which approximates the root of the absolute value of dp, times the sign of dp, to provide a finite result which is smooth at dp = 0.

Flash Tank

Another important component is the flash tank. The flash tank is modeled as a lumped volume as in Qiao et al. (2015). The model assumes ideal liquid and vapor separation and that the vapor and liquid within the tank are at thermal equilibrium. The pressure drop within the tank is assumed to be negligible, as is the heat loss from the tank. The component has three ports: an inlet port, a vapor outlet port and a liquid outlet port. The component requires both mass and energy balances since the total refrigerant quantity in the flash tank changes over time. The equations governing the behavior of the flash tank are

$$\frac{dM}{dt} = \dot{m}_{in} + \dot{m}_{out,liq} + \dot{m}_{out,vap} = V\left[\frac{\partial\rho}{\partial p}\Big|_h \frac{dP}{dt} + \frac{\partial\rho}{\partial h}\Big|_P \frac{dh}{dt}\right]$$

$$\frac{dU}{dt} = \dot{m}_{in}h_{in} + \dot{m}_{out,liq}h_{liq} + \dot{m}_{out,vap}h_{vap}$$

$$= V\left[(h\frac{\partial\rho}{\partial p}\Big|_h - 1)\frac{dP}{dt} + (h\frac{\partial\rho}{\partial h}\Big|_P - \rho)\frac{dh}{dt}\right]$$

$$M_{tot} = M_{liq} + M_{vap}$$

$$M_{vap} = M_{tot} * x$$

$$M_{liq} = V * \frac{H_{liq}}{H_{tank}} * \rho$$

$$U = M_{tot} * (h - \frac{P}{\rho})$$

The enthalpy of the liquid and vapor phases are assumed to be the saturated liquid and vapor enthalpy levels respectively at the pressure of the flash tank. As modeled, the height of liquid refrigerant in the flash tank did not cross the orifice ports, however such cases could be accommodated.

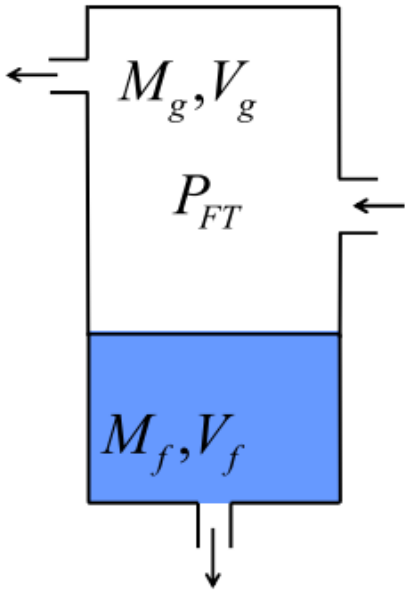

Figure 49: Schematic of Flash Tank Model (reproduced from Qiao et al 2012)

Controls

The control logic for the simulated cycle was duplicated from the settings of the commercially-available control software used for the system in the laboratory for validation modeling. Among key control points are the flash tank pressure, suction pressure for the MT compressor, saturated suction pressure for each evaporator,

superheat and gas cooler pressure. These values were selected to match the equipment and controls of the tested hardware, rather than to optimize performance (for example, gas cooler pressure was based on the control of the test equipment, not optimized for capacity or efficiency). A Modelica PID component was used for each of these with set points as shown in Table 9. The control logic of the subcooler is again the same as the laboratory set-up, which is on-off control based on a water/glycol temperature of approximately 4.4°C; the shut-off condition was not observed in the tests discussed here.

Control of the cycle is performed with a series of proportional-integral controllers. The Modelica *PID* component is used for simulating this control. The following are the PI controllers and their control points, derived from the actual control software for the laboratory equipment. In later sections these points are modified to simulate a real-world installation.

Table 9 Set-Points for Control in Validation Simulations

Description	Control Input	Validation Set-Point	k	Ti
Condenser pressure regulator	Gas cooler pressure	(varies with temperature)	$5.0*10^{-5}$	0.5
Bypass valve	Flash tank pressure	3.46 MPa	$1.0*10^{-7}$	1
MT expansion valve	Superheat	5K	$7.5*10^{-5}$	10
LT expansion valve	Suction pressure	1.535 MPa	$5.0*10^{-7}$	0.5
MT compressor speed	Suction pressure	2.86 MPa	$7.5*10^{-5}$	1
SLHX Valves	Superheat to MT Compressor	15K	$1.0*10^{-4}$	1
Subcooler expansion valve	Suction pressure	0.30 MPa	$5*10^{-7}$	10

Brine Tanks

The laboratory test set-up was also modeled for validation purposes. The test set-up consisted of two insulated tanks containing a water/propylene glycol blend. The volumes were 0.492m^3 for the MT load bank and 0.303 m^3 for the LT load bank. The fluid was circulated to each evaporator using pumps which are not modeled in detail here (the flow rate, which was measured in the laboratory, is set as a parameter). The electric resistance heat is simulated using a simple fixed-heat-transfer pipe component, and controlled with a simple on-off control with a 2K dead band. The storage tanks are modeled as lumped parameter volumes and losses are neglected.

For modeling the brine system, a brine tank component and fixed-heat-flow pipe components are used. The pipe flow uses a lumped control volume, like that in the heat exchanger components. The properties of brine are calculated from the following equations:

$$h = T - 258.15 * c_p$$

$$\rho = -0.4689 * (T - 273.15) + 1044.8$$

$$\lambda = 0.0006 * T + 0.3889$$

$$c_p = (0.0033 * (T - 273.15) + 3.6357) * 1000$$

$$\mu = (-0.4302 * (T - 273.15) + 16.144)/1000$$

Energy balance in each control volume is calculated:

$$m * c_p * \frac{dT}{dt} = Q + \dot{m}_{in} h_{in} + \dot{m}_{out} h_{out}$$

For fixed-heat transfer pipes (used to simulate heaters) the value of Q is provided as an input. The glycol tanks are modeled as a single control volume using the same method. The storage tanks are set to have a node pressure of 1 atmosphere, thereby "grounding" the pressure in each closed loop.

Results: Transient Behavior and Model Validation

To understand behavior in transient conditions, laboratory tests were performed for the following scenarios:

(1) Shed MT load by shutting expansion valve for MT evaporator. Transcritical, 35.0°C outdoor temperature.

(2) Shed LT load by shutting off expansion valve for LT evaporator. Transcritical, 35.0°C outdoor temperature.

(3) Switch the subcooler system from "on" to "off'. Subcritical, 12.0°C outdoor temperature.

The results of laboratory testing and the model validation are presented together here. The results for the MT shed are discussed first. The values of key parameters are averaged before, during, and after the event in

Table 10. In model results, the first 200 seconds are omitted as the model initializes. In the simulated event, the MT evaporator expansion valve control was manually interrupted, and set to "close" at time 1100 seconds in the results. The duration is 1800 seconds, and the system is allowed to resume normal operation at that time.

Table 10 MT Shed Laboratory and Simulation Results

		Before Shed				During Shed				After Shed			
		Model	Lab	Delta	Pct	Model	Lab	Delta	Pct	Model	Lab	Delta	Pct
MT Compressor Power	(kW)	5.94	5.76	0.19	3%	3.55	3.91	-0.36	-10%	6.08	6.16	-0.09	-1%
LT Compressor Power	(kW)	1.41	1.55	-0.13	-9%	1.41	1.58	-0.17	-11%	1.42	1.53	-0.12	-8%
MT Evaporator Capacity	(kW)	5.13	5.45	-0.32	-6%	0.23	-0.22	0.45	NA*	5.28	5.76	-0.48	-9%
LT Evaporator Capacity	(kW)	6.56	5.99	0.57	9%	6.56	6.43	0.13	2%	6.56	6.30	0.26	4%
MT Comp. Ref. Flow Rate	(kg/s)	0.07	0.06	0.01	14%	0.04	0.04	0.00	-5%	0.07	0.07	0.01	8%
LT Comp. Ref. Flow Rate	(kg/s)	0.02	0.02	0.00	0%	0.02	0.03	0.00	-8%	0.02	0.03	0.00	-5%
MT Evap. Ref Flow Rate	(kg/s)	0.02	0.02	0.00	-2%	0.00	0.00	0.00	NA*	0.02	0.02	0.00	-3%
LT Evap. Pressure	(MPa)	1.54	1.47	0.06	4%	1.54	1.56	-0.02	-1%	1.54	1.53	0.00	0%
MT Evap. Pressure	(MPa)	2.89	2.86	0.03	1%	2.47	2.66	-0.20	-8%	2.89	2.90	0.00	0%
Flash Tank Pressure	(MPa)	3.46	3.47	-0.01	0%	3.46	3.48	-0.02	0%	3.46	3.47	-0.01	0%
Cond./Gas Cooler Pressure	(MPa)	8.58	8.63	-0.05	-1%	8.55	8.35	0.20	2%	8.58	8.65	-0.07	-1%
COP	(-)	1.40	1.35	0.05	4%	1.14	1.04	0.10	9%	1.40	1.36	0.04	3%

*comparison not applicable for components turned “off” during shed

The power for the MT and LT compressors is shown in Figure 50. The LT compressor power, shown in blue, is approximately flat and agrees closely throughout the simulation for the laboratory and model results. The model power is consistently a bit lower, and the difference in power is 8-11% at each stage of the simulation. The MT compressor power varies during the shed event, as the MT compressor speed reduces to minimum speed. The power agrees to within 3% prior to the shed, 10% during the shed, and 1% after the shed. In the figure, the power may be observed to rise and fall during steady periods (outside the shed) as the simulated load temperature increases and decreses. These increases and decreases are not quite synchronized between laboratory and model, because of slight differences in laboratory and simulated conditions arising from the intial conditions and initialization period.

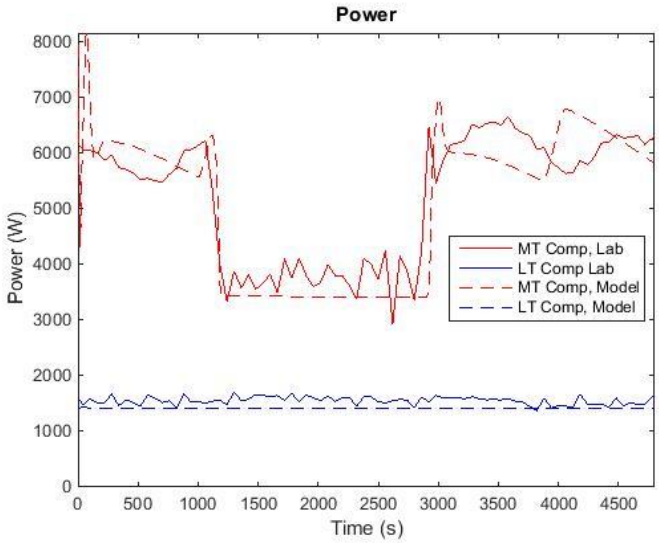

Figure 50 MT and LT Compressor Power for Laboratory (solid) and Model (dash) for MT Capacity Shed

The refrigerant flow rates are shown in Figure 51. The MT and LT evaporator flow rates, in red and blue respectively, agree closely on average. The flow rates in the laboratory test show some perodic cycling and variation that is not captured in the model. The MT compressor flow is higher outside of the shed, by 14% on average before and 8% on average after, and lower by 5% during the shed. Since the MT evaporator flow rate agrees closely, the primary difference is the bypass flow, which is higher in the model. This corresponds to higher refrigerant temperature leaving the subcooler, which was 3-6K higher in the model.

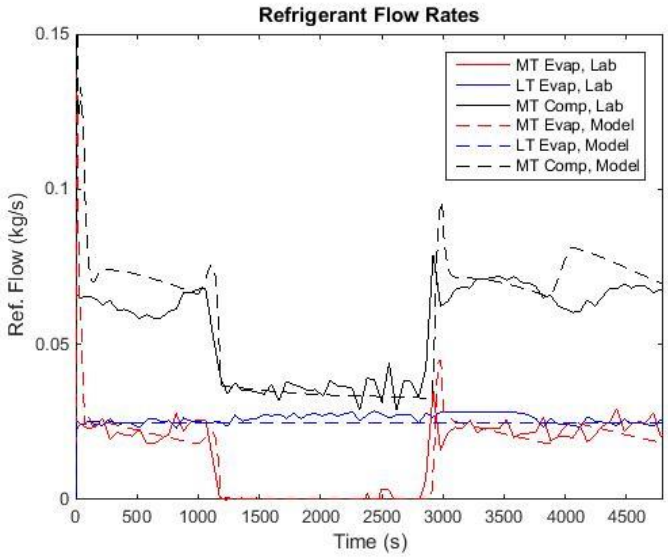

Figure 51 Refrigerant Flow Rates for Laboratory (solid) and Model (dash) for MT Capacity Shed

The refrigerating capacity, shown in Figure 52, agrees closely. The COP Figure 53 agrees within 3-4% outside of the shed, and 9% during the shed.

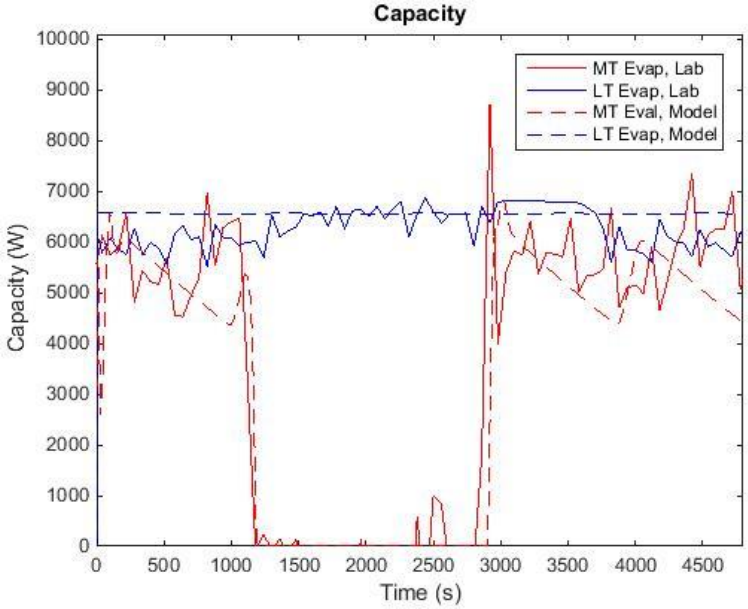

Figure 52 MT and LT Evaporator Capacity for Laboratory (solid) and Model (dash) for MT Capacity Shed

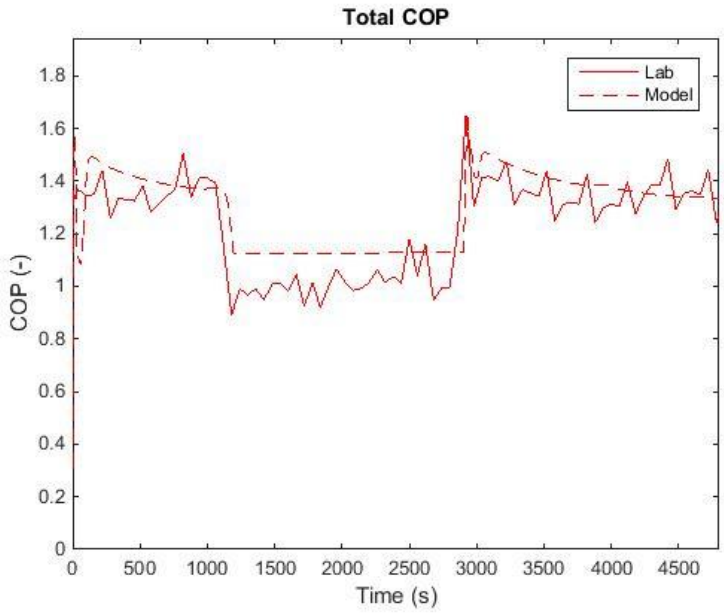

Figure 53 Total System COP for Laboratory (solid) and Model (dash) for MT Capacity Shed

The LT shed test was performed similarly, and the results are shown in Table 11. In the laboratory, the LT evaporator pressure often settled at slightly different steady levels per test; in the LT demand response test, the steady pressure was approximately 1.8 MPa prior to the shed, and ramped down to about 1.5 MPa after the shed; this was emulated in the model using different set pressures before and after the shed. Similar to the MT shed results, the first 200 seconds of simulation time are omitted from the calculated results. At 1300 seconds, the LT expansion valve was manually set to close, and after 1800 seconds, re-opened. The LT compressor is controlled to shut down on low pressure sensing approximately 1.2 MPa, and turn on sensing approximately 1.8 MPa. As such, the compressor turned off during the event. The model and laboratory results showed fair agreement. The MT compressor power agreed within 10% before, 8% during, and 11% after the shed; the LT compressor power agreed within 16% before

and 17% after the shed. The capacity of the MT evaporator agreed within 12% before, 2% during, and 7% after the shed; the LT evaporator results agreed within 10% before and 1% after the shed.

Table 11 LT Shed Laboratory and Simulation Results

		Before Shed				During Shed				After Shed			
		Model	Lab	Delta	Pct	Model	Lab	Delta	Pct	Model	Lab	Delta	Pct
MT Compressor Power	(kW)	7.99	7.23	0.76	10%	4.15	4.50	-0.35	-8%	6.37	5.69	0.68	11%
LT Compressor Power	(kW)	1.31	1.54	-0.23	-16%	0.03	0.07	-0.04	NA*	1.19	1.41	-0.22	-17%
MT Evaporator Capacity	(kW)	5.40	4.80	0.59	12%	9.26	9.04	0.22	2%	4.66	4.34	0.32	7%
LT Evaporator Capacity	(kW)	8.03	8.90	-0.87	-10%	0.14	0.68	-0.54	NA*	8.29	8.22	0.07	1%
MT Comp. Ref. Flow Rate	(kg/s)	0.10	0.08	0.01	15%	0.04	0.05	0.00	-11%	0.08	0.06	0.01	20%
LT Comp. Ref. Flow Rate	(kg/s)	0.03	0.03	0.00	-7%	0.00	0.00	0.00	NA*	0.04	0.03	0.00	15%
MT Evap. Ref Flow Rate	(kg/s)	0.02	0.02	0.00	14%	0.04	0.04	0.00	4%	0.02	0.02	0.00	10%
LT Evap. Pressure	(MPa)	1.84	1.85	-0.01	-1%	1.24	1.58	-0.35	-25%	1.95	1.80	0.15	8%
MT Evap. Pressure	(MPa)	2.89	2.91	-0.02	-1%	2.57	2.62	-0.05	-2%	2.94	2.91	0.03	1%
Flash Tank Pressure	(MPa)	3.46	3.49	-0.03	-1%	3.38	3.47	-0.09	-3%	3.45	3.48	-0.03	-1%
Cond./Gas Cooler Pressure	(MPa)	8.60	8.66	-0.06	-1%	8.56	8.63	-0.07	-1%	8.58	8.66	-0.08	-1%
COP	(-)	1.31	1.38	-0.07	-5%	1.85	1.71	0.14	8%	1.54	1.53	0.02	1%

*comparison not applicable for components turned “off” during shed

The results are graphed in Figure 54 through Figure 57. A summary of the average power and capacity agreement between laboratory and model is shown in Figure 60.

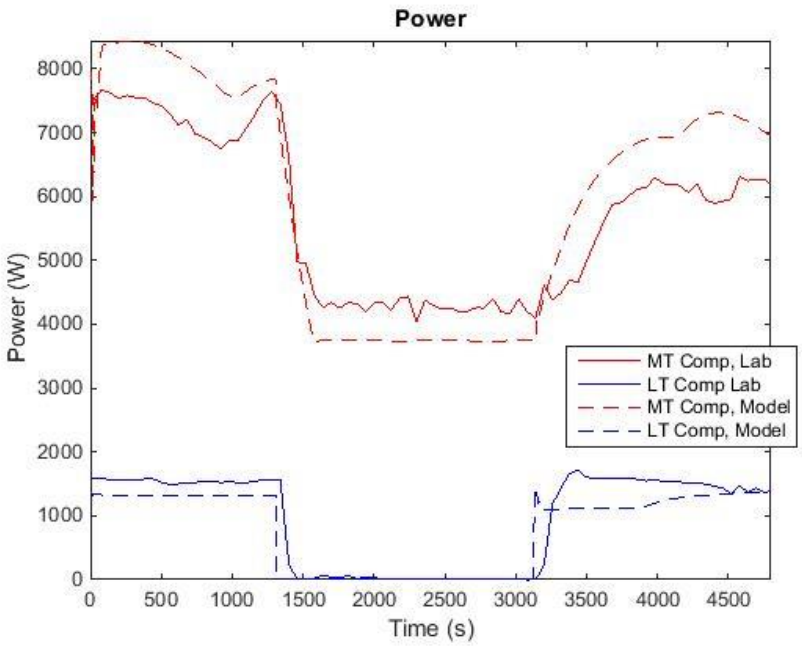

Figure 54 MT and LT Compressor Power for Laboratory (solid) and Model (dash) for LT Capacity Shed

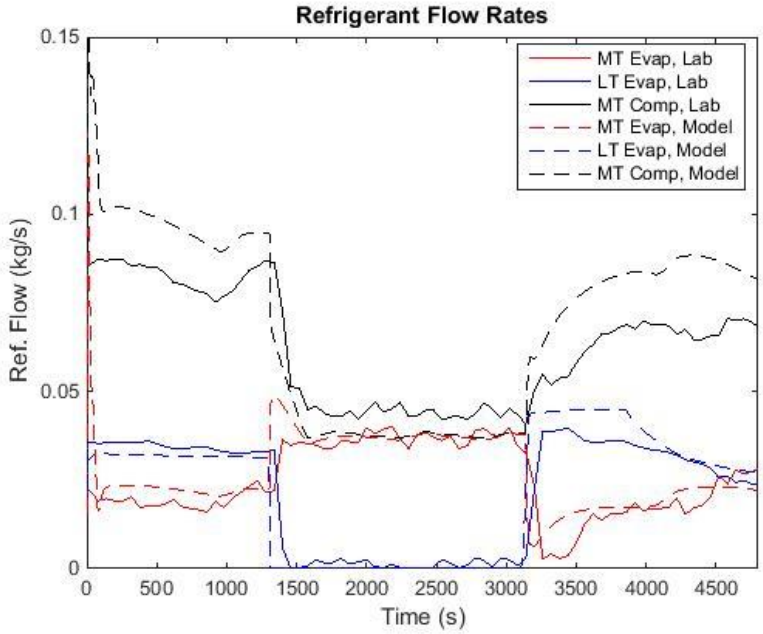

Figure 55 Refrigerant Flow Rates for Laboratory (solid) and Model (dash) for LT Capacity Shed

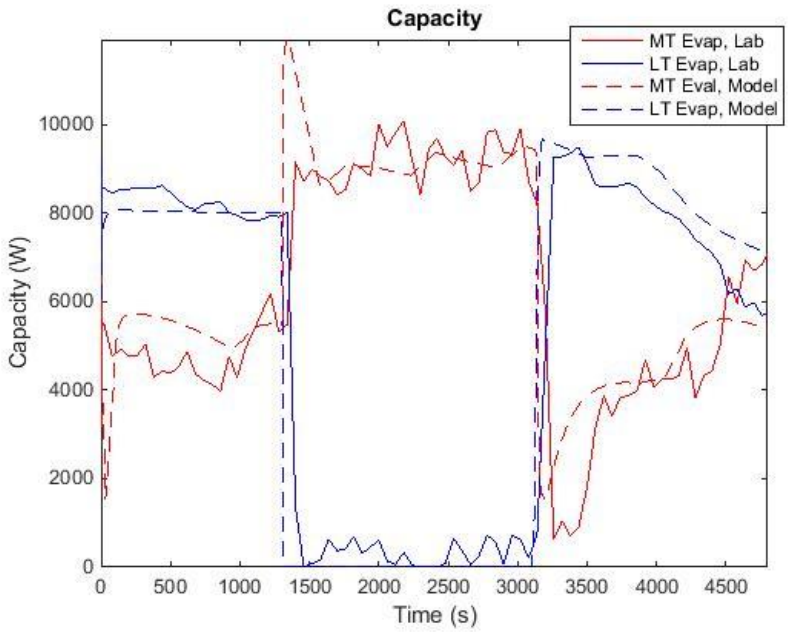

Figure 56 MT and LT Evaporator Capacity for Laboratory (solid) and Model (dash) for LT Capacity Shed

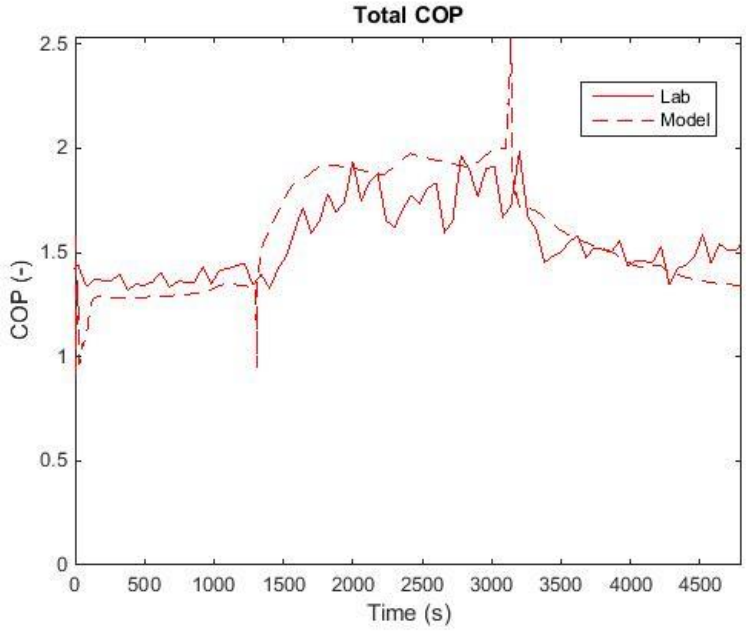

Figure 57 Total System COP for Laboratory (solid) and Model (dash) for LT Capacity Shed

For the subcritical transient validation test, a different approach was taken. A laboratory test in which the subcooler was off at the beginning, and then turned on, was used as the condition for validation. The resulting values are again summarized in Table 12.

Table 12 Subcooler Off-to-On Test Summary

		Before Shed				During Shed				After Shed			
		Model	Lab	Delta	Pct	Model	Lab	Delta	Pct	Model	Lab	Delta	Pct
MT Compressor Power	(kW)	6.92	6.64	0.28	4%	6.25	5.44	0.81	14%	4.32	3.82	0.51	12%
LT Compressor Power	(kW)	1.44	1.48	-0.04	-3%	1.43	1.5	-0.07	-5%	1.42	1.53	-0.11	-8%
MT Evaporator Capacity	(kW)	2.62	2.21	0.41	17%	5.28	4.83	0.45	9%	5.3	5.42	-0.12	-2%
LT Evaporator Capacity	(kW)	6.55	6.66	-0.11	-2%	6.56	6.69	-0.13	-2%	6.55	6.98	-0.42	-6%
MT Comp. Ref. Flow Rate	(kg/s)	0.14	0.14	0.01	4%	0.12	0.11	0.01	5%	0.09	0.08	0.01	13%
LT Comp. Ref. Flow Rate	(kg/s)	0.02	0.02	0	0%	0.02	0.02	0	0%	0.02	0.03	0	-4%
MT Evap. Ref Flow Rate	(kg/s)	0.01	0.01	0	19%	0.02	0.02	0	11%	0.02	0.02	0	1%
LT Evap. Pressure	(MPa)	1.53	1.51	0.02	2%	1.54	1.5	0.03	2%	1.54	1.51	0.02	1%
MT Evap. Pressure	(MPa)	3.07	3.01	0.06	2%	2.86	2.88	-0.03	-1%	2.89	2.87	0.01	0%
Flash Tank Pressure	(MPa)	3.46	3.52	-0.05	-2%	3.46	3.5	-0.04	-1%	3.46	3.48	-0.02	-1%
Cond./Gas Cooler Pressure	(MPa)	5.99	5.74	0.25	4%	5.83	5.49	0.35	6%	5.62	5.44	0.18	3%
COP	(-)	1.1	0.95	0.14	14%	1.4	1.44	-0.04	-3%	1.78	1.91	-0.12	-7%

In this case the first 400 seconds were removed from the calculations as the model intialized. In the event, the system is operating without subcooling for the intial 3600 seconds. The subcooler was engaged at that time in the laboratory and similarly the modeled subcooler was changed to "on." The transition time was judged to be 1200 seconds from simulation time 3600 to 4800, and the post-change period was calculated from simulation time 4800 to 8000. Prior to the change, the MT compressor was running at full power and the power of the modeled and laboratory compressors agreed within 4%. The power of the MT compressor in the model decreased over a similar time period but the reduction was smaller in magnitude, and the MT compressor power was 12% higher in the post-change results. The LT compressor agreed closely in both

cases, within 2% before and 8% after. Figure 58 shows the MT and LT compressor power in the laboratory and simulation.

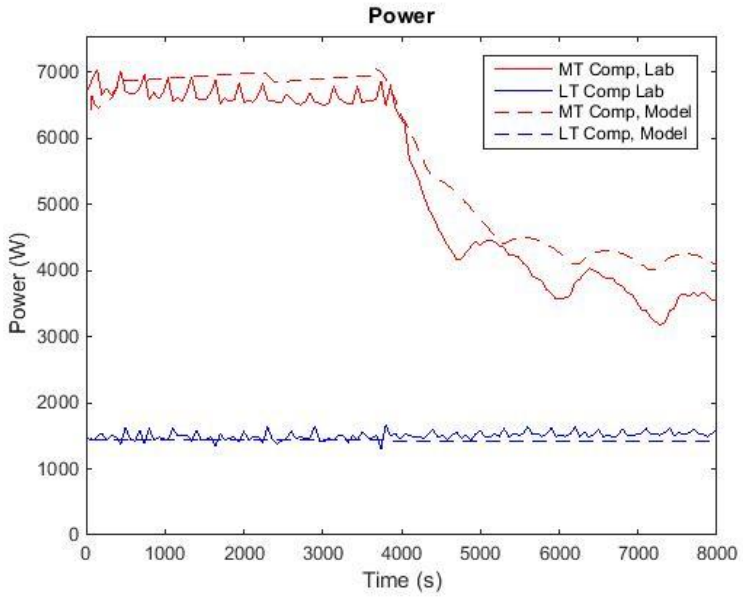

Figure 58 MT and LT Compressor Power for Laboratory (solid) and Model (dash) During Subcooler Off-On Test

The MT evaporator flow and capacity was higher in the model than the laboratory during the time the subcooler was off. With the compressor at full speed, this result is to be expected: the bypass flow requirement dictates how much flow is available to the MT evaporator (based on the total MT compressor flow). The MT evaporator flow and capacity in both cases are considerably less than the capacity with the subcooler running, and small differences in the refrigerant enthalpy returning to the flash tank would be expected to drive a difference in available capacity for the MT evaporator. The difference is much smaller after the subcooler turns on. These results are shown in Figure 59 and Figure 60.

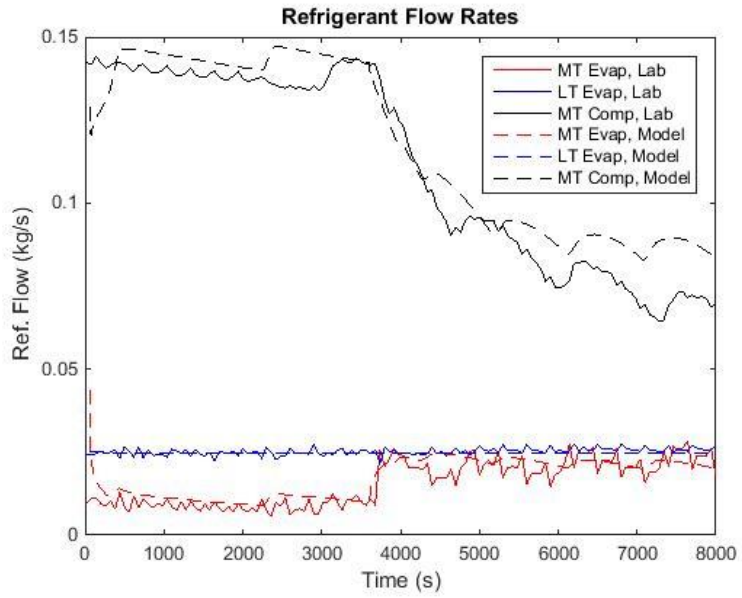

Figure 59 Refrigerant Flow Rates for Laboratory (solid) and Model (dash) for Subcooler Off-On Test

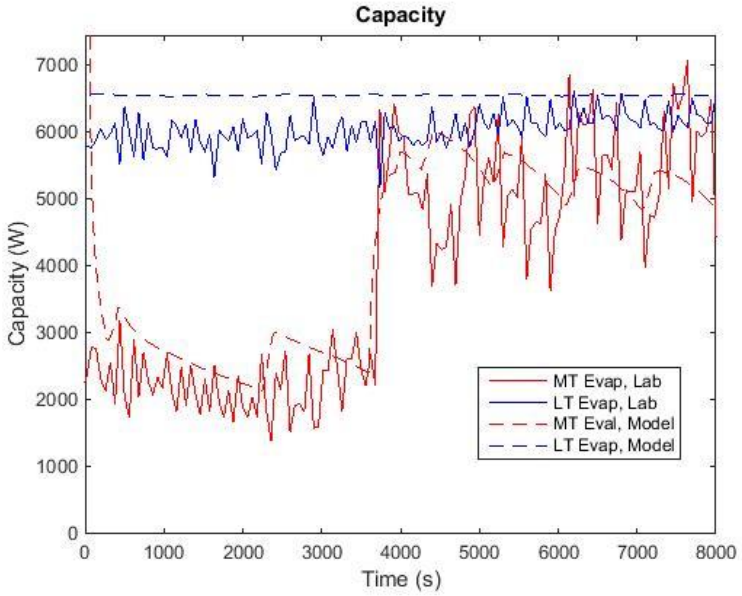

Figure 60 MT and LT Evaporator Capacity for Laboratory (solid) and Model (dash) for Subcooler Off-On Test

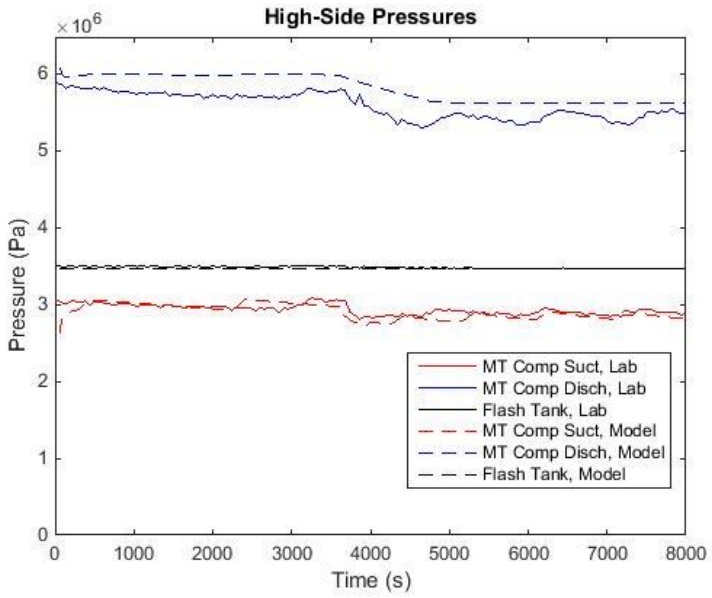

Figure 61 High-Side Refrigerant Pressure for Laboratory (solid) and Model (dash) for Subcooler Off-On Test

The pressures during steady operation agree well as in previous cases as they are set by user parameters. These are shown in Figure 61 and Figure 62. Interestingly, the laboratory and model results both show an increased MT compressor suction pressure as the subcooler is off and the MT compressor runs at full speed; the MT compressor is not quite able to satisfy the control set point for suction pressure at the test conditions until the subcooler turns on and reduces the bypass flow requirement.

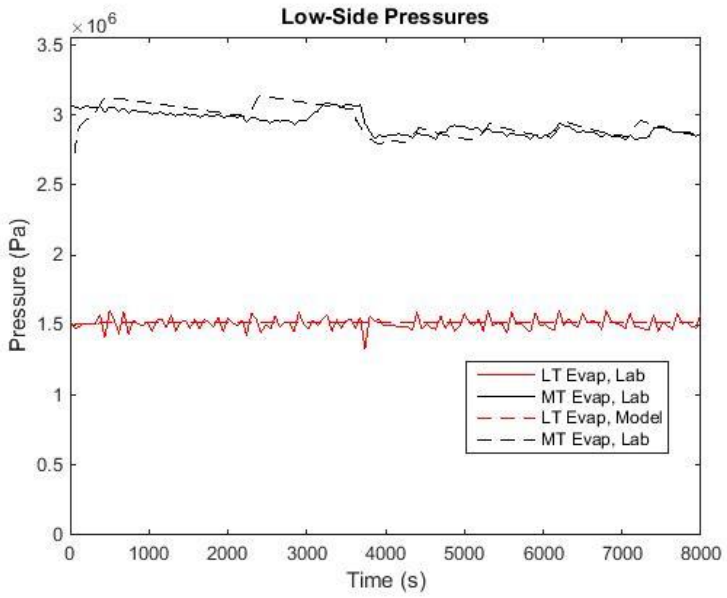

Figure 62 Low-Side Refrigerant Pressure for Laboratory (solid) and Model (dash) for Subcooler Off-On Test

COP, shown in Figure 63, agreed within 6% after the subcooler was on, and 14% before. During the transition period most variables agreed within less than 10%, except MT compressor power and MT evaporator flow, which were within 14% and 11% respectively.

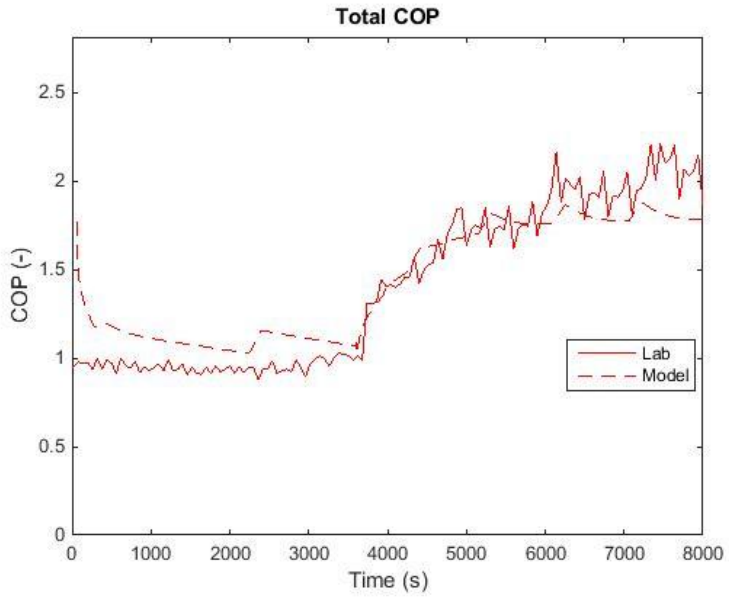

Figure 63 COP for Laboratory (solid) and Model (dash) for Subcooler Off-On Test

The results show good agreement in general for averaged values and with the system-level trends of power, capacity and efficiency; the average values for each stage across the three validation tests are shown in Figure 64. The model does not capture some of the short-term cycling in particular of the expansion valves, for example as observed in the MT evaporator refrigerant flow. The researchers observed that the simulation speed was significantly affected by PID control oscillations. Since the objective of the research is to capture system-level variations in behavior rather than optimize control of individual valves, the PID controls were not fine-tuned to capture these short-term variations.

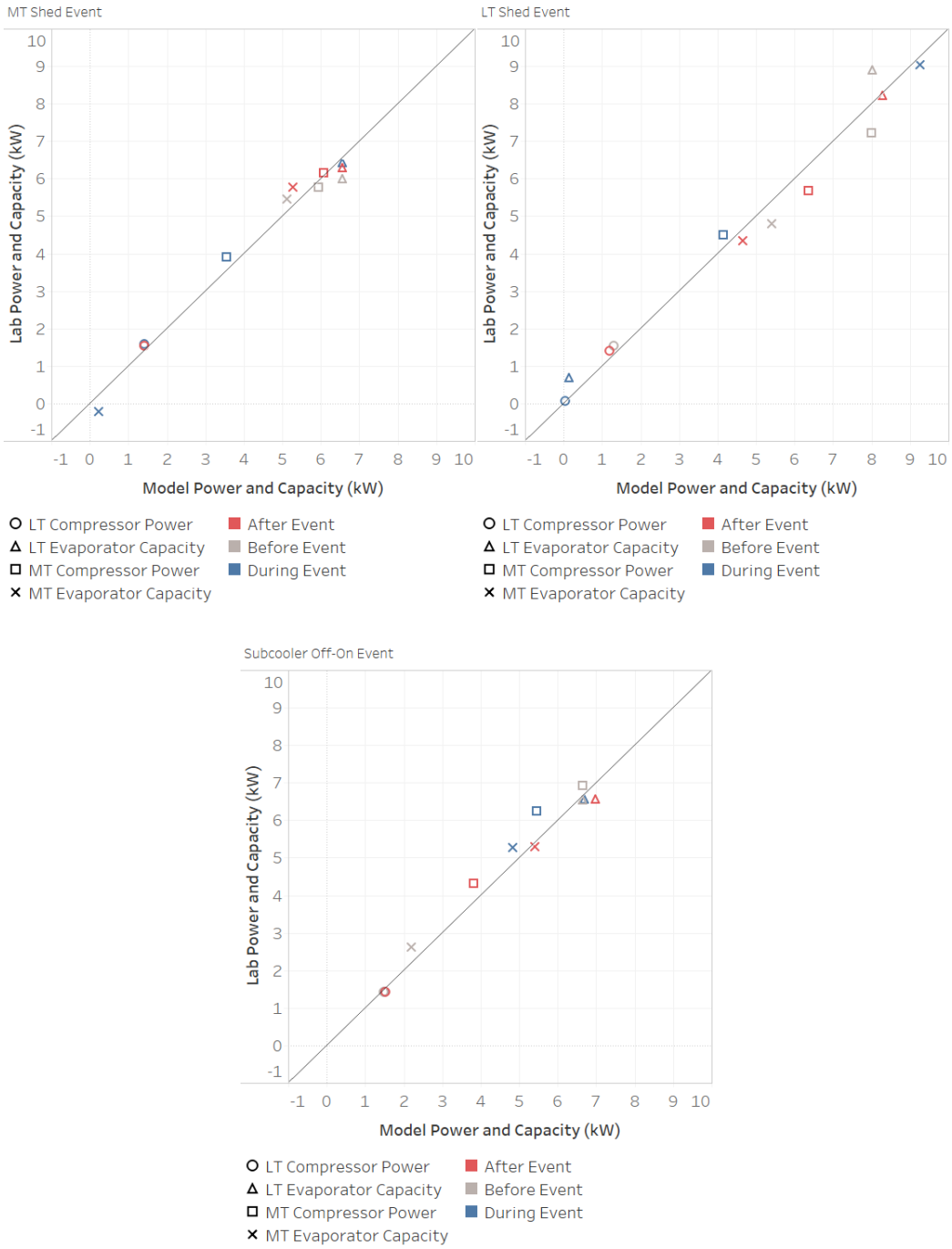

Figure 64 Summary Results of Transient Model Validation

Load Shed Simulations

The model was subsequently adjusted to perform parametric analysis. The simulated load banks were adjusted have fixed re-heat load (rather than "on-off"

control). In order to simulate a scenario where load and capacity can be varied on both the MT and LT loads, the LT compressor control was swiched from simple “on-off” control to variable compressor speed control using the same control logic as the MT compressor, including a compressor speed range of 550-1750 rpm. These changes allow the loads to be set, and adjusted to simulate the transient response of the rack to changes to either load. Simulations were then run of 30-minute “load shed” events to study how the system responds to load reductions of varied magnitude on either the LT or MT evaporator. To simulate a shed, the fixed re-heat capacity on the MT or LT load bank could be reduced, and the simulated volume of the load banks was significantly reduced to allow a quick response.

Two scenarios were evaluated. First, remaining close to the laboratory configuration, a one-to-one ratio of MT and LT loads was used. 6.0 kW of continuous re-heating load was selected as a near-match to typical laboratory conditions. Reductions of 1, 2, 3, 4, 5 and 6 kW were imposed on each evaporator load for a duration of 30 minutes, from the same initial conditions. In the second scenario, a two-to-one MT to LT ratio was simulated. In this case, 8.0 kW of MT load and 4.0 kW of LT load were simulated. Reductions of 0.5, 1.0, 1.5, 2.0, 2.5, and 3.0 kW were imposed on each evaporator load, again for 30 minutes.

An example of the system response is shown for a partial shed of LT load with 2:1 load ratio in Figure 65. The LT capacity reduction (shown with a blue dotted line) is met with a corresponding reduction of LT compressor power, and a larger reduction in MT compressor power. Since the MT compressor provides all heat rejection flow through the condenser/gas cooler, the reduction in heat rejection requirement manifests

in reduction in MT compressor work. For comparison, a shed of MT load with 2:1 load ratio is shown in Figure 66. In this case, the reduction in capacity of the MT evaporator is met with a similar reduction in power of the MT compressor, and the LT compressor and evaporator are unaffected.

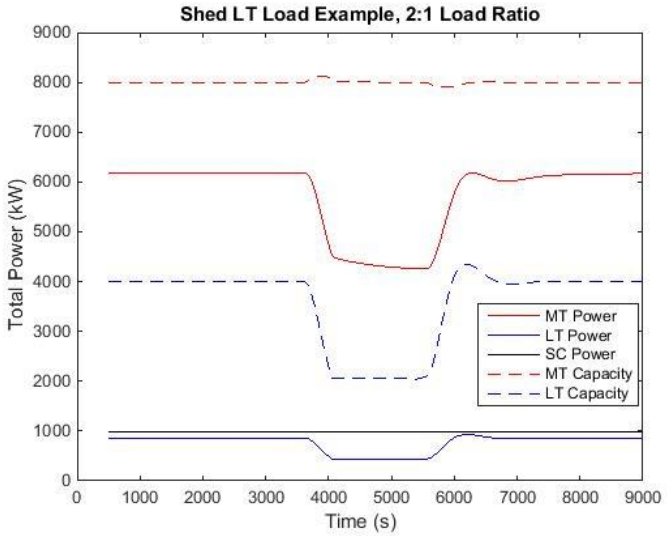

Figure 65 Example of Load Shed with 2kW Re-Heat Power Reduction on LT Evaporator, with 2:1 Load Ratio

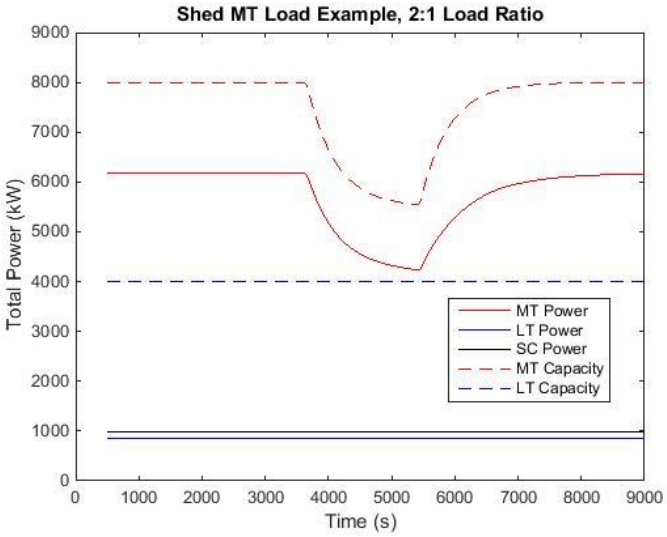

Figure 66 Example of Load Shed with 2kW Re-Heat Power Reduction on MT Evaporator with 2:1 Load Ratio

Closer inspection shows the impact of a load reduction on the cycle. For each of the cases discussed above, Table 13 shows some key operating conditions at simulation time of 3000 seconds (prior to the shed) and 5000 seconds (during the shed). The steady condition was the same for both simulations. While the combined capacity reduction is essentially the same in both cases, the total compressor power reduction is greater in the LT shed case. In turn, the total heat rejection required through the condenser and subcooler is less during the LT shed than the MT shed. The temperature of refrigerant leaving the subcooler was lower during the LT shed, leading to a lower refrigerant quailty (more liquid) to the flash tank from the subcooler. Since the LT compressor also discharges to the flash tank, the quality of refrigerant considering both returning flows (subcooler and LT compressor) can also be considered. The difference here is pronounced: in the pre-shed period, the total returning refrigerant quality is 0.455; during the LT shed it is 0.382, compared with 0.437 in the MT shed. This pronounced difference corresponds with a significant difference in the bypass flow ratio: in the steady-state condition the bypass flow percentage is 54.9%; it reduces to 54.1% during the MT shed, and to 45.5% during the LT shed. In sum, a reduction in LT capacity results in less bypass flow required at the MT stage than a reduction in MT capacity. With less flow required to provide heat rejection, the refrigerant returning from the subcooler produces slightly less flash gas, amplifying the overall reduction. This creates a greater power reduction per kW of shed load in the LT case than the MT case. A subtlety of the subcooler can also be noted. Considering the gas cooler and the subcooler, the gas cooler operates with a fixed entering air temperature, while the subcooler has roughly fixed power but the temperature of the subcooler fluid changes

in response to the reduced refrigerant flow. Because of this, the condenser capacity reduces more than the subcooler capacity in both shed cases.

Table 13 Changes of Key Parameters Before and During a Shed of 1 kW of MT or LT Load with Simulated 2:1 Load Ratio

		Before Shed	During LT Shed	Change	During MT Shed	Pct. Change
MT Evap. Capacity	W	8000	8001	0%	7051	-13%
LT Evap. Capacity	W	4000	3044	-27%	4000	0%
MT Comp. Power	W	6175	5153	-18%	5370	-14%
LT Comp. Power	W	853	646	-28%	852	0%
Subcooler Comp. Power	W	982	990	1%	987	1%
Condenser & SLHX Capacity	W	12714	10753	-17%	11183	-13%
Subcooler Capacity	W	6249	5887	-6%	5932	-5%
MT Evap. Flow	kg/s	0.033	0.033	0%	0.0291	-13%
LT Evap. Flow	kg/s	0.0151	0.0115	-27%	0.0151	0%
MT Comp. Flow	kg/s	0.0732	0.0606	-19%	0.0634	-14%
Bypass Flow	kg/s	0.0402	0.0276	-37%	0.0343	-16%
Quality - Subcooler to Flash Tank	-	0.3281	0.2704	-19%	0.2859	-14%
Quality - Combined to Flash Tank	-	0.4553	0.3824	-17%	0.4371	-4%
Ref. Temp. Leaving Subcooler	K	302.2	298.5	-1%	299.5	-1%

Simulations of different magnitudes of load shed were performed for each scenario (LT or MT evaporator shed and 1:1 or 2:1 load ratio). The purpose of these simulations is to quantify the benefit of a given capacity reduction in terms of power reduction, first for a load ratio similar to that tested in the laboratory, and then also for a situation in which there are more MT loads than LT loads. A summary of the results is shown in Table 14.

Table 14 Summary of Load Shed Simulation Results

	Total Capacity			Total Power			
Test	Before Shed (W)	During Shed (W)	(Delta) (W)	Before Shed (W)	During Shed (W)	(Delta) (W)	Ratio
Baseline, 2:1 LR	12000	12000	0	8010	8010	0	
LT Shed 0.5kW	12000	11574	426	8010	7485.2	524.8	1.23
LT Shed 1kW	12000	11144	856	8010	6968	1042	1.22
LT Shed 1.5kW	12000	10710	1290	8010	6484	1526	1.18
LT Shed 2kW	12000	10382	1618	8010	6158.7	1851.3	1.14
LT Shed 2.5 kW	12000	10282	1718	8010	6080.5	1929.5	1.12
LT Shed 3kW	12000	10196	1804	8010	6019	1991	1.10
MT Shed 0.5kW	12000	11642	358	8010	7713	297	0.83
MT Shed 1kW	12000	11283	717	8010	7425	585	0.82
MT Shed 1.5kW	12000	10924	1076	8010	7145	865	0.80
MT Shed 2kW	12000	10563	1437	8010	6882	1128	0.78
MT Shed 2.5kW	12000	10201	1799	8010	6636	1374	0.76
MT Shed 3kW	12000	9831	2169	8010	6393	1617	0.75

	Total Capacity			Total Power			
Test	Before Shed (W)	During Shed (W)	(Delta) (W)	Before Shed (W)	During Shed (W)	(Delta) (W)	Ratio
Baseline, 1:1 LR	12000	12000	0	8906	8906	0	
LT Shed 1kW	12000	11227	773	8906	7912	994	1.29
LT Shed 2kW	12000	10412	1588	8906	6970	1936	1.22
LT Shed 3kW	12000	9555	2445	8906	6096	2810	1.15
LT Shed 4kW	12000	9062	2938	8906	5624	3282	1.12
LT Shed 5kW	12000	8917	3083	8906	5520	3386	1.10
LT Shed 6kW	12000	8806	3194	8906	5452	3454	1.08
MT Shed 1kW	12000	11271	729	8906	8269	637	0.87
MT Shed 2kW	12000	10519	1481	8906	7667	1239	0.84
MT Shed 3kW	12000	9743	2257	8906	7119	1787	0.79
MT Shed 4kW	12000	8839	3161	8906	6539	2367	0.75
MT Shed 5kW	12000	8294	3706	8906	6289	2617	0.71
MT Shed 6kW	12000	7898	4102	8906	6188	2718	0.66

Figure 67 shows the reduction in total power corresponding to the reduction of LT load for a 1:1 load ratio. Each load reduction is shown with a different color; the load reductions indicated in the legend are the adjustment to the simulated re-heat power,

rather than the measured capacity (which is indicated in the results of Table 14). The power reduction in this case slightly exceeds the capacity reduction; this would be expected, since the efficiency of the low-temperature portion of the refrigeration load is low. The power reduction is limited in this simulation case to the minimum speed of 550 rpm. In these cases the simulated load is "over-cooled", and a slight delay can be seen before power increases again. Figure 68 shows the total power when shedding MT load. In this case the magnitude of power reduction is smaller for a given load reduction. Since the efficiency of MT refrigeration is relatively more efficient, this is to be expected. The power reduction is similarly limited to the minimum compressor speed.

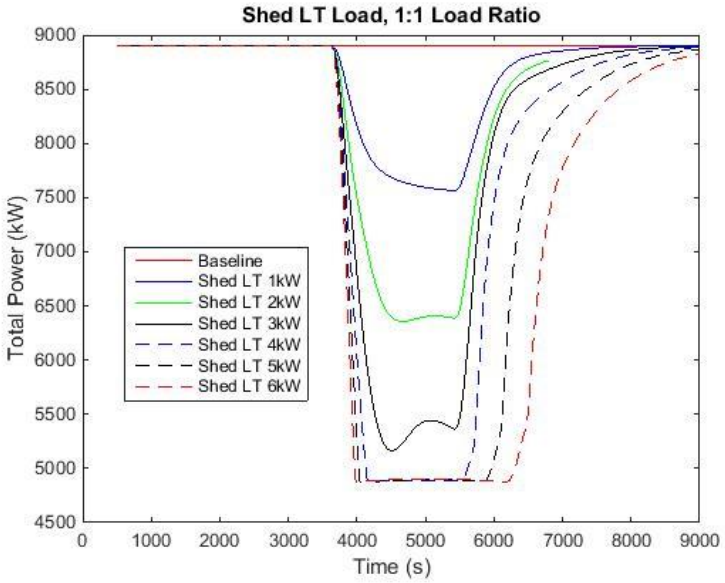

Figure 67 Total System Power with 30-Minute LT Load Shed with 1:1 Load Ratio

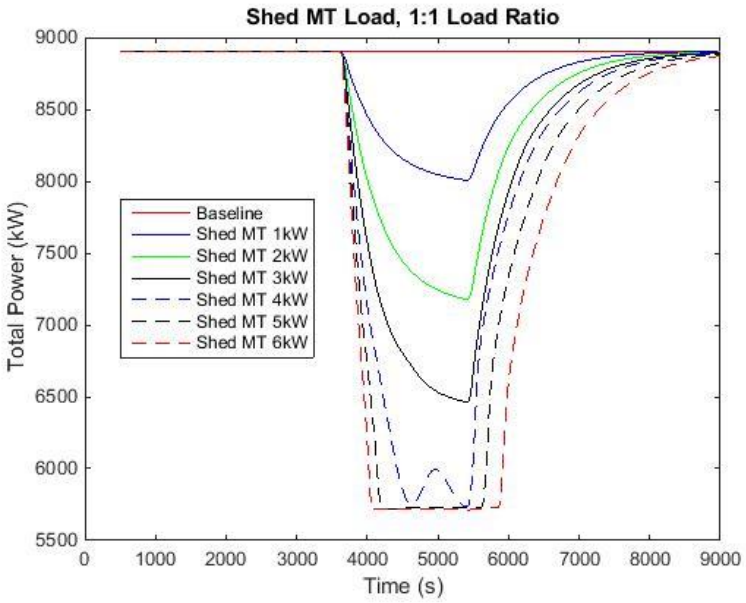

Figure 68 Total System Power with 30-Minute MT Load Shed with 1:1 Load Ratio

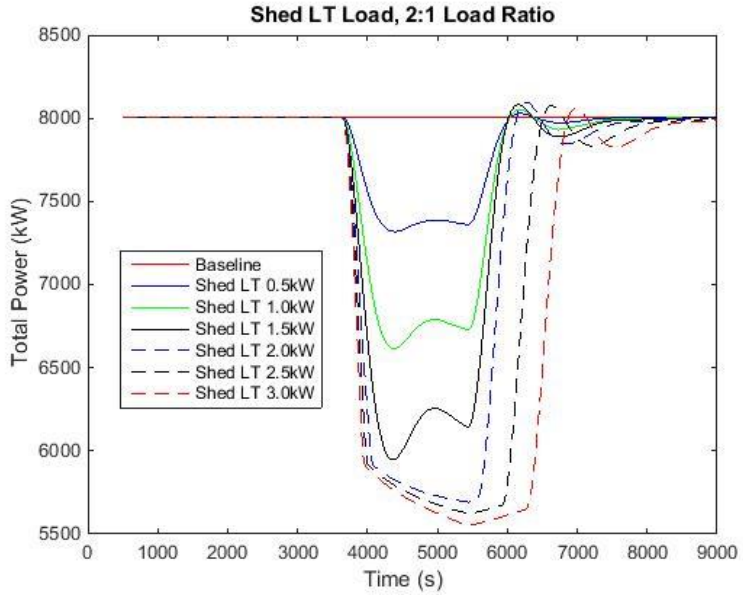

Figure 69 Total System Power with 30-Minute LT Load Shed with 2:1 Load Ratio

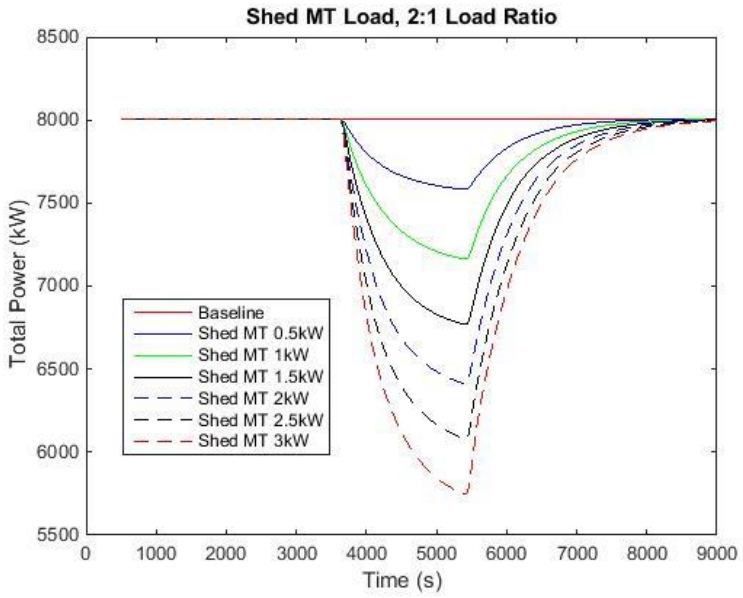

Figure 70 Total System Power with 30-Minute MT Load Shed with 1:1 Load Ratio

Figure 69 and Figure 70 show similar results for a 2:1 load ratio. Since the LT load is smaller in this simulation, the capacity reduction step size was reduced. However, again the reduction in total power is slightly larger than the reduction in capacity. With the MT load shed, the power reduction is smaller in magnitude.

Figure 71 shows the average, 30-minute reduction of power plotted against the average, 30-minute reduction in delivered capacity. The LT sheds are shown in blue and the MT sheds in red. The results show a significantly higher power reduction for a given capacity reduction when shedding LT load.

An important factor which is not captured in this chapter is the characterstics of the thermal mass in the refrigerated goods. The results here show the general response characteristics of a reduction of load on each suction group, but does not consider how the reduction in load is achieved (e.g., shutting off a certain number of display cases), nor the dynamic response of the load itself (rise in temperature of the product). This is examined in Chapter 7.

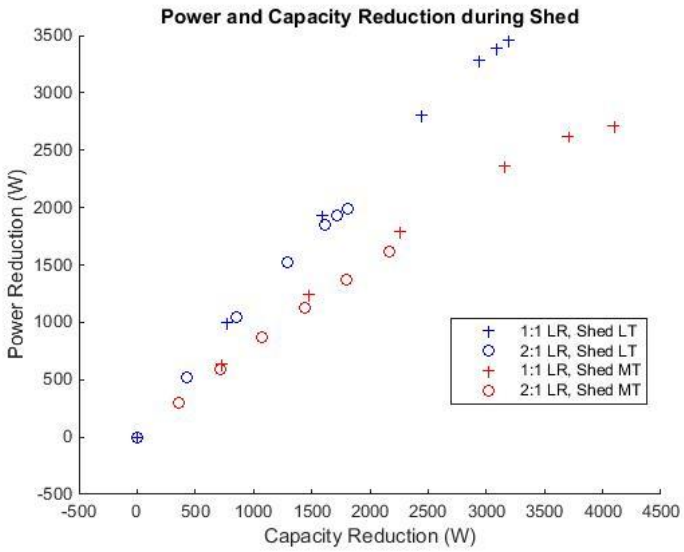

Figure 71 Average Power Reduction vs. Average Capacity Reduction during Sheds

Chapter Summary

This chapter introduces a Modelica-based transient simulation of the CO_2 transcritical booster cycle using dedicated mechanical subcooling. The model was developed and compared with laboratory tests of simulated load-shed events. In the laboratory tests, the full capacity of one evaporator stage was shut off for a duration of 30 minutes. The model validation results showed good agreement with laboratory results, particularly for the simpler MT shed where power and capacity agreed within 11% or less for all conditions before, during and after the simulated shed events. In the LT shed event the power and capacity agreed within 16% before, during and after the simulated shed.

Using the model to simulate load sheds, the interaction between the two stages can be observed. When shedding MT load, the LT stage is essentially unaffected. The MT compressor must still provide heat rejection for the low temperature evaporator stage,

as well as bypass flow to balance the flash tank. The power reduction per kW of load shed was 0.75-0.83 for a 2:1 MT to LT load ratio. Shedding LT load impacts both compression stages, and the power reduction per kW of capacity shed was higher, from 1.10-1.23 kW of power reduction per kW of shed load for the 2:1 load ratio. The relative reduction was higher with smaller shed. Shedding LT loads offers a bigger power reduction in return for a given load reduction. While this finding is intuitive, the authors believe this effort to be a novel exploration for the booster cycle. Subsequent research efforts should consider giving preference to the reduction of LT loads first as a way to provide the best demand reduction for a given capacity reduction.

Chapter 5: Load Modeling

This chapter describes the development and implementation of simulated display case models for transient modeling. There are numerous approaches documented in the literature. For demand response modeling, it is important to capture both the refrigerant-side behavior, as well as the load-side behavior such as product temperature increase during a shed event. The objectives of this effort are to:

- Identify an approach that captures load-side response with reasonable accuracy while minimizing computational complexity to allow faster simulations
- Develop appropriate component models to simulate realistic end-use loads with appropriate dynamic response to capture demand response behavior
- Identify appropriate load profiles for 24-hour simulation of supermarket conditions

Modeling Refrigerated Loads

At a high level, the modeling of refrigerated loads can be accomplished several ways ranging from black-box models, to semi-empirical gray-box approaches, to detailed physical models. The simplest approach would be with a simple black-box component with a user-specified heat load imposed on the refrigerant. This approach allows the user to impose any arbitrary load on the refrigerating system, and observe how the system responds to changes in load. This may be useful for understanding how the stages of the booster cycle interact (as discussed in Chapter 4). Polzot et al. (2016) use a model that could be described as black box, in that the heat flows are input from prior knowledge such as manufacturer specifications. The researchers were modeling thermal storage, but with the assumption that the load-side was not interrupted, therefore load and capacity did not deviate at each end-load, so this

approach was appropriate. However, the simplified fixed-load model omits many of the key details required to understand the control, response and limitations of demand response in detail if the load-side device is to be interrupted. Demand response necessarily includes considerations of the response of the load and limitations of critical parameters to allowable ranges. For instance in the case of a supermarket, different food products have different thermodynamic properties, and sensitivity to temperature deviations must be considered. The load itself dynamically changes as temperatures deviate, and the control of the hardware under demand response control is itself of interest. Therefore any models representing loads which are under demand response control should be more detailed than the black-box approach.

More detailed approaches incorporate some consideration for the interactions between refrigerant and air, air and refrigerated product, and the case itself and the ambient space. O'Connell et al. (2014) implemented a gray-box approach. This approach uses a series of stochastic differential equations tuned with measurement data; the complexity is adjusted by the number of states (e.g., refrigerant inlet temperature, outlet temperature, internal air temperature, food temperature) that are included in the model. The researchers used store measurement data, which included normal operation and defrost. Because of the requirement to tune the model with measurement data, this approach was ruled out.

Another approach is taken by researchers such as Glavan et al. (2016), Vinther et al. (2013) and Shafiei et al. (2013) adopt a simplified physical model of the hardware

and heat flows. These models incorporate energy balances between each thermal system, with parameters such as the heat capacity of the food as model inputs. The researchers apply different approaches to modeling the refrigerant-side components, frost formation, and disturbances, but derive their efforts from a similar form. The overarching model approach is visualized in Figure 72.

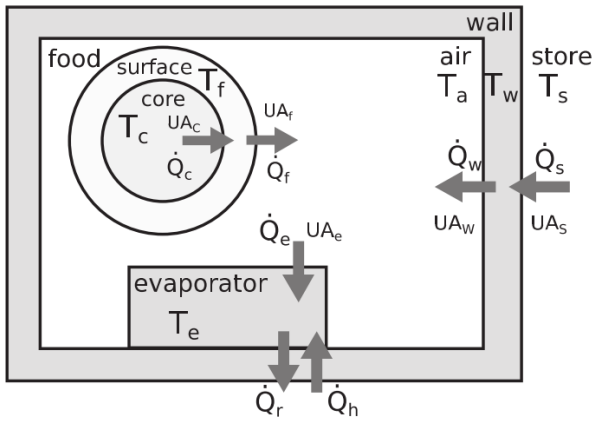

Figure 72 Schematic of the Simplified Physical Model Approach to Display Case Modeling (Glavan et al. 2016).

The advantage of this simple physical model is that it is easily adopted to Modelica, and existing heat exchangers models can be readily incorporated. Therefore, a version of the simplified physical model approach was adopted for this work.

Display Case Model Development

The method applied here is derived from the approach taken by Glavan et al. (2016), Shafiei et al. (2013), and others. This model approach was selected for providing sufficient detail to capture transient changes to model variables, while having low computational burden to allow reasonable simulation times. The model was adapted

to interact with the refrigerant control volume and heat exchanger architecture already developed in Modelica. The model is described here.

The display case is modeled as consisting of two primary masses: the mass of the food products inside the case, and the mass of the case itself. Each is treated as a lumped-temperature mass with parameters which may be set and adjusted by the user. The following equations describe the energy balances:

$$Mc_{p_{food}} * \frac{dT_{food}}{dt} = -Q_{food-case}$$

$$Mc_{p_{case}} * \frac{dT_{case}}{dt} = Q_{case-ambient} + Q_{food-case} + Q_{evap} + Q_{defrost} + Q_{usage}$$

The value of Q_{usage} is an input used to simulate customer interaction loads, and is described in a subsequent section. The value of $Q_{defrost}$ is an input from the user (as defrost for the LT cases is electric resistance heat, and for the MT cases the defrost power is zero as forced-off-cycle defrost is used). The value of the case load is calculated as:

$$Q_{case-ambient} = UA_{case-ambient} * (T_{ambient} - T_{case})$$

And the value of the heat transfer between the food and the case is

$$Q_{food-case} = UA_{food-case} * (T_{food} - T_{case})$$

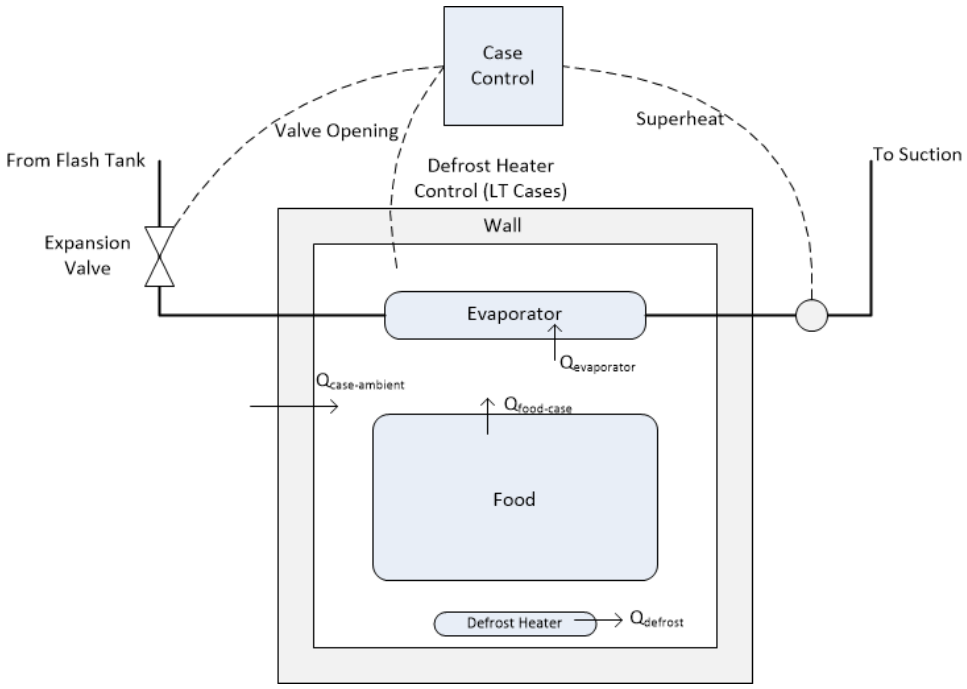

Figure 73 Schematic of the Model Configuration for Display Case Modeling

A simplifying assumption applied here is to replace the terms for door openings, air infiltration, and product removal and addition with a general usage term. The term Q_{usage} in the above description is used to simulate case interaction that comes from normal store operation. The loads on cases vary in time, particularly as customers and employees interact with them. In order to capture the time-dependent nature of external loading on the cases, the measured, normalized loads observed by Heerup and Fredslund (2016) were adopted here. Simulations of each case showed a baseline ambient loss of 700 watts for each MT case and 760 watts for each LT case. This was used as the baseline load, equal to the total load during overnight hours where it is assumed there is no external interaction with the case. The external load is then calculated as additional load based on the relative loading measured by Heerup and Fredslund; a modification is made by removing the defrost load from this calculation,

since defrost is modeled separately. The loads as a fraction of nameplate load from Heerup and Fredslund is shown in Figure 74.

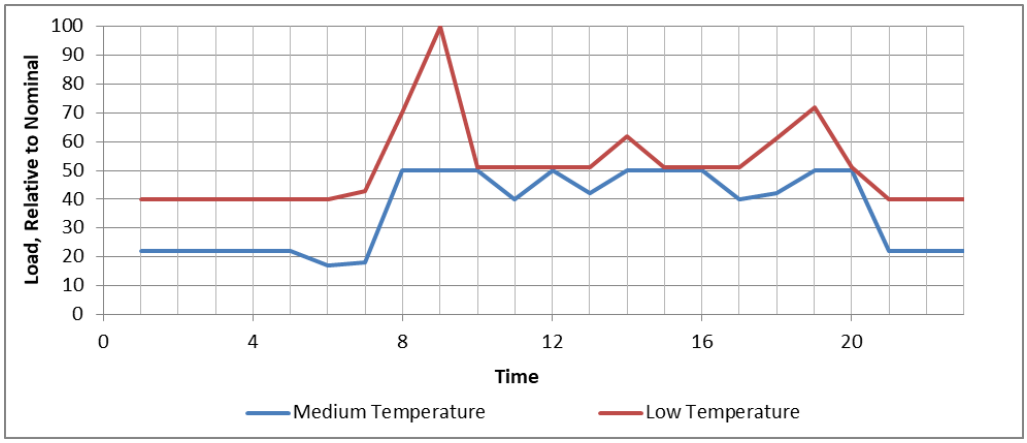

Figure 74: 24-Hour Refrigeration Loads, Relative to Nameplate Capacity, Reproduced from Heerup and Fredslund (2016)

Normalized to the baseline loads of the modeled MT and LT cases, the auxiliary loads are shown in Figure 75, which shows the external load on the case in addition to the baseline. From these values, two further adjustments were made. The defrost effect in the LT load profile was removed (as defrost is handled separately) and for each refrigeration level, two cases were modeled, with 15% higher or lower external loads. These higher and lower loads may represent more and less frequently used cases, for example.

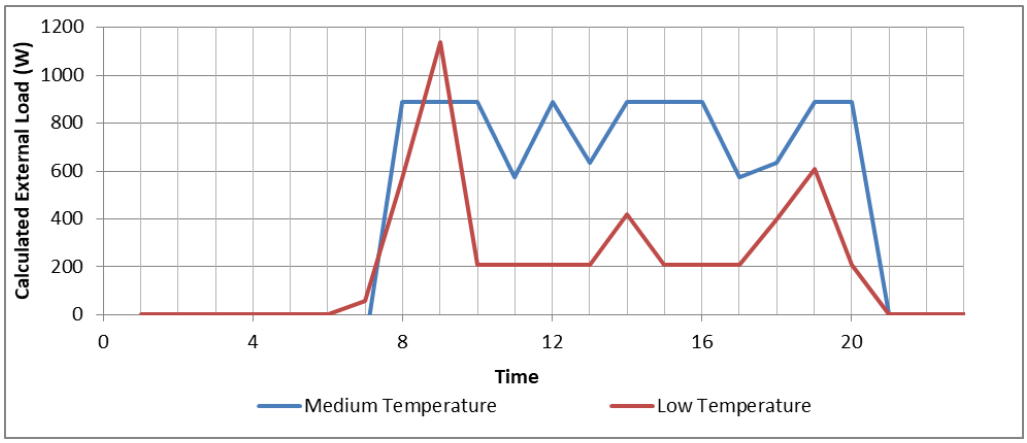

Figure 75: Calculated, External Loads on MT and LT Cases Calculated From Relative Loads

The above changes lead to a new external load profile shown in Figure 76.

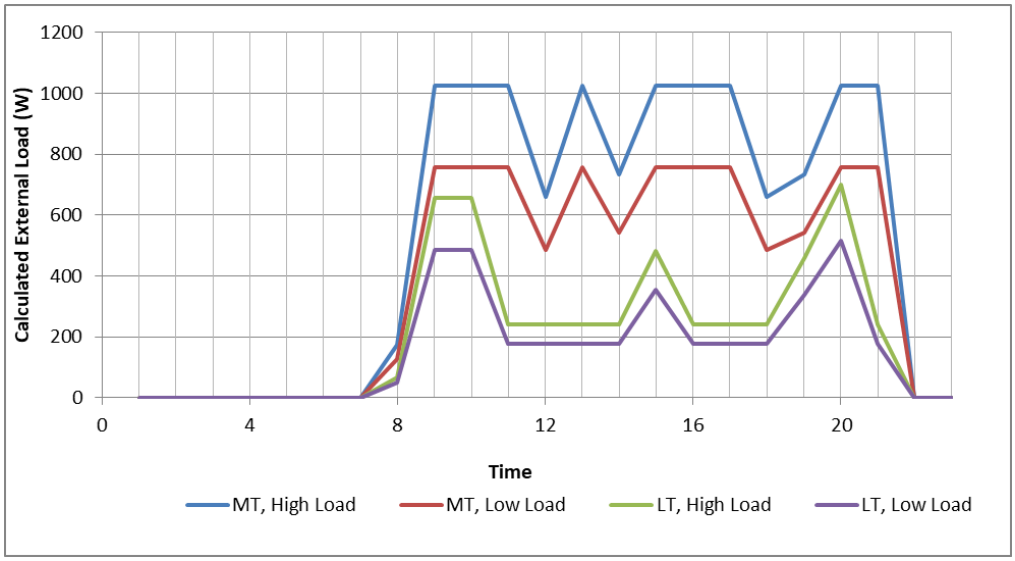

Figure 76 External Loading Used for Simulations

An additional external load is defrost. The defrost approach is different for each of the refrigeration groups. For the LT cases, an electric resistance defrost is used; in this case, the refrigerating capacity is shut off and a 1-kW electric resistance element is modeled (simulated as an external, 1,000 watt load). For the MT cases, an off-cycle defrost is used; in this case, the refrigerating capacity is shut off and the case allowed

to naturally warm. Two cycles per day at thirty minute duration were selection for each stage.

Evaporator modeling uses the same approach to the heat exchanger components described in Chapter 4. The *SingleNode* heat transfer component incorporates the geometry and materials of the evaporator pipe; the *FiniteVolumeFluidCV* component is used for calculating refrigerant properties and flows as described in Chapter 4. The other port of the *SingleNode* component connects to the *DisplayCaseBody* component, which contains the display case energy balances described above.

The parameters for the display cases were derived from Shafiei et al. (2013) and are described in Table 15.

Table 15 Display Case Parameters Derived from Shafiei et al. (2013)

	$UA_{case\text{-}ambient}$	$UA_{food\text{-}case}$	$M*Cp_{case}$	$M*Cp_{food}$	$T_{ambient}$
MT Cases	41.9	72.9	$1.9*10^5$	$4.6*10^5$	19.85
LT Cases	21	36	$9.5*10^4$	$2.3*10^5$	19.85

An example of the case model operation is shown in Figure 77, which shows the case temperature and food temperature (left) and delivered refrigerating capacity (right). In this example scenario, the case capacity is shed for a short period and then returned. The case air temperature increases rapidly, with the food temperature slowly increasing after. The air temperature increases approximately 6.7°C during the 20 minutes that capacity is interrupted; in this time the food temperature increases by

0.6°C. The food temperature continues to increase after capacity is returned, until the air temperature drops below the food temperature.

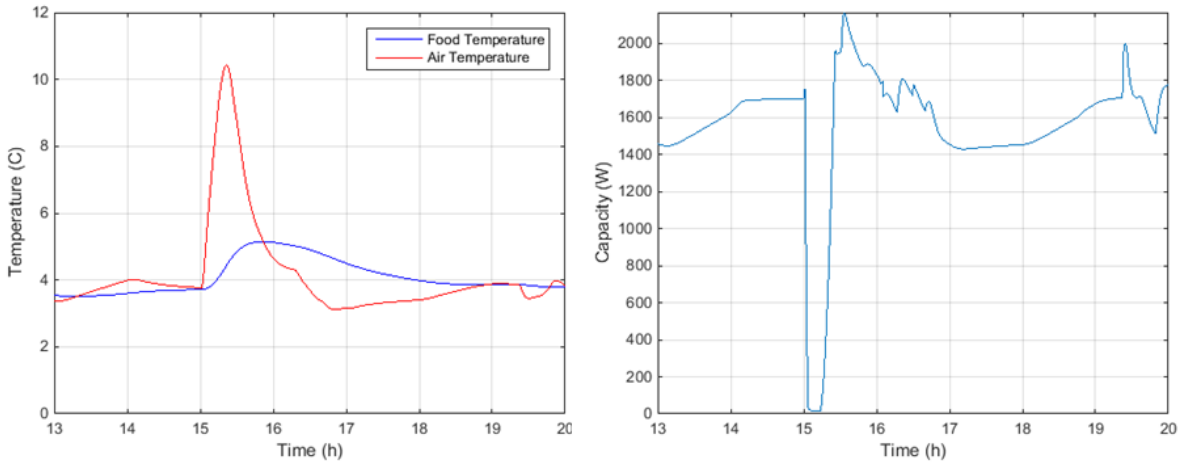

Figure 77 Case Temperatures and Capacity

Figure 78 shows the refrigerant pressure and refrigerant mass flow rate during this period. The pressure drops quickly when capacity is interrupted, before increasing (compressor speed adjusts to compensate). There is a second capacity shed on the other display case (not shown) thirty minutes after the beginning of the case shown here; this explains the second drop in pressure. The pressure drop is equivalent to approximately 1.3°C saturated suction temperature difference, from a starting saturated suction temperature of -6.7°C.

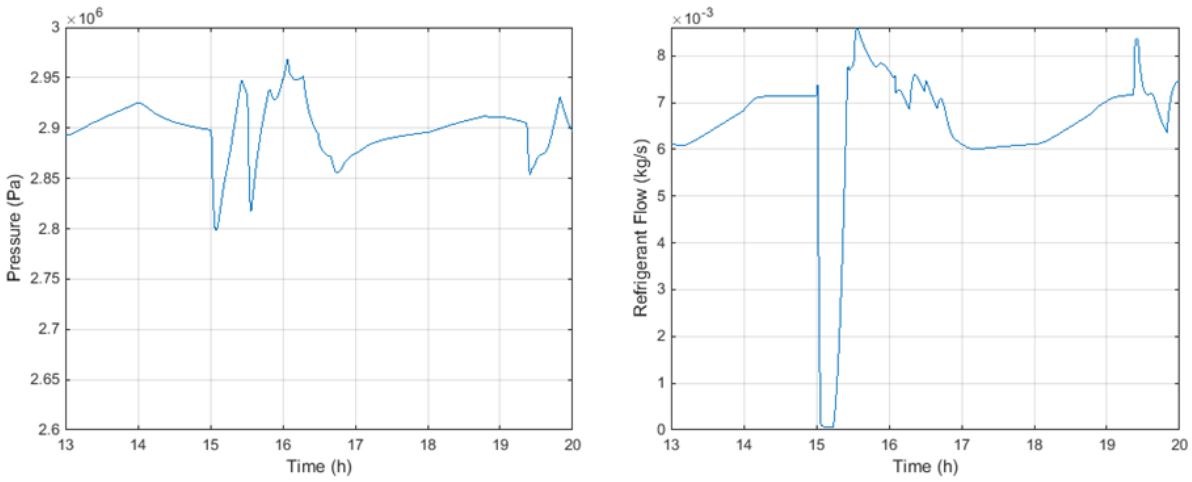

Figure 78 Suction Pressure and Refrigerant Flow

Chapter Summary

This chapter describes the development of load-side models of display cases, and an external loading strategy used to simulate the in-store interactions imposed upon cases in normal operation. A simplified modeling approach is used where the food and air are each treated as lumped parameter masses interacting with each other and, through the case walls, the ambient environment. The approach selected is computationally simple, avoiding significant simulation slow-down, while still providing a representation of the condition of the air and food in the case to allow further modeling developments to consider those parameters in control.

Chapter 6: Thermal Storage Implementation

This chapter describes the modeling of phase change materials for thermal storage integration into the refrigeration cycle. The objectives of the PCM modeling effort are to identify and develop a method that is versatile enough to incorporate a range of PCMs quickly and simply, while reflecting the physical behaviors of true PCMs with reasonable accuracy. Since the effort hinges upon integrating the PCM model into an already-complex and computationally-intensive model, computational simplicity is an important criterion. The work described in this chapter is intended to:

- Identify an approach to modeling PCM thermal storage systems that allows integration to the larger supermarket refrigeration system model with adequate accuracy and minimal computational complexity
- Develop appropriate component models and, using available data in the literature, verify that the model provides reasonable replication of critical behavioral characteristics

Approaches to Modeling PCM Thermal Storage

Models of phase change thermal storage systems are abundant in the literature. The primary difference in the modeling approaches is whether or how to incorporate both the convective and conductive processes of phase change. The most detailed models include convective and mass transfer phenomena. To reduce complexity, many researchers simplify the calculations by combining these into a single equivalent conductive heat transfer value and using a lumped-parameter approach. The accuracy of these models is generally still sufficient, especially for high-level integration studies. Wang et al. (2007) described the advantages of lumped-parameter models,

but pointed out that some detail is missed in terms of subcooling and superheating of the material. However, for the purposes of this effort, where different PCMs are desired to be tested with the goal of assessing system level impacts, this trade-off is acceptable.

Wang et al. describe various, similar approaches to PCM system modeling. An interesting approach was taken by Leonhardt and Muller (2017) using Modelica. In this case an energy balance is performed on a discretized volume of phase change materials, and the thermal properties of the PCM are approximated into two equations describing the enthalpy-temperature relationship and the heat capacity of the material. An example calculation of these properties is shown in Figure 79.

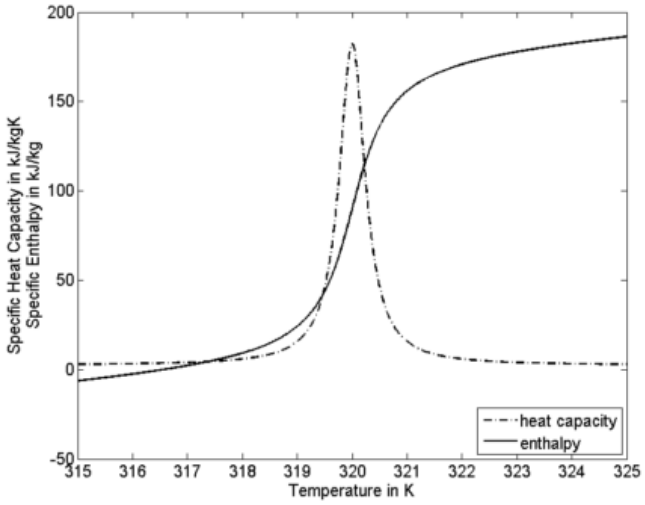

Figure 79: Example properties of PCM as Calculated Using the Method Described in Leonhardt and Muller (2017).

This approach is attractive in its simplicity, but a more accurate description of the properties can readily be adopted using a property table as described below.

A similar approach is that used by Dhumane et al. (2017). In this approach, the enthalpy-temperature relationship is tabulated and read into Modelica using the *CombiTable1D* component. The other properties are input as parameters of the model. The advantage of this approach is that any arbitrary PCM can be incorporated into the model by simply changing the source table and property parameters, and the table may include any resolution of detail. This approach was used as a basis for the model developed here.

Thermal Storage Model Development

To satisfy the objectives of flexibility and limited computational complexity, a lumped-parameter approach was selected which significantly reduces complexity by removing the need to model mass flow from convection. The approach is similar to that adopted by Dhumane et al. (2017). The PCM component is described as follows. The system is modeled as a cylindrical storage tank. The tank is broken into six nodes in the vertical axis. At each node an energy balance is calculated:

$$m_{node} * \frac{dh_{node}}{dt} = Q_{evap,node} + Q_{ambient,node} + Q_{cond,node}$$

Where:

$$Q_{evap,node} = HTC * A_{HX,node} * (T_{HX\ wall,node} - T_{PCM,node})$$

$$Q_{ambient,node} = U_{tank} * A_{HX,node} * (T_{ambient} - T_{PCM,node})$$

$$Q_{cond,node} = k * \frac{A_{cond}}{L_{Node}} * \left(T_{PCM,node+1} - T_{PCM,node}\right) + k * \frac{A_{cond}}{L_{Node}} * (T_{PCM,node-1} - T_{PCM,node})$$

The relationship between temperature and enthalpy is calculated from material properties from a variety of sources (Sharma et al. 2009, Oro et al. 2012) using the relationships:

$$h(T) = \begin{cases} c_{p,solid} * \left(T_{pcm} - T_{sat,solid}\right) + h_{sat,solid} & T < T_{sat,solid} \\ 0 & T = T_{sat,solid} \\ h_{l-s} & T = T_{sat,liquid} \\ c_{p,liquid} * \left(T_{pcm} - T_{sat,liquid}\right) + h_{sat,liquid} & T > T_{sat,liquid} \end{cases}$$

The PCMs investigated here are tabulated in 16. The materials were selected to represent a range of phase change temperatures, which is expected to in turn provide a range of subcooling capacity to the cycle when in use. The average density of the liquid and solid phase was used, and so volume change is neglected.

Table 16 Summary Properties of Phase Change Materials used in Simulations

Material	Density (kg/m^3)	Latent heat of phase change (kJ/kg)	Specific heat (kJ/kg K)	Melting Phase Change Temperature (°C)
Fatty acid with pentadecane 50:50 (PCM5050) [1]	839.1	157.8	2.44 (s) 2.89 (l)	10.2
Single paraffin wax $C_{14}H_{30}$ [2]	760	230	1.68 (s) 2.18 (l)	6
Single paraffin wax $C_{13}H_{28}$ [3]	756	154.5	1.68 (s) 2.18 (l)	-5.3
Water	956.4	334	2.05 (s) 4.22 (l)	0
1: Li et al. (2012)				
2: Kouskou et al. (2010)				
3: Li et al. (2013)				

An important simplifying assumption is that the heat transfer within the PCM can be described by a combined heat transfer coefficient and the behavior within the PCM is uniform. The heat transfer coefficient of the PCM was selected as 65 W/m^2-K, which was calculated from results presented in Tay et al. (2012).

The heat exchanger geometry approximates an ice-on-coil or similar heat exchanger system with a long length of pipe coiled within the tank, creating a relatively large heat transfer surface. The heat exchanger is itself modeled as a linear approximation of this with the length of heat exchanger per node of the storage tank calculated as

$$L_{node} = \frac{L_{total}}{n}$$

Like the display case models, this model approach allows integration with other existing components in the CEEE Modelica library. The *SingleNode* component describes the pipe geometry and heat transfer between the brine, the pipe wall and the PCM. The *FiniteVolumeBrineControlVolume* component calculates the brine properties and flows.

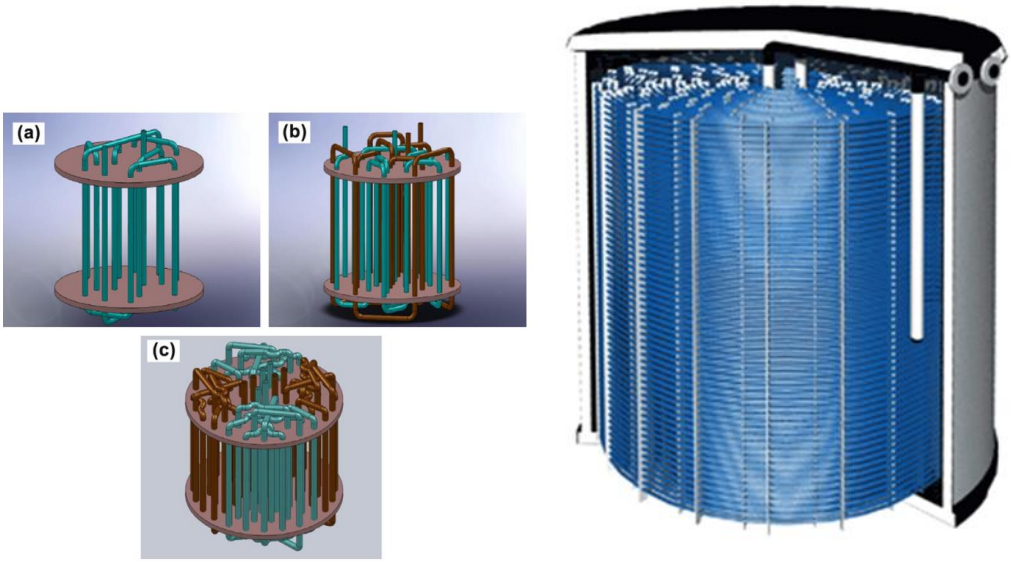

Figure 80 Example schematic of a PCM tank with PCM-on-Tube Heat Exchange (Tay et al. 2012) and a Typical Ice Storage Tank (Calmac)

The relatively low heat transfer rate between the PCM and the working fluid is one of the main challenges for PCM systems. To overcome this barrier a large heat transfer surface area is required. In typical tube-in-tank approaches this is accomplished by using a densely-packed tube array in the tank, such as pictured in Figure 80. With a long length of tube it is possible to use a lower-cost, resilient material such as polyethylene. The material properties of copper were used in this effort.

The PCM storage tank model is implemented into the subcooler-to-main-cycle brine circuit; the control allows the following operating scenarios:

- The R134a subcooler heat exchanger and CO_2 subcooler heat exchanger are engaged, the PCM is disengaged. This is the baseline operating mode.

- The R134a subcooler heat exchanger and PCM are engaged, the CO_2 subcooler heat exchanger is disengaged; this is the "charge" mode.
- The R134a subcooler heat exchanger is disengaged, the CO_2 subcooler heat exchanger and PCM are engaged. This is the "discharge" mode.
- All are disengaged. This is the "off" mode.

Thermal Storage Model Verification

In order to verify that the thermal storage model provides a reasonable approximation of real physical behavior, two scenarios were replicated from Tay et al. (2012) and an additional scenario from López-Navarro et al. (2014) using the PCM model developed here.

In Tay et al. the researchers provided experimental results for a similar configuration of PCM-containing tank, using a -27°C phase change material (referred to as PCM-27) for melting evaluations, and water (referred to by the authors as PCM0) for freezing evaluations. The properties of the -27°C material were estimated based on results of Tay et al. (2012) and Trp (2005), who performed prior analysis of a similar system and PCM. Tay et al. also provides geometry for the tank and heat exchanger, which were replicated as inputs to the model of the PCM. For one experiment with each phase change material, the results are shared with both the heat transfer fluid inlet and outlet temperature as well as the temperature measured at nine points inside of the tank, at three heights and an inside, middle, and outside tank location. For the PCM-27 evaluation, a run with a total of 5.46 m of tube is run with full results shown, and for the PCM0 test, a run with 23.83 m of tube is run with full results shown. The

tank is 0.35 m tall and 0.29 m in diameter. The tube used for heat transfer fluid is 0.01 m in diameter. The material is polyvinyl chloride. The system under test is shown in Figure 81.

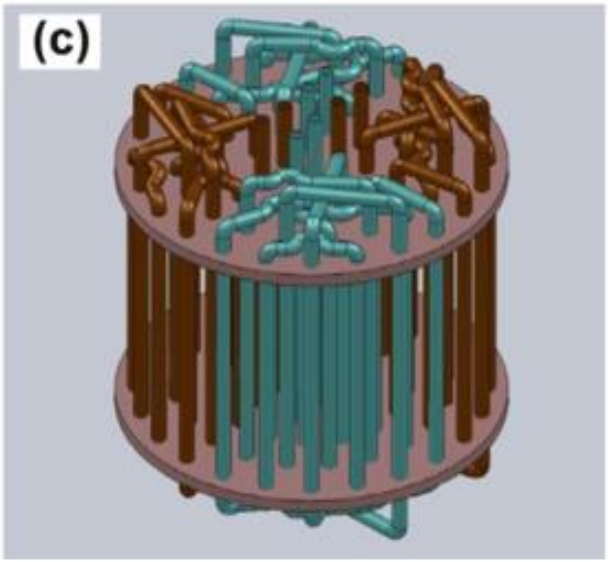

Figure 81: PCM Tank System from Tay et al. (2012)

Each of these geometric parameters were replicated using Modelica, as well as the properties of the heat transfer fluid as described by the authors. The results are shown in the figures below. For the Modelica model, the node temperatures represent lumped volumes with geometric centers which were at slightly different locations than the measurement locations described in the laboratory evaluation; all six of the modeled nodes are shown. The laboratory results are at locations approximately between modeled nodes 2-3, 3-4, and 4-5. For each effort, the starting temperature of the PCM and heat transfer fluid were estimated visually from the graphed results of laboratory testing and input to the model as starting conditions. In the case of the PCM-27 material, the density was calculated based on measured data reported in the

paper, to match the mass of PCM between the model and test results. The latent heat of phase change was also replicated from the values reported; the specific heat and conductivity were estimated based on other PCMs with similar phase change temperatures from Li et al. (2013) and Oró et al. (2012). Observation from the results reported also suggested a melting temperature range of approximately -27°C to -22°C. For water, 1.0°C to 0.0°C was used for phase change. In all three simulations, the simplified, constant heat transfer coefficient of 65 W/m^2-K is used.

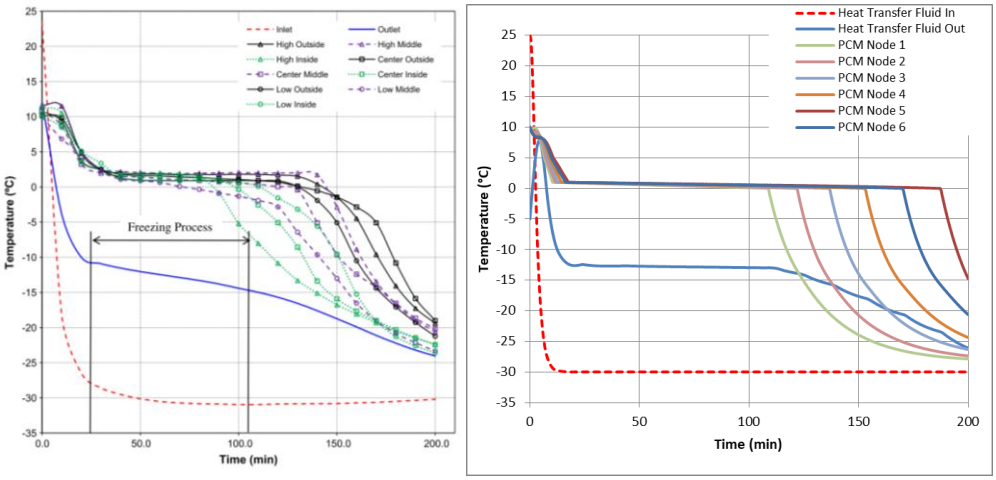

Figure 82 PCM Melt with PCM-0 Material (Tay et al. 2012)

The laboratory test case using water as the PCM is shown in Figure 82 with the simulated result. The results of the laboratory test, on the left, show a freeze process lasing approximately 80 minutes, which the authors indicate on the graph based on the approximate time the first measured regions in the tank begin to rapidly decrease below the phase change temperature. The lower portion solidifies first, followed by the middle and upper nodes; there is some variation between the inside, center and outside locations. The ending temperature after 200 minutes is between approximately -18°C and -24°C. The model shows reasonable behavioral similarity,

with the nodes crossing through the two-phase region and solidifying in sequence, and an ending temperature in the range of -25°C to -30°C. In the simulated case, the time to freeze was slightly longer, and the temperature difference between inlet and outlet of the heat transfer fluid remained constant while the temperature difference gradually decreased in the laboratory experiment. This likely reflects a difference between a heat transfer coefficient which is treated as constant in the model, and the real-world decrease in heat transfer that occurs as ice forms around the coil.

The results of the validation effort are shown in Figure 83 for the PCM-27 case. The results on the left show the laboratory result, which shows the upper portion of the tank appearing to melt first at approximately 150 minutes, followed by lower nodes melting beginning at approximately 250 minutes. The ending temperature after 450 minutes was approximately 5°C to 12°C. The model results, to the right, again show similar behavior.

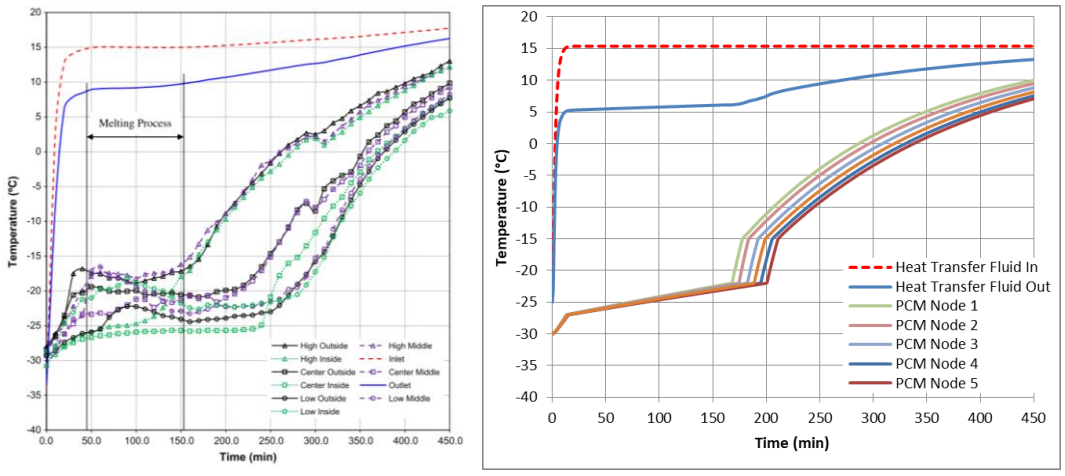

Figure 83: PCM Melt with PCM-27 Material (Tay et al. 2012)

The López-Navarro et al. (2014) test used a stainless steel-body tank with copper coil, which consists of eight sections each 13.3 m in length and 0.016 m outside diameter. The volume of PCM is 0.235 m^3; the author states that 0.032 m^3 of the material is in a center portion not in direct contact with the coils. A commercial PCM, Rubitherm 8, is used. The PCM temperature-enthalpy properties are documented with a polynomial fitting curve for heating and cooling. The heating and cooling curves are quite similar, and the cooling curve is used here. The curve is described by:

$$h_{cooling}(2°C \leq T < 8.1°C)[\frac{kJ}{kg}] = 2.6080 * 10^{-3} * T^6 + 2.7400 * 10^{-2} * T^5 - 1.6791 * T^4 + 1.9583 * 10 * T^3 - 1.0030 * 10^2 * T^2 + 2.5611 * 10^2 * T - 3.7774 * 10^2$$

$$h_{cooling}(8.1°C \leq T < 16°C)[\frac{kJ}{kg}] = 1.6113 * T - 22.705$$

The system under test is shown in Figure 84.

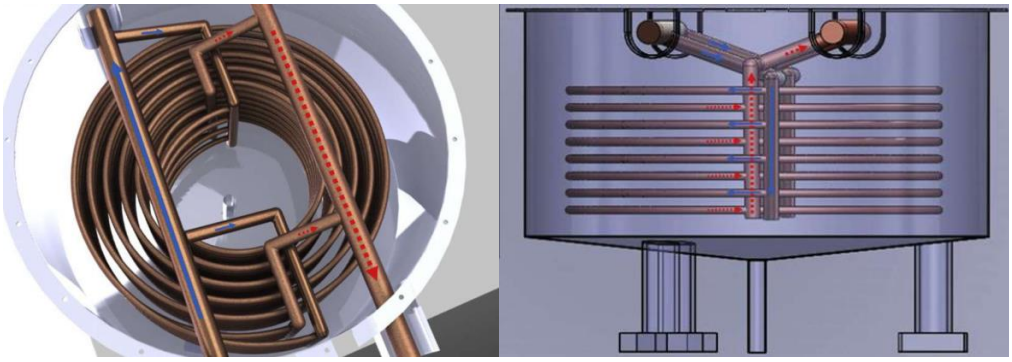

Figure 84: Images of the PCM Tank Configuration from López-Navarro et al. (2014)

The results of the simulation are shown in Figure 85. The laboratory test results start at time = 50 minutes, and the cooling begins at approximately time = 70 minutes. In

both scenarios, there is an approximately 30-minute period of sensible cooling (with rapid temperature decrease) followed by approximately 420 minutes of latent cooling with ending PCM temperatures in the range of approximately 1.0°C to 2.25°C in the laboratory case, and approximately 1.75°C to 2.75°C in the simulation case. One element captured in laboratory testing which is not reflected in the model is the temperature of the PCM far away from the heat transfer tubes, which stays nearly constant above 8°C after the initial cooling period; since the modeled case assumes all of the mass together as lumped-sum blocks, this area of warmer PCM is not reflected. This also provides some explanation for the slightly slower cooling and higher end-temperature of the modeled case.

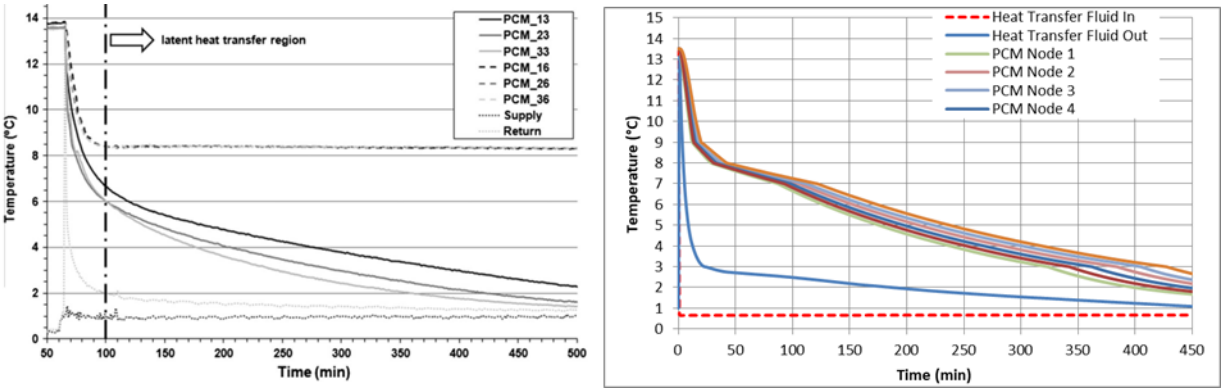

Figure 85 PCM Freezing with PCM8 (López-Navarro et al. 2014)

The results of the model verification effort show that the simplified thermal storage model applied here provides a reasonable approximation of behavior of a PCM system, with the same model and simplifying assumptions applied to two different tank configurations, one with two PCMs (water and PCM-27) and another with a third separate PCM (Rubitherm 8) with widely different phase change temperatures and properties. The laboratory tests of the first two cases show full transition from

single phase, through transition, to single phase with a long period of single-phase heating or cooling after the transition; in both simulations, the approximate time to pass through phase change and the beginning and ending conditions are similar, though the model shows much more orderly transitions and tighly-bunched temperatures within the PCM, and does not fully capture the change in heat transfer as the make-up of two-phase PCM changes. The third case shows a different system and the agreement is good between model and laboratory; the model does not capture an area of the tank in the laboratory that was far removed from the heat transfer coil, though this is an issue specific to the given configuration of the system. For the purposes of simulating behavior as part of a large system with a range of PCMs studied, the results show adequate replication of real system behavior.

Material Cost

The cost of material should be considered for such a system in order to understand whether its' installation is worthwhile. López-Navarro et al. presented costs for the system they evaluated, as presented in the below:

Tank feature	Value
Tube material	Copper
Container material	INOX AISI 316L
Horizontal pitch	41 mm
Vertical pitch	37 mm
Length of tubes	13,300 mm
Inner diameter of tubes	12 mm
Outer diameter of tubes	16 mm
Total area (A) of heat transfer	5.75 m^2
Number of turns	6
Number of tubes	8
Total volume of PCM	235 l
Volume of PCM around the tubes	176 l
Volume of PCM in the center	32 l
Volume of PCM in the drainage system	27 l
External insulation	Polyurethane 150 mm

	Cost (€)	% Of total cost
Wall of the tank, lid, drainage system	1700	36.5
Insulation	1500	32
Copper tubes	400	8.6
Collectors	240	5.1
PCM (165 kg)	814	17.5
Total	4654	100

Figure 86 Material Cost Presented by López-Navarro et al. (2014)

Two variables of particular interest are the price of the tube and the price of the tank itself. For reference on copper tube pricing, an online hardware supply price list is consulted: the price of soft copper tube with 19mm OD is listed from $5.17/m to $9.48/m. Larger tube with 22mm OD is listed from $9.12/m to $12.80/m. A high-end estimate for tube price assuming a 200m run of tube is approximately $2,000. Based on internet search results, uninsulated high-density polyethylene tanks in the range of 250 gallons (0.95 m^3) to 275 gallons (1.04 m^3) may be purchased for approximately $300 to $500. Adhesive insulation sheets may be expected to cost approximately $80-$100 more. As will be discussed in a later chapter, water is considered to be the most viable for application in the near-term, and therefore the cost may be negligible. If a different phase change material is selected there is potentially considerable cost. The prices of PCMs varies, and commercial-grade PCMs are less expensive than the higher-grade substances for which prices are readily available. The PCM listed in Navarro et al. has a cost of $4.93/kg. For a PCM with a latent heat of phase change of

180,000 J/kg, storing 20 kWh would require 400 kg of material and a cost of $1,970 at this price.

Chapter Summary

A thermal storage system using various PCMs was developed and modeled. The PCM system consists of a tank with a long coil of copper tube, through which water-glycol heat transfer fluid is pumped to provide charging or discharging of the PCM. The model approach selected was intended to provide adequate accuracy and replication of real-world behaviors while remaining computationally simple to reduce simulation burden. A six-node cylinder of PCM is modeled and a temperature-enthalpy table is used to calculate the properties at each location.

In order to verify the behavior of the modeled PCM system, laboratory efforts by several researchers were consulted and their laboratory efforts were replicated in simulations. The scenarios used in the verification were widely varied, with two different tank configurations and three phase change materials with widely different phase change temperatures. The results of the verification effort showed that the approach selected here provides a reasonable approximation of behavior of the PCM systems. The modeled PCM system has more consistent heat transfer and more orderly transition through the two-phase region, with the nodes more tightly bunched than was observed in the laboratory tests, particularly for a PCM with a wider phase change temperature band. Also, for one of the configurations a large portion of the tank in the laboratory test was relatively removed from the heat exchanger surface; the model, with constant properties per node, did not capture this nuance. However,

overall the agreement between model and laboratory was decided to be satisfactory for the purposes of this modeling effort.

Chapter 7: Transient Modeling of Demand Response

This chapter describes simulations of demand response scenarios with and without thermal energy storage. The chapter includes description of the model used including modifications from the system as evaluated in laboratory testing, and transient model validation. Then, demand response scenarios and thermal storage load-shifting scenarios are examined, followed by a combination of both approaches. The work in this chapter is intended to:

- Provide a baseline model of energy consumption on a typical peak summer day for a "small-scale" supermarket
- Model basic demand response load-shed events by shedding display cases in an otherwise-unmodified cycle
- Model basic demand response load shifting events using a dedicated PCM subcooling system to provide subcooling capacity during shed. Examine strategies for meeting shed objectives (depth of reduction, duration)
- Model combined demand response approach, using both load shifting with PCM subcooling and display case sheds
- Quantify the peak demand, energy consumption, and operating costs of the above for a variety of rate/incentive scenarios

Model Description

The model of the laboratory system was adapted to simulate a scaled-down food retail application. The following describes the major modifications incorporated.

Outdoor temperature is imposed upon the condenser/gas cooler and subcooler condenser, with the temperature profile derived from the National Renewable Energy Laboratory's Typical Meteorological Year (TMY) data (Wilcox and Marion 2008), selected for summer days from Baltimore, MD. The *CombiTable1Ds* Modelica component is used to interpolate temperature readings in time.

In the laboratory test configuration, the LT compressor was operated at fixed speed with on-off control. In supermarkets, it is typical to have multiple compressors per stage and to have a single "leading" compressor operated under variable-speed control to approximately match load. Like the MT compressor in the laboratory testing, the LT compressor in modeling is controlled via P-I control to maintain a suction pressure level; the suction pressure of 1.535 MPa was selected corresponding to a saturated suction temperature of -27.8°C. the expansion devices for evaporators on the LT stage are then controlled via P-I control to maintain a desired superheat of 5K.

In laboratory testing, a single plate heat exchanger on each stage provides load using on-off electric resistance heaters for control. In the modeling effort, two display case models are added per stage for simulated control and demand response; to provide additional total load with minimal modeling complexity, the same plate heat exchanger components are retained and used for additional load. The glycol storage tank was also retained in the model to maintain thermal mass. However, the on-off control of simulated resistance heat is replaced with a continuous, time-varying heat

load. As described in Chapter 5, the loads imposed upon each evaporator were read from an input table derived from the measurements of Heerup and Fredslund (2016). Figure 87 shows the schematic of the modeled system including the loads, subcooler, thermal storage media, and primary cycle.

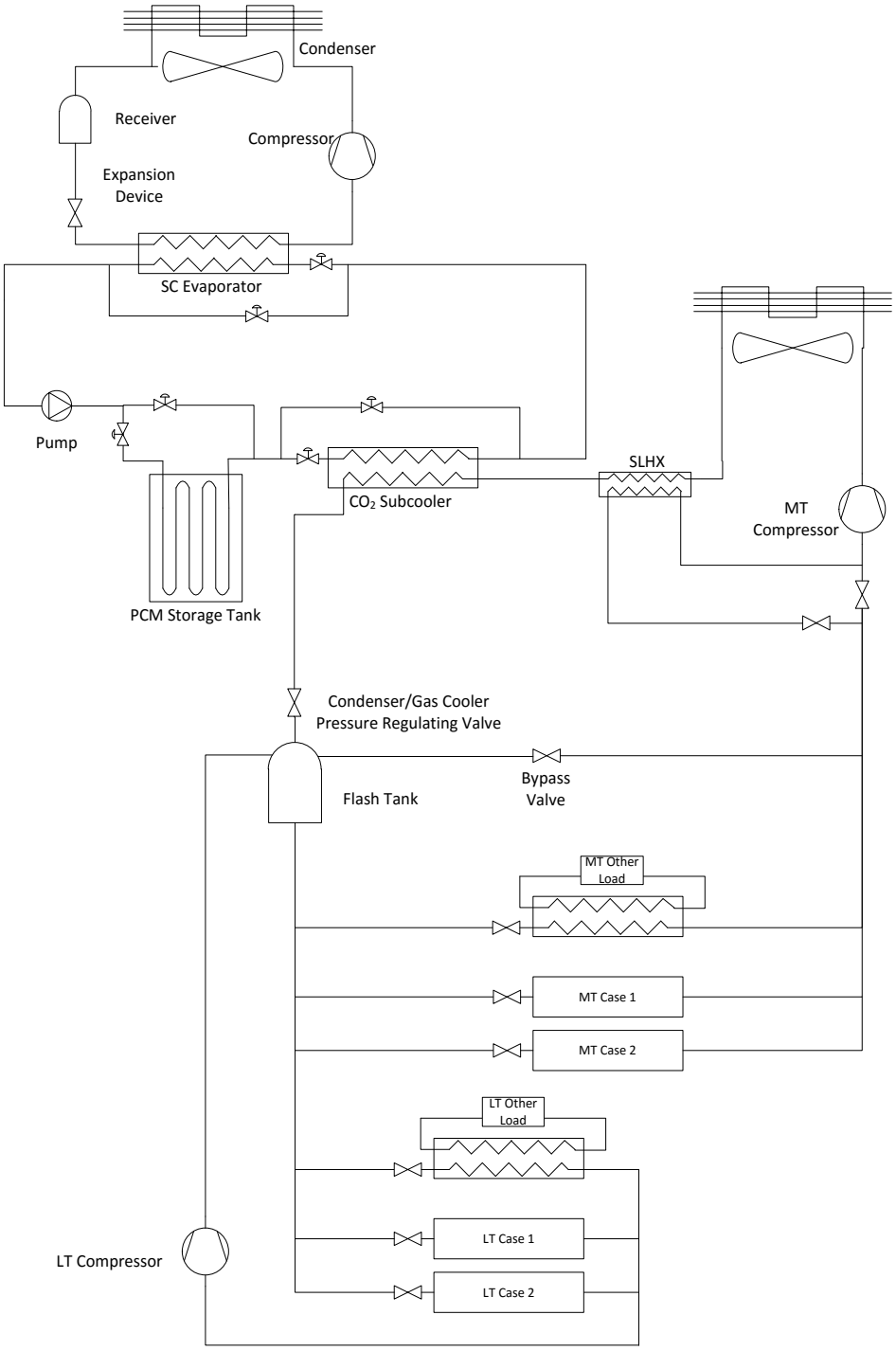

Figure 87 Schematic of Refrigeration Cycle as Modeled for Simulated Use Scenarios

The load profile is shown in Figure 88.

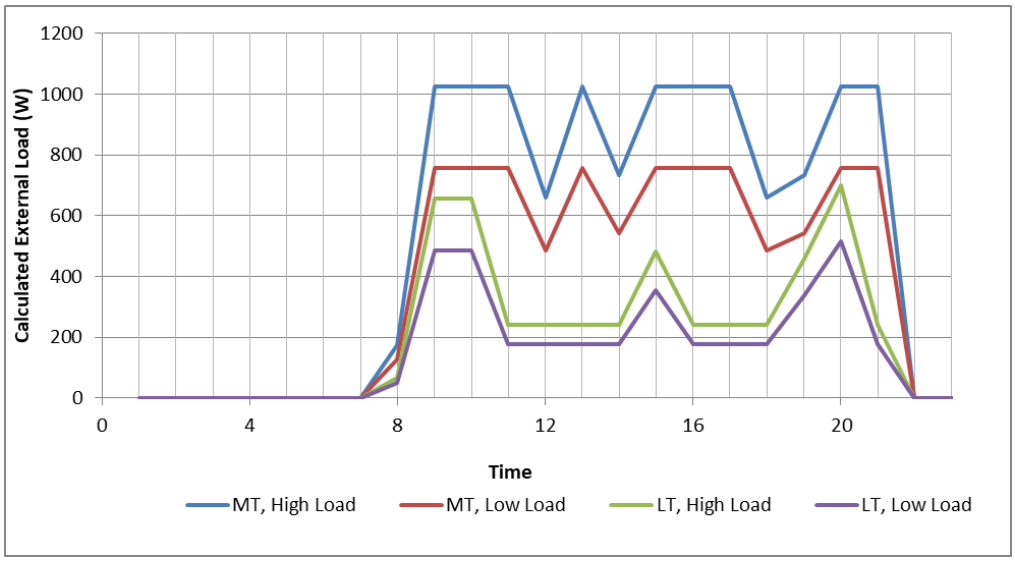

Figure 88 External Loading on Each Case Used for Simulations

In laboratory testing, the subcooler was in the laboratory space and the expansion device was generally at a fixed position; for modeling, the subcooler ambient air condition is the same as the condenser gas/cooler, and is input from a table of simulated weather conditions. The expansion device is controlled via P-I control to provide fixed superheat. This allows better efficiency, and also allows the subcooler to operate flexibly regardless of the PCM selected in the simulation.

Another critical difference is in the control of the condenser/gas cooler pressure regulating valve. The laboratory system had a control configuration that set pressure as a function of ambient temperature, and the pressure was the same with or without subcooling. However, the performance of the system can be improved by adjusting this pressure, in particular when subcooling is not provided. The control of the pressure regulating valve was modified to improve performance as will be shown in the next section.

Demand response and defrost signals are also implemented in the model here. The demand response and defrost signals are read using the *CombiTable1Ds* Modelica component; the table provides a binary on/off signal for each. The expansion valves are controlled using a variable input signal: in normal operation, they control to measured superheat. In the event of a demand response signal or defrost signal, the superheat signal is replaced with a fixed constant value 0.2K below the target superheat value; this allows the PI control to operate continuously and prevents the valve component from responding too quickly and causing model instability. Because the PI control never satisfies set-point, it smoothly transitions to close the valve.

Modification of High-Side Pressure Control

Through laboratory testing and model development it was observed that the system capacity and efficiency were generally limited by the heat rejection of the condenser and gas cooler. This problem is particularly visible in cases with no subcooling, where the refrigerant returning to the flash tank may be more than 50% vapor as operated in the laboratory. Further investigation shows that the pressure-outdoor temperature profile followed by the laboratory equipment agrees with that identified in Gullo et al. (2006). However, as was seen in laboratory test results, the performance of this system declined significantly in conditions where the pressure in the gas cooler/condenser was close to and just below the critical point; therefore, an alternate pressure control calculation was developed.

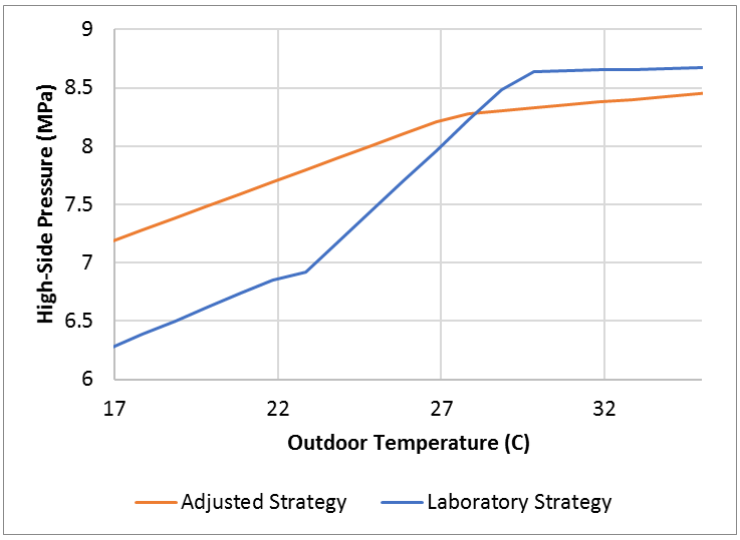

Figure 89 Adjusted Condenser/Gas Cooler Control Strategy

The primary purpose of the adjusted strategy was to prevent the system from dropping below the critical point too early and losing capacity. To demonstrate the effectiveness of the alternate strategy, two simulations are shown in Figure 90 for a short temperature profile with decreasing outdoor temperature and fixed loads. The power is shown with solid lines and the total delivered capacity with dotted lines, black for the new strategy and blue for the altered strategy. The laboratory control strategy encounters lost capacity and a drastic increase in compressor power as temperature approaches approximately 24°C; in the alternative approach, the power decreases and capacity stabilizes as might be expected.

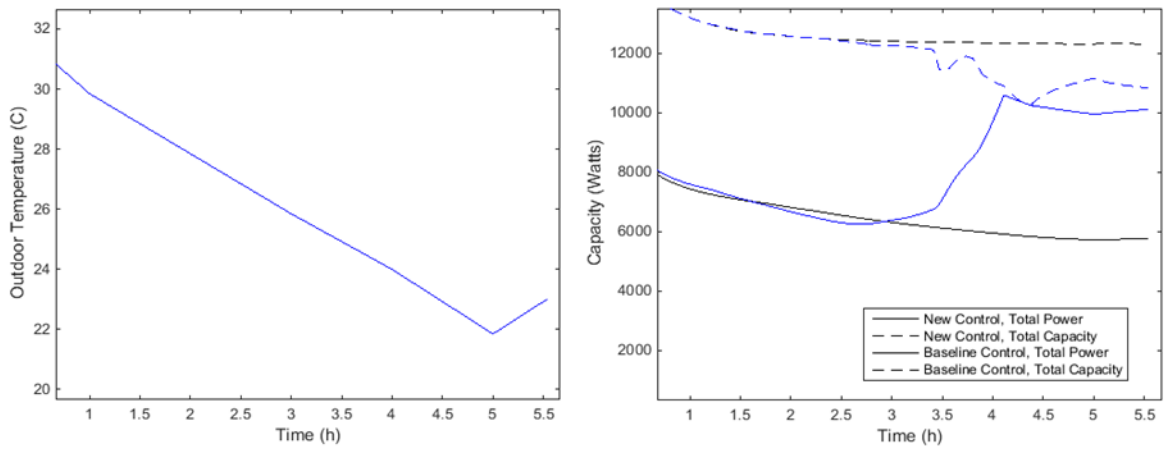

Figure 90 Outdoor Temperature (left) and Power and Capacity (right) for Pressure Control Strategies During a Period of Decreasing Outdoor Temperature

The COP vs. outdoor temperature of the new strategy during the period shown above, is plotted in Figure 91. The high-temperature portion contains some effects of model initialization, and the low-temperature portion includes a change from decreasing to increasing outdoor temperature leading to slight differences in COP.

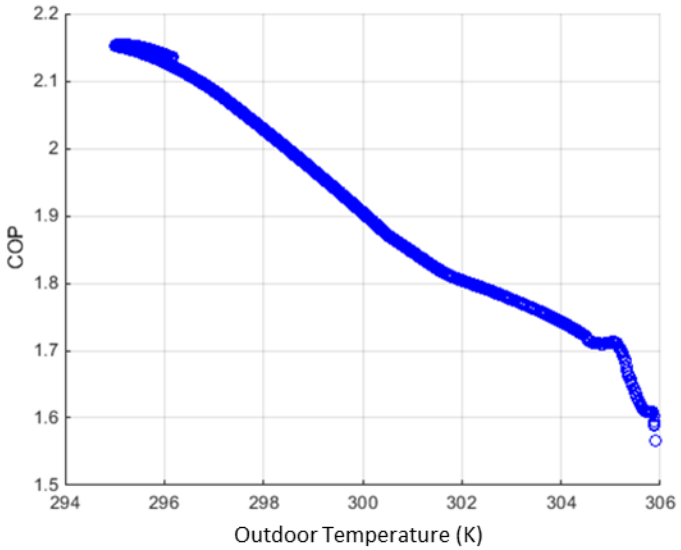

Figure 91 COP vs. Outdoor Temperature with New Pressure Control Strategy from the Period Shown in Figure 90

Baseline Simulation

A baseline simulation is used as the basis for comparing energy and demand. For this simulation, the PCM is excluded, and no demand response events are triggered. The subcooler is always on since this was found to be best for overall COP at all test conditions. The model is simulated for full 24-hour cycle with an additional simulated "run-in" time ending at 5:00 AM. The results are presented for 24 hours, with 5:00AM to 5:00 AM selected as the interval to allow capturing a full overnight re-charge in subsequent thermal storage simulations. Figure 92 shows the outdoor temperature profile that is used for the simulations. This temperature profile is reflective of a hot summer day with still-warm evening temperatures, which could be expected to present a challenging operating environment for transcritical CO_2.

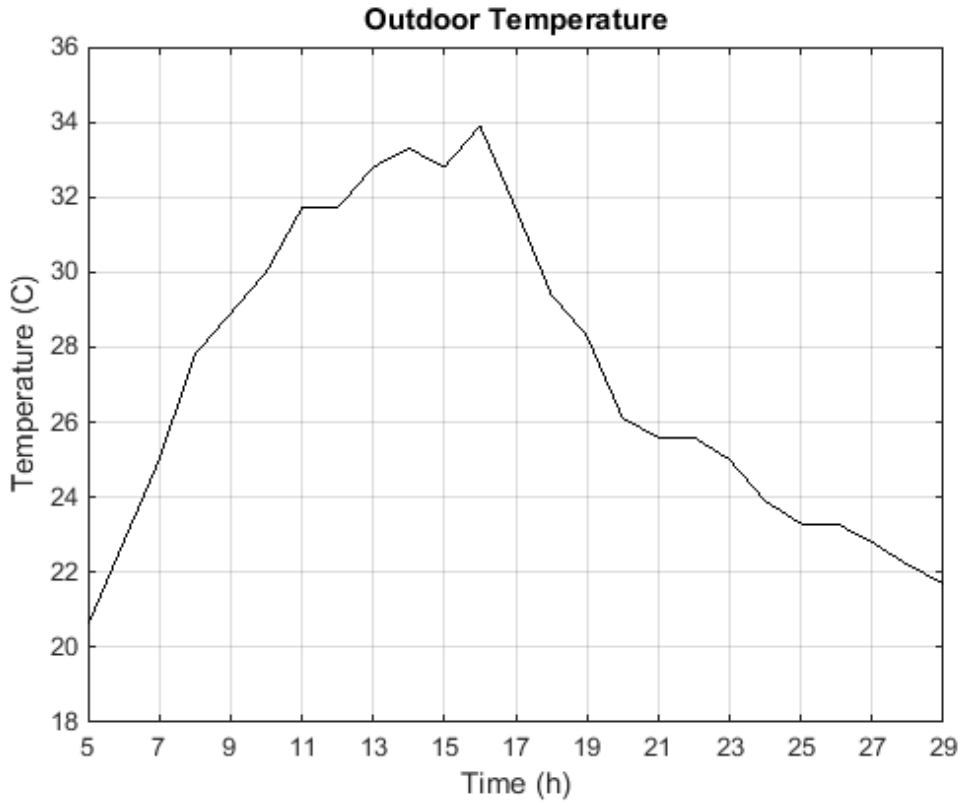

Figure 92: Outdoor Temperature Profile for Simulations

The baseline simulation results are shown in the following figures. The simulation is shown with hour "24" indicating midnight. There are three defrosts in the modeled period: at approximately hour 6, hour 20, and hour 28. The defrosts are staggered, with one MT and one LT case defrosting at a given time.

The total system power for the whole period is shown in Figure 93 alongside the component-by-component power. The MT compressor power, in blue, is the largest component; the LT compressor power and subcooler system power are similar in magnitude. The defrost power for the LT cases is shown in green and light blue; the MT defrost times overlap with the LT defrost times (there is no heater power for the MT defrost).

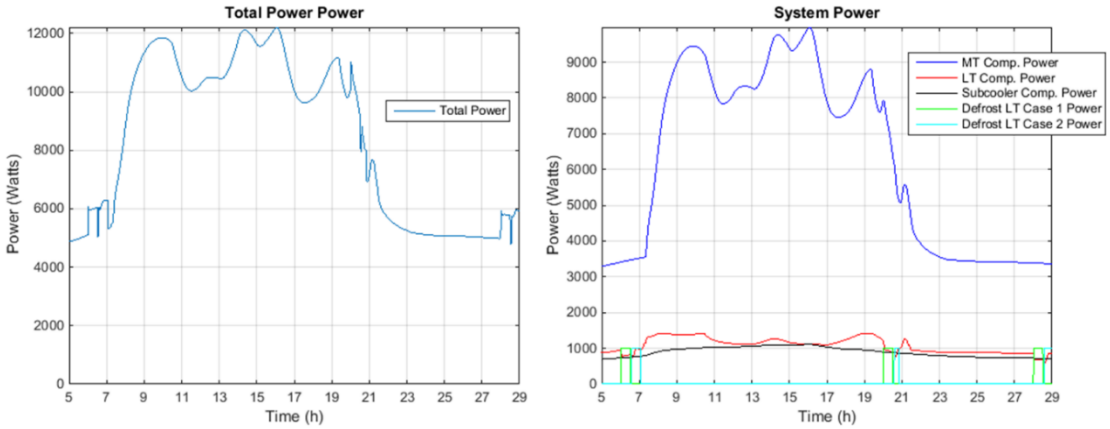

Figure 93 Total System Power (left) and Subsystem Power (right), Baseline Test

The total delivered refrigerating capacity is shown in Figure 94, with the total MT capacity in blue and the total LT capacity in red. The drop and subsequent rebound in refrigeration capacity is clearly seen around each defrost period.

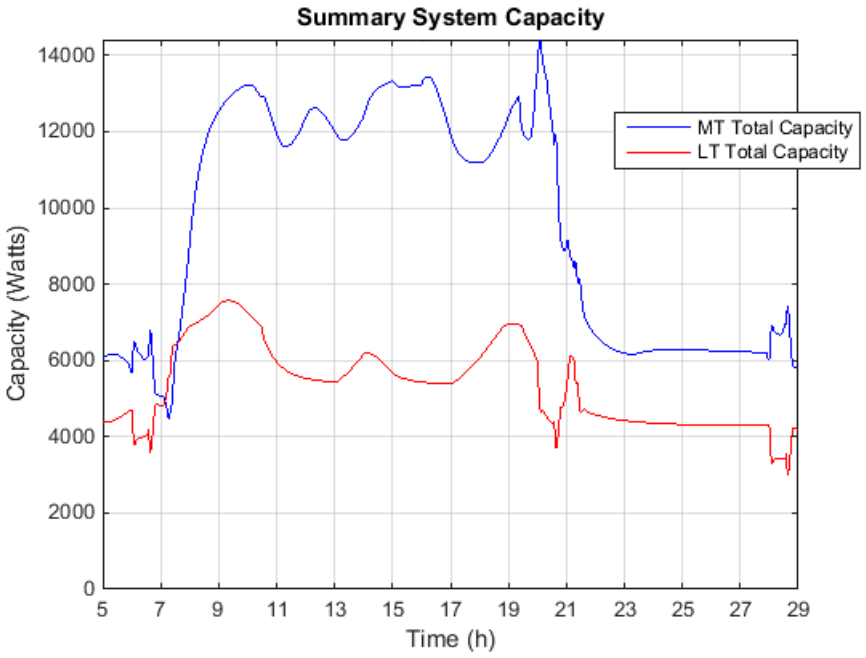

Figure 94 MT and LT Stage Capacity, Baseline

Figure 95 shows the capacity, separated into the individual load components; each case has a drop to zero capacity during the defrost period, and a subsequent capacity rebound indicated by a pronounced spike in capacity immediately after the defrost ends.

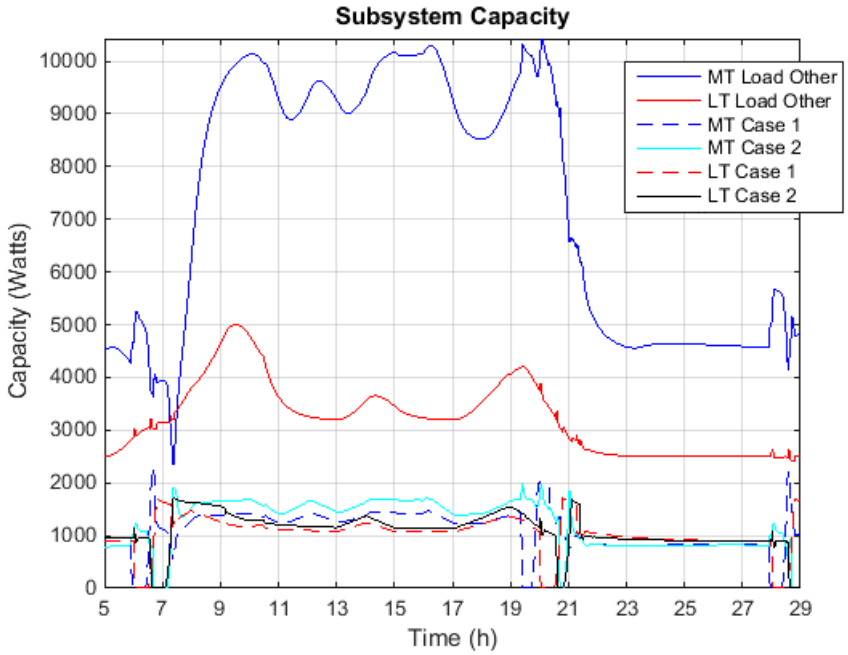

Figure 95 Capacity of Each Evaporator, Baseline

The temperature of the refrigerated air and food in the LT and MT cases is shown in Figure 96; this shows the effect of the defrost on temperature within the case. The LT air temperature deviates by approximately 25°C in a typical defrost, to a level of about 0°C; the load on the case includes the defrost heater in this case. For the MT case the temperature departures are smaller. Another observation may be made from this and the previous graphs: the MT case temperature reaches an equilibrium under daytime load of approximately 3°C-4°C. During the overnight hours where load is low, the temperature decreases. The cause of this is that, as modeled, the capacity of

the MT compressor at minimum speed is slightly larger than the load, and the temperature is drawn down slightly. In a real-world system, the entire MT compressor stage might cycle off, or the compressor may have a mechanical unloader to produce still-lower capacity.

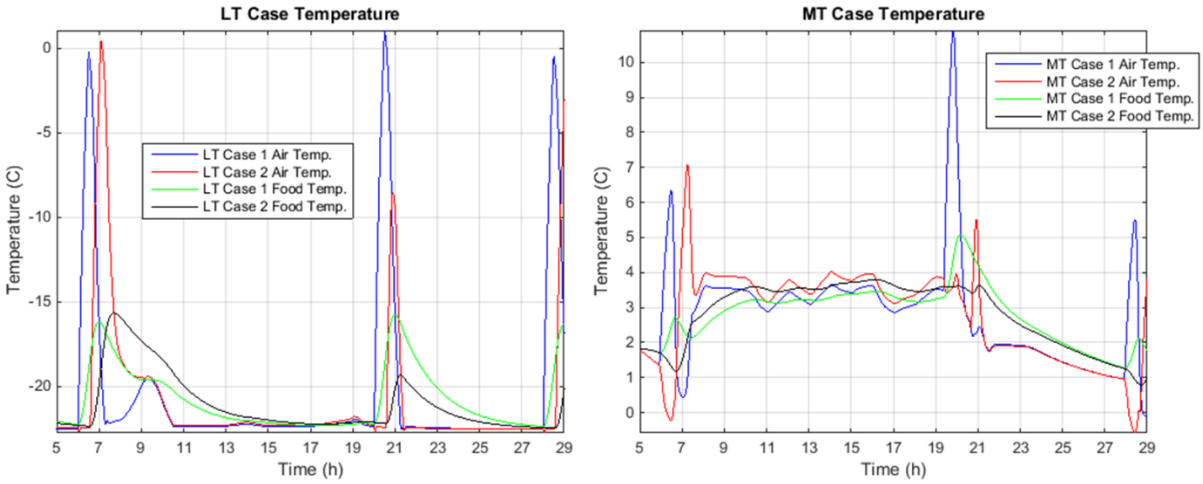

Figure 96 LT and MT Case Temperatures, Baseline

This is also reflected in Figure 96 which shows the refrigerant pressure at the MT compressor suction and discharge and the flash tank (left), and each plate evaporator (right). The evaporator pressures deviate slightly at times. For the MT evaporator, as mentioned above, in the overnight hours the capacity of the MT stage is slightly higher than load, drawing pressure downwards. The pressure also deviates and recovers during the disturbance caused by defrost. On the LT evaporator, the load briefly exceeds capacity at about 9:00 AM – the display cases are still recovering from defrost, and the daytime load increases during this timeframe.

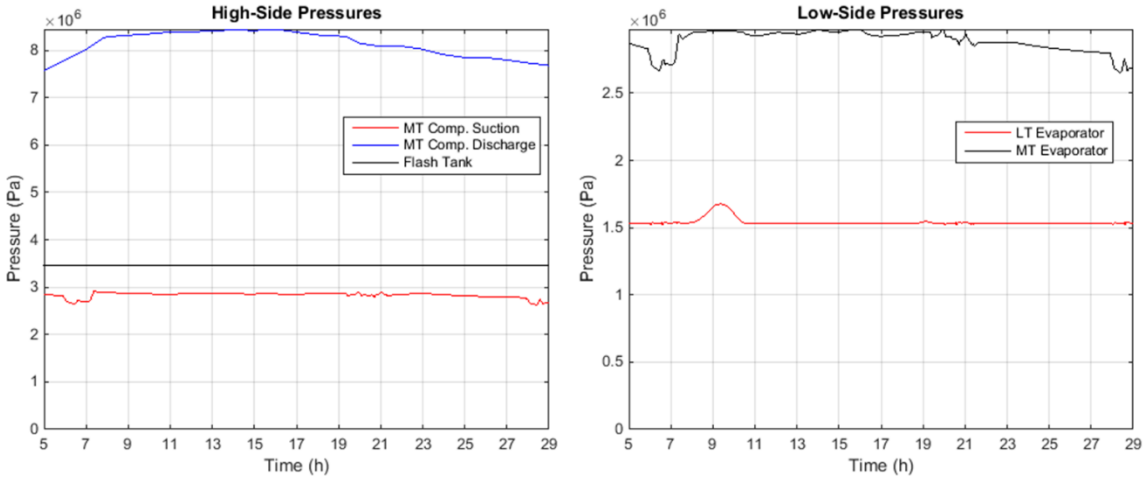

Figure 97 Refrigerant Pressures, Baseline

The refrigerant flow rates of each evaporator stage (plate heat exchangers and display cases combined) and the MT compressor are shown in Figure 98.

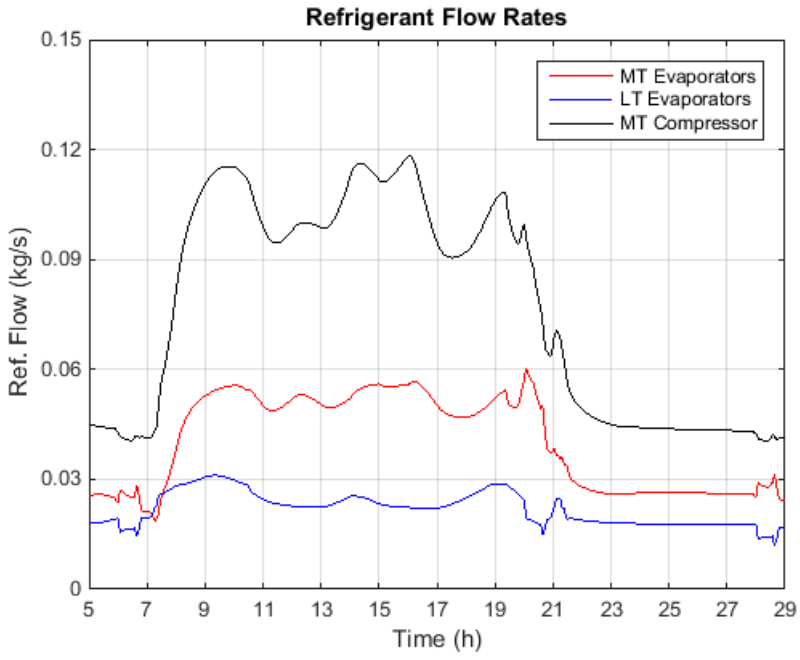

Figure 98 Refrigerant Flow Rates, Baseline

The bypass flow percentage is shown in Figure 99. The bypass flow mostly is in the range of approximately 40-52%, except deviations relating to defrosting and transitioning loads.

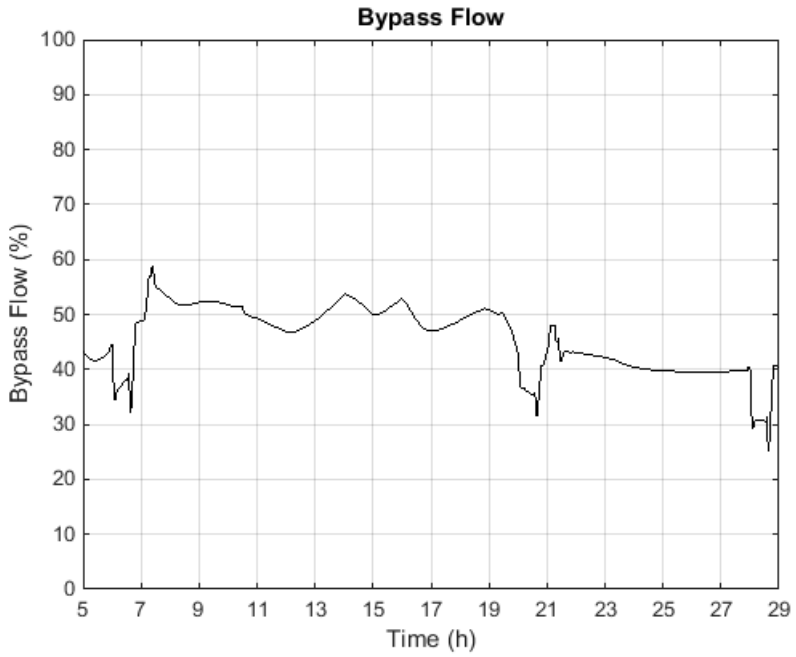

Figure 99 Bypass Flow, Baseline

Refrigerant charge distribution is also of interest. The system charge is shown in Figure 100. The total charge remains constant as expected, and the large majority of the charge resides in the flash tank, followed by the condenser/gas cooler. The charge variation during the day is largely driven by the mass of refrigerant in the gas cooler; in particular as the leaving enthalpy increases, the density of refrigerant in the subcooler decreases, reducing the charge volume in the heat exchanger.

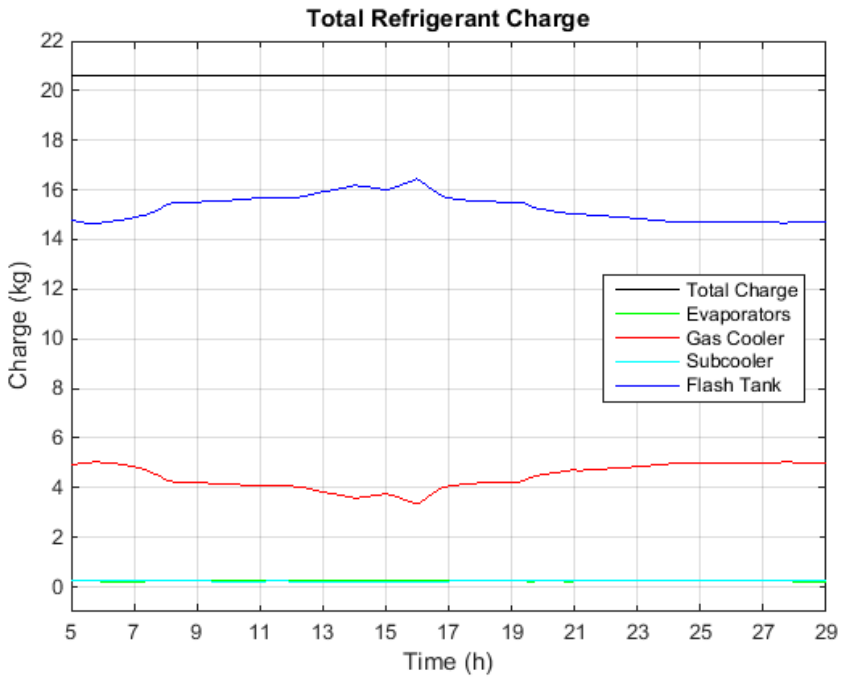

Figure 100: System Refrigerant Charge for Primary Components, Baseline Simulation

Baseline System, Demand Response

The baseline system was simulated with load sheds on one or both of each of the LT and MT evaporator case levels. The results of these sheds are examined here. First, MT case sheds are examined. Two scenarios are examined: one with one case shed, and one with both cases shed together. In each case, a simulated shed is executed at hour 15 (3:00 PM). In the baseline case, hour 15 to hour 16 had relatively flat capacity and power that is at a local minimum at hour 15, increasing to a peak close to hour 16 before dropping off. These sheds would be expected to reduce power and capacity during the period of interest.

Shed of One MT Case

A single case shed is triggered at hour 15 (3:00 PM) with a duration up to 30 minutes. The capacity of MT Case 2 (light blue on Figure 60) drops to zero quickly. However, as MT Case 2 drops to zero, there is some corresponding increase in capacity in MT Case 1 and the MT Load heat exchanger. The other loads on the MT stage respond with short increases in capacity which taper downwards. This occurs because the relatively sudden closing of the MT Case 2 expansion valve reduces flow through that evaporator to zero more quickly than the MT compressor, or the other expansion valves, respond. Immediately after the MT Case 2 valve closes, the MT compressor speed remains close to the balance point for the full load, and so a sudden increase in flow through the other valves is observed.

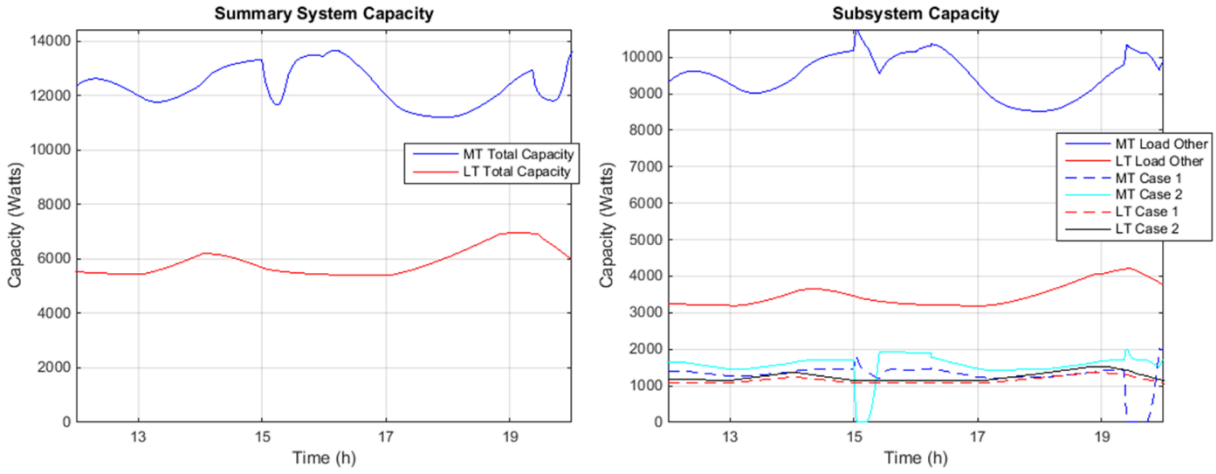

Figure 101 Refrigerating Capacity with MT Case 2 Shed at Hour 15

The response of temperatures in the display cases is shown in Figure 102. MT case 2 has a rapid increase in air temperature and gradual increase in food temperature. The food temperature fairly quickly reaches the 4°C threshold and the shed ends, though

the case air temperature remains above the food temperature and the food temperature increases to approximately 5°C. MT Case 1 is also affected: the air temperature briefly deviates down due to the sudden change in capacity, quickly recovering. This deviation is not enough to have a noticeable impact on food temperature in MT Case 1. The LT cases are not affected.

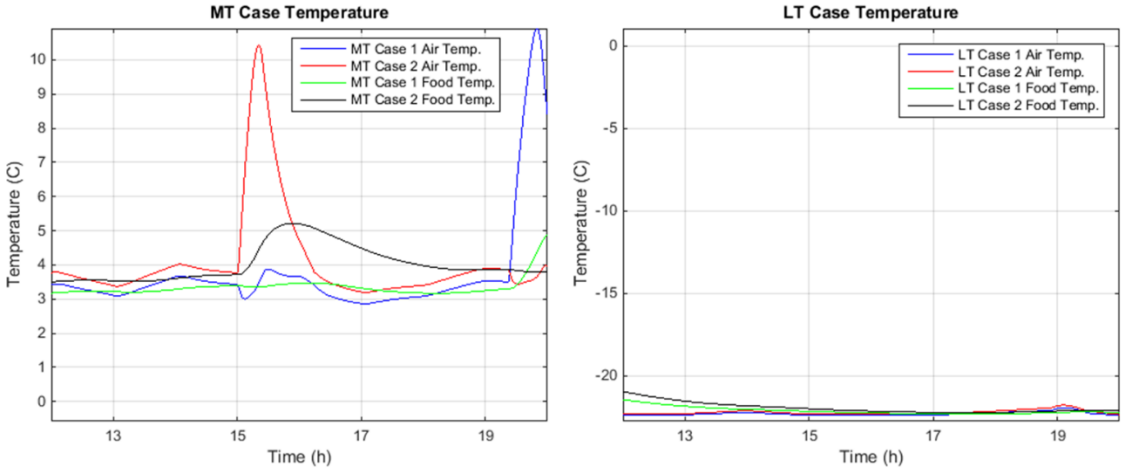

Figure 102 MT and LT Case Temperatures with MT Case 2 Shed at Hour 15

The refrigerant pressures shown in Figure 103 show the effect of the change: a sharp downward shift in MT evaporator pressure as the event begins, which gradually recovers, while the LT evaporator, flash tank, and MT discharge are essentially unaffected.

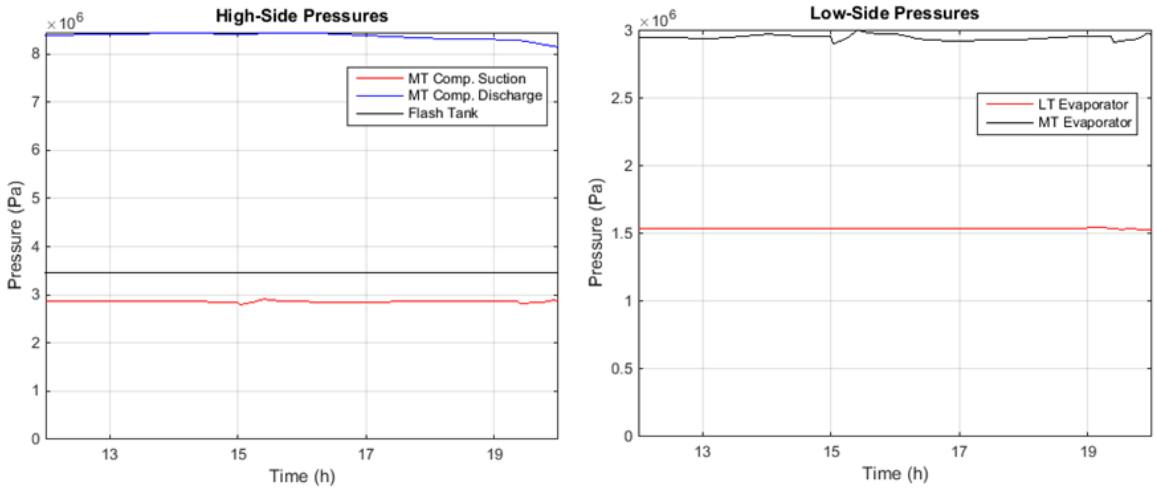

Figure 103 Refrigerant Pressures with MT Case 2 Shed at Hour 15

The total power and subsystem power are shown in Figure 104. From this the effect of the shed can be seen at the system level. The MT combined capacity immediately prior to the shed was 13.3 kW; it reached a minimum of 11.6, a reduction of 1.7 kW (12% reduction). The minimum was reached after approximately 14 minutes, near the same time that the shed was cut short by the MT case temperature reaching the cut-off threshold. The total system power at the beginning of the shed was 11.6 kW, and reduced to 10.6 kW, a reduction of 1 kW or 9% of total power. The MT compressor power was initially 9.4 kW, and reduced by the same amount. The minimum power was reached approximately 100 seconds after the minimum capacity.

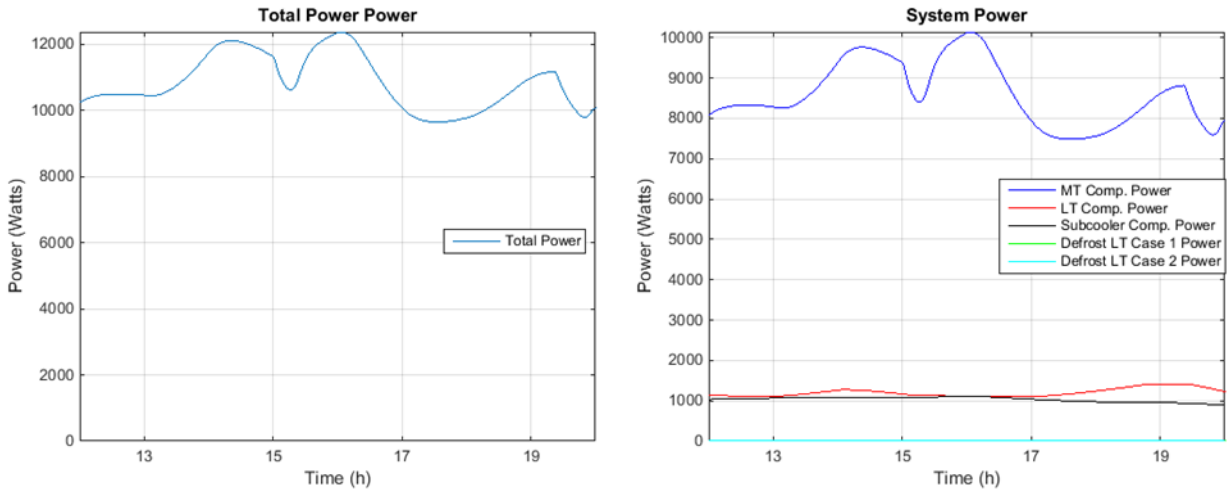

Figure 104 Total Power and Subsystem Power with MT Case 2 Shed at Hour 15

The bypass flow is only slightly altered by the event, as shown in Figure 105.

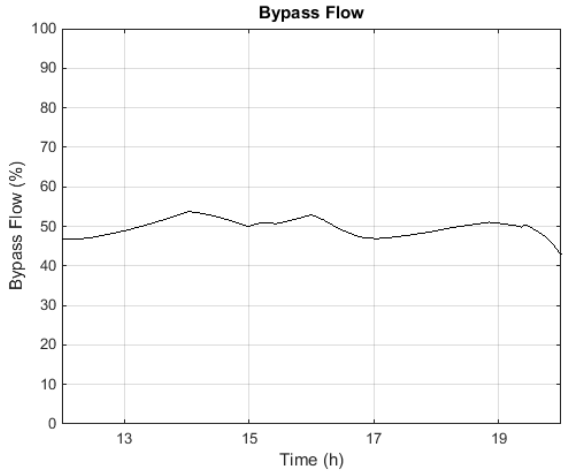

Figure 105 Bypass Flow with MT Case 2 Shed at Hour 15

Shed of Two MT Cases

A similar shed was run with both MT cases shedding at the same approximate time. The total MT-stage capacity, shown in Figure 106, decreases from 13.3 kW to 10.3 kW at minimum, a reduction of 3.0 kW or 22.5% of the MT load. There is a similar sudden spike in capacity on the load which is not part of the shed, in this case the MT load evaporator. The magnitude is larger than with only one case shedding; with two

of the three evaporators on the stage shutting, the MT compressor and the MT load evaporator valve both must adjust in response.

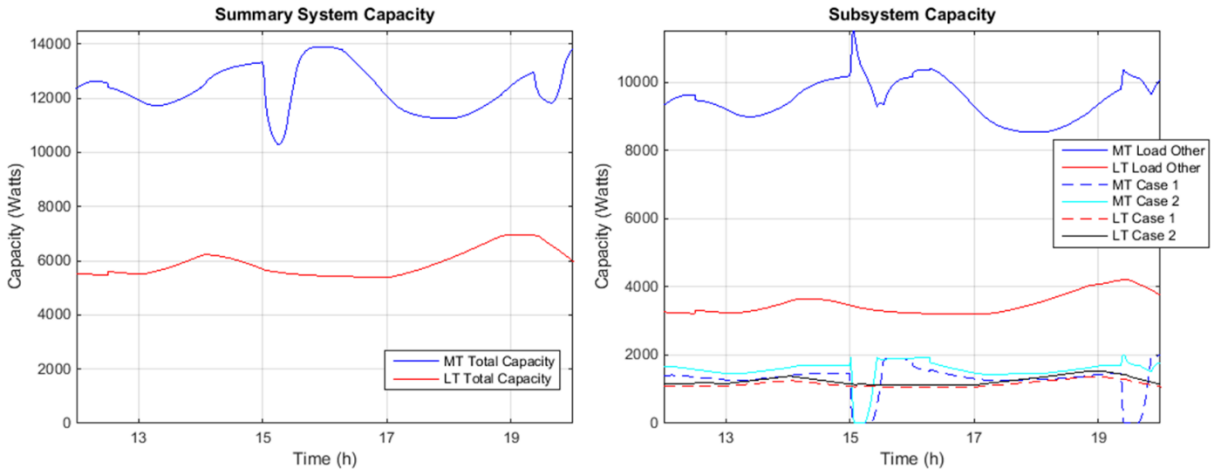

Figure 106 Capacity with MT Case 1 and MT Case 2 Sheds at Hour 15

The total power reduction is from 11.6 kW to 9.8 kW, a 1.8 kW or 15.5% reduction in total power. The reduction is, like the above case, entirely from the MT compressor.

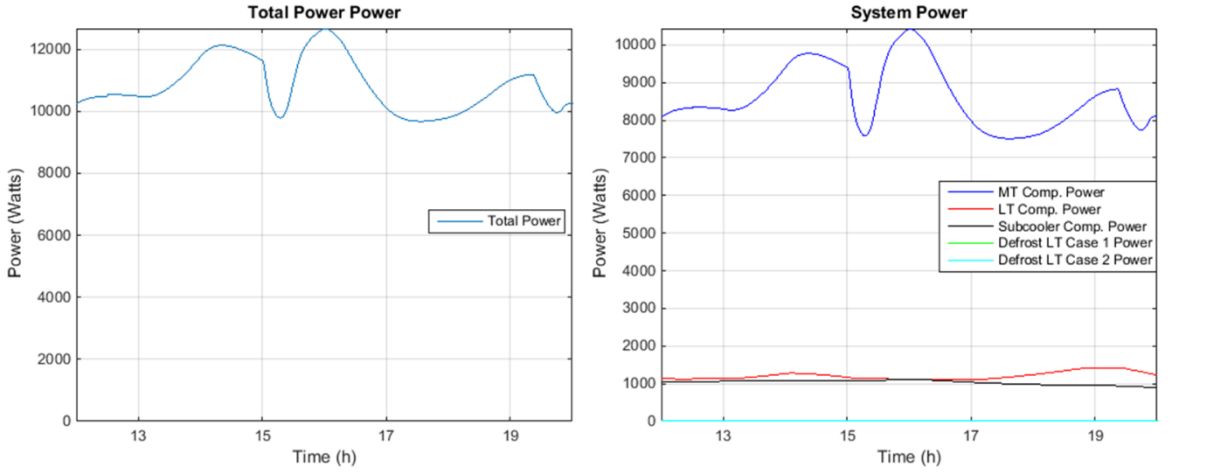

Figure 107 Total Power and Subsystem Power with MT Case 2 Shed at Hour 15

Shed of One LT Case

The shed of only LT Case 2 is examined next. The shed is again at hour 15 (3:00 PM) for a duration of up to thirty minutes. The capacity results are shown in Figure 108. The capacity reduction on the LT stage is met with a corresponding response on the other evaporators: both small increases on the other LT evaporators, and also small increases on the MT evaporators. The responses on the MT evaporators are significantly smaller in magnitude than those when a MT case was shed. The LT capacity reduction is from 5.7 kW to 4.4 kW, a reduction of 1.3 kW or 22.8% of the LT load.

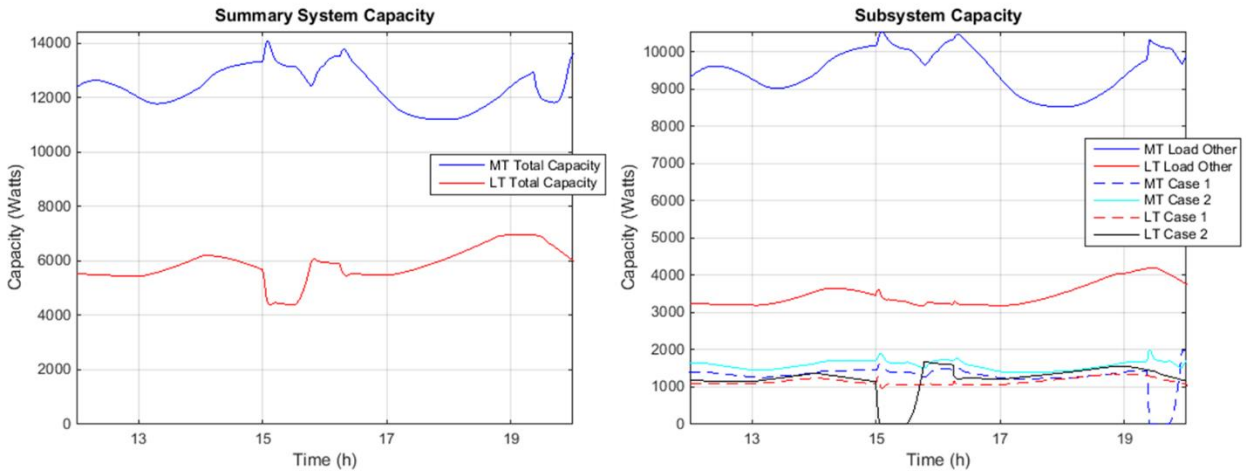

Figure 108 Refrigerating Capacity with LT Case 2 Shed at Hour 15

The bypass flow is shown in Figure 109. At the time of the event there is a sharp decrease in bypass flow, from approximately 50% to 45%, which lasts for the duration of the shed. This change is part of the interaction between the LT and MT stages.

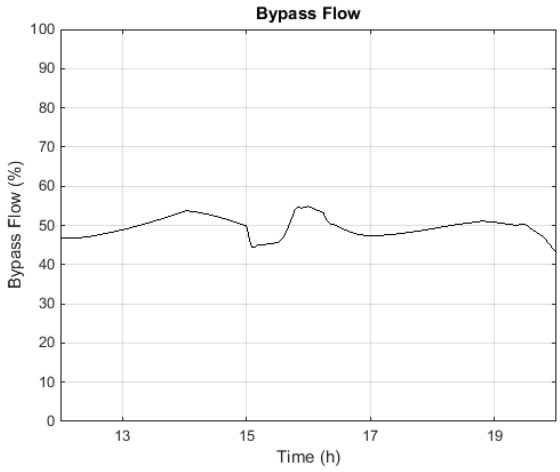

Figure 109 Bypass Flow with LT Case 2 Shed at Hour 15

The case temperatures are shown in Figure 110. The LT Case 2 air temperature increases by approximately 15°C during the shed, during which time the food temperature increases by approximately 5°C. LT Case 1 is minimally affected. The MT cases have small deviations in air temperature corresponding to the capacity adjustments.

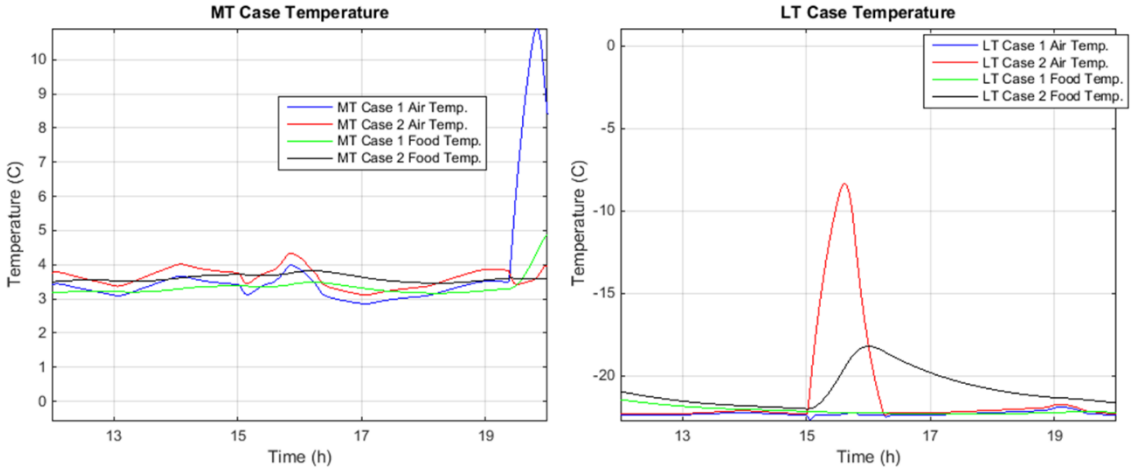

Figure 110 MT and LT Case Temperatures with LT Case 2 Shed at Hour 15

The change to power is shown in Figure 111. The total power reduces from 11.6 kW to 10.5 kW, a 1.1 kW or 9.5% reduction. The LT compressor power at the beginning

of the shed was 1.2 kW and reduces to 0.9 kW. The MT compressor power reduced from 9.4 kW to 8.5 kW.

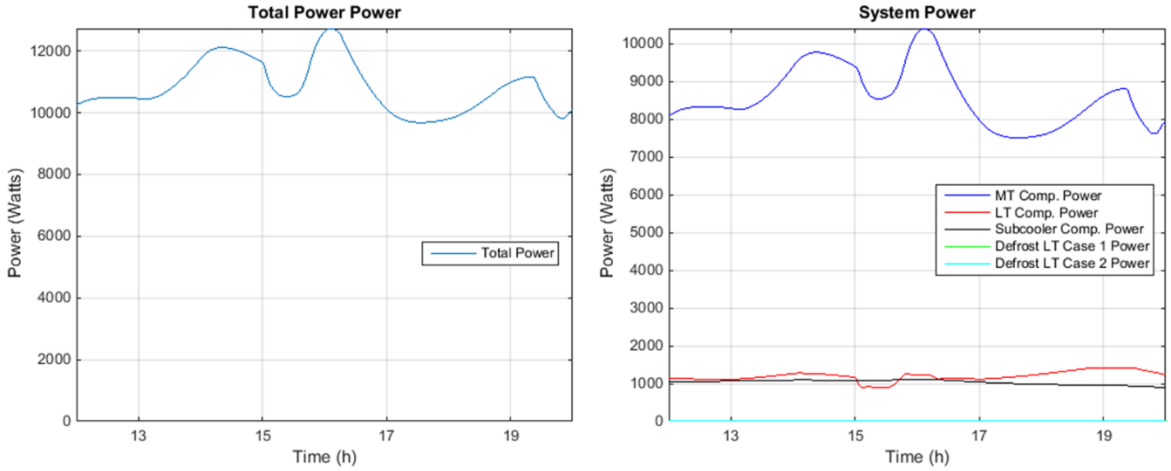

Figure 111 Total Power and Subsystem Power with LT Case 2 Shed at Hour 15

Shed of Two LT Cases

A case of two LT case sheds is also run. In this case the capacity reduction, shown in Figure 112 is from 5.7 kW to 3.4 kW, a 40.4% reduction. The total power, shown in Figure 113, is from 11.6 kW to 9.5 kW, an 18.1% decrease. The LT compressor power reduction is from 1.2 kW to 0.7 kW. The MT compressor power decrease is from 9.4 kW to 7.7 kW.

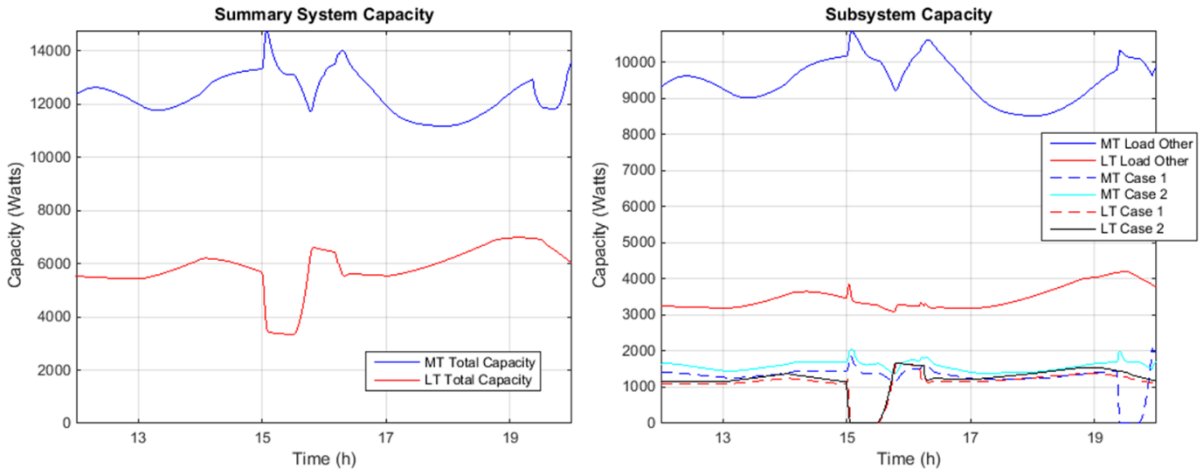

Figure 112 Capacity with LT Case 1 and LT Case 2 Sheds at Hour 15

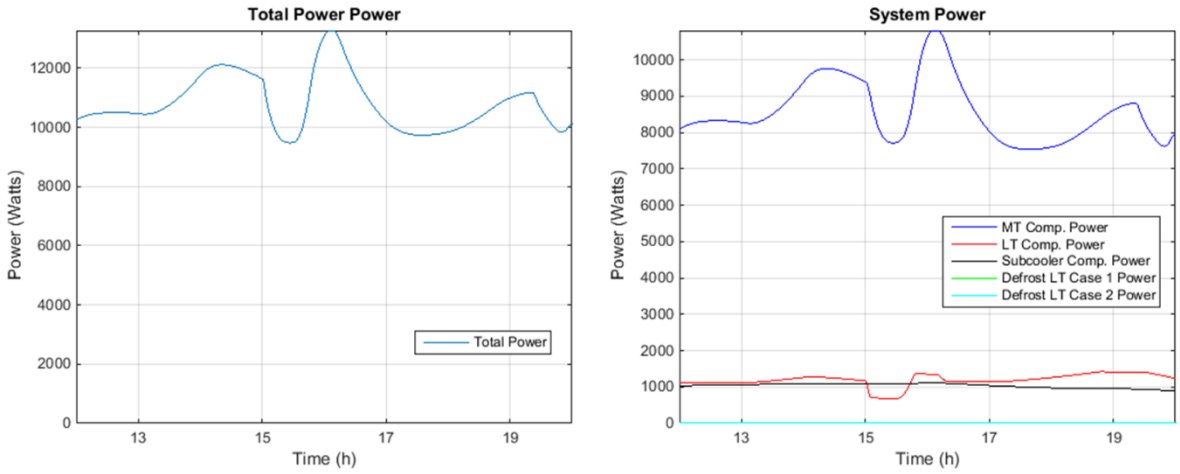

Figure 113 Total Power and Subsystem Power with LT Case 1 and LT Case 2 Shed at Hour 15

Baseline System, Demand Response with Shed Schedules

The baseline system was also simulated in demand response load-shed simulations with different schedules tested to examine the possibility of prolonging the power reduction or otherwise benefitting from shedding multiple cases at different times. Eight scenarios were selected and simulated first without any thermal storage. The scenarios are listed in Table 17, which shows the "shed" period or periods for each

case. In general the start and end of each shed is staggered by one minute if they are intended to coincide. This allows better stability in the control response to reduced load.

Table 17 DR Shed Schedule Showing Times for "Shed" for Each Case (all times PM)

Shed:	LT Case #1	LT Case #2	MT Case #1	MT Case #2
DR1	1:00 - 1:30; 3:00 - 3:30	1:58 - 2:28; 3:56 - 4:26	1:29 - 1:59; 3:27 - 3:57	2:27 - 2:57; 4:25 - 4:55
DR2	1:00 - 1:20; 1:40 - 2:00; 2:20 - 2:40; 3:00 - 3:20; 3:40 - 4:00; 4:20 - 4:40	1:10 - 1:30; 1:50 - 2:10; 2:30 - 2:50; 3:10 - 3:30; 3:50 - 4:10; 4:30 - 4:50	1:20 - 1:40; 2:00 - 2:20; 2:40 - 3:00; 3:20 - 3:40; 4:00 - 4:20; 4:40 - 5:00	1:30 - 1:50; 2:10 - 2:30; 2:50 - 3:10; 3:30 - 3:50; 4:10 - 4:30; 4:50 - 5:10
DR3	1:00 - 1:15; 1:40 - 1:55; 2:20 - 2:35; 3:00 - 3:15; 3:40 - 3:55; 4:20 - 4:35	1:10 - 1:25; 1:50 - 2:05; 2:30 - 2:45; 3:10 - 3:25; 3:50 - 4:05; 4:30 - 4:45	1:20 - 1: 35; 2:00 - 2:15; 2:40 - 2:55; 3:20 - 3:35; 4:00 - 4:15; 4:40 - 4:55	1:30 - 1:45; 2:10 - 2:25; 2:50 - 3:05; 3:30-3:45; 4:10 - 4:25; 4:50 - 5:05
DR4	4:30 - 5:00	4:00 - 4:32	4:31 - 5:01	4:01 - 4:33
DR5	3:30 - 4:00	3:00 - 3:32	3:31 - 4:01	3:01-3:33
DR6	2:30 - 3:00	2:00 - 2:31	2:32 - 3:02	2:01 - 2:33
DR7	1:30 - 2:00	1:00 - 1:31	1:32 - 2:02	1:01 - 1:33
DR8	1:00 - 5:00	1:02 - 5:02	1:01 - 5:01	1:03 - 5:03

For each scenario, the LT and/or MT cases are given a "shed" signal of a given duration. The shed is interrupted either by the end of the one-hour duration, or the temperature of the food in the case reaching -15°C for the LT cases, or +4°C for the MT cases.

For illustration, two cases will be examined in depth: DR4 is shown first. This is a simple example with each case shedding once. Detailed results are then shown for DR1, which has each shed multiple times, with a rebound period in between. After showing the system behavior in detail, summary data for all eight tests are shown.

Figure 114 shows the total power consumption of case DR4 for the hours of interest, in red, with the baseline power profile in black for reference. The power reduction can be observed beginning at 4:00 PM, with total power dropping by approximately 2,000 watts. There is a rebound period, beginning at 5:00 PM, during which the power consumption of the system is higher than the baseline period. The power is higher by approximately 600-1,000 watts for a period of approximately 45 minutes, and then slightly higher for the ensuing three hours.

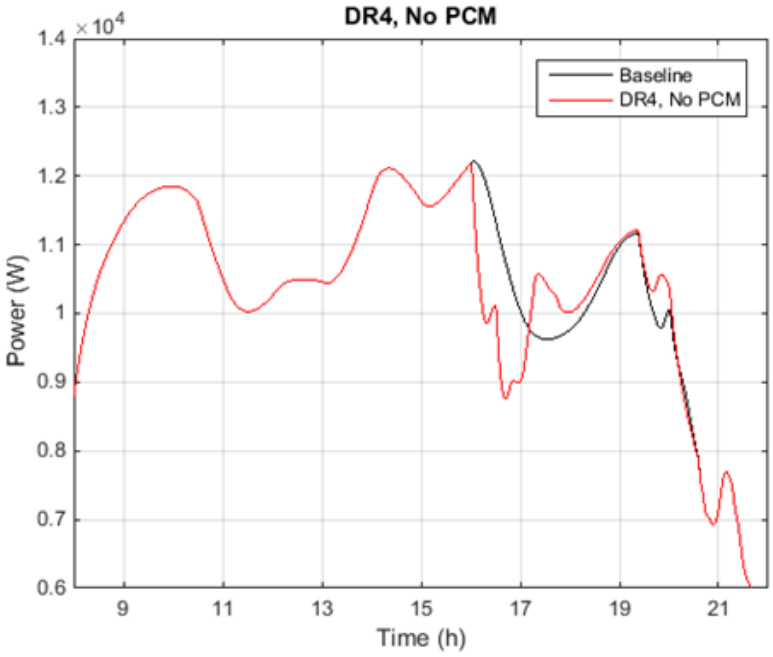

Figure 114 Total Power, Baseline and DR4, no PCM

Figure 115 shows the total and subsystem power consumption of the refrigeration rack for the 24-hour period starting at 5:00 AM. The DR event occurs begins at 4:00 PM, when cases MT2 and LT2 shed for 30 minutes, after which MT1 and LT1 shed for 30 minutes, and the event ends at 5:01 PM (with the staggered shed termination). The system response includes a drop in power consumption from each compressor, with some small rebound occurring at 4:30 PM, when the cases which are shedding switch. A subsequent graph shows detail of the case temperatures.

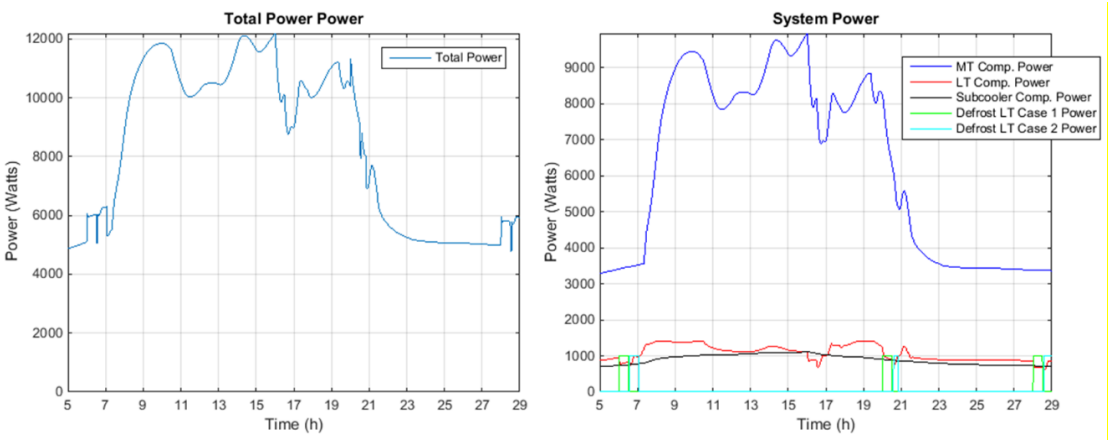

Figure 115 Total Power and Subsystem Power DR4, no PCM

Figure 116 shows the summary capacity of each stage of refrigeration, for the DR4 case (left) and the baseline case (right). In the baseline operation, the period of 4:00-5:00 PM is a high-load period transitioning to lower load. The demand response event can be clearly seen in the left figure: at 4:00 PM, both the MT and LT stages have a pronounced drop in capacity reflecting the shed of one display case per stage; at approximately 4:30, the MT stage capacity increases and then abruptly decrease again; this reflects one case returning to operation and the other dropping out. Similar is seen for the LT stage, except with different sequence: the capacity drops, and then

drops again prior to a two-stage rebound from each case returning to operation. There is a higher capacity after the shed on both stages as the cases recover. The delivered capacity outside of the period of interest is nearly identical.

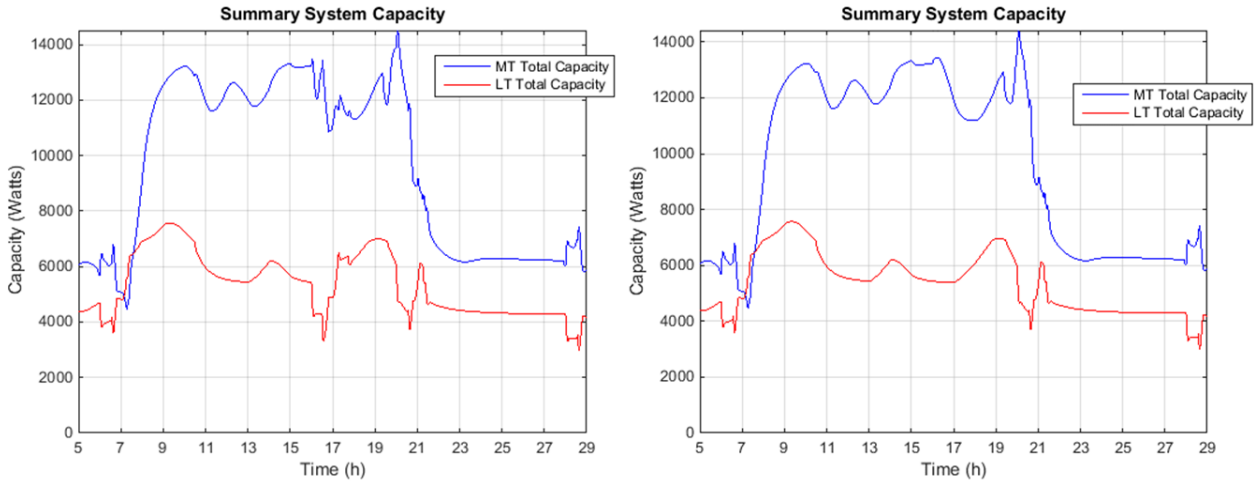

Figure 116 Capacity, DR4, no PCM (Left); Baseline (Right)

Figure 117 shows the temperature of each case during the 24-hour period. The three defrost periods, around 6:00 AM, 8:00 PM and the end of the sample period are shown; in addition, the temperature deviates during the shed. In the LT side, the temperature of the case air during the shed increases to slightly above -10°C during the shed for each case, for Case #2 first and then Case #1. The temperature increase of the food product lags behind. MT case air increases to slightly below 10°C for each shed. The food product temperature increases to nearly 5°C in each case. A difference to note between the LT and MT cases: the food temperature in the LT cases do not reach the threshold to interrupt the shed (-15°C), but the MT cases do reach the threshold (4°C). The MT shed event is interrupted for each case, after approximately 15 minutes of shed.

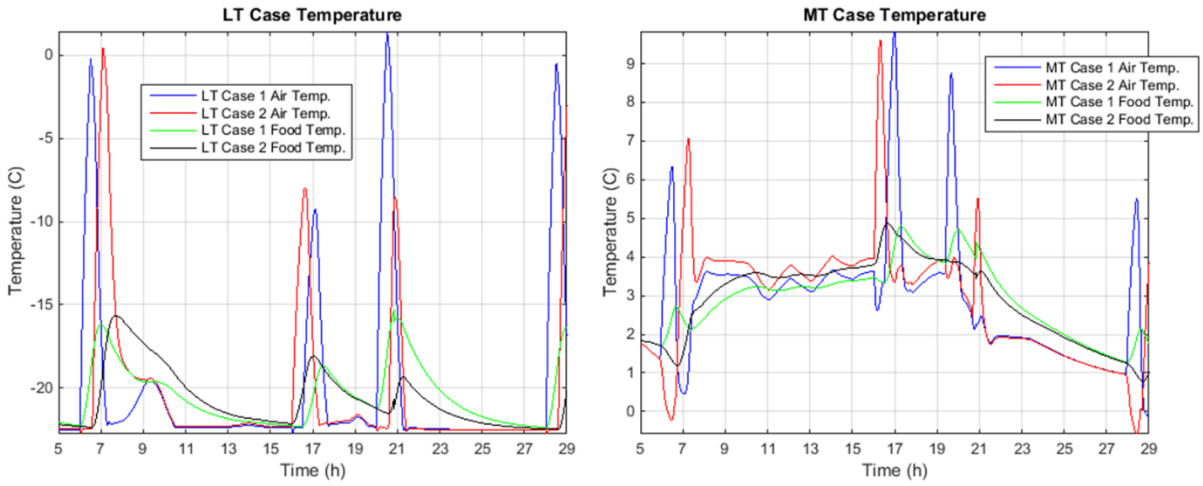

Figure 117 MT and LT Case Temperatures DR4, no PCM

The refrigerant pressure profiles for each stage are shown in Figure 118; by visual comparison with Figure 97 (the baseline case) there are only small differences in the pressure at each evaporator/suction stage as the system compensates for changing flow rates during the shed events.

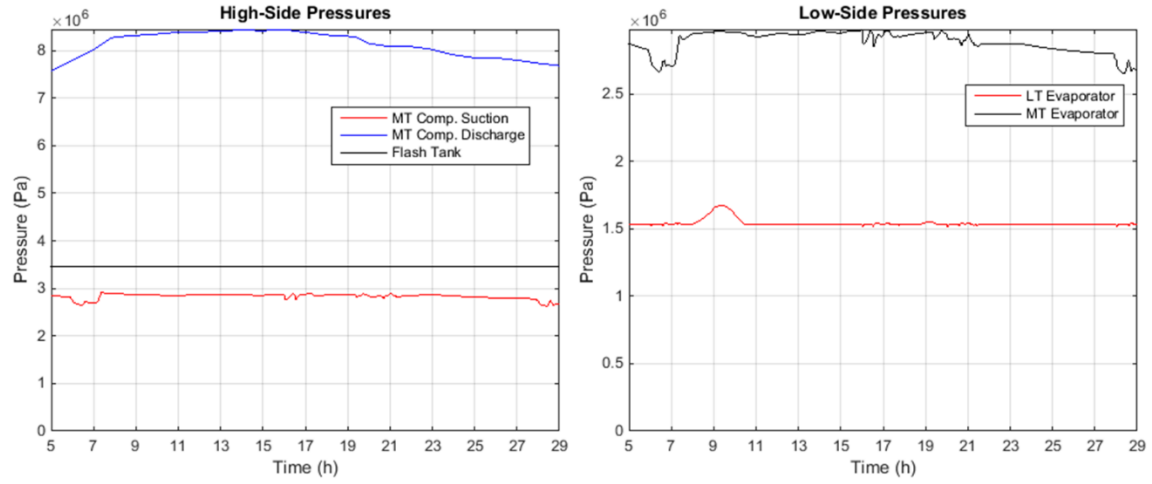

Figure 118 Refrigerant Pressures, DR4, No PCM

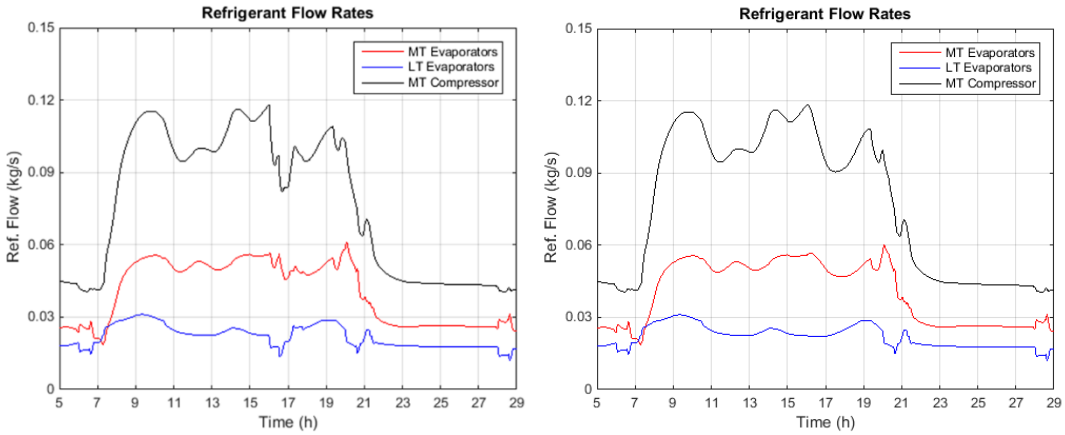

Figure 119 Refrigerant Flow Rates, DR4, no PCM (left) and Baseline (right)

The refrigerant mass flow rates are shown for the DR4 case (left) and baseline case (right) in Figure 119. Like the above figures, the change during the DR event is pronounced, as the mass flow in each evaporator stage declines and the MT compressor mass flow rate decreases by approximately 25% during the shed event. The bypass flow rate, shown in Figure 120, similarly shows this change, where the bypass flow rate drops by approximately 10% during the shed event.

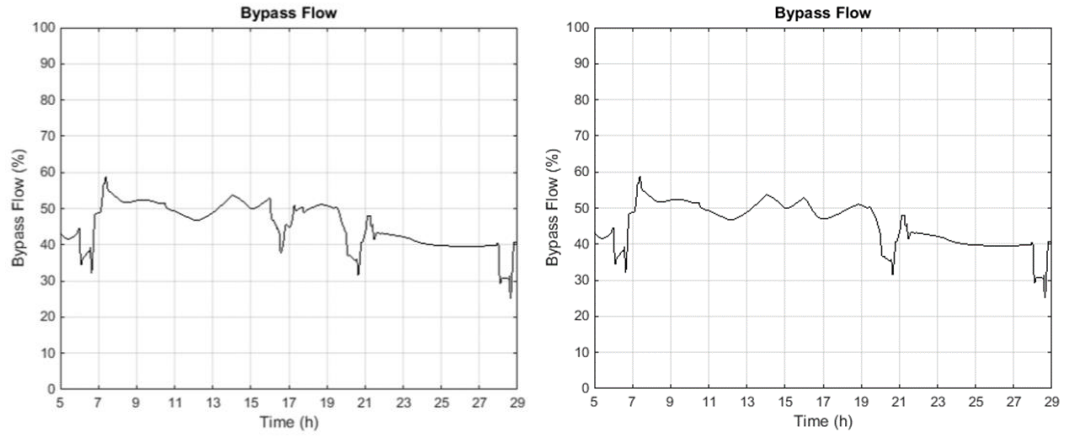

Figure 120 Bypass Flow, DR4, no PCM (left) and Baseline (right)

Results for DR1 are shown below, which is a more complicated scenario: multiple shed calls are made to each case. The total power profile, along with the baseline power profile, are shown in Figure 121. The event begins at 1:00 PM and continues to 4:55 PM, which each case called to shed twice for thirty minutes during the duration. In this example, only one case sheds at any given time. The power profile shows the power in the DR case is significantly reduced for much of the baseline period, but is higher than the baseline shortly before 3:00 PM, and again before 5:00 PM.

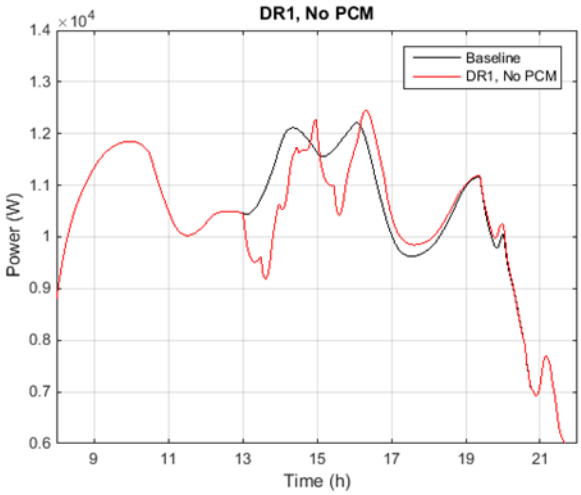

Figure 121 Total Power, Baseline and DR1, no PCM

The subsystem power is shown in Figure 122. As in the prior example, power reduction on both compressor stages is followed by a rebound and recovery.

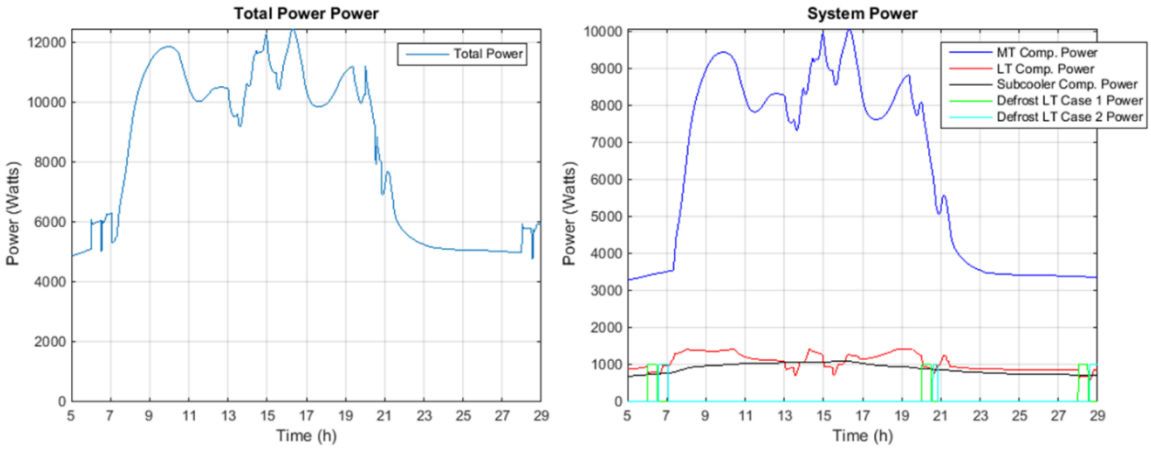

Figure 122 Total Power and Subsystem Power, DR1, no PCM

The total capacity of each evaporator stage is shown in Figure 123 alongside the baseline. The first shed, which is a LT case only, causes response in the high side capacity as well: the reason for this is that the decrease in LT load leads to reduced LT compressor speed, in turn reducing the heat rejection requirement for the MT compressor; since the MT compressor speed is controlled by refrigerant pressure, the abrupt change to LT load manifests in the form of decreased MT suction pressure, leading to a MT compressor reduction which lags behind the LT delivered capacity reduction. This causes a brief increase in delivered capacity on the MT stage.

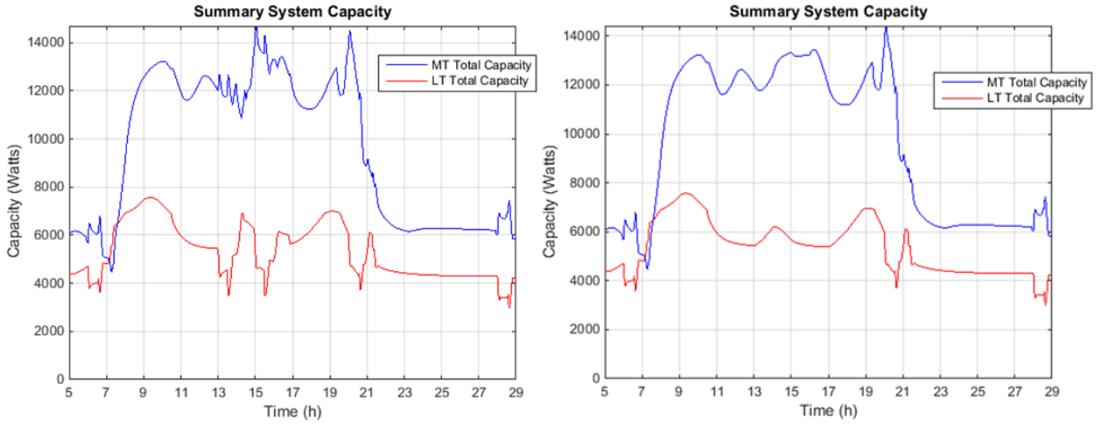

Figure 123 Capacity, DR1, no PCM (left) Baseline (right)

The slight oscillations in MT suction pressure can be seen in Figure 65.

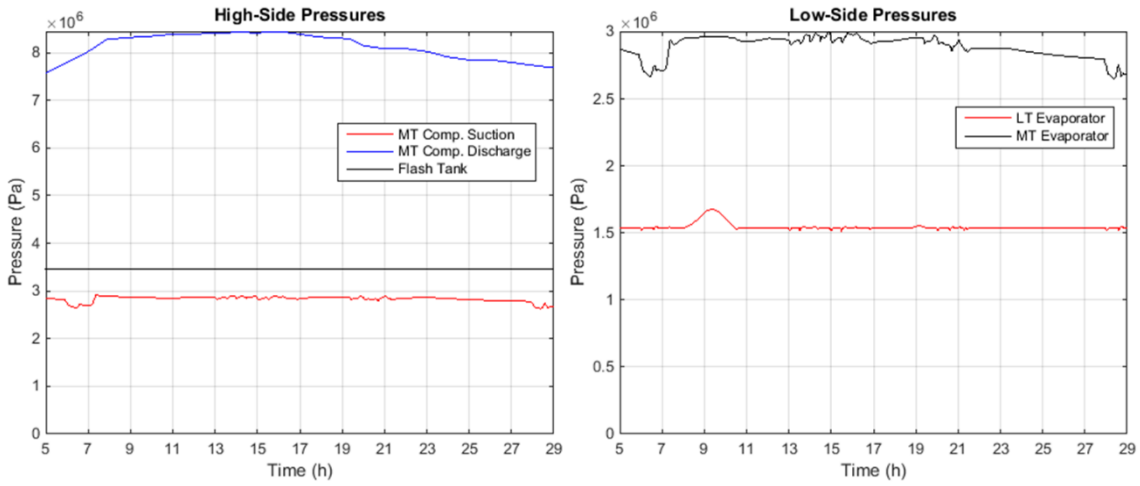

Figure 124 Refrigerant Pressure, DR1, no PCM

Figure 125 shows the LT and MT case temperatures. On the LT stage, two events per display case occur, with food temperature increasing in two stages in response to the two events. The MT cases are triggered to shed twice each, but only provide meaningful response once due to food temperatures remaining above the cutoff threshold of 4°C.

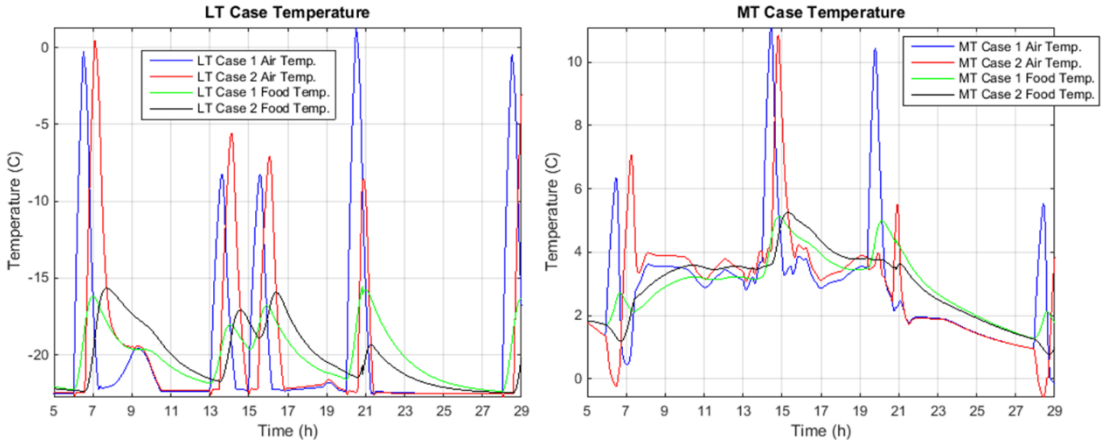

Figure 125 MT and LT Case Temperatures, DR 1, no PCM

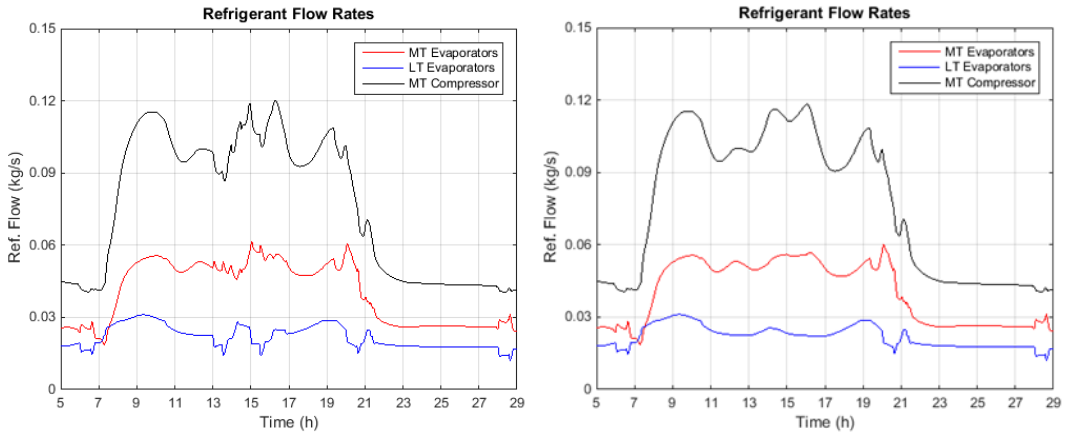

Figure 126 Refrigerant Flow Rates, DR1, no PCM

The refrigerant flow rates for DR1 and the baseline case are shown in Figure 126, and the bypass flow rate in Figure 127. The benefits of the shed are less clear in this example than in the DR4 example: the bypass flow percentage, which decreased followed by a small increase in the case of DR4, varies more significantly above and below the level of the baseline in DR1.

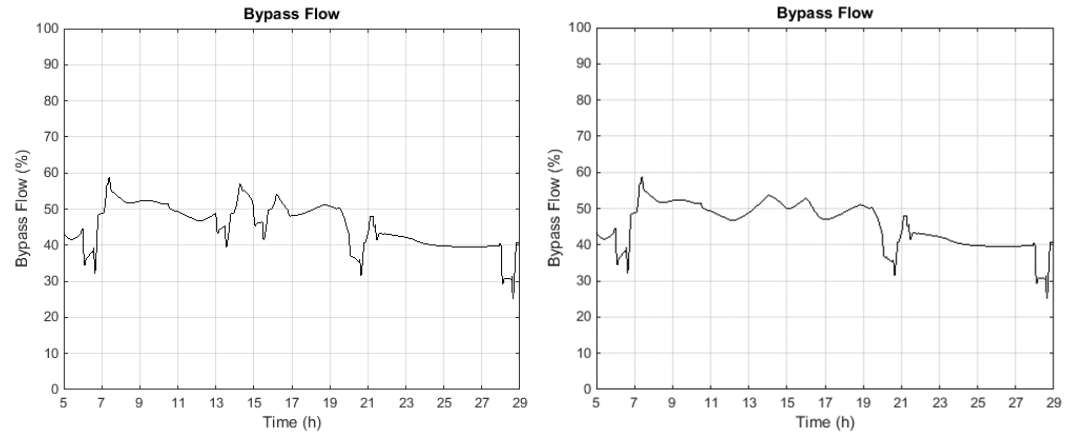

Figure 127 Bypass Flow, DR1, no PCM (left) and Baseline (right)

The above two examples show a simple case of load shedding and a more complex example, in qualitative terms. The results highlight that performing simple load sheds can be relatively complicated, particularly if a long-duration reduction is the desired

outcome. The LT case shed potential is greater because of the larger allowable temperature variation for the products. The MT cases have only a small allowable temperature deviation, and recovery from a shed may last too long to allow a reliable, second call to a given case.

The results of each of the eight DR cases can be looked at in terms of instantaneous power, or energy intervals. The following figures show all eight cases with the baseline power profile for comparison. Figure 128 shows the average total system power of the baseline scenario, in black, and with the DR event, in red. The hours of interest are shown, as the power is identical outside of the DR event and subsequent rebound hours. Since the power varies and is at times lower and at times higher than the baseline, it is helpful to consider overall energy. Figure 129 shows hourly energy comparing baseline and treatment. For this calculation, the simulated power is integrated using *Matlab's* trapezoidal numerical integration to compute energy consumption for each hour.

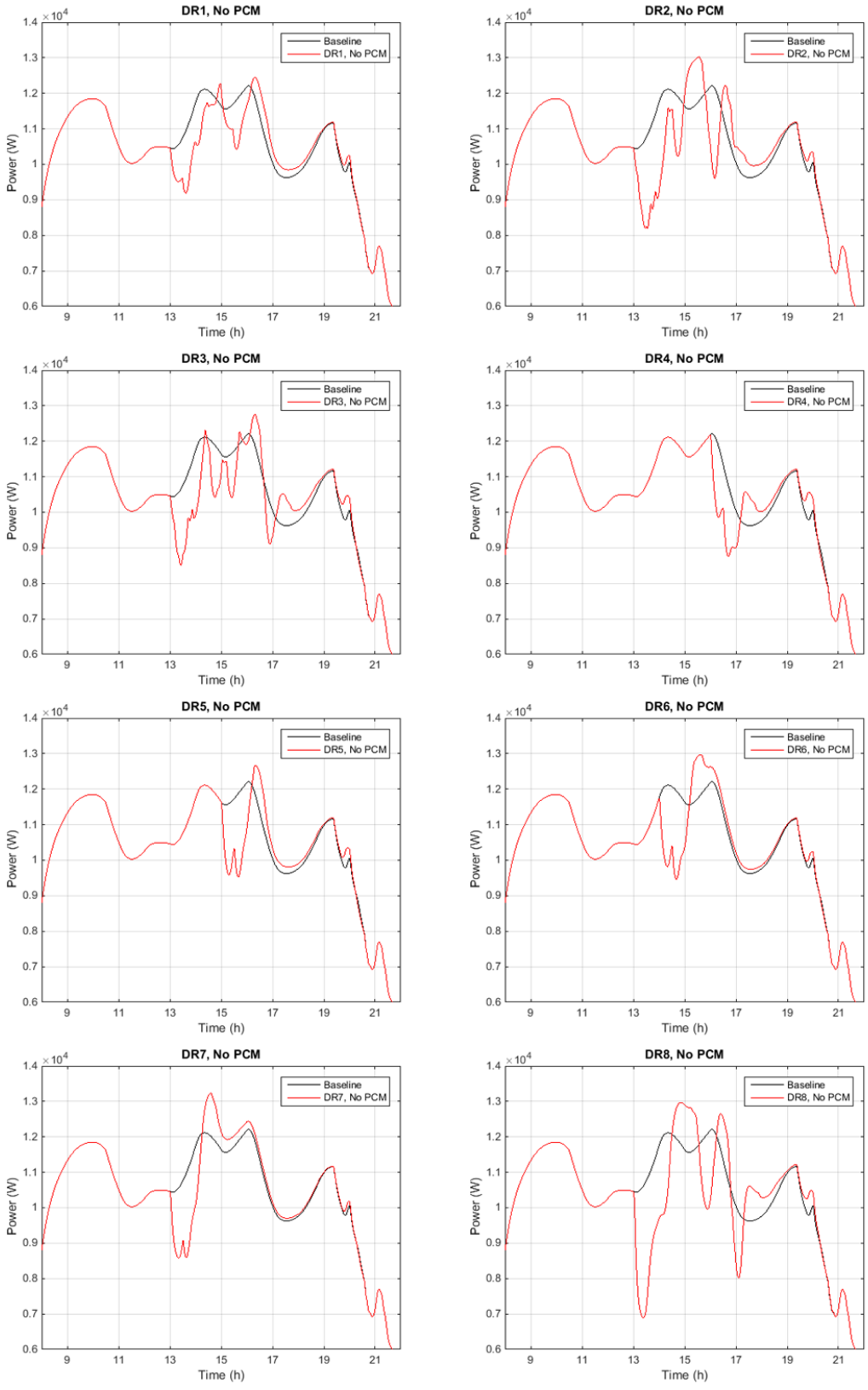

Figure 128 Total Power During DR Events, with Baseline Power, No PCM

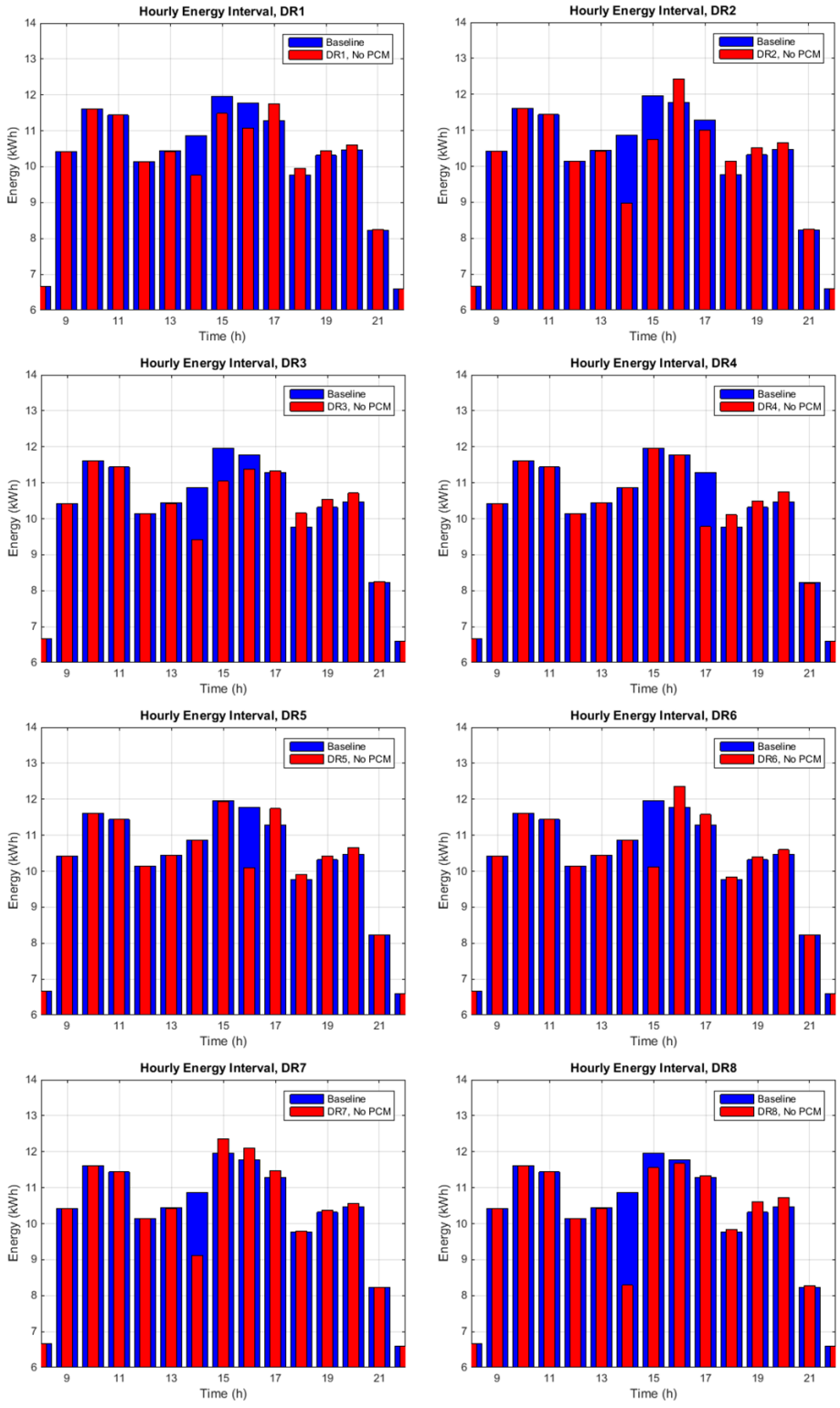

Figure 129 Total Hourly Energy During DR Events (red) and Baseline Energy (blue) (intervals are "hour-ending")

The results above show that for the scenarios where each case is called to shed several times, there is a reduction overall in energy during the hours of 1:00 to 5:00 PM; there are periods in which there is significant reduction in instantaneous power and periods with increased instantaneous power, as sheds and rebounds overlap. In cases DR4, DR5, DR6, and DR7, a one-hour period of "shed" is performed in two parts, with one MT and one LT case shed at a time for 30 minutes each. The shed and rebound are clear when examining power or hourly energy in these cases, with reduction of 1.5-1.8 kWh in the hour of the shed, and a rebound increase of 0.4-0.6 kWh in the hour following the shed. The rebound is most pronounced in the hour after the shed, and a small increase is observed for several hours following. Scenario DR8 is the most aggressive strategy: all cases are called to shed for four hours, and the temperature of the cases dictates when capacity is delivered or interrupted. This strategy shows the deepest short-term drop: a reduction of 2.6 kWh in the first hour (a 24% reduction) which is followed by a rebound and subsequent smaller reductions and rebounds. In this case, the hourly energy is lower or approximately the same for all hours but the effect is most drastic during the first hour of the shed.

Mechanical Subcooler Shed with PCM Thermal Storage

Another possible approach to shedding load for this system is to shed the dedicated mechanical subcooler, replacing the mechanical cooling with the PCM heat sink. This section describes the implementation of storage, without other demand response. The model was simulated using a four-hour window of "shed" during which the mechanical subcooler is off, and the PCM is engaged. Four PCMs are studied with three different heat exchanger sizes, providing a range of subcooling heat transfer

conditions. For water as the PCM (0°C median phase change temperature), two additional heat exchanger sizes are tested to add more granularity. A single case, using water as the PCM with 200m heat exchanger, is examined first in depth to understand qualitative effects, and then the test are compared.

Figure 130 shows the total power consumption during the hours of interest for the system with PCM and subcooler shed, and for the baseline shown with the black line. The result shows a shed of approximately 1,000 watts continuously for the four-hour duration, with the power profile following the same shape but shifted down for the duration of the shed; then, an overnight period of significantly higher power consumption which begins at approximately 8:00 PM (coinciding with a defrost) and ending at approximately 4:00 AM (again coinciding with the beginning of defrost, by chance). During this time, the subcooler is running, but not providing subcooling to the refrigeration cycle; rather, it is cooling the PCM.

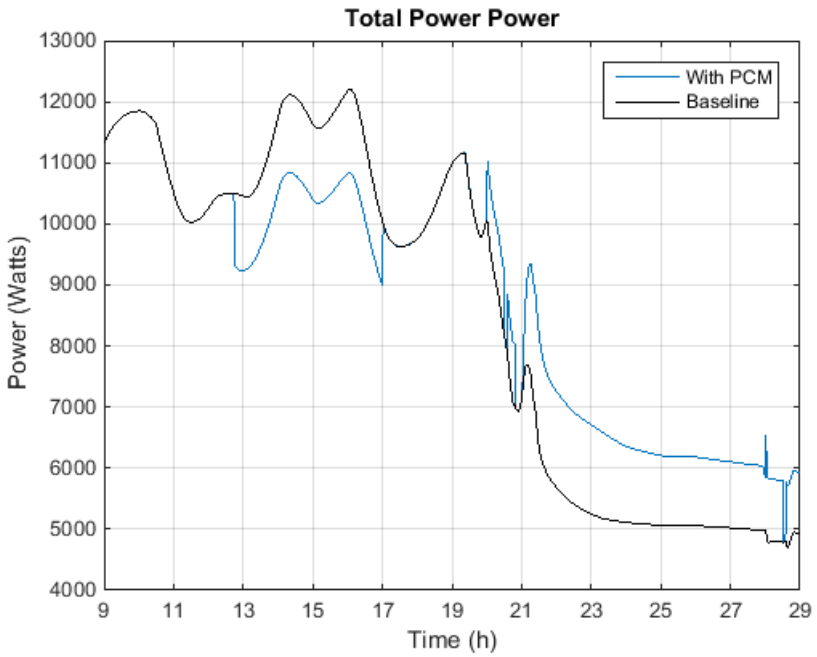

Figure 130 Water, 200m HX, No DR, PCM Engaged 1:00 PM to 5:00 PM

Figure 131 shows the total system power and the subsystem power. The power profile of the MT and LT compressors are quite similar to the baseline, but the subcooler power drops to zero during the period of the shed. In the overnight hours, the MT compressor power is higher than the baseline until the subcooler returns to normal operation at approximately 4:00 AM.

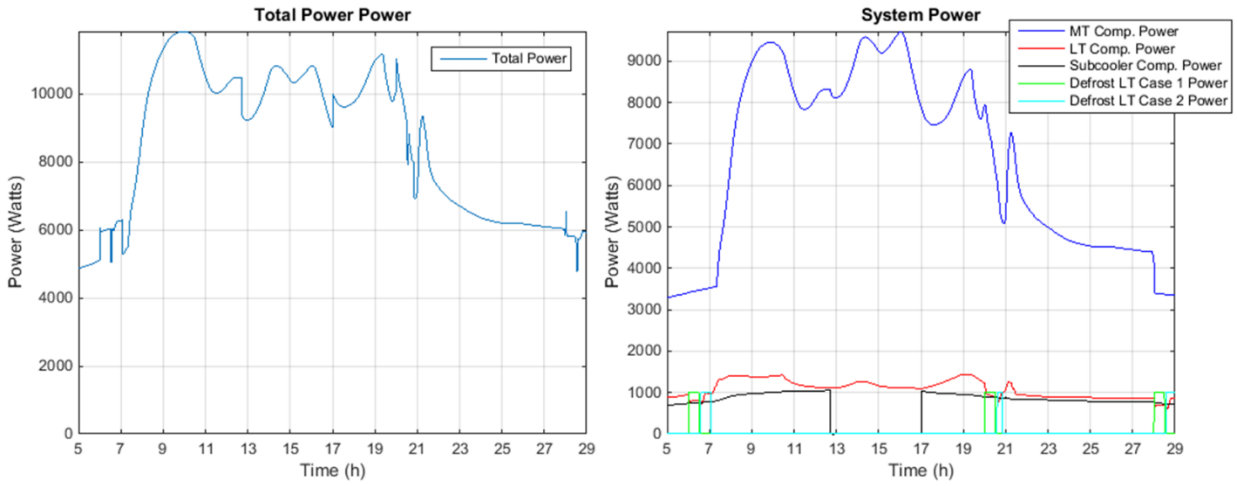

Figure 131 Water, 200m HX, No DR, PCM Engaged 1:00 PM to 5:00 PM

Figure 132 shows the summary capacity profiles for the PCM case (left) and the baseline (right). The capacity is essentially the same even during the shed. This is as expected: the only shed occurs on the subcooler, not on any load.

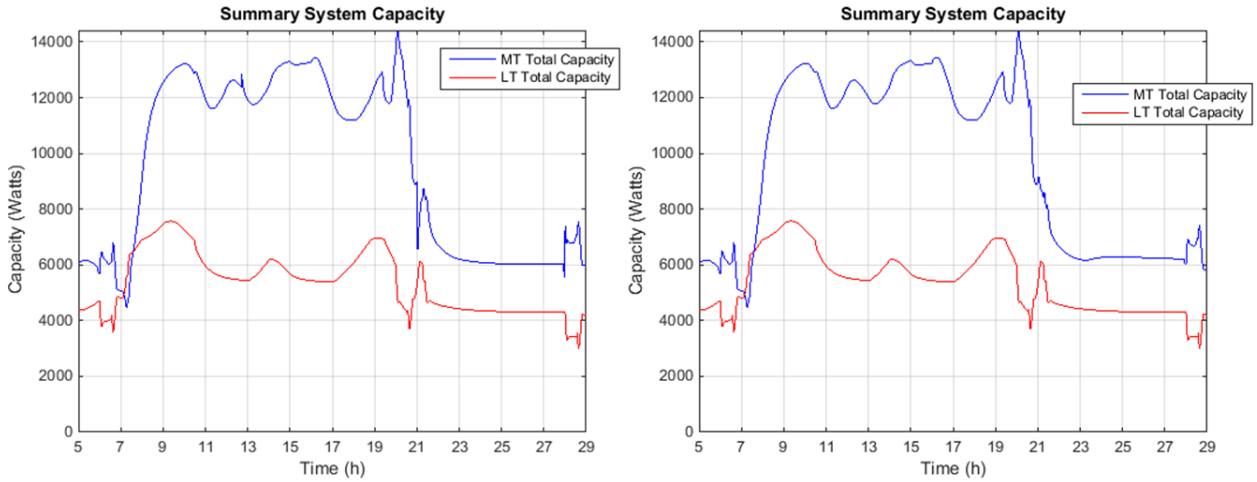

Figure 132 Water, 200m HX, No DR, PCM Engaged 1:00 PM to 5:00 PM (left); Baseline (right)

The LT and MT case temperatures are shown in Figure 133. The LT case profile is essentially the same as the baseline; the MT case profile is also quite similar, although there is a noteworthy difference in the overnight hours. In the baseline case,

the system operated at minimum compressor speed (a phenomenon which would not necessarily be observed in a real system), while as modeled here, the mechanical subcooler is during this time not providing subcooling to the cycle, leading to higher bypass flow requirement and a corresponding higher compressor speed. Since the compressor is not at its minimum speed, the air temperatures reach an equilibrium.

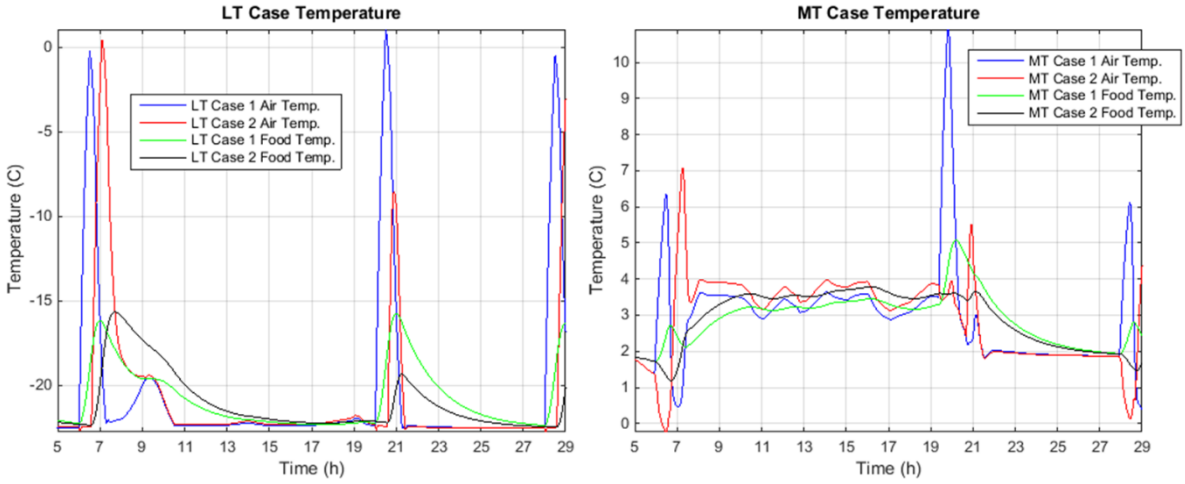

Figure 133 Water, 200m HX, No DR, PCM Engaged 1:00 PM to 5:00 PM

The refrigerant flow rates, shown in Figure 134, demonstrate the same behavior: the CO_2 flow rates are nearly the same when the subcooling is provided by the PCM rather than the mechanical subcooler, and the evaporator flow rates are quite similar at all times. The MT compressor flow is substantially higher in the overnight charging period in the PCM case than the baseline, for the reasons described above.

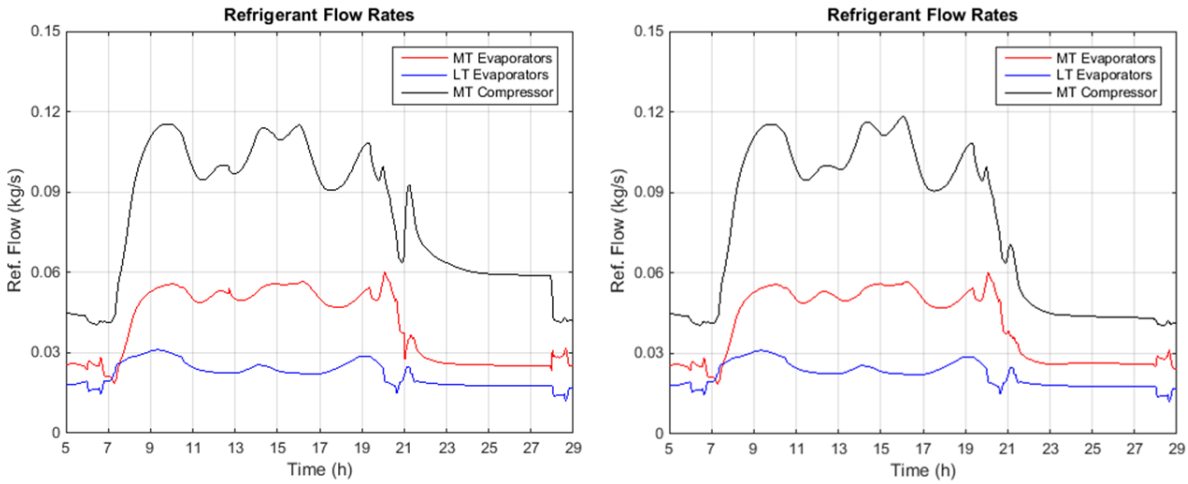

Figure 134 Water, 200m HX, No DR, PCM Engaged 1:00 PM to 5:00 PM (left); Baseline (right)

The bypass flow rate is shown in Figure 135 for the PCM case and the baseline. Again, the profiles are nearly the same until the "charge" period; the bypass flow is approximately 40% overnight in the baseline, and approximately 60% overnight while subcooling is not available for the CO_2 cycle.

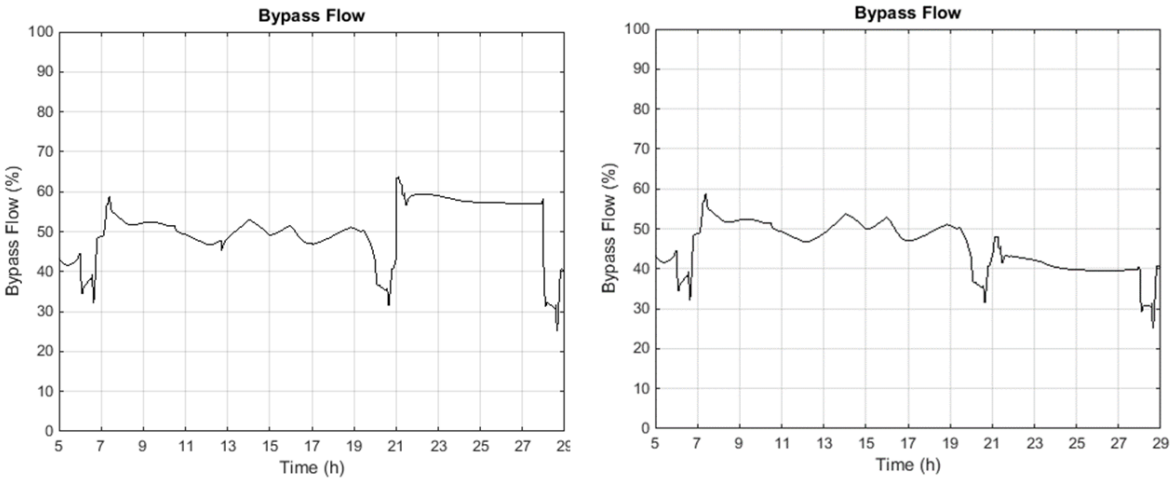

Figure 135 Water, 200m HX, No DR, PCM Engaged 1:00 PM to 5:00 PM (left); Baseline (right)

The charts above show the general behavior when shedding the mechanical subcooler, using thermal storage via the PCM to replace the subcooling for the cycle. The close similarities in behavior observed during the shed period shown here are attributable to two factors: on the evaporator side, there is ample capacity in either case (mechanical subcooling or PCM subcooling), and there is no reason for the evaporator behavior to differ. For the bypass flow rate and the behavior of the MT compressor, another factor is at play: in the case shown here, the amount of subcooling provided by the PCM is similar to the capacity of the mechanical subcooler under these conditions. Therefore, from the perspective of the CO_2 cycle, there is little change when switching. This is not necessarily the case, as the temperature and heat exchanger properties of the PCM system can lead to a higher or lower subcooling capacity than the mechanical subcooler, which in turn changes the CO_2 cycle during PCM subcooling. The following section shows high-level comparison of the different PCMs and heat exchanger sizes, followed by summary observations of these differences.

Water as PCM

Figure 136 shows the results, keeping water as the PCM. For water, five heat transfer capacities are shown. The power, shown in the figure on the left, decreases during the shed with increasing heat transfer size. However, there is a diminishing return, which will be discussed in more depth below. On the right, the hourly energy difference is shown. The hourly energy reduction during the shed is between 730 and 760 watt-hours in the 100m case, 1,020 to 1,090 watt-hours in the 150m case, 1,160 to 1,280 in

the 200m case, 1,250 to 1,380 watt-hours in the 250m case, and 1,320 to 1,460 watt-hours in the 300m case.

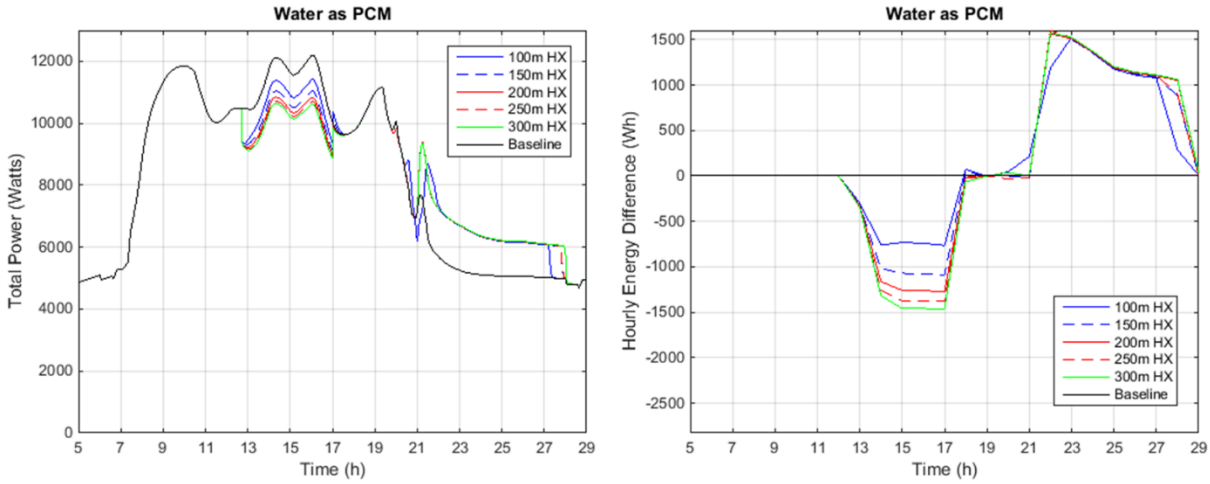

Figure 136 Total Power and Hourly Energy Difference vs. Baseline, Water as PCM, Different HX Sizes

The temperature of the PCM is shown during each simulation in Figure 137. The PCM was modeled with a temperature-enthalpy table, with phase change occurring between -0.5°C and 0.5°C; as expected, the latent heat capacity of the storage volume is substantially larger than is used in the discharge period.

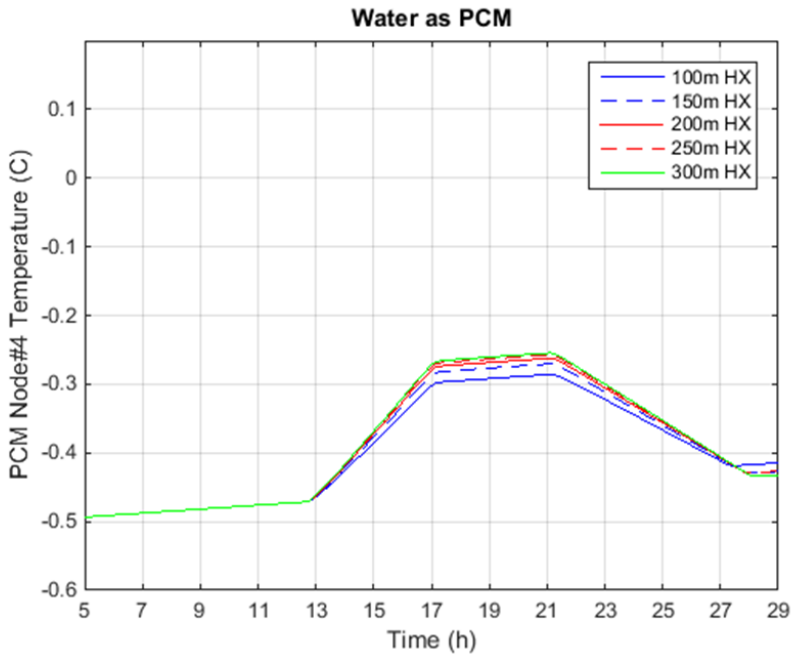

Figure 137 PCM Node Temperature During Operation, Water as PCM, Different HX Sizes

The charging and discharging capacity is shown in Figure 138. The capacities again vary with heat exchanger size, with discharge ranging from a maximum of 4,710 W in the 100m case to 5,960 W in the 300m case. During discharge, the capacity varies as the MT compressor flow rate and CO_2 refrigerant temperature entering the subcooler vary. During recharge, the capacity stabilizes at approimatey 2,880W to 2,910W in the 100m case and 3,420W to 3,460W in the 300m case. The capacity increases slightly as the outdoor air temperature decreases; the PCM temperature is essentially constant during the charging.

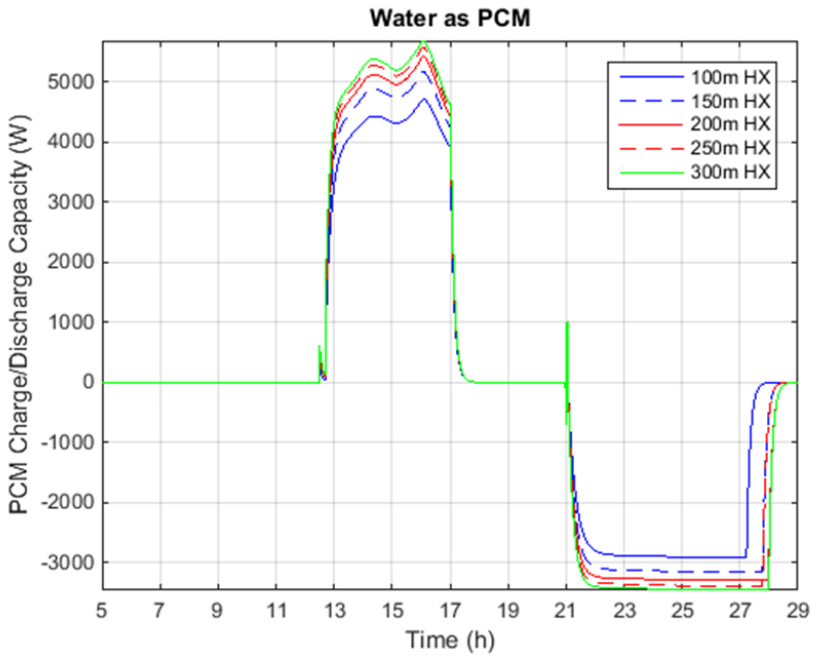

Figure 138 PCM Charging and Discharging Capacity, Water as PCM, Different HX Sizes

For each of the tests, the discharge capacity is plotted against heat exchanger length at 4:00 PM in Figure 139. The discharge capacity with 300m pipe is approximately 20% higher than the capacity with the 100m pipe; however, the improvement in capacity dimishes with increasing heat exchanger size. With 100m as a baseline, doubling heat exchanger size achieves 73% of the benefit that tripling heat exchanger size achieves.

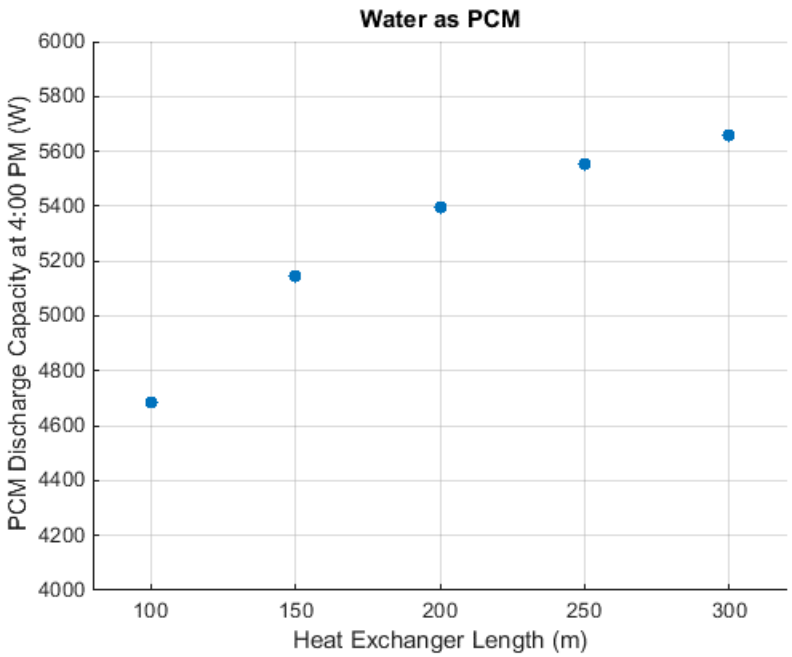

Figure 139 PCM Instantaneous Discharging Capacity at 4:00 PM vs. Heat Exchanger Size, Water as PCM

Viewed differently, the addition of heat exchanger surface for a given PCM provides greater reductions in total system power during the discharge. Figure 140 shows the total system power, at 4:00 PM, with each heat exchanger size. The system power is approximately 7% lower with the 300m heat exchanger than with the 100m heat exchanger. However, again much of the benefit can be achieved with a smaller heat exchanger. The power with the 200m heat exchanger is 5% lower than with the 100m heat exchanger.

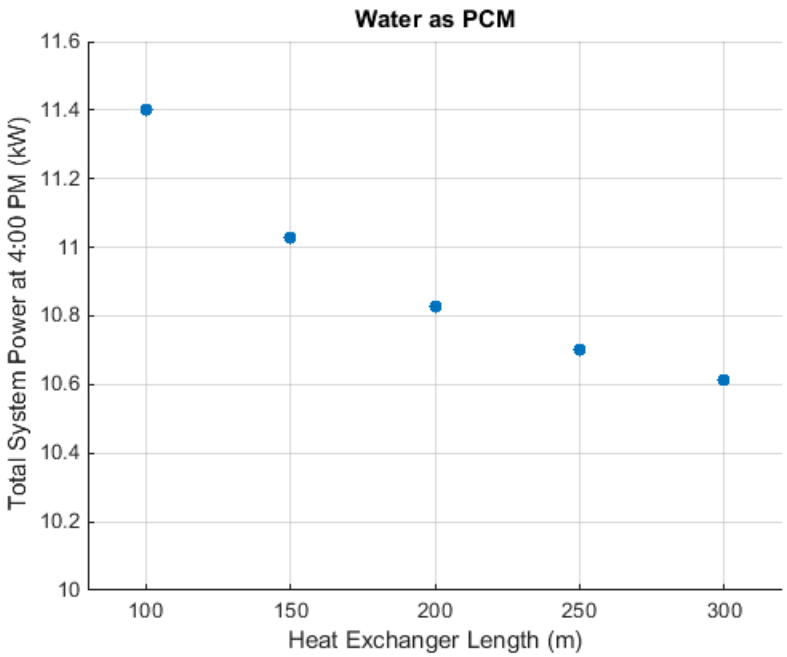

Figure 140 Total System Power at 4:00 PM vs. Heat Exchanger Size, Water as PCM

Other PCMs

Three other PCMs are investigated. Two have higher phase change temperatures than water, and one has lower phase change temperature. First, $C_{13}H_{28}$ (phase change between -5.8°C and -4.8°C) is shown. In this case, a larger subcooling effect is observed during the shed than the water case. The hourly reduction in energy during the period of interest is 1,120 Wh to 1,140 Wh with the 100m heat exchanger, 1,550 Wh to 1,680 Wh with the 200m heat exchanger and 1,700 to 1,880 Wh in the 300m heat exchanger case. The lower PCM temperature leads to greater reduction during the shed period because a higher degree of subcooling is provided for a given heat exchanger size. On the other hand, the power increase in the overnight re-charge period is approximately the same: the CO_2 cycle operates without subcooling in either

case, and therefore the impact on the main cycle because of no subcooling is the same.

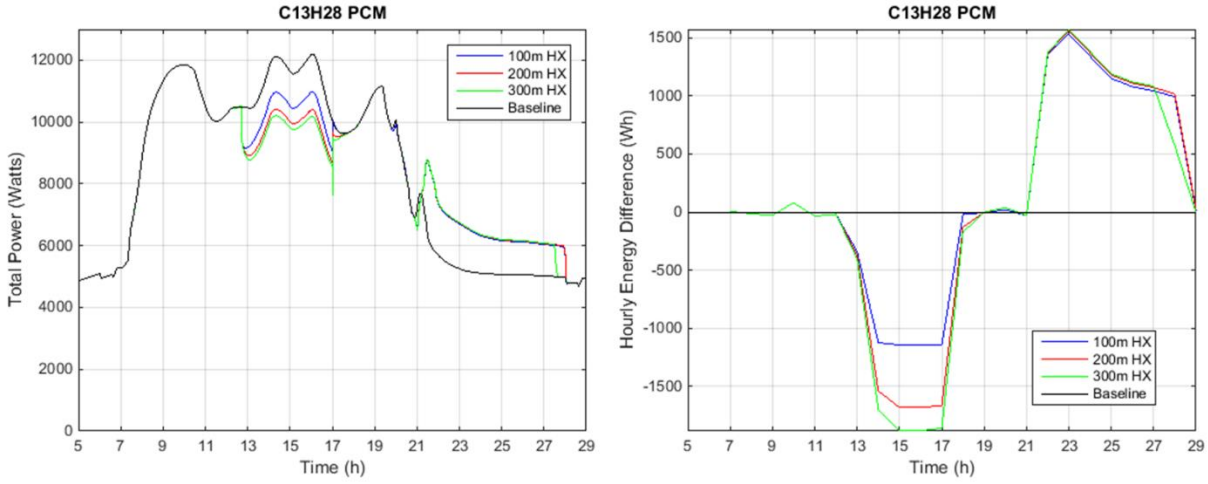

Figure 141 Total Power and Hourly Energy Difference vs. Baseline, $C_{13}H_{28}$ as PCM, Different HX Sizes

Figure 142 shows the temperature profile, again showing a narrow temperature band throughout. The temperature profile also reveals that the PCM is not returned to the starting temperature by the re-charge shown here. One factor impacting this is a reduced charging capacity by the mechanical subcooler, due to the lower PCM temperature.

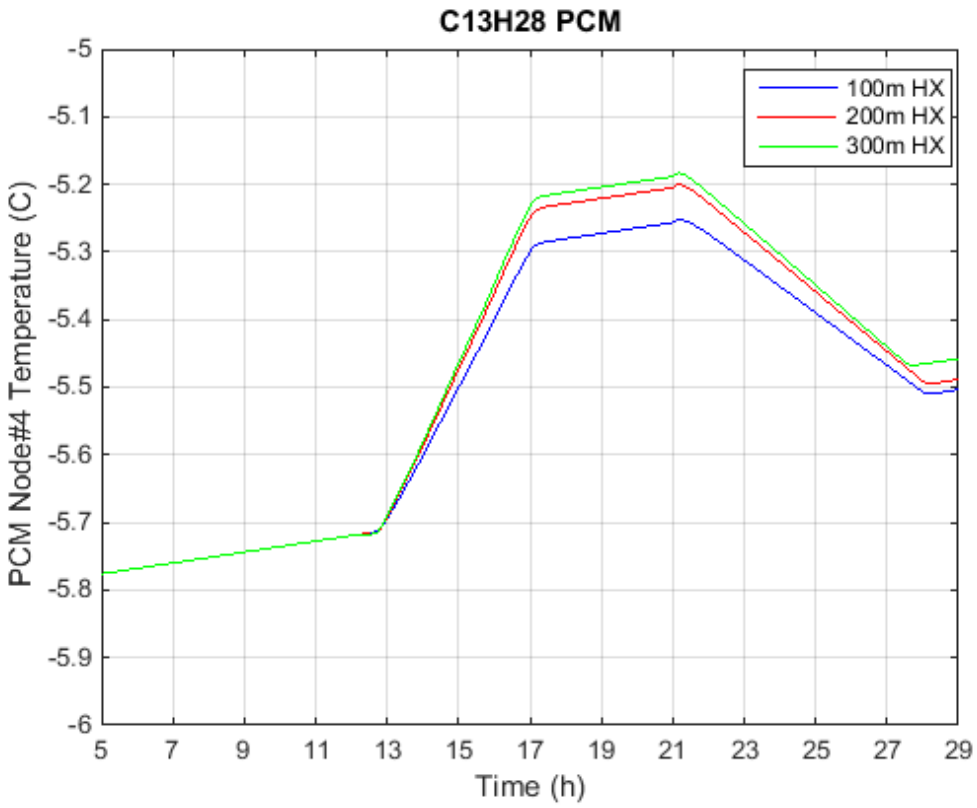

Figure 142 PCM Node Temperature During Operation, $C_{13}H_{28}$ as PCM, Different HX Sizes

Figure 143 shows the charge and discharge capacities for $C_{13}H_{28}$, and also for water. The discharge rate is higher with the lower-temperature PCM, but the charge rate is lower.

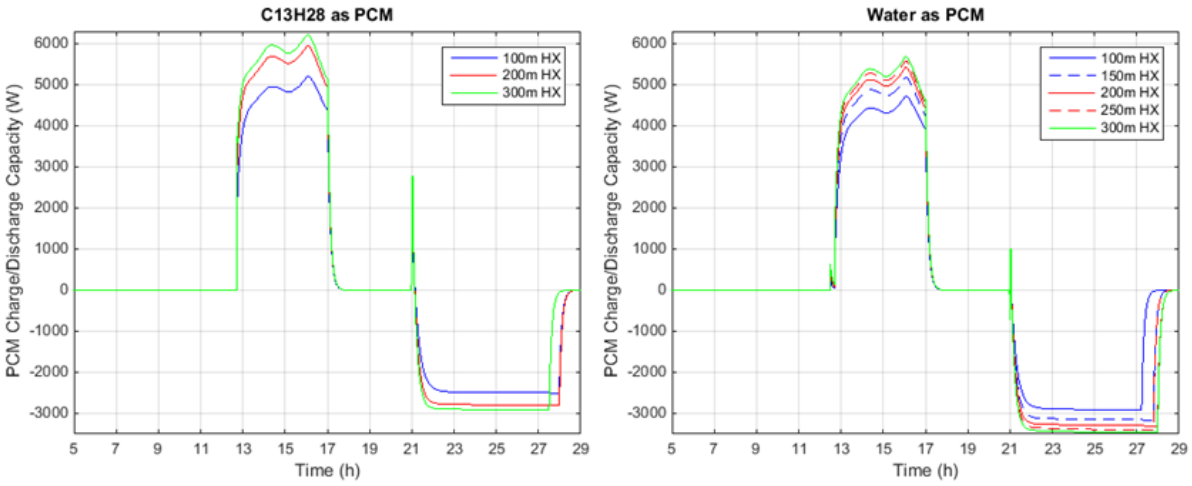

Figure 143 PCM Charging and Discharging Capacity, $C_{13}H_{28}$ as PCM, Different HX Sizes

$C_{14}H_{30}$ is shown next (5.5°C to 6.5°C phase transition). Figure 144 shows the power (left) and hourly energy difference (right) for the PCM and baseline cases. The higher PCM temperature results in a smaller reduction in power, compared with the water case, given the same heat exchanger cases. The duration, however, is shorter, and normal subcooler operation resumes at approximately 3:00 AM.

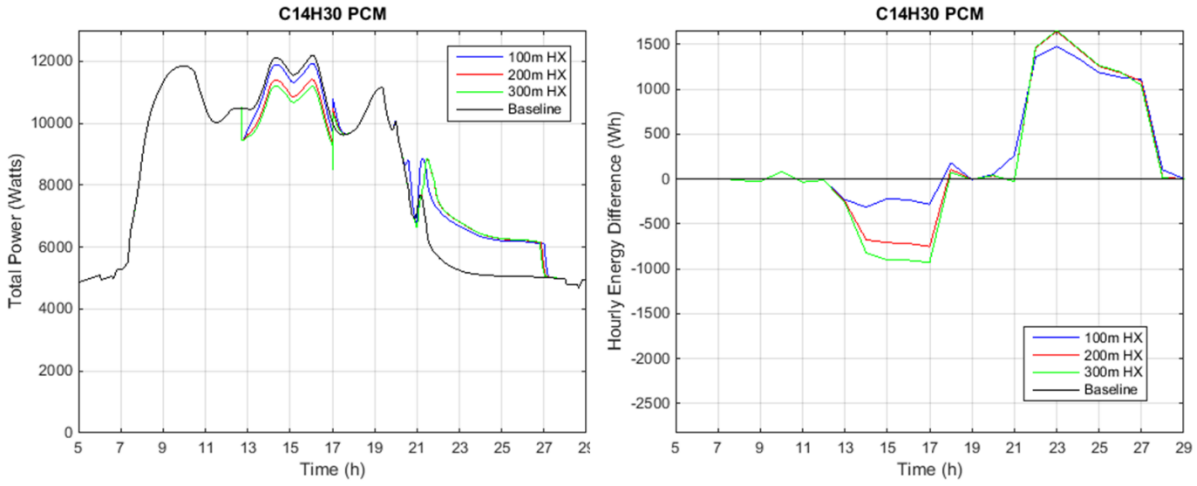

Figure 144 Total Power and Hourly Energy Difference vs. Baseline, $C_{14}H_{30}$ as PCM, Different HX Sizes

The PCM temperatures are shown in Figure 145. Similar to the water case, the temperature remains relatively close to the saturated solid temperature, because of the large storage volume in the model.

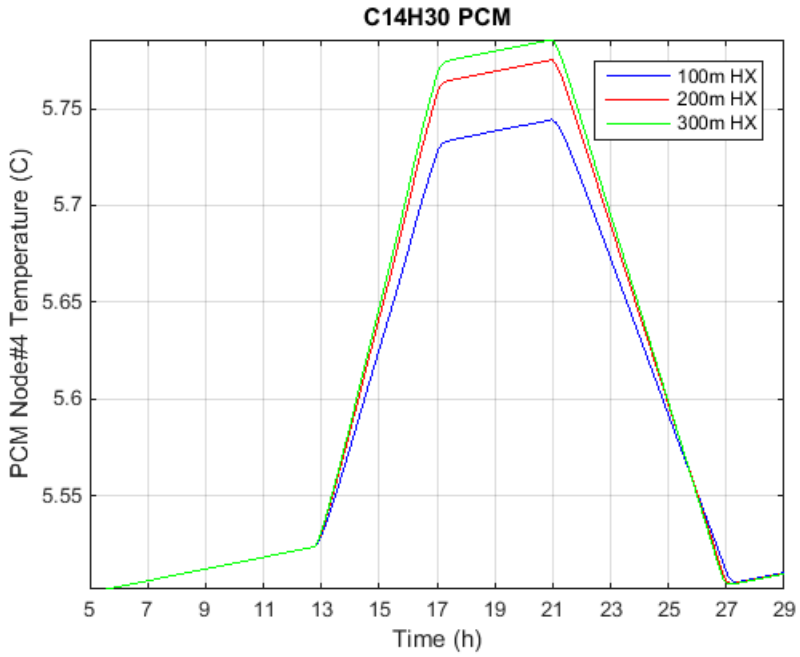

Figure 145 PCM Node Temperature During Operation, $C_{14}H_{30}$ as PCM, Different HX Sizes

To provide a comparison against PCMs with a very narrow phase change temperature band, the PCM5050 is also shown, modeled with 3.4°C to 10.2°C phase change temperature. The power profile shown in Figure 146 is visually similar to that in Figure 144 for $C_{14}H_{30}$. The difference in the hourly energy graphs shows a subtle difference: the energy reduction gets slightly larger over time for the 200m and 300m heat exchanger cases with $C_{14}H_{30}$ (as it does with the other PCMs), but gets slightly smaller over time for those cases with the PCM5050 case. This may be explained by examining the temperature shown in Figure 147. In the other PCM cases, the phase change material temperature varies by less than 0.5°C during the discharge; in this

case, the temperature increases by over 2°C over the course of the discharge period. This difference manifests in a gradually-reducing subcooling effect over the course of the discharge.

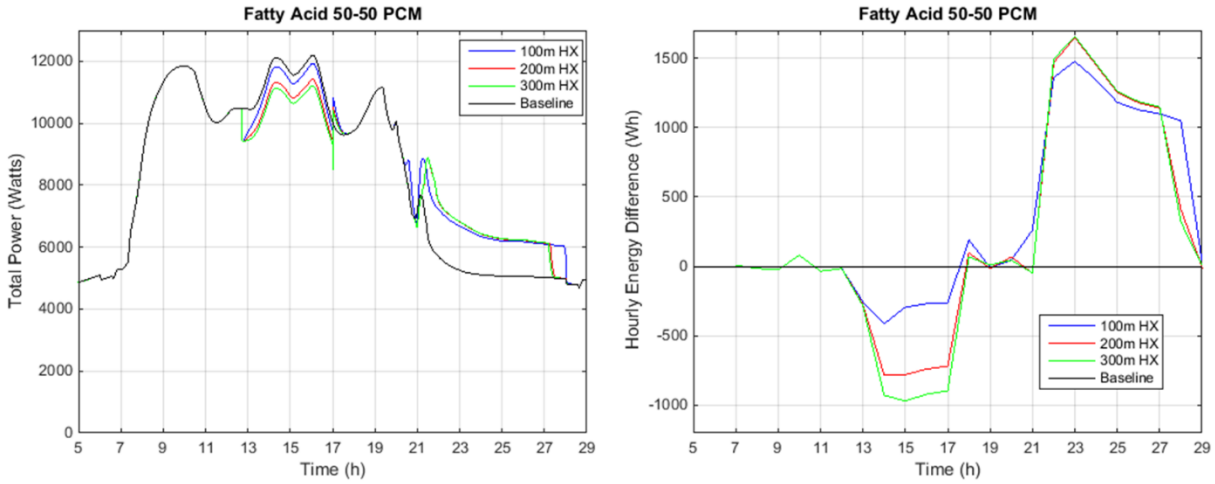

Figure 146 Total Power and Hourly Energy Difference vs. Baseline, PCM5050, Different HX Sizes

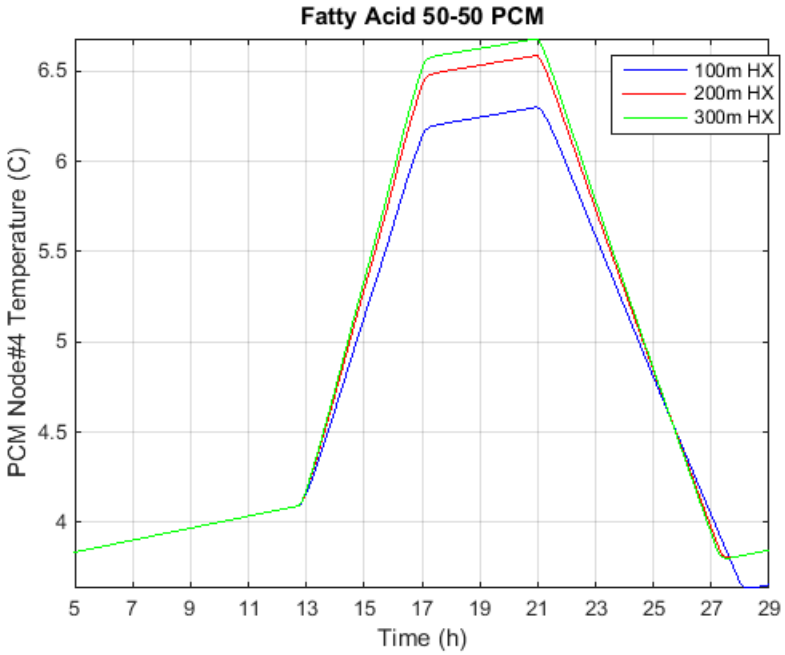

Figure 147 PCM Node Temperature During Operation, PCM5050, Different HX Sizes

Comparison of Different PCMs with Same Heat Exchanger

Finally, a comparison between the different PCMs with a fixed heat exchanger size is shown. Figure 148 shows the power and hourly energy difference versus baseline for each. It is important to note that the recharge is not necessarily equivalent: the system as modeled could not fully recharge the $C_{13}H_{28}$ case, which presents an apparent advantage if not considered.

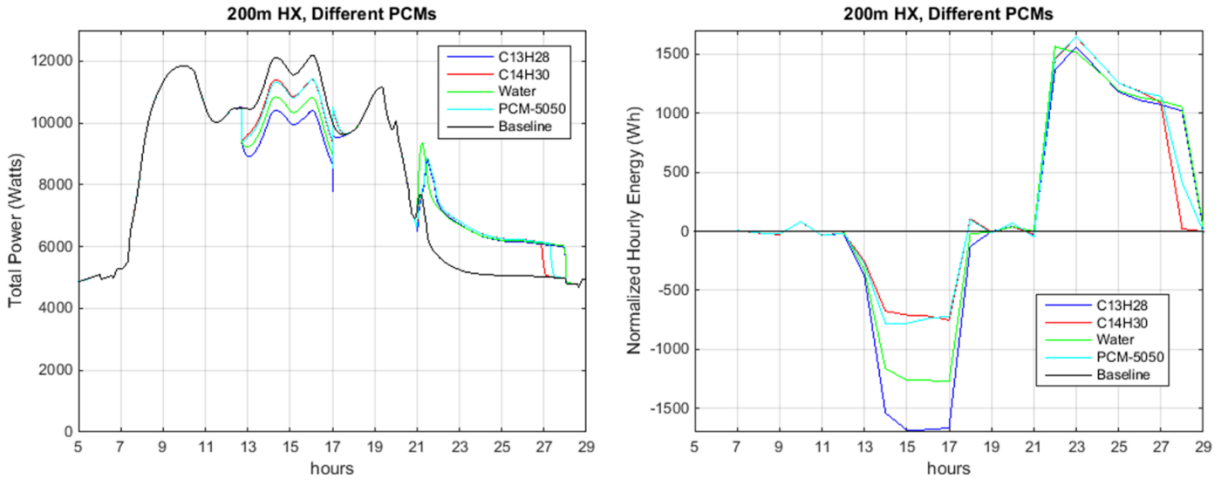

Figure 148 Total Power and Hourly Energy Difference vs. Baseline, Different PCMs with 200m Heat Exchanger Size

Figure 149 shows the temperature range of each PCM for the simulation.

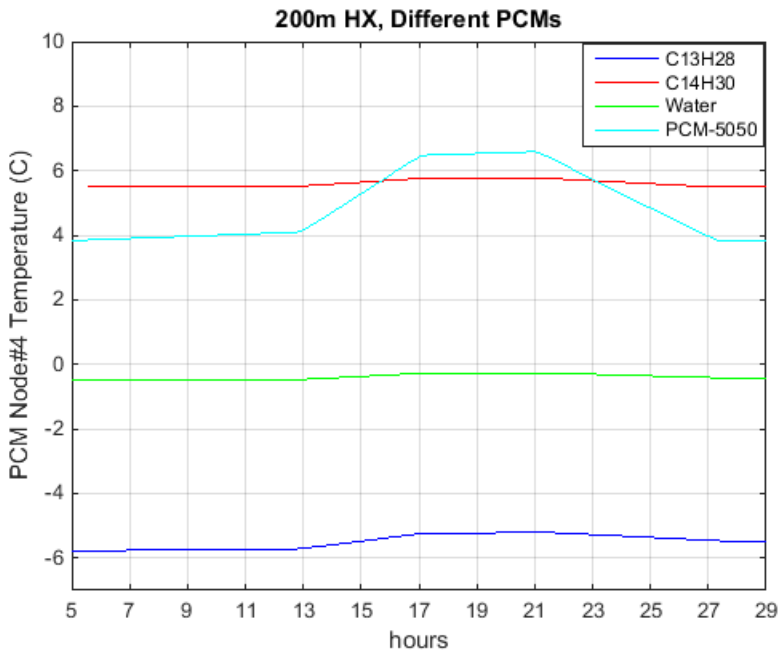

Figure 149 PCM Node Temperature During Operation, Different PCMs with 200m Heat Exchanger Size

The most pronounced difference on the CO_2 cycle side is the refrigerant enthalpy leaving the subcooler. The subcooler leaving enthalpy is plotted over time in Figure 150, illustrating the impact of the subcooling system on the cycle. The baseline case is shown in black. The water PCM case, shown in green, produces a slight reduction in leaving enthalpy, while the two higher-temperature PCMs lead to higher enthalpy, and the $C_{13}H_{28}$ case produces a significant reduction. The implication of these differences is higher flash gas and corresponding bypass flow requirement for the higher enthalpy case, and lower required bypass flow for the lower enthalpy cases. In the recharge period, the behavior is essentially the same: the subcooler leaving enthalpy is drastically higher with the mechanical subcooler charging the PCM compared with the baseline case.

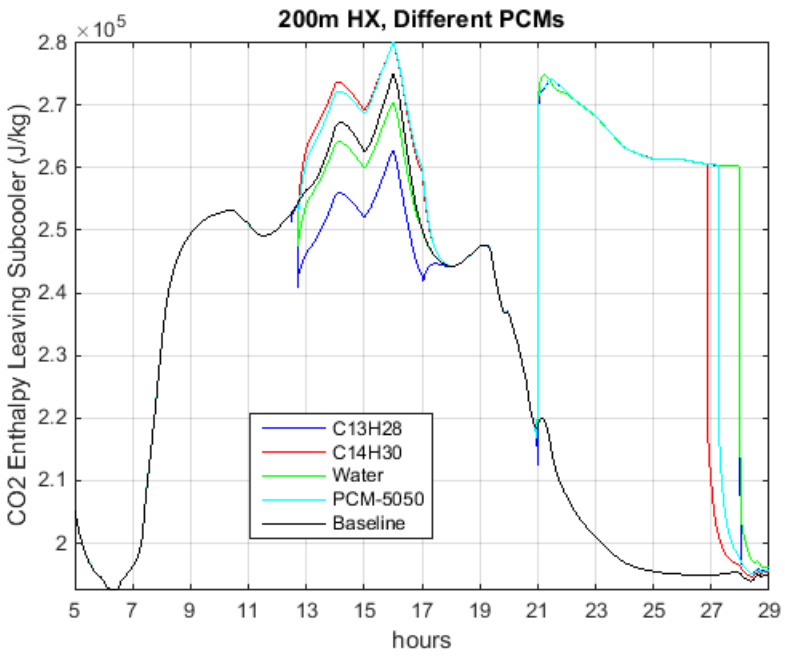

Figure 150 Refrigerant Enthalpy Leaving Subcooler with Different PCMs with 200m Heat Exchanger Size

The effect of the above on overall performance is shown in Figure 151 and Figure 152. Figure 151 shows the impact on system power instantaneously at each hour of the shed. The total power and the MT compressor power are shown, plotted against the enthalpy leaving the subcooler at 1:00 PM, 2:00 PM, 3:00 PM and 4:00 PM. Considering total power, the baseline stands out as an outlier, and the power for each of the PCM cases decreases linearly as subcooler leaving enthalpy decreases. In all cases shown here, the power is lower with the mechanical subcooler being shed, but the difference in reduction from the highest to lowest leaving enthalpy condition is significant. The MT compressor power, it can be seen from this chart, drives the difference in total system power.

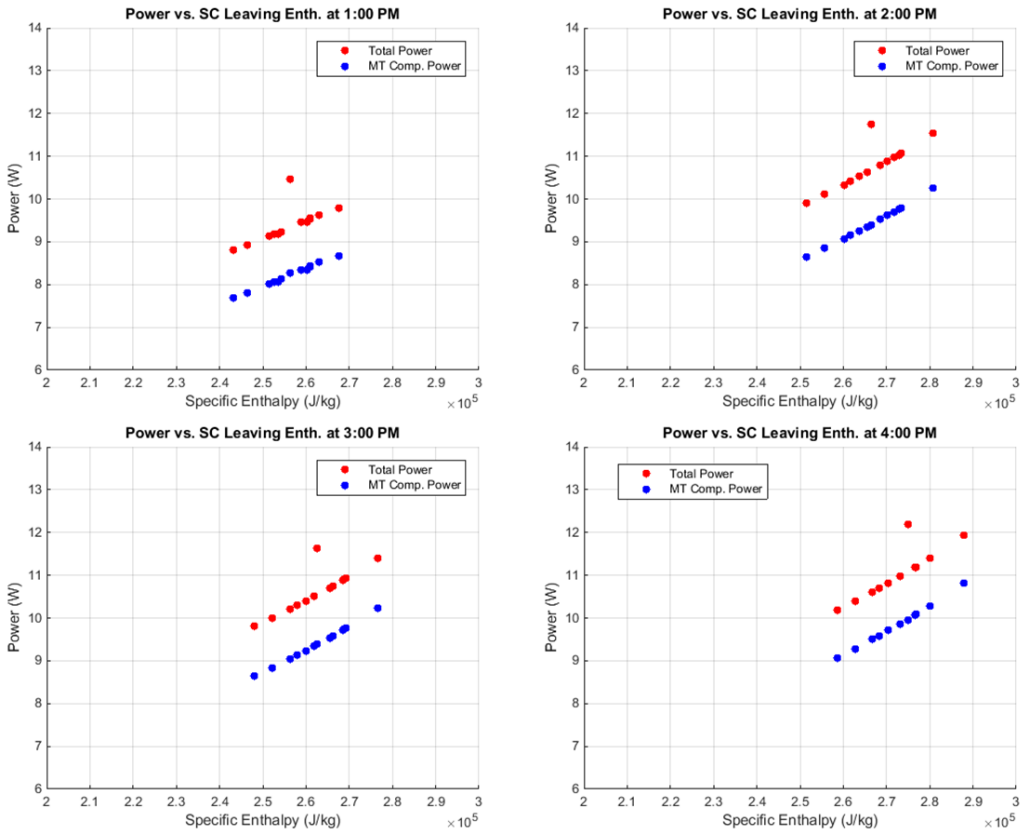

Figure 151 Instantaneous Whole-System Power vs. Subcooler Leaving Enthalpy for Different Hours, All Tests

Previously it was shown that the capacity is the same during the shed in each of these cases. Since the power varies considerably, the COP can be expected to vary similarly. In Figure 152 the COP is plotted against subcooler leaving refrigerant enthalpy. There is again an improvement in all cases, ranging from a very small improvement in the highest-enthalpy cases (where subcooler power is off, but MT compressor power increases due to bypass flow) to a considerable improvement at the other extreme. Examining the 4:00 PM case, the baseline COP is 1.53, and the refrigerant enthalpy leaving the subcooler is 275,000 J/kg. In the least-improved COP case, the enthalpy leaving the subcooler is 288,000 Btu/h and the COP is 1.56, a 2% improvement. Interpolating the PCM results, a case with identical leaving enthalpy

(275,000 J/kg) would produce a COP of 1.69, a 10.5% increase. This improvement is attributable to the subcooler power being zero, with the same subcooling capacity. In the most extreme case modeled here, with 259,000 J/kg leaving enthalpy, the COP is 1.84 or a 20.2% increase.

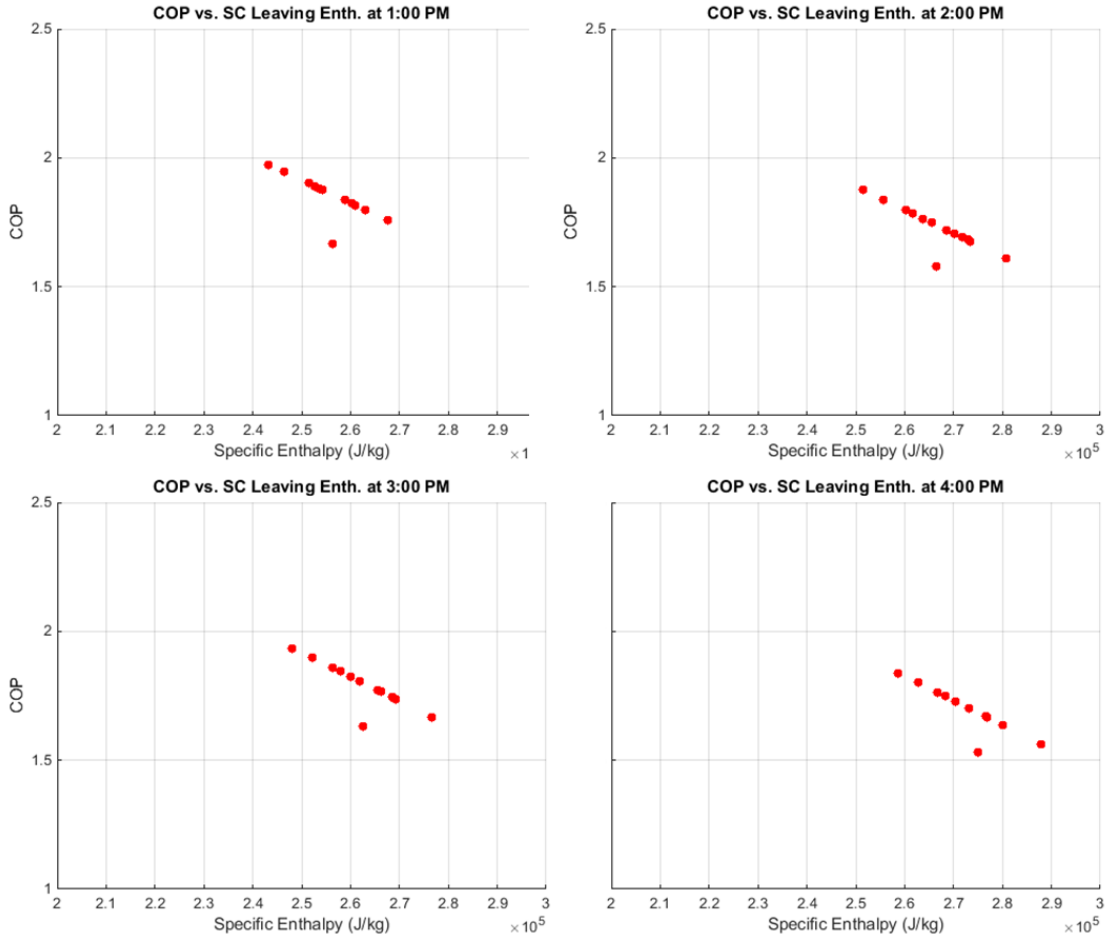

Figure 152 Instantaneous COP vs. Subcooler Leaving Enthalpy for Different Hours, All Tests

DR With PCM Using Water

In the above sections, two cases are examined: display case load sheds and subcooler sheds using PCM subcooling. This section examines the combination of the two: load shedding using the display cases with subcooler shed using the phase change material

to provide passive, dedicated subcooling. The results are presented for two cases, first using water with 200m heat exchanger. For simplicity of qualitative overview, DR4 is examined in detail, before summary results for all DR cases.

Figure 153 shows the power of this case along with the baseline. The resulting power profile resembles the additive impact of each shed as presented above. The instantaneous power reduction is approximately 1,000 watts during the period where the subcooler is shed, and is approximately 3,000 watts to 3,400 watts during the period where both sheds are active.

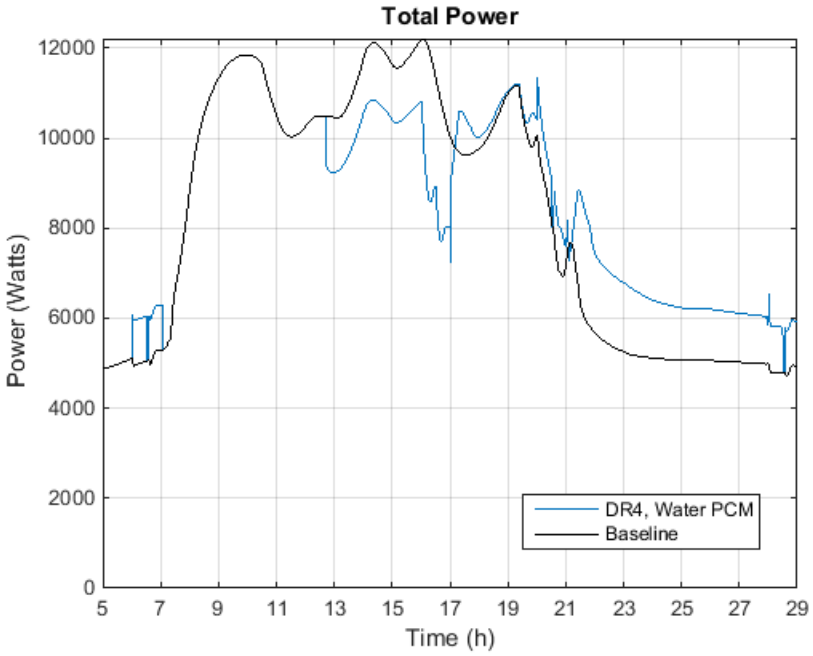

Figure 153 Total Power, Baseline and DR4 with Water PCM

Figure 154 shows the total power and the subsystem component power. Since the PCM scenario used here is that in which the PCM-discharge subcooling capacity is very closely matched to that of the mechanical subcooler, the MT compressor and LT compressor power profiles closely match the DR4 scenario shown in Figure 115.

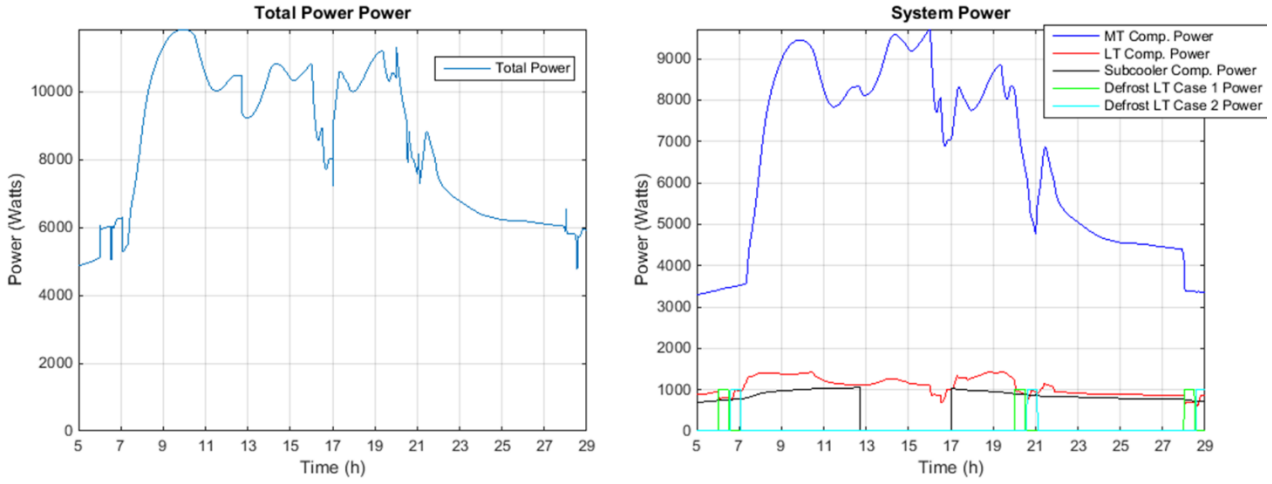

Figure 154 Total Power and Subsystem Power, DR4 with Water PCM

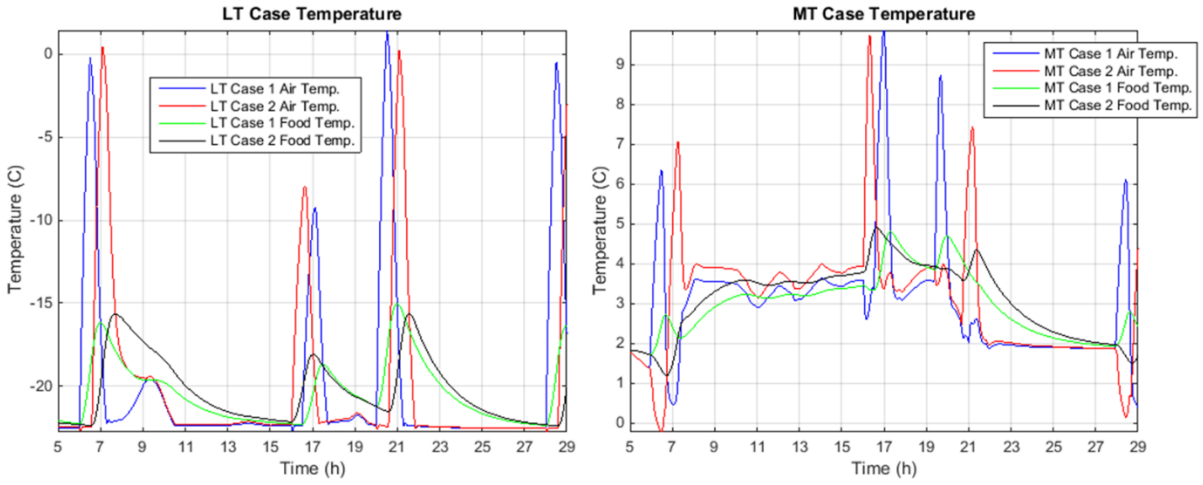

Figure 155 LT and MT Case Temperatures, DR4 with Water PCM

Similarly, the temperature profile in the cases, shown in Figure 155, and the subsystem capacity, shown in Figure 156, are quite similar to the DR4 case without subcooler shed.

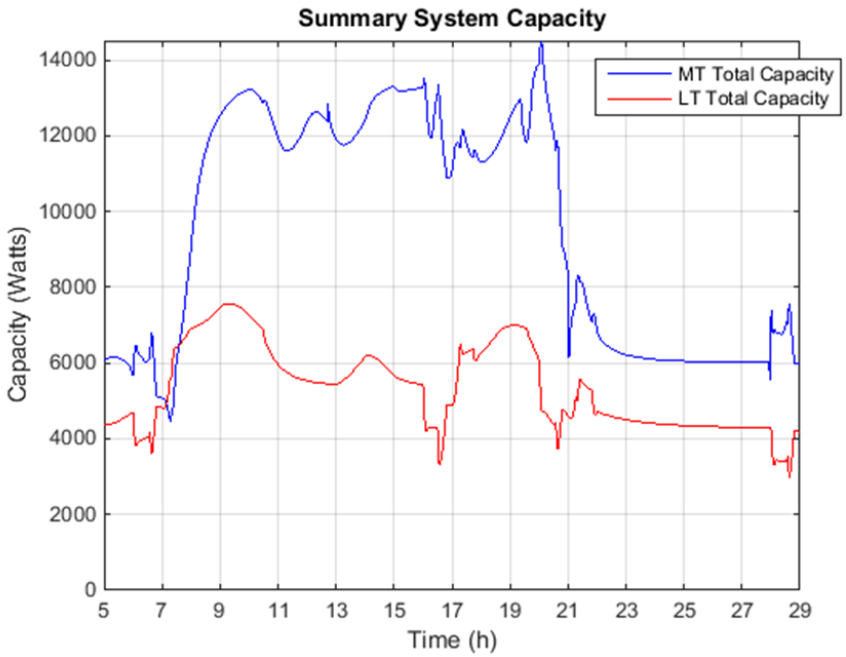

Figure 156 Refrigerating Capacity, DR4 with Water PCM

The combined effects of the subcooler shed and the DR events are shown for each of the simulated DR cases in terms of total system power in Figure 157, and hourly energy interval in Figure 158. For ease of comparison, the DR cases with only case sheds and no mechanical subcooler shed are also shown, with a dotted blue line in Figure 157, and a narrow black bar in Figure 158. In terms of power consumption, the benefits are additive: the reduction during the shed in the case of both a subcooler shed and case sheds is approximately the same as the reduction during the DR shed, plus the reduction attributable to the subcooler shed alone. Considering energy the same observation can be made: the reduction when using both shed approaches is approximately equal to the additive effects of each individually.

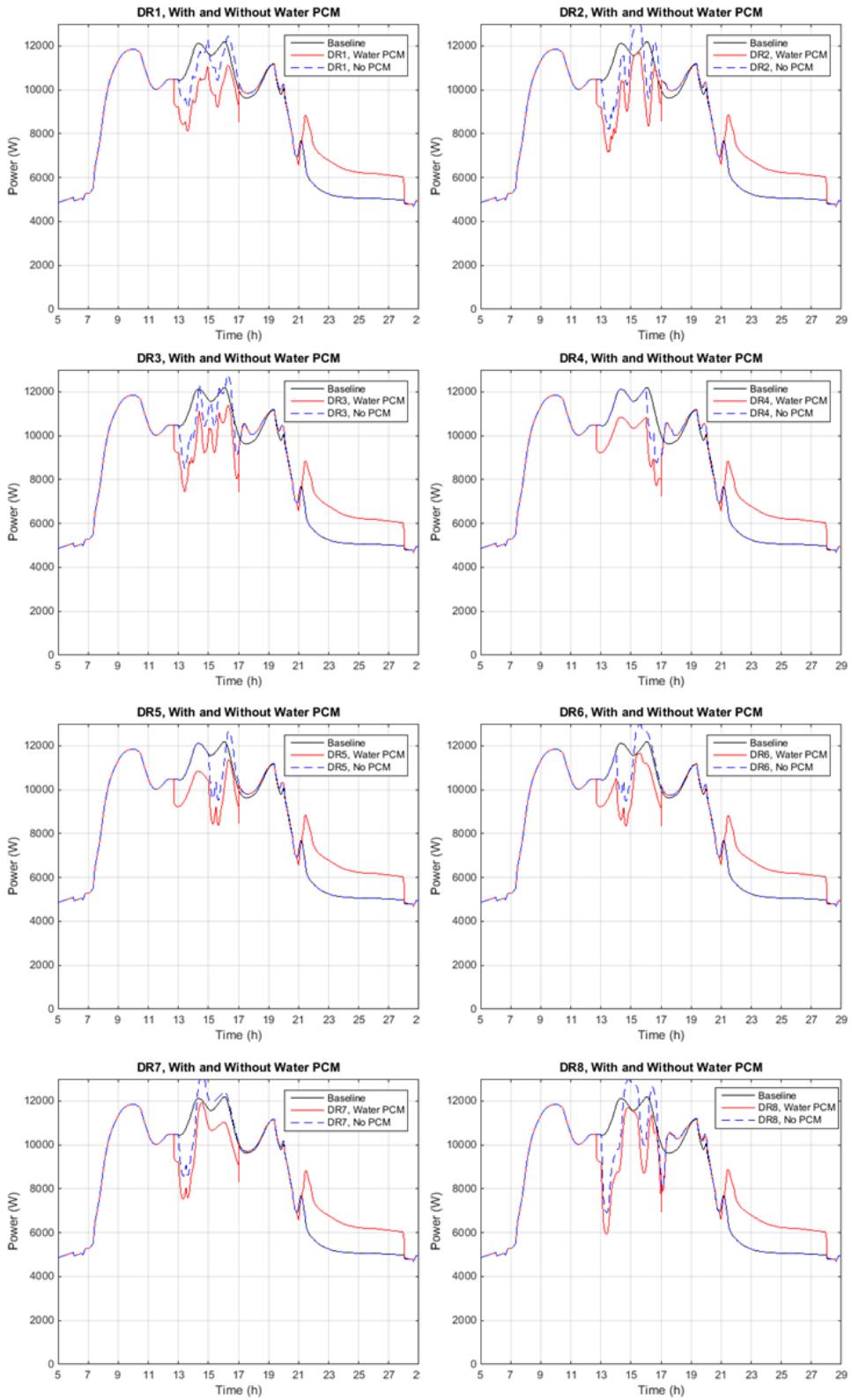

Figure 157 Total Power During DR Events, with Baseline Power, Water as PCM and no PCM (dash)

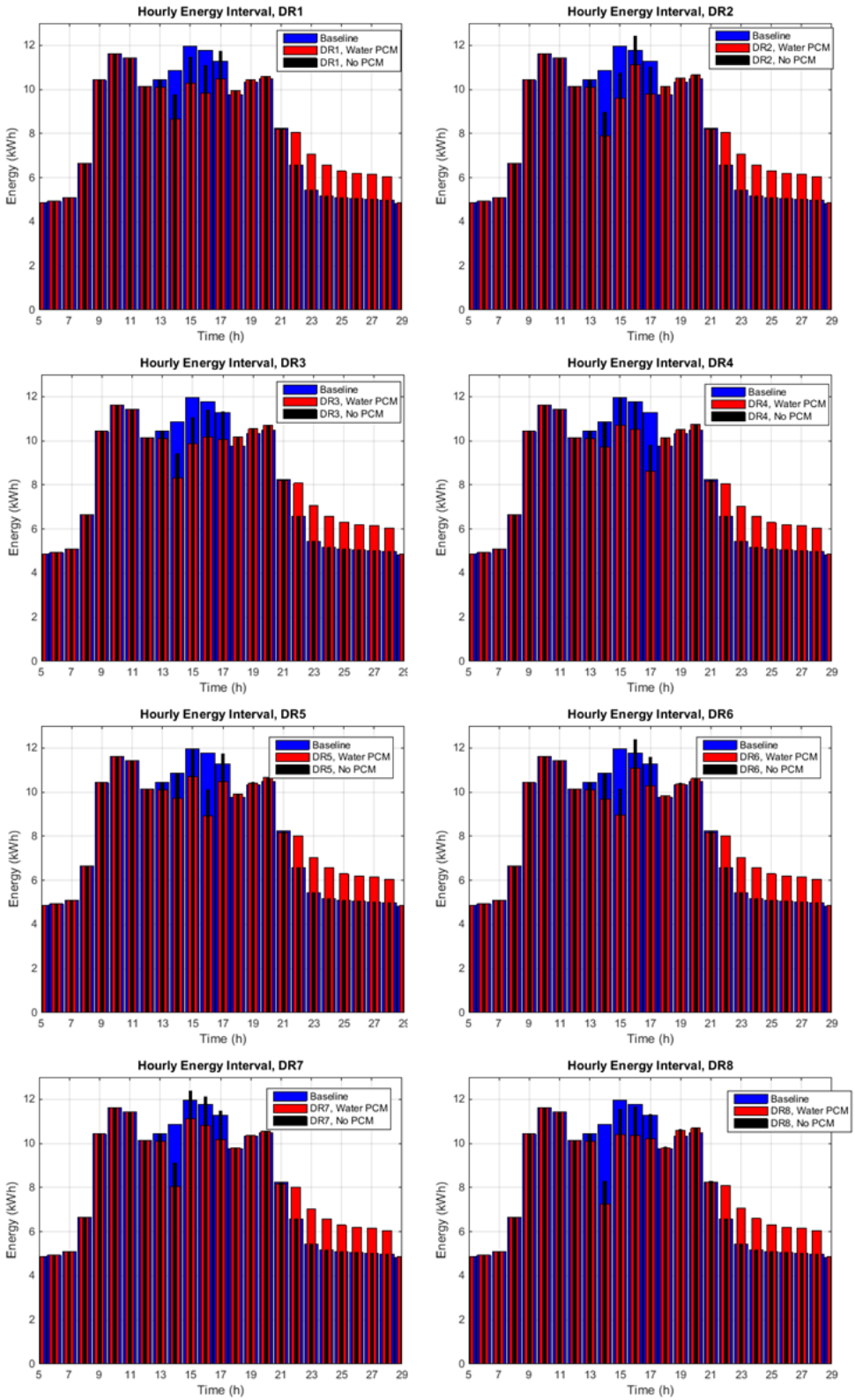

Figure 158 Total Hourly Energy During DR Events with Water PCM (red), with no PCM and Baseline Energy (blue) (intervals are "hour-ending")

Demand Response with PCM Using $C_{13}H_{28}$

The same comparison is performed for the case using $C_{13}H_{28}$ as the PCM, in Figure 159 and Figure 160. The power consumption is again lower in all cases during the PCM shed, regardless of refrigerated case sheds and rebounds. The magnitude of the power reduction is greater because the $C_{13}H_{28}$ PCM provides lower-temperature subcooling; for example, in case DR5, the power reduction during the period of the case shed ranges from 3.0 kW to 3.9 kW.

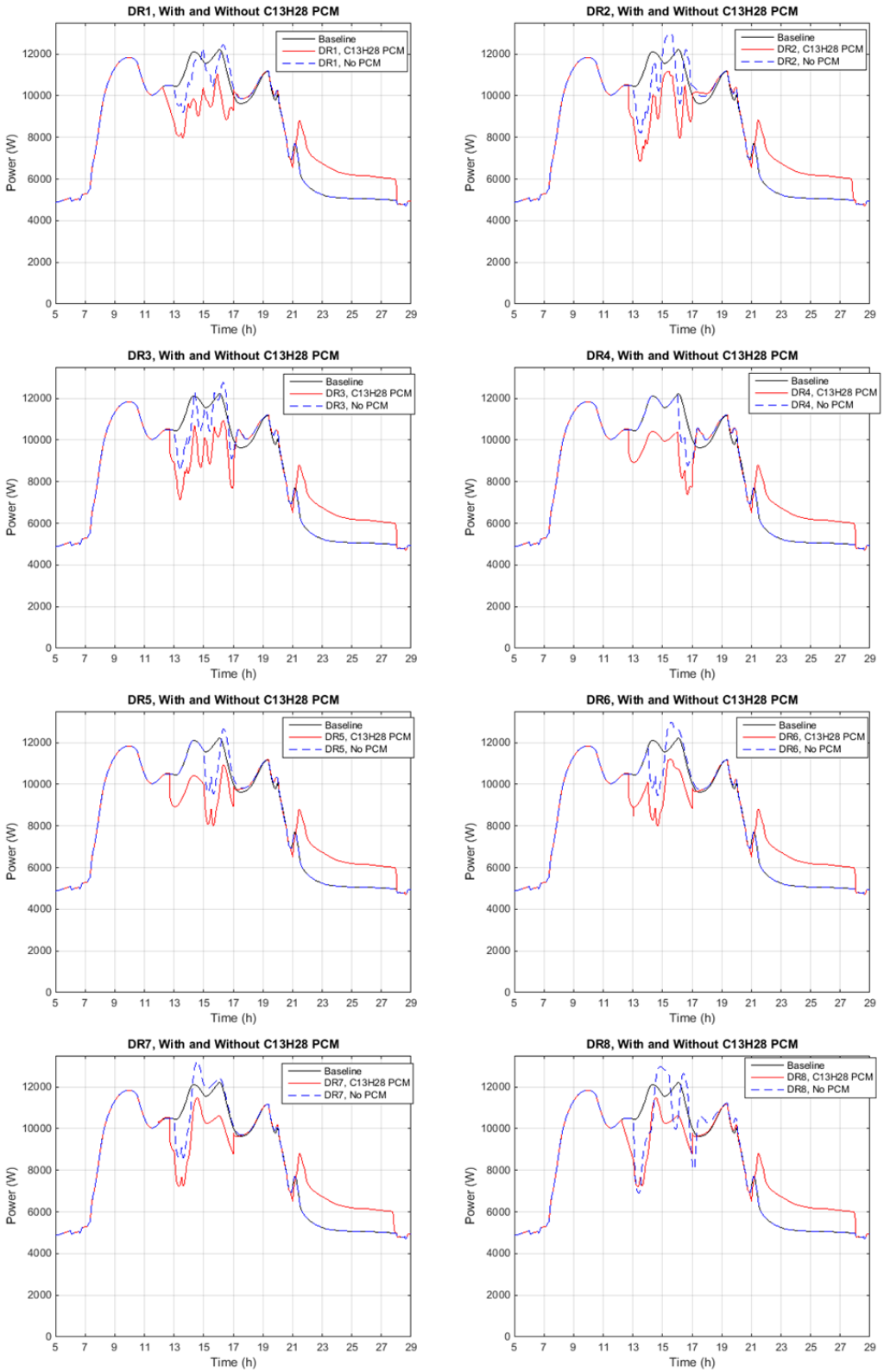

Figure 159 Total Power During DR Events, with Baseline Power, $C_{13}H_{28}$ as PCM and no PCM (dash)

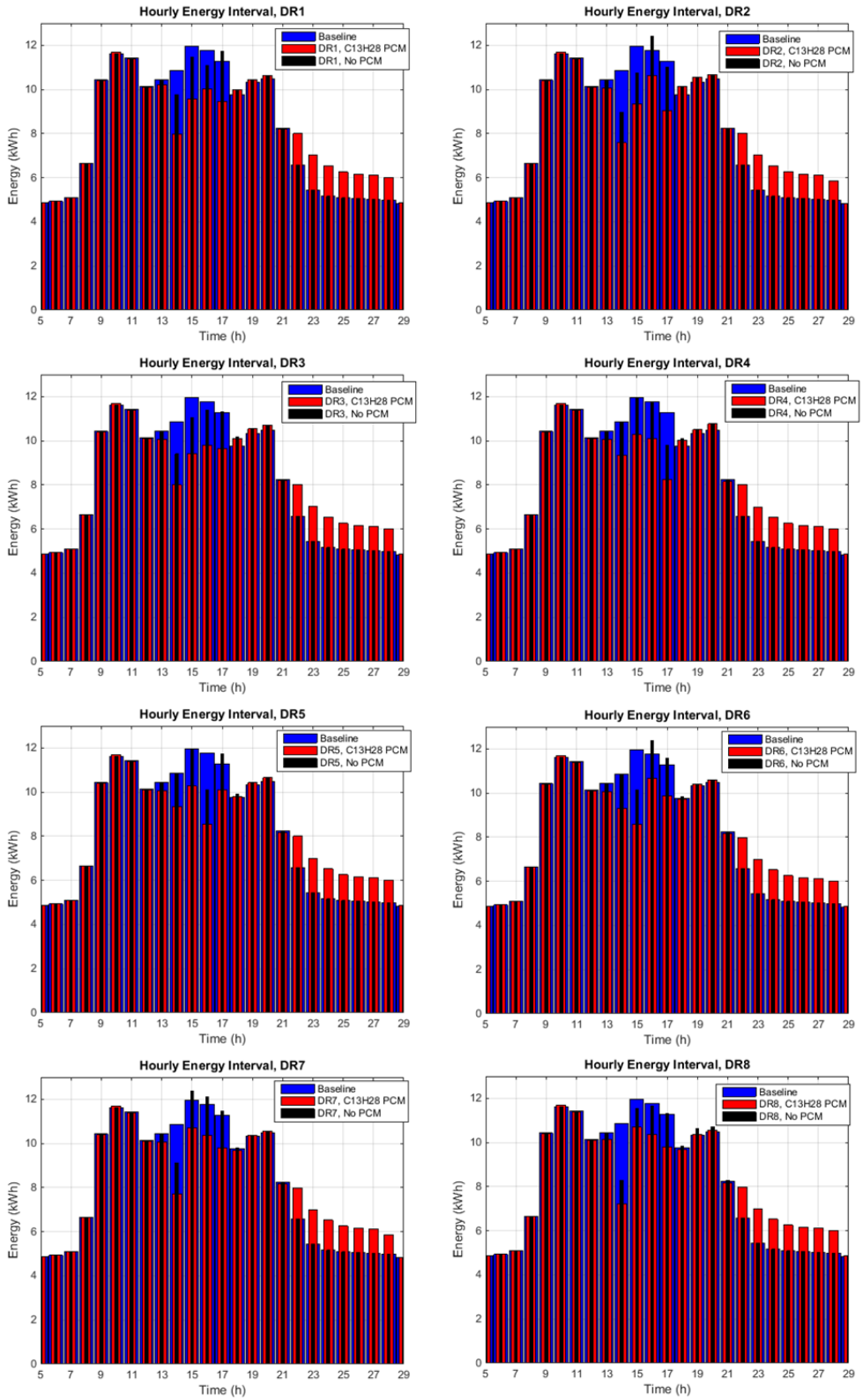

Figure 160 Total Hourly Energy During DR Events with $C_{13}H_{28}$ PCM (red), with no PCM and Baseline Energy (blue) (intervals are "hour-ending")

Re-Charge State of PCM and Correction for Cost Calculations

An important consideration is that for a PCM system to be continuously useful, it must be fully re-charged each day (at least prior to days on which it will be used). Review of the results shows that with the configuration selected here, this is not always the case. The results shown in Figure 137, Figure 142, Figure 145, and Figure 147 show that the two PCMs with higher-than-water phase change temperatures were fully re-charged in the time allocated by the simulated control strategy. In the case of water and $C_{13}H_{28}$, the PCM was not fully re-charged at the end of the cycle. For water, the re-charge was 81% of the discharge (including standby losses). For $C_{13}H_{28}$, the re-charge was only 57% of the discharge. In the water case, to re-charge the tank completely would take an additional approximately 2 hours of run-time.

Standby losses are a major variable in this consideration; the standby losses as modeled averaged 330W in the water case and 425W in the $C_{13}H_{28}$ case. Since the tank never discharges out of two-phase, re-running simulations with different insulation values would yield the same results, but the difference in standby losses can be estimated without doing so. With increased insulation on a real tank, it might be expected that standby losses could be reduced by 50% or more.

In the water scenario, the total discharge from the tank during the subcooler shed, excluding standby losses, was 20.9 kWh. The total standby losses over 24 hours, as simulated, was 8.0 kWh. Therefore, reducing standby losses by 50% would reduce

total discharge by 14%. The required additional run-time in the water case could be reduced from 2 hours to approximately 40 minutes.

In subsequent calculations of operating cost for the water-as-PCM scenarios, in order to adjust the simulated results to reflect the additional run-time in "charge" mode one hour of morning energy consumption is altered to be equal to one hour of "charge" energy consumption.

Operating Cost Comparison

An important consideration in any energy efficiency, demand response or thermal storage scenario is to consider the utility rate and determine if the provision saves or costs more money. To evaluate this each case is calculated against several rate scenarios, including tiered pricing and peak demand pricing.

There are many utility rates and programs to incentivize the use of storage or demand response. The general categories are demand pricing, time-of-use rates, load curtailment programs and real-time pricing. Each provides a slightly different mechanism but all may be considered for potential cost savings. For this effort, real-time pricing and time of use rates are evaluated since ample data is available with real rates to provide examples. Also, demand response incentives are considered.

Time-of-use rates refer to rates where there is a step-change in pricing based on time of day. TOU rates consist of off-peak and on-peak periods, and may also include "shoulder" periods between off- and on-peak hours. A typical summer TOU rate may

include off-peak hours overnight, shoulder hours in the late morning and evening, and on-peak hours during the afternoon. In the winter in most climates the TOU rate may include an off-peak period that is most of the daytime and an on-peak period that is in the morning. TOU rates may or may not include demand charges. Time of use rates vary in how extreme their price difference is. In some cases, the peak price may be in the range of 20-40% higher than the off-peak price. Others are more aggressive. The most aggressive rate identified in this effort was the Georgia Power rate examined here. The overnight rate is near zero, and the peak price is approximately 24 times higher.

Load curtailment programs are generally “riders”, meaning they are adjustments to another rate plan, and offer an incentive for the customer to curtail power consumption in response to a request from the utility. A load curtailment program for large commercial equipment is often a custom agreement between the utility and the end-user. The agreement will often feature either an agreed-upon demand reduction in kW, or an agreed upon maximum demand, in kW. The utility agrees to a minimum advanced notification (which may be minutes, hours, or day-ahead), a not-to-exceed duration per event, and a not-to-exceed cumulative duration or number of calls. The end-user’s bill may typically be adjusted per month for availability, or per event based on successful completion or measured curtailment, or both. Typical payments for commercial customers may be in the range of $15-$40/kW per month of enrollment, and $0.02-$0.50/kWh for actual shed. It is important to note that demand response is typically paid for shed when compared with a baseline (which may be for

example based on the trailing several days' power profile for the same meter). Therefore, if a permanent load shifting asset (such as thermal storage) is deployed every day, it cannot be counted as demand response and further capture a DR payment.

Demand pricing is simply a utility rate which includes both energy (per kWh) charges as well as demand (per kW) charges. The demand charges are based on the maximum average power during a pre-determined interval (typically 15- or 20-minute duration). The demand may be calculated based on the maximum during the whole billing period regardless of hour, or they may be the maximum during a pre-set "on peak" period (for example, 12:00 PM – 9:00 PM during the summer). Demand pricing will be part of a larger rate structure, and demand pricing may be included with a flat rate or a varying rate.

Real time pricing (RTP) refers to a situation in which the consumer is charged a rate that varies in short intervals and is determined and quoted one day or less in advance. The price of electricity typically varies hourly and reflects the marginal cost of supplying electricity. In RTP conditions, the price of electricity may vary quite widely; in some scenarios the price of electricity may increase by a factor of two or more from one hour to the next, or may even be negative for some hours, for instance if renewable generation exceeds demand. Typically day-ahead pricing is significantly less volatile than same-day real-time pricing. The price paid by an end user includes several subcomponents: a locational marginal price (LMP), which reflects the cost of

generation at a specific location within the grid (this is the portion that varies), as well as other, often fixed monthly and fixed-rate ($/kWh) costs such as delivery and transmission fees. The effective rate at a given hour can be calculated as the sum of the LMP and the other fixed-rate charges. RTP may be challenging for supermarkets, who have a considerable 24-hour load, but opportunities may arise if thermal storage and load shedding can be deployed flexibly.

Summary of Considered Rate Scenarios

The following scenarios are considered in this evaluation. In each case, the fixed monthly costs and other bill considerations are not included; only the per-kWh costs and (where applicable) demand incentives are considered. Several flat rates are included, a particularly aggressive time-of-use rate is considered, and LMP rates from the PJM market and the NEISO market are also used for hot summer days.

- Flat Rates:
    - Representative Flat Rate (FLAT):
        - Based on Georgia Power Medium Service Business Rate with Assumed Monthly Total Bill of 125,000 kWh
            - $0.0956/kWh
- Time-of-Use Rates:
    - George Power Time Of Use “Multiple Business” (GP-TOU)
        - Midnight to 7:00 AM: $0.008823/kWh
        - 7:00 AM to 1:00 PM: $0.041315/kWh
        - 1:00 PM to 6:00 PM: $0.212233/kWh
        - 6:00 PM to 11:00 PM: $0. 041315/kWh

            - 11:00 PM to Midnight: $0. 008823/kWh
    - SRP Business Time-of-Use Rate (SRP-TOU):
        - Midnight to 10:00 AM: $0.0558/kWh
        - 10:00 AM to 1:00 PM: $0.1113/kWh
        - 1:00 PM to 6:00 PM: $0.1691/kWh
        - 6:00 PM to 10:00 PM: $0. 1113/kWh
        - 10:00 PM to Midnight: $0.0558/kWh
    - Modified Version of SRB Business Time-of-Use (ModSRP-TOU):
        - (Modified while having same 24-hour average rate of $0.0956/kWh)
            - Midnight to 10:00 AM: $0.0258/kWh
            - 10:00 AM to 1:00 PM: $0.1113/kWh
            - 1:00 PM to 6:00 PM: $0.1691/kWh
            - 6:00 PM to 10:00 PM: $0.1113/kWh
            - 10:00 PM to Midnight: $0.0258/kWh
- Real-Time Price
    - New England ISO Node 4605, July 18, $0.04 fixed-rate (see Figure 148) (RTP-NEISO)
    - PJM BG&E, Calverton Node, July 18, $0.04 fixed-rate (see Figure 148) (RTP-PJM)
- Demand Response Incentives
    - Range of price and duration
        - $0.05/kWh
        - $0.10/kWh
        - $0.15/kWh
        - $0.20/kWh

The rates are visualized in Figure 161.

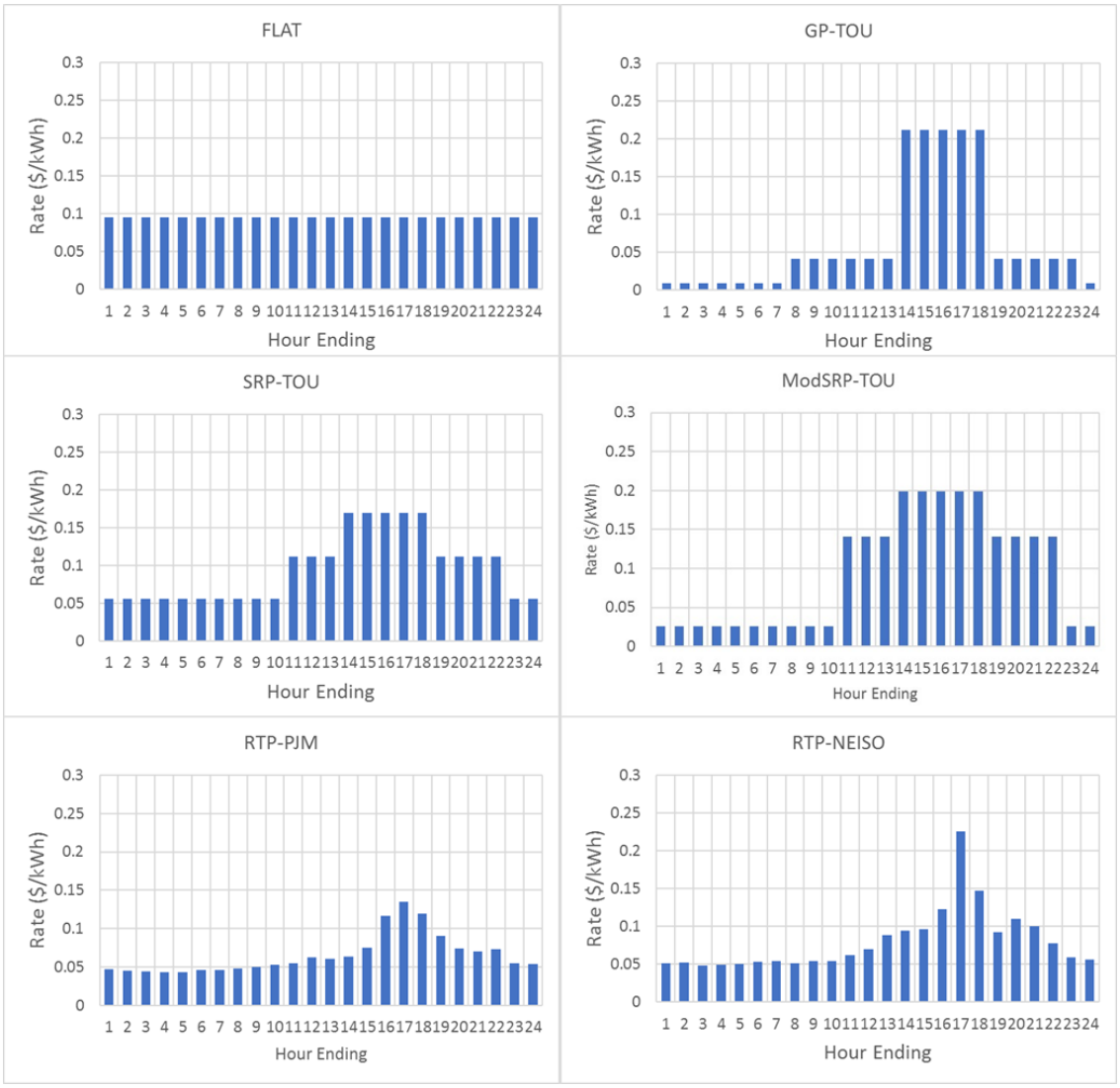

Figure 161 Hourly Rate Scenarios

Because the energy management approach of a building should vary with the rate, the cases will be considered for each rate category.

Flat-Rate

The flat rate costs scale simply with energy consumption. The results are shown in Table 18 for each simulated case. The highest cost is seen in the case with the water

phase change material and no case load sheds. This should be expected as the PCM system adds a recharge "penalty", but there is no incentive to shed load during hot hours in this rate scenario.

Table 18 Daily Energy Costs with FLAT Rate

FLAT Rate		
Control	24-h Cost	Difference (%)
Baseline	18.89	0.0%
Water PCM, No DR	19.38	2.6%
No PCM, DR1	18.76	-0.7%
No PCM, DR2	18.70	-1.0%
No PCM, DR3	18.71	-0.9%
No PCM, DR4	18.82	-0.4%
No PCM, DR5	18.81	-0.4%
No PCM, DR6	18.82	-0.4%
No PCM, DR7	18.83	-0.3%
No PCM, DR8	18.66	-1.2%
Water PCM, DR1	19.27	2.0%
Water PCM, DR2	19.22	1.8%
Water PCM, DR3	19.24	1.8%
Water PCM, DR4	19.33	2.3%
Water PCM, DR5	19.32	2.3%
Water PCM, DR6	19.32	2.3%
Water PCM, DR7	19.32	2.3%
Water PCM, DR8	19.19	1.6%

The lowest cost is in the DR8 scenario with no PCM, which has the longest period of elevated display case temperatures, after a deep power reduction at the beginning of the load shedding. The hourly energy is plotted against baseline and the hourly rate in Figure 162.

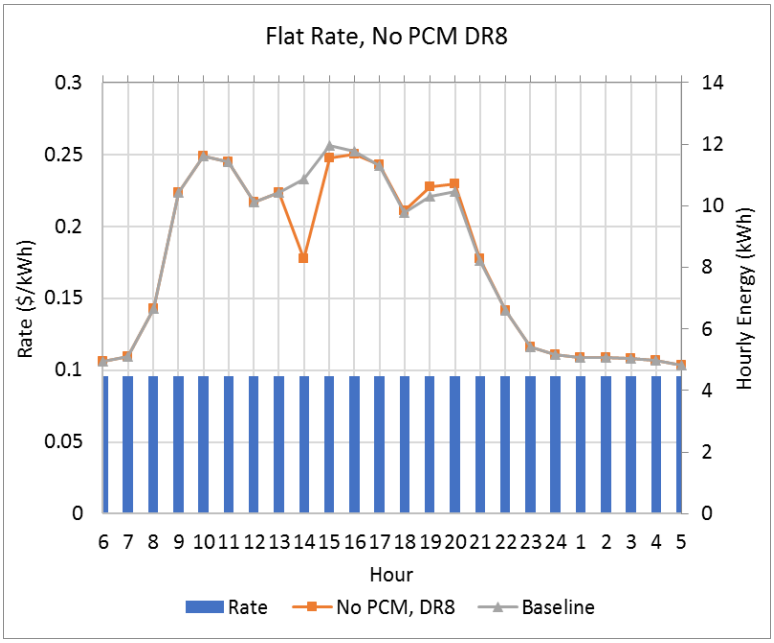

Figure 162 Hourly Energy for Baseline and DR8 with No PCM

Time-of-Use Rate

Demand response behavior reduces operating cost in most cases compared with the baseline scenario, because the load shed reduces overall energy because of a brief period of higher refrigerating temperatures. The benefit of this depends upon the rate. The total costs are summarized in Table 19. In this case the highest-cost scenario is the baseline for all three rates. The water PCM system shifting load produces a cost reduction, from 1% in the least-aggressive TOU rate structure (SRP-TOU), to 5.4% in the most aggressive rate structure (GP-TOU). The lowest overall operating cost is in the case of the PCM storage system with DR8, a strategy with prolonged elevated case temperatures. In this scenario the total reduction in cost is 8.4% compared to the baseline. DR2 and DR3 similarly produce high savings in this case, 8.0 and 7.0% respectively.

Table 19 Daily Energy Costs with TOU Rates

GP-TOU			SRP-TOU			SRP-ModTOU		
Control	24-h Cost	Difference (%)	Control	24-h Cost	Difference (%)	Control	24-h Cost	Difference (%)
Baseline	16.37	0.0%	Baseline	21.09	0.0%	Baseline	22.55	0.0%
Water PCM, No DR	15.49	-5.4%	Water PCM, No DR	20.87	-1.0%	Water PCM, No DR	21.97	-2.6%
No PCM, DR1	16.03	-2.1%	No PCM, DR1	20.84	-1.2%	No PCM, DR1	22.27	-1.3%
No PCM, DR2	15.88	-3.0%	No PCM, DR2	20.73	-1.7%	No PCM, DR2	22.14	-1.8%
No PCM, DR3	15.89	-2.9%	No PCM, DR3	20.74	-1.6%	No PCM, DR3	22.16	-1.8%
No PCM, DR4	16.14	-1.4%	No PCM, DR4	20.94	-0.7%	No PCM, DR4	22.38	-0.8%
No PCM, DR5	16.15	-1.3%	No PCM, DR5	20.93	-0.7%	No PCM, DR5	22.38	-0.8%
No PCM, DR6	16.19	-1.1%	No PCM, DR6	20.95	-0.6%	No PCM, DR6	22.40	-0.7%
No PCM, DR7	16.20	-1.0%	No PCM, DR7	20.96	-0.6%	No PCM, DR7	22.41	-0.6%
No PCM, DR8	15.76	-3.7%	No PCM, DR8	20.65	-2.1%	No PCM, DR8	22.04	-2.3%
Water PCM, DR1	15.20	-7.2%	Water PCM, DR1	20.66	-2.0%	Water PCM, DR1	21.70	-3.8%
Water PCM, DR2	15.06	-8.0%	Water PCM, DR2	20.56	-2.5%	Water PCM, DR2	21.59	-4.3%
Water PCM, DR3	15.07	-7.9%	Water PCM, DR3	20.57	-2.4%	Water PCM, DR3	21.61	-4.2%
Water PCM, DR4	15.29	-6.6%	Water PCM, DR4	20.75	-1.6%	Water PCM, DR4	21.81	-3.3%
Water PCM, DR5	15.30	-6.5%	Water PCM, DR5	20.74	-1.6%	Water PCM, DR5	21.80	-3.3%
Water PCM, DR6	15.33	-6.4%	Water PCM, DR6	20.75	-1.6%	Water PCM, DR6	21.81	-3.3%
Water PCM, DR7	15.34	-6.3%	Water PCM, DR7	20.76	-1.5%	Water PCM, DR7	21.82	-3.2%
Water PCM, DR8	14.95	-8.7%	Water PCM, DR8	20.49	-2.8%	Water PCM, DR8	21.51	-4.6%

It is also worth comparing this rate against the flat rate, since both would be available as options to a supermarket. This comparison is shown in Table 20. Simply switching from the flat to the TOU rate would yield over 13% cost reduction; this is because the supermarket load profile, while much higher during the daytime, still has considerable overnight energy consumption. In this aggressive TOU rate, overnight energy consumption is drastically less expensive. Combining the rate change with the thermal storage system and the DR2, DR3, or DR8 control approach each resulted in 20% lower total energy cost.

Table 20 Daily Energy Costs with GP-TOU and FLAT Rates

	Flat Rate	GP-TOU	
Control	24-h Cost	24-h Cost	Difference (%) Relative to Flat, Baseline
Baseline	18.89	16.37	-13.3%
Water PCM, No DR	19.38	15.49	-18.0%
No PCM, DR1	18.76	16.03	-15.1%
No PCM, DR2	18.70	15.88	-15.9%
No PCM, DR3	18.71	15.89	-15.9%
No PCM, DR4	18.82	16.14	-14.6%
No PCM, DR5	18.81	16.15	-14.5%
No PCM, DR6	18.82	16.19	-14.3%
No PCM, DR7	18.83	16.20	-14.2%
No PCM, DR8	18.66	15.76	-16.6%
Water PCM, DR1	19.27	15.20	-19.6%
Water PCM, DR2	19.22	15.06	-20.3%
Water PCM, DR3	19.24	15.07	-20.2%
Water PCM, DR4	19.33	15.29	-19.0%
Water PCM, DR5	19.32	15.30	-19.0%
Water PCM, DR6	19.32	15.33	-18.9%
Water PCM, DR7	19.32	15.34	-18.8%
Water PCM, DR8	19.19	14.95	-20.9%

The hourly energy consumption and the rate are plotted in Figure 163. From this graph it is clear that the penalty associated with overnight charging is minimal compared to the cost reduction in the peak hours. Slight modifications to the control strategy could have further reduced cost, as some of the recharge occurs during the shoulder pricing and the load reduction ends during the last hour of high pricing.

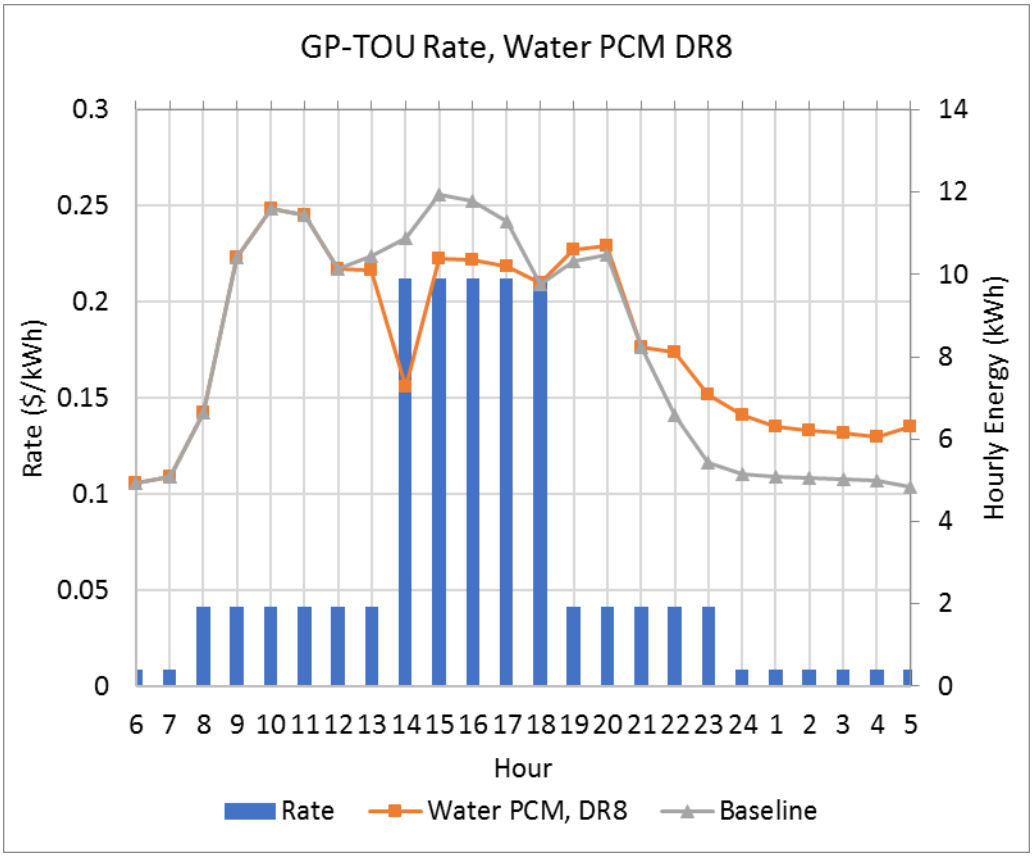

Figure 163 Hourly Energy for Baseline and DR8 with Water PCM

Real Time Price

The RTP scenarios similarly feature relatively high peak pricing with relatively low overnight rates; the high peak price is more concentrated into a few hours, and the difference between maximum and minimum price is much smaller than the GP-TOU example.

Table 21 Daily Energy Costs with RTP Rates

RTP-PJM			RTP-NEISO		
Control	24-h Cost	Difference (%)	Control	24-h Cost	Difference (%)
Baseline	13.96	0.0%	Baseline	17.31	0.0%
Water PCM, No DR	13.99	0.2%	Water PCM, No DR	17.19	-0.7%
No PCM, DR1	13.88	-0.6%	No PCM, DR1	17.23	-0.4%
No PCM, DR2	13.86	-0.7%	No PCM, DR2	17.13	-1.1%
No PCM, DR3	13.84	-0.8%	No PCM, DR3	17.15	-0.9%
No PCM, DR4	13.83	-0.9%	No PCM, DR4	17.06	-1.4%
No PCM, DR5	13.86	-0.7%	No PCM, DR5	17.26	-0.3%
No PCM, DR6	13.95	-0.1%	No PCM, DR6	17.30	-0.1%
No PCM, DR7	13.95	0.0%	No PCM, DR7	17.28	-0.2%
No PCM, DR8	13.81	-1.0%	No PCM, DR8	17.09	-1.3%
Water PCM, DR1	13.92	-0.3%	Water PCM, DR1	17.13	-1.0%
Water PCM, DR2	13.91	-0.3%	Water PCM, DR2	17.04	-1.6%
Water PCM, DR3	13.89	-0.5%	Water PCM, DR3	17.06	-1.4%
Water PCM, DR4	13.88	-0.6%	Water PCM, DR4	16.97	-1.9%
Water PCM, DR5	13.91	-0.4%	Water PCM, DR5	17.16	-0.9%
Water PCM, DR6	13.98	0.2%	Water PCM, DR6	17.18	-0.7%
Water PCM, DR7	13.98	0.2%	Water PCM, DR7	17.17	-0.8%
Water PCM, DR8	13.87	-0.6%	Water PCM, DR8	17.02	-1.7%

The NEISO RTP offers slightly better savings opportunity (but higher total cost) due to a higher peak price; in that case the DR4 control combined with the PCM system produces the lowest total cost. DR4 has a narrow demand reduction from the display

cases coinciding with the hour of highest price. This scenario was lower-cost overall than the DR strategies that have elevated case temperatures for the whole time period; this suggests that in RTP scenarios, if a short and particularly high price signal is expected in upcoming hours, it can be more cost effective to target a large kW reduction for that hour than to provide greater energy savings spread out over several hours.

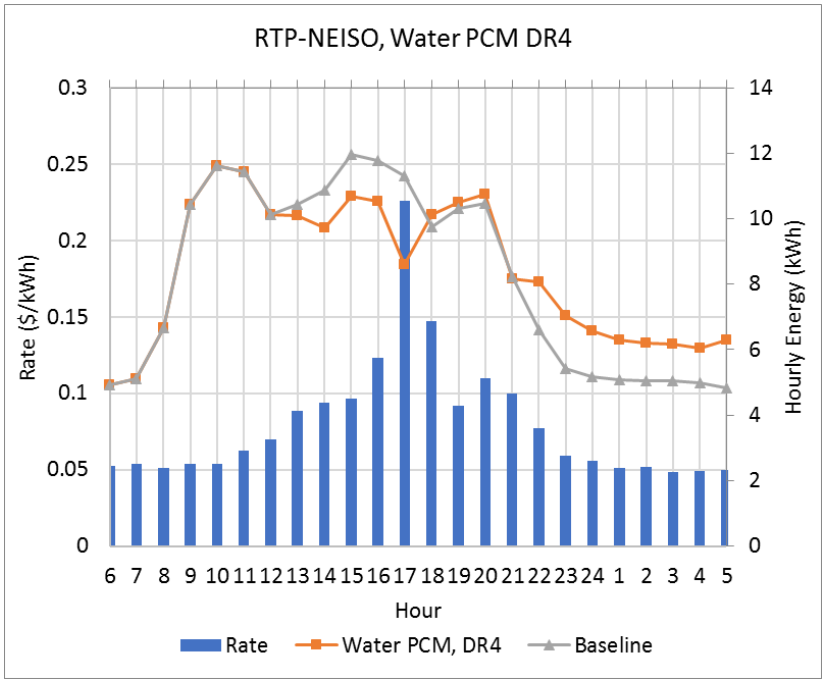

Figure 164 Hourly Energy for Baseline and DR4 with Water PCM

Demand Response

Demand response incentives are considered for two cases: applied to the flat-rate plan, and applied to the time-of-use plans. Different durations are examined. One factor that is not included in calculation but should be considered is that a demand response payment may require some minimum guarantee of reduction and duration; for example, a two-hour event may require a two-hour duration of power reduction

during which time the average power remains below baseline. This can present a challenge, one way around which is the pooling of loads into an aggregated group (which would be managed centrally). Since these rules may vary, it is not directly included in the calculations here. However, since none of the evaluated demand response approaches sustained a 1-kW average reduction for longer than two hours, durations longer than two hours were not considered. The energy difference calculated for demand response compensation is equal to the baseline energy during the same interval, minus the energy in the demand response scenario. For cases with the thermal storage, only the part of the load reduction which is executed in response to a signal may be credited. Therefore, those sheds are treated the same way, with the portion receiving demand response compensation calculated as the difference between the water-as-PCM, no DR case, and the DR case simulated. While it is conceivable that the PCM storage could also be deployed for individual demand response events rather than as regular load shifting, since demand response events are sporadic, the PCM is considered here as a permanent shift option.

The results are presented here for a selection of the scenarios. The complete results are shown in Appendix A. In each table, the total daily cost is shown for the simulated cases with the greatest improvement in savings from the DR event, as well as baseline, and water with a subcooler shed but no case sheds. Cases where there is no or very small difference from the incentive (such is when the shed in the simulation does not overlap with the incentive) are not shown. Four incentive cases are shown, from $0.05/kWh to $0.20/kWh. The first two tables show demand

response events added to the FLAT rate; the second set show DR events added to the GP-TOU rate.

The first case shown is a two-hour duration shed, for hours ending 2:00 PM and 3:00 PM (shed between 1:00-3:00 PM), in Table 22. The results without a DR incentive (the left column, the same results as in Table 18) show slight decrease in cost with each DR case due to the reduction in total cooling delivered, and increase in cost with each case using the PCM due to higher energy consumption associated with re-charge. In the DR cases, each of the presented scenarios produces an increased cost savings associated with the shed. The largest reduction is in the DR2 case. In the DR2 case without the water PCM, the energy reduction during hour ending 2:00 PM is 1.89 kWh, or a 17% reduction compared to the same hour in baseline. For hour ending 3:00 PM, the reduction is 1.2 kWh or 10%. The following hour outside of the incentive period, the rebound leads to approximately 5% higher energy consumption in the DR case.

Table 22 Two-Hour Shed, Flat Base Rate

	FLAT, No DR Incentive		FLAT, DR HE 2:00 & HE 3:00 PM, $0.05/kWh		FLAT, DR HE 2:00 & HE 3:00 PM, $0.10/kWh		FLAT, DR HE 2:00 & HE 3:00 PM, $0.15/kWh		FLAT, DR HE 2:00 & HE 3:00 PM, $0.2/kWh	
Control	24-h Cost	Diff (%)	24-h Cost	Diff. (%)	24-h Cost	Diff. (%)	24-h Cost	Diff. (%)	24-h Cost	Diff. (%)
Baseline	18.89	0.00%	18.89	0.00%	18.89	0.00%	18.89	0.00%	18.89	0.00%
No PCM, DR1	18.76	-0.70%	18.68	-1.10%	18.6	-1.50%	18.52	-1.90%	18.45	-2.40%
No PCM, DR2	18.7	-1.00%	18.55	-1.80%	18.39	-2.60%	18.24	-3.50%	18.08	-4.30%
No PCM, DR3	18.71	-0.90%	18.6	-1.60%	18.48	-2.20%	18.36	-2.80%	18.24	-3.40%
No PCM, DR6	18.82	-0.40%	18.73	-0.80%	18.64	-1.30%	18.55	-1.80%	18.46	-2.30%
No PCM, DR7	18.83	-0.30%	18.76	-0.70%	18.69	-1.10%	18.62	-1.40%	18.56	-1.80%
No PCM, DR8	18.66	-1.20%	18.63	-1.40%	18.61	-1.50%	18.58	-1.70%	18.55	-1.80%
Water PCM, No DR	19.38	2.60%	19.38	2.60%	19.38	2.60%	19.38	2.60%	19.38	2.60%
Water PCM, DR1	19.27	2.00%	19.2	1.60%	19.13	1.30%	19.06	0.90%	18.98	0.50%
Water PCM, DR2	19.22	1.80%	19.08	1.00%	18.94	0.20%	18.79	-0.50%	18.65	-1.30%
Water PCM, DR3	19.24	1.80%	19.12	1.20%	19.01	0.60%	18.9	0.10%	18.79	-0.50%
Water PCM, DR6	19.32	2.30%	19.24	1.80%	19.15	1.40%	19.06	0.90%	18.97	0.40%
Water PCM, DR7	19.32	2.30%	19.26	2.00%	19.2	1.60%	19.14	1.30%	19.08	1.00%
Water PCM, DR8	19.19	1.60%	19.06	0.90%	18.92	0.20%	18.78	-0.60%	18.65	-1.30%

The calculated hourly energy cost is shown in Figure 165 for the $0.10/kWh incentive level. The orange line shows the cost calculated without the DR incentive; the gray line shows the cost calculated with the DR incentive applied. The DR incentive is applied only to reductions occurring within the shaded blue period.

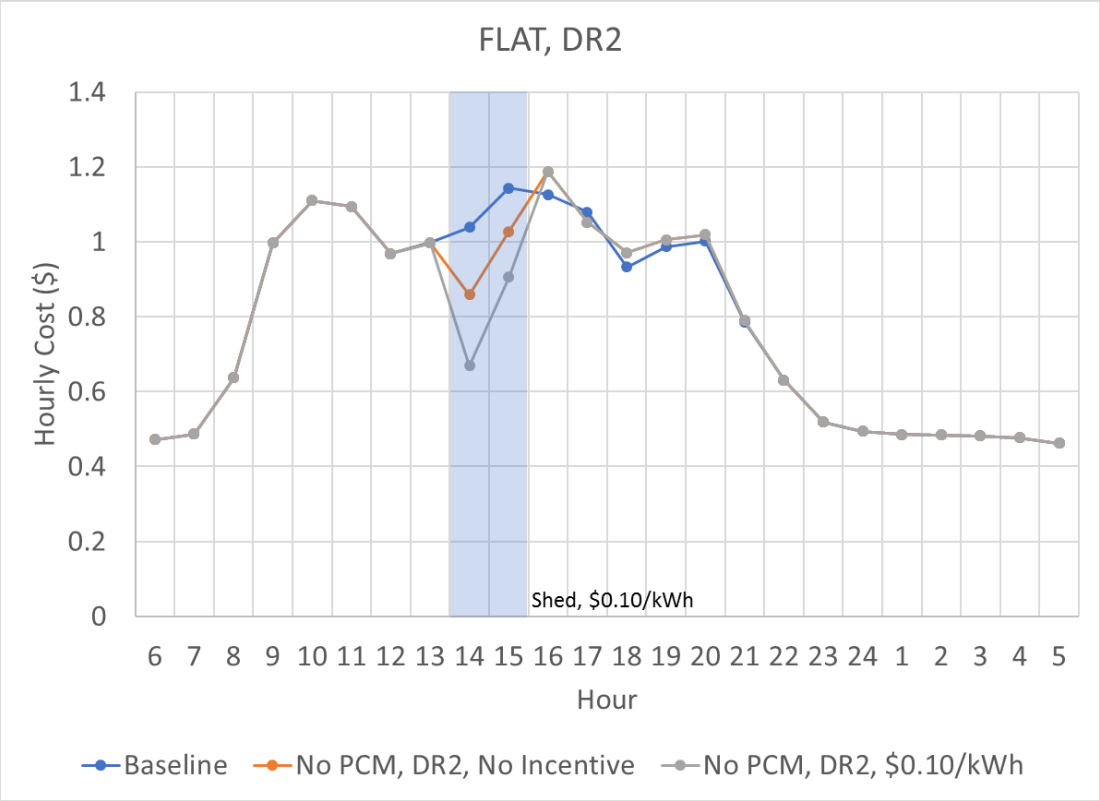

Figure 165 Hourly Cost for DR2 with no PCM in FLAT rate

The results are also shown for a one-hour duration event. This shows a slight difference, where for the smallest DR incentive, the overall cost of case DR8 (which has lower total energy consumption) is still the least-expensive case. However, with a larger DR incentive, the higher first-hour reduction of DR2 becomes more valuable than the overall energy reduction of case DR8.

Table 23 One-Hour Flat Base Rate

	FLAT, No DR Incentive		FLAT, DR HE 2:00 PM, $0.05/kWh		FLAT, DR HE 2:00 PM, $0.10/kWh		FLAT, DR HE 2:00 PM, $0.15/kWh		FLAT, DR HE 2:00 PM, $0.2/kWh	
Control	24-h Cost	Diff (%)	24-h Cost	Diff. (%)	24-h Cost	Diff. (%)	24-h Cost	Diff. (%)	24-h Cost	Diff. (%)
Baseline	18.89	0.00%	18.89	0.00%	18.89	0.00%	18.89	0.00%	18.89	0.00%
No PCM, DR1	18.76	-0.70%	18.71	-1.00%	18.65	-1.30%	18.6	-1.60%	18.54	-1.90%
No PCM, DR2	18.7	-1.00%	18.61	-1.50%	18.51	-2.00%	18.42	-2.50%	18.32	-3.00%
No PCM, DR3	18.71	-0.90%	18.64	-1.30%	18.57	-1.70%	18.5	-2.10%	18.42	-2.50%
No PCM, DR7	18.83	-0.30%	18.74	-0.80%	18.65	-1.30%	18.56	-1.70%	18.48	-2.20%
No PCM, DR8	18.66	-1.20%	18.59	-1.60%	18.52	-2.00%	18.45	-2.30%	18.38	-2.70%
Water PCM, No DR	19.38	2.60%	19.38	2.60%	19.38	2.60%	19.38	2.60%	19.38	2.60%
Water PCM, DR1	19.27	2.00%	19.22	1.70%	19.17	1.50%	19.12	1.20%	19.06	0.90%
Water PCM, DR2	19.22	1.80%	19.14	1.30%	19.05	0.80%	18.96	0.30%	18.87	-0.10%
Water PCM, DR3	19.24	1.80%	19.17	1.50%	19.1	1.10%	19.03	0.70%	18.96	0.40%
Water PCM, DR7	19.32	2.30%	19.24	1.90%	19.16	1.40%	19.08	1.00%	18.99	0.50%
Water PCM, DR8	19.19	1.60%	19.07	1.00%	18.95	0.30%	18.83	-0.30%	18.71	-1.00%

Next, DR incentives applied to the most aggressive TOU rate are considered. In such a scenario, utilities may provide DR incentives less frequently or in smaller amounts since the rate itself is intended to shift load off-peak. Table 24 shows the hourly costs with the TOU rate and incentive for the hour-ending 3:00 PM and hour-ending 4:00 PM period. In this scenario, the benefits of the PCM and subcooler power shed make the PCM cases lower-cost. The largest reduction of all cases was DR8 with the PCM, except for with the $0.20 incentive level for the load shed.

Table 24 Two-Hour Shed, Aggressive TOU Rate

	GP-TOU, No DR Incentive		GP-TOU, DR HE 3:00 PM & HE 4:00 PM, $0.05/kWh		GP-TOU, DR HE 3:00 PM & HE 4:00 PM, $0.1/kWh		GP-TOU, DR HE 3:00 PM & HE 4:00 PM, $0.15/kWh		GP-TOU, DR HE 3:00 PM & HE 4:00 PM, $0.2/kWh	
Control	24-h Cost	Diff. (%)	24-h Cost	Diff. (%)	24-h Cost	Diff. (%)	24-h Cost	Diff. (%)	24-h Cost	Diff. (%)
Baseline	16.37	0.00%	16.37	0.0%	16.37	0.0%	16.37	0.0%	16.37	0.0%
No PCM, DR1	16.03	-2.08%	15.98	-2.4%	15.92	-2.8%	15.86	-3.1%	15.80	-3.5%
No PCM, DR2	15.88	-2.99%	15.86	-3.1%	15.83	-3.3%	15.80	-3.5%	15.77	-3.7%
No PCM, DR3	15.89	-2.93%	15.83	-3.3%	15.76	-3.7%	15.70	-4.1%	15.63	-4.5%
No PCM, DR4	16.14	-1.41%	16.14	-1.4%	16.14	-1.4%	16.14	-1.4%	16.14	-1.4%
No PCM, DR5	16.15	-1.34%	16.07	-1.9%	15.98	-2.4%	15.90	-2.9%	15.81	-3.4%
No PCM, DR6	16.19	-1.10%	16.12	-1.5%	16.06	-1.9%	16.00	-2.3%	15.93	-2.7%
No PCM, DR7	16.2	-1.04%	16.24	-0.8%	16.27	-0.6%	16.31	-0.4%	16.35	-0.2%
No PCM, DR8	15.76	-3.73%	15.86	-3.1%	15.96	-2.5%	16.06	-1.9%	16.16	-1.3%
Water PCM, No DR	15.49	-5.38%	15.49	-5.4%	15.49	-5.4%	15.49	-5.4%	15.49	-5.4%
Water PCM, DR1	15.2	-7.15%	15.14	-7.5%	15.09	-7.8%	15.03	-8.2%	14.98	-8.5%
Water PCM, DR2	15.06	-8.00%	15.04	-8.2%	15.01	-8.3%	14.99	-8.4%	14.96	-8.6%
Water PCM, DR3	15.07	-7.94%	15.01	-8.3%	14.95	-8.7%	14.89	-9.0%	14.83	-9.4%
Water PCM, DR4	15.29	-6.60%	15.29	-6.6%	15.29	-6.6%	15.29	-6.6%	15.29	-6.6%
Water PCM, DR5	15.3	-6.54%	15.22	-7.0%	15.14	-7.5%	15.07	-8.0%	14.99	-8.5%
Water PCM, DR6	15.33	-6.35%	15.27	-6.7%	15.21	-7.1%	15.15	-7.4%	15.09	-7.8%
Water PCM, DR7	15.34	-6.29%	15.38	-6.1%	15.42	-5.8%	15.45	-5.6%	15.49	-5.4%
Water PCM, DR8	14.95	-8.67%	14.93	-8.8%	14.91	-8.9%	14.88	-9.1%	14.86	-9.2%

Table 25 shows a one-hour incentive for hour-ending 4:00 PM. The DR8 case has the lowest overall cost, though the actual reduction during the hour-ending 4:00 PM interval is so small that the difference between no incentive and $0.20/kWh incentive is only $0.03. The next-lowest cost is DR5 with water PCM, which is a targeted load shed at the same hour. In this case, with no incentive paid, the full-day cost reduction from simply performing the shed is $1.07 or 6.5%. With the incentive at $0.10/kWh, the total day operating cost is $1.23 lower or reduced by 7.5%.

Table 25 One-Hour Shed, Aggressive TOU Rate

	GP-TOU, No DR Incentive		GP-TOU, DR HE 4:00 PM, $0.05/kWh		GP-TOU, DR HE 4:00 PM, $0.1/kWh		GP-TOU, DR HE 4:00 PM, $0.15/kWh		GP-TOU, DR HE 4:00 PM, $0.2/kWh	
Control	24-h Cost	Diff. (%)	24-h Cost	Diff. (%)	24-h Cost	Diff. (%)	24-h Cost	Diff. (%)	24-h Cost	Diff. (%)
Baseline	16.37	0.00%	16.37	0.0%	16.37	0.0%	16.37	0.0%	16.37	0.0%
No PCM, DR1	16.03	-2.08%	16.00	-2.3%	15.96	-2.5%	15.93	-2.7%	15.89	-2.9%
No PCM, DR2	15.88	-2.99%	15.92	-2.8%	15.95	-2.6%	15.98	-2.4%	16.01	-2.2%
No PCM, DR3	15.89	-2.93%	15.87	-3.0%	15.85	-3.2%	15.83	-3.3%	15.81	-3.4%
No PCM, DR4	16.14	-1.41%	16.14	-1.4%	16.14	-1.4%	16.14	-1.4%	16.14	-1.4%
No PCM, DR5	16.15	-1.34%	16.07	-1.9%	15.98	-2.4%	15.90	-2.9%	15.82	-3.4%
No PCM, DR6	16.19	-1.10%	16.22	-1.0%	16.24	-0.8%	16.27	-0.6%	16.30	-0.4%
No PCM, DR7	16.2	-1.04%	16.22	-0.9%	16.23	-0.8%	16.25	-0.7%	16.27	-0.6%
No PCM, DR8	15.76	-3.73%	15.82	-3.4%	15.88	-3.0%	15.93	-2.7%	15.99	-2.3%
Water PCM, No DR	15.49	-5.38%	15.49	-5.4%	15.49	-5.4%	15.49	-5.4%	15.49	-5.4%
Water PCM, DR1	15.2	-7.15%	15.16	-7.4%	15.13	-7.6%	15.09	-7.8%	15.06	-8.0%
Water PCM, DR2	15.06	-8.00%	15.09	-7.8%	15.12	-7.6%	15.15	-7.5%	15.18	-7.3%
Water PCM, DR3	15.07	-7.94%	15.05	-8.1%	15.04	-8.2%	15.02	-8.3%	15.00	-8.4%
Water PCM, DR4	15.29	-6.60%	15.29	-6.6%	15.29	-6.6%	15.29	-6.6%	15.29	-6.6%
Water PCM, DR5	15.3	-6.54%	15.22	-7.0%	15.15	-7.5%	15.07	-8.0%	14.99	-8.5%
Water PCM, DR6	15.33	-6.35%	15.36	-6.2%	15.38	-6.0%	15.41	-5.8%	15.44	-5.7%
Water PCM, DR7	15.34	-6.29%	15.36	-6.2%	15.37	-6.1%	15.39	-6.0%	15.40	-5.9%
Water PCM, DR8	14.95	-8.67%	14.94	-8.7%	14.94	-8.8%	14.93	-8.8%	14.92	-8.9%

The DR5 with water PCM case is illustrated in Figure 166. The figure shows the shed occurring at hour ending 4:00 PM with a corresponding $0.10/kWh paid for reductions below the baseline, which in this case would be the water PCM with no other load sheds. The hourly cost is heavily influenced by the aggressive TOU rate. This also shows the benefit of the low overnight rate for charging: the energy during

overnight charge intervals is approximately 20% higher, but the cost difference is approximately $0.01, whereas in the mid-day periods, a power reduction of 10% results in approximately $0.26 return.

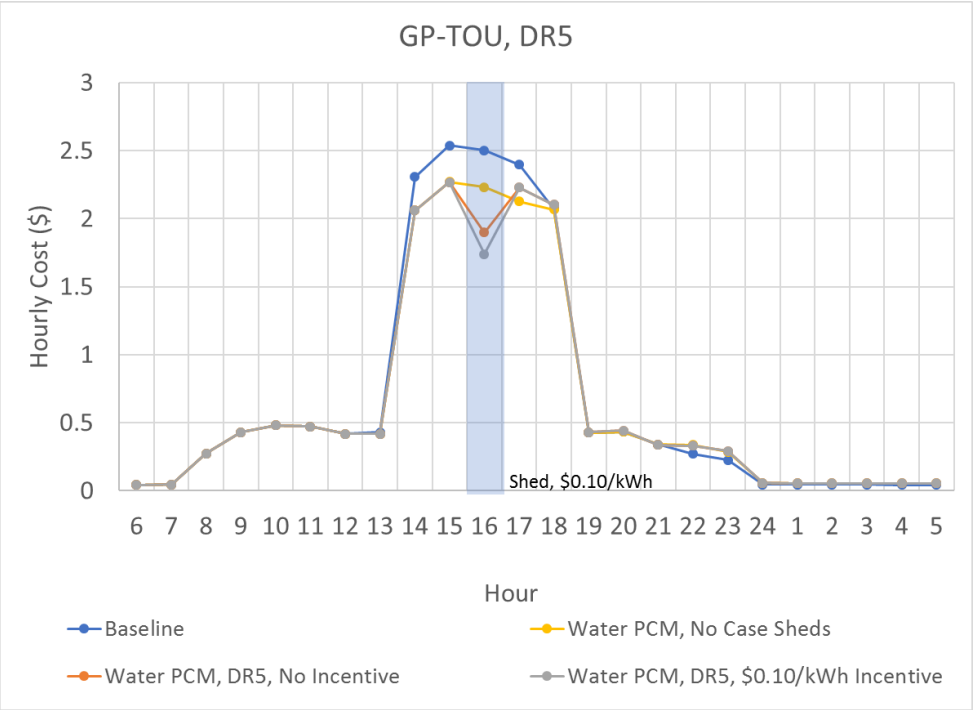

Figure 166 Hourly Cost for DR5 with water PCM in GP-TOU rate

Scaling to Full-Scale Systems

The energy and cost savings identified here are calculated on the basis of the laboratory-scale system which was modeled. The approximate modeled capacity was 12kW of MT load and 6 kW of LT load. Supermarket-scale systems are much larger: for example the systems examined by Sawalha et al (2017) and documented in Table 3 had MT capacity ranges of 87-410 kW and LT of 18-81kW. The MT capacity of these full-scale systems is between 7-34 times larger than that modeled here. While there are many important differences between the full-scale, field systems and the

laboratory-scale model here, an assumption of linear scaling may provide an order-of-magnitude estimate of the cost reduction potential of this approach. Considering each of the above scenarios then, the expected baseline, single-day operating cost of this system scaled up by 7-34 times would be $132 to $642 on the flat $0.0956/kWh rate. The simple difference in energy consumption associated with the various DR events (excluding incentive payments) without the PCM led to changes in total energy consumption up to 1.2% or $1.59 to $7.70 for the day. Including demand response incentives, the benefit depends on the incentive. If the incentive is similar to the avoided cost in the FLAT load profile scenario ($0.10/kWh incentive), a 2.6% cost savings was calculated, or $3.40-$16.70 per day.

Simply switching from the flat rate to the aggressive GP-TOU rate reduced the daily cost by 13.3% or $18-$85. The daily cost under this case is $115-$557. The most significant improvement, implementing case load reduction (without direct demand response incentive) and subcooler load shedding with the PCM in the GP-TOU rate would reduce cost by 8.7% or $10-$48. The new cost in this case would be $105-$508. Compared with the flat-rate, un-altered case, the reduction is 21%, or for a small or large supermarket, $28-$134. The largest part of the benefit on the aggressive TOU plan comes from the use of the PCM to offset subcooler operation, taking advantage of very low overnight rates. Of the cost reductions from the flat rate to the GP-TOU with load shedding, 13.3 percentage points out of a maximum of 21% is achieved by switching rates; an additional 4.7 percentage points are added only by using the PCM to shed subcooler power; 3 additional percentage points are gained by

reducing case loads. Since these reductions are considering shifts that take advantage of the TOU rate, but not yet considering incentivized DR events, this savings may be achievable on many days out of the year. However, the benefit is not present if on a flat rate, because of the energy penalty associated with the re-charge period.

Dedicated Charging System

The energy penalty associated with the PCM system could be reduced by adding a dedicated system for re-charging the PCM. The power of the baseline case subcomponents and the simple water PCM case with no case shedding are shown in Figure 167. The water PCM case is shown with dotted lines, and differences may be observed in the subcooler power and the MT compressor power. The power increase in the MT compressor is greater in magnitude (approximately 1,000 watts to 1,400 watts higher) during the recharge than the power of the subcooler, which is during the recharge not providing subcooling. The power of the subcooler is slightly different but the magnidtude is much smaller: approximately 15-40 watts difference. The power of the subcooler during these hours is between 780-830 watts.

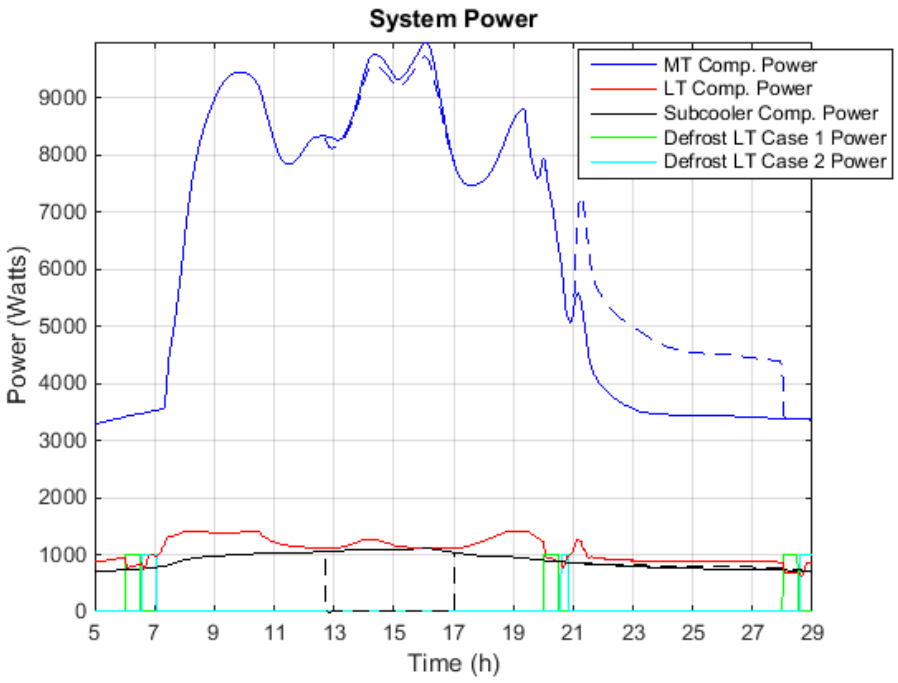

Figure 167 Subsystem Power for Baseline (solid) and Water PCM (dash)

An improved power profile would be possible by allowing the mechanical subcooler to provide subcooling to the cycle during the recharge, while a separate system charges the phase change material. To approximate the difference, the hourly energy values are re-calculated based on the two previous profiles (baseline and water PCM with no case sheds) with the following assumptions:

- The power during all hours outside the charging period is equal to the power in the water PCM, with subcooler shed scenario.
- The power during the charging hours is equal to the power during the charging hours for the baseline case, plus the power of the subcooler only as calculated in the water-as-PCM charging case.

The resulting hourly energy values are tabulated in Table 26.

Table 26 Hourly Energy for MT Comp and Subcooler, with Recalculated Energy for Dedicated Charging System Configuration

	Baseline			Water PCM			Recalculated, Dedicated Charging System		
Hour	MT Comp.	Subcooler	Total	MT Comp.	Subcooler	Total	MT Comp.	Subcooler Plus Charging System	Total
6	3.32	0.71	4.94	3.32	0.71	4.94	3.32	0.71	4.94
7	3.48	0.76	5.10	3.48	0.76	5.10	3.48	0.76	5.10
8	4.59	0.83	6.66	4.59	0.83	6.66	4.59	0.83	6.66
9	8.07	0.95	10.42	8.07	0.95	10.42	8.07	0.95	10.42
10	9.26	0.98	11.61	9.26	0.98	11.61	9.26	0.98	11.61
11	9.06	1.02	11.44	9.06	1.02	11.44	9.06	1.02	11.44
12	7.94	1.03	10.13	7.94	1.03	10.13	7.94	1.03	10.13
13	8.27	1.05	10.44	8.23	0.76	10.11	8.27	1.05	10.11
14	8.62	1.08	10.87	8.53	0.00	9.71	8.62	1.08	9.71
15	9.63	1.09	11.96	9.46	0.00	10.70	9.63	1.09	10.70
16	9.56	1.10	11.78	9.39	0.00	10.52	9.56	1.10	10.52
17	9.10	1.08	11.29	8.91	0.00	10.02	9.10	1.08	10.02
18	7.59	1.01	9.76	7.58	1.00	9.74	7.59	1.01	9.74
19	8.01	0.97	10.32	8.01	0.97	10.31	8.01	0.97	10.31
20	8.19	0.92	10.47	8.22	0.93	10.51	8.19	0.92	10.51
21	6.41	0.88	8.23	6.41	0.88	8.23	6.41	0.88	8.23
22	4.70	0.85	6.59	6.27	0.84	8.16	4.70	0.85	6.59
23	3.71	0.81	5.43	5.20	0.83	6.94	3.71	1.64	6.26
24	3.49	0.78	5.16	4.82	0.81	6.52	3.49	1.59	5.97
1	3.44	0.76	5.08	4.59	0.80	6.27	3.44	1.56	5.88
2	3.43	0.75	5.06	4.52	0.79	6.19	3.43	1.55	5.85
3	3.42	0.75	5.04	4.48	0.79	6.14	3.42	1.54	5.83
4	3.39	0.73	4.99	4.40	0.78	6.04	3.39	1.51	5.77
5	3.38	0.72	4.84	3.41	0.78	6.27	3.38	1.46	5.85
	Total Energy:		197.61	Total Energy:		202.68	Total Energy:		198.14
	Difference (%)		0.0%	Difference (%)		2.6%	Difference (%)		0.3%

Using this energy profile for energy costs, the per-day cost under each scenario can be re-calculated. The findings are tabulated in Table 27. In all cases the cost is lower with the dedicated recharging system than with the original water PCM configuration.

Table 27 Per-Day Cost with Recalculated Energy for Dedicated Recharge System

	FLAT	GP-TOU	SRP Bus TOU	ModSRP-TOU	RTP-NEISO	RTP-PJM
Baseline	18.89	16.37	21.09	22.55	17.31	13.96
Water PCM	19.38	15.49	20.87	21.97	17.19	13.99
Diff. vs. Baseline (%)	2.6%	-5.4%	-1.0%	-2.6%	-0.7%	0.2%
Water PCM, Dedicated Recharge	18.95	15.38	20.54	21.67	16.91	13.73
Diff. vs. Baseline (%)	0.3%	-6.1%	-2.6%	-3.9%	-2.3%	-1.7%

Chapter Summary

This chapter describes modeling of the transcritical booster cycle under simulated load conditions for a "peak" day in Baltimore, MD. The validated cycle model that was developed and described in Chapter 4 is modified to include simulated loads (described in Chapter 5) and a thermal storage system (described in Chapter 6) which can be used to offset the subcooler system. The cycle is then modeled for simple demand response load sheds in which only display cases are adjusted; the results support those of Chapter 4, showing that a MT evaporator shed has a relatively smaller impact on total power than an equivalent shed of LT evaporator capacity. This is compounded by another issue: the MT display case quickly reaches a threshold temperature and must end the shed early.

Subsequently the model is used to examine a variety of possible control strategies to seek options to prolong the load shed. These strategies include short efforts to stagger

one after the other, or longer strategies of rolling cases sequentially in and out of load sheds. The strategies have varying success; all reduced energy due to a period of higher average evaporator temperatures. However, in the cases where prolonged sheds (more than an hour) are attempted, the power after the initial shed period oscillates above and below the baseline level as the cases rebound from each shed. The average power remains lower, but brief departures can be considerably higher.

The phase change material subcooler is initially examined in a separate operating strategy, where the subcooler itself is shed for a fixed duration and its' cooling replaced by the PCM. Four materials were examined, including water, two PCMs with higher phase change temperatures and one with lower phase change temperature. As configured, the water case could achieve approximately equal subcooling to the mechanical subcooler if a large heat exchanger is used. This results in approximately equal power of the MT and LT compressors, equal subcooling and approximately the same bypass flow as if the subcooler were running instead. The major difference is reduction in power due to the subcooler being off. Further improvement can be had with lower subcooling temperatures. The lower-temperature PCM could provide further power reductions by providing lower-temperature subcooling. In general the range of conditions tested show a strong dependency of total system power on the subcooler refrigerant leaving enthalpy. However, the PCM recharge incurs an energy penalty, and in the main configuration examined, the required time to re-charge the lowest temperature PCM would have been approximately 6 hours longer than the allocated time. Water was selected for further examination due to the combination of

performance and cost and availability considerations; the PCM itself can be expensive. A particular advantage of the load shed technique demonstrated here is that the load side of the cycle is unaffected; because the PCM storage system replaces the subcooler with little difference in behavior, there is no impact to the capacity delivered to the loads.

Demand response events executed in addition to the subcooler shed with thermal storage were examined to explore further peak load reduction. The combined effect of the PCM with demand response allowed scenarios in which the power could be continuously lower than baseline for four hours as simulated, with shorter reductions of approximately 3.5-4 kW sustained for approximately one hour.

In order to estimate the operating cost impact, several utility rate scenarios are considered, including flat rates, time-of-use rates, examples of real-time price operation, and demand response incentives applied to flat or time-of-use rates. The results show that in many cases, the PCM system has either higher operating cost or only small savings, because of the increased overnight power consumption associated with charging. This is especially true in cases where the rate is flat or there is not a large difference between the lowest and highest rates. However, in aggressive time of use rates, the PCM provides higher savings. One real-world time of use rate was identified with particularly low overnight rates that, with no change at all to operating strategy from the baseline, would be expected to reduce refrigeration operating cost

by 13%. Adding the PCM system and case load shedding to reduce on-peak load could reduce operating cost by approximately 20%.

An issue identified with the PCM system is that, as the PCM charges, subcooling is not provided to the refrigeration system, and the increase in MT compressor power to provide bypass flow is larger in magnitude than the power of the subcooler itself. An alternative approach, with a dedicated system for charging the PCM to allow the subcooler to continue running, was considered. In this case, the energy penalty from the recharging of the PCM is almost eliminated. The simple subcooler load shifting strategy then produces cost savings between 1.7-6.1% for the variable rate cases that were evaluated.

Chapter 8: Summary and Conclusions

This dissertation describes laboratory testing and transient modeling of CO_2 booster refrigeration systems with dedicated mechanical subcooling, model validation, development of a thermal storage integration approach for the cycle, and examination of the potential for demand response with and without thermal storage using a booster system. The conclusions are summarized here.

Laboratory Testing and Steady State Evaluation

A CO_2 booster system was investigated in laboratory testing with and without dedicated mechanical subcooling to quantify the effects of the subcooler on cycle performance. The subcooler was found to provide significant enhancements to capacity and efficiency across all test points, by reducing the refrigerant enthalpy leaving the subcooler and thereby reducing flash gas and bypass flow. The testing and analysis also revealed that at condensing pressures slightly below the critical point, there is a local efficiency minimum caused by a lower condenser effectiveness. This leads to an increase in flash gas, higher compressor power and lower efficiency. The effect was particularly pronounced because of the approximately 1:1 ratio of MT and LT loads in the testing. Control strategies to carefully navigate the transition from transcritical to subcritical should be applied. Steady-state modeling was also performed to investigate the effect of adding subcooling capacity. Additional subcooling capacity can significantly improve the COP of the primary CO_2 cycle, and as the COP of the primary cycle improves and the COP of the subcooler reduces (due

to lower evaporating temperature), the benefit shrinks. The benefit of added subcooler capacity is greater at hotter outdoor conditions where the primary cycle COP is lower.

Transient Modeling

A Modelica-based transient model of the cycle was developed and validated with transient laboratory tests of three different behaviors: transcritical operation with interruption of the MT evaporator, transcritical operation with interruption of the LT evaporator, and subcritical operation with an off-to-on step of the mechanical subcooler. The model is subsequently used to study demand response behavior, first with fixed-capacity simulations. This allows an assessment of the relative impact of load sheds on each stage. The results show a greater power reduction per unit of capacity reduction with shedding of the LT loads. In particular, the reduction of power per kW of load reduction was less than 1.0 for sheds of MT capacity, and greater than 1.0 for sheds of LT capacity. This reflects a temporary transition to a higher MT-to-LT load ratio, so an improvement of COP occurs during the shed. The MT capacity sheds, on the other hand, do not cause any impact to the LT evaporator stage, but LT sheds cause responses throughout the cycle as the LT compressor adjustment causes corresponding adjustments to the MT compressor and bypass flow.

Simulated Supermarket and Demand Response

Models of display cases were developed to allow simulation of realistic load conditions. A simulation scenario was developed with two display cases per stage, plus an additional evaporator with an externally fixed load. A peak-day weather profile for Baltimore, MD was used and the load profile for the store was derived

from the literature. The high-side pressure control of the system was modified to delay transition through the critical point, which was observed to improve COP and avoid the significant drop in capacity and efficiency observed in the laboratory. In the modified strategy the system remains transcritical for the full 24 hours as the outdoor temperature overnight remains above 20°C.

Subsequent simulations were performed with various demand response sheds of the MT and LT refrigerating cases. These simulations include capacity sheds of one or both display cases on each stage. The MT cases are of limited value because of the lower power reduction per kW of capacity reduction, and also because the MT case temperature is much closer to the upper threshold for food temperature than in the LT cases. In the scenarios modeled here, the MT cases could sustain approximately 15 minutes of shed during peak loading conditions until the food temperature rose to a shut-off threshold. The LT cases provide larger magnitude power reduction and longer duration sheds. In a simple shed of two LT cases equaling approximately 40% of the total LT capacity, the corresponding power reduction for the whole system reached 18%. Strategies to extend the duration of power reductions were examined and the staging of case sheds can provide somewhat longer power reductions. In the longest case, a duration of approximately 2 hours of continuously lower power relative to baseline is achieved. In all of the demand response cases, even if power oscillates above and below the baseline after the initial shed period, the average power over time remains lower than baseline because of elevated average case temperatures.

Thermal Storage Integration

Thermal energy storage was also investigated, using phase change materials to provide storage for subcooling. The PCM is applied to offset mechanical subcooling operation during peak hours, and then recharged using the subcooler in overnight hours. The use of different PCMs was investigated. Four PCMs are investigated in detail including water. For all cases, the PCM can replace the mechanical subcooler to provide a subcooling benefit without mechanical subcooler operation. In the case of water as the PCM, for the heat exchanger sizes investigated here the subcooling capacity was similar to that of the mechanical subcooler, and the change in the CO_2 cycle behavior is small. For PCMs with a phase change temperature above 0°C for a given heat exchanger size, the subcooling capacity with the PCM was smaller and while the mechanical subcooler power is zero, the MT compressor power increases due to higher bypass flow. With a PCM below 0°C, additional subcooling capacity is available and there is a dual benefit, with reduced MT compressor power along with the shut-off of the mechanical subcooler. A similar effect could be achieved with higher-temperature PCMs including water, with enhanced heat transfer between the PCM and the refrigerant.

The PCM was modeled under the same loading conditions as the baseline and load shed cases. Using the PCM alone to shed the mechanical subcooler, a continuous reduction of over 1kW (with the total magnitude depending on the PCM and heat exchanger) can be sustained for several hours without any impact on the refrigerating capacity. The PCM subcooler is also modeled in scenarios where both the

mechanical subcooler shed and the LT and MT display cases are also used. These scenarios can produce still deeper power reductions. The effect of the two approaches combined is approximately equal to the additive reduction of each approach.

Operating Cost Savings

Daily operating cost calculations were also performed for a range of rate scenarios, including flat rates, example real-time-price days, and tiered time-of-use rates. Demand response incentive payments were investigated for a range of incentive levels. Considering a case where the incentive payment is approximately equal to the offset rate price, on the flat rate plan, an approximate 2.6% savings on total daily cost is achieved for demand response only without thermal storage. At full supermarket scale this could amount to a modest savings, estimated to be $3.40-$16.70 per event at scale. While this is a small relative savings, the DR alone does not require hardware modifications, and could potentially be replicated across multiple stores within a given region. Considering alternative rate structures also shows savings potential. Permanent load shifting with an aggressive time-of-use rate structure is more likely to have large cost savings. Using thermal storage in the most aggressive TOU rate identified, a Georgia Power Time-of-Use plan with particularly low overnight rates, could produce significant cost savings in the range of 20% when compared to the baseline controls strategy on the same utility's flat rate plan. In a large supermarket, switching to the time of use rate and using load shifting and peak load shedding with the display cases could reduce cost by over $100 per day. The subcooler shedding in particular is repeatable on not just hot days, as the subcooler

power can be shed at any time. If the overnight rate (during recharging) is very low, this could provide savings on any given day. A further improvement to this strategy could be achieved using a dedicated recharging system for the PCM: using the mechanical subcooler to recharge the PCM has the effect of significantly reducing the efficiency of the primary CO_2 cycle overnight. Simply using a duplicate mechanical subcooling compressor to recharge the PCM while the main mechanical subcooler operates as normal would effectively eliminate the energy penalty associated with recharging.

Chapter 9: Contributions and Future Work

The following summarizes the key contributions presented here, and outlines suggested future work to expand upon this effort.

- A new detailed laboratory data set investigating a full booster cycle with dedicated mechanical subcooling was developed. The system was operated with and without subcooling to quantify the benefits of the dedicated mechanical subcooler.
- A transient model of the laboratory-scale system as developed and validated using laboratory data.
- Transient behavior of the booster cycle was investigated in detail.
    - In laboratory study, the booster is examined with abrupt interruptions to MT or LT capacity. These tests show the interaction between stages that is inherent to the cycle.
    - In transient modeling, the relative benefits and system-wide effects of load sheds on each evaporator stage are investigated. New insights into how load shed events may be prioritized and deployed are developed.
- Demand response load shedding scenarios were developed and simulated. The ability to provide demand response with sheds of display cases, including individual sheds and sequenced sheds of multiple cases were investigated.
    - The research demonstrates that sequencing display cases may provide longer durations of load shed and delay the rebound effect.
- An approach to thermal storage integration for subcooling is introduced. The use of a phase change material as a thermal storage medium for offsetting operation of the mechanical subcooler was investigated.

    - This strategy was found to provide long-duration power reduction by allowing the mechanical subcooler to be turned off, while the storage system provides subcooling.
    - An advantage of this approach is that there is no impact to the load side of the cycle. There may be an energy penalty associated with recharge, which could be reduced through deployment of a dedicated recharge system.
- The combined approach of offsetting the mechanical subcooler using thermal storage, and providing load reduction by shedding display cases was investigated.
    - The combined effect of both methods can be used for prolonged, smaller-scale demand reduction, or a short but deep demand reduction, depending on how the case sheds are deployed.
- Daily operating costs were calculated for a variety of utility rate scenarios.
    - The research identifies significant cost savings, but aggressive time-of-use rates are needed to offset the cost associated with recharging overnight.

Publications

Peer reviewed journal papers:

- Bush, J, M. Beshr, V. Aute & R. Radermacher (2017) Experimental evaluation of transcritical CO2 refrigeration with mechanical subcooling, Science and Technology for the Built Environment
- Bush, J, V. Aute & R. Radermacher. Transient Simulation of CO_2 Booster Refrigeration System with Mechanical Subcooler in Demand Response Operation, Science and Technology for the Built Environment. Manuscript Accepted December, 2017
- Upcoming: Bush, J, V. Aute & R. Radermacher. Transcritical Booster Refrigeration with Integrated Thermal Storage Subcooling: Peak Load Reduction and Demand Response. Submission expected March 2018

Conference papers:

- Beshr, Mohamed, John Bush, Vikrant Aute, and Reinhard Radermacher. 2016. "Steady State Testing and Modeling of a Co 2 Two-Stage Refrigeration System With Mechanical Subcooler," 12th IIR Gustav Lorentzen Natural Working Fluids Conference, Edinburgh, 2016
- Submitted: Bush, John, Vikrant Aute and Reinhard Radermacher. 2018. "Transient Simulation of a CO_2 Booster Refrigeration System with Mechanical Subcooler in Demand Response Operation." 13th IIR Gustav Lorentzen Natural Working Fluids Conference, Valencia, 2018

Recommendations for future work

There are several promising areas for future work related to this research. Some suggested research areas include:

- This research included simulation of peak-day conditions under loading. Further investigation of the year-round integration of the thermal storage subcooling system could provide additional insight.
- Investigate improvements to the phase change material storage and implementation to improve overall efficiency, and reduce size, cost and complexity. Possible refrigerant-to-PCM heat transfer configurations which should be investigated. The design of such a configuration may prove challenging as, unless CO_2 is also used as the "charging" system working fluid, two separate heat exchangers may be needed.
- Researchers have investigated the cost and benefit of CO_2 refrigeration systems compared to alternatives, but expanding the investigation of the costs and benefits of enhanced CO_2 systems is important. A cost-benefit evaluation of dedicated mechanical subcooling, with and without integrated thermal energy storage, should

also be undertaken for different climates and rate and incentive scenarios. This will help encourage the deployment of efficient and effective systems in the most appropriate applications.

- Investigate methods to improve the flexibility of display cases in providing load shedding. Case-by-case pre-cooling and/or thermal storage in the display cases could be implemented. In particular for the MT cases, this could improve the duration of shed that is possible for each individual case. The potential risk of demand response in supermarkets includes risk of lost product due to excessive temperature variation. This risk needs to be understood for supermarket demand response to be deployed at a wide scale. Future research should investigate the risk of increased food waste associated with demand response. In addition, any differences that might exist due to the use of CO_2 refrigerant as opposed to other alternatives in the risk of lost product quality should be examined.
- In parallel to this effort, other researchers have extensively investigated other CO_2 cycle enhancements intended to improve efficiency in hot weather, such as ejectors and parallel compression. These enhancements should be investigated in the context of demand response and in cooperation with dedicated mechanical subcooling.
- The value of the thermal storage system as used to offset subcooler operation has the potential to be aggregated with other loads as part of a broader grid integration strategy. Since the subcooler shed can be done with no impact to refrigerating capacity, it can in theory be charged and discharged in any arbitrary control scheme. The potential to control many such systems in an aggregated fleet for larger-scale grid interaction should be investigated.

Appendix A: Demand Response Scenario Results

Table 28

	FLAT, DR HE 1:00 & HE 2:00 PM, $0.05/kWh		FLAT, DR HE 1:00 & HE 2:00 PM, $0.1/kWh		FLAT, DR HE 1:00 & HE 2:00 PM, $0.15/kWh		FLAT, DR HE 1:00 & HE 2:00 PM, $0.2/kWh	
Control	24-h Cost	Diff. (%)	24-h Cost	Diff. (%)	24-h Cost	Diff. (%)	24-h Cost	Diff. (%)
Baseline	18.89	0.0%	18.89	0.0%	18.89	0.0%	18.89	0.0%
No PCM, DR1	18.71	-1.0%	18.65	-1.3%	18.59	-1.6%	18.54	-1.9%
No PCM, DR2	18.61	-1.5%	18.51	-2.0%	18.42	-2.5%	18.32	-3.0%
No PCM, DR3	18.64	-1.3%	18.57	-1.7%	18.49	-2.1%	18.42	-2.5%
No PCM, DR4	18.82	-0.4%	18.82	-0.4%	18.82	-0.4%	18.82	-0.4%
No PCM, DR5	18.81	-0.4%	18.81	-0.4%	18.81	-0.4%	18.81	-0.4%
No PCM, DR6	18.82	-0.4%	18.82	-0.4%	18.82	-0.4%	18.82	-0.4%
No PCM, DR7	18.74	-0.8%	18.65	-1.3%	18.56	-1.7%	18.47	-2.2%
No PCM, DR8	18.61	-1.5%	18.55	-1.8%	18.50	-2.1%	18.44	-2.4%
Water PCM, No DR	19.38	2.6%	19.38	2.6%	19.38	2.6%	19.38	2.6%
Water PCM, DR1	19.22	1.7%	19.17	1.5%	19.11	1.2%	19.06	0.9%
Water PCM, DR2	19.13	1.3%	19.04	0.8%	18.95	0.3%	18.86	-0.1%
Water PCM, DR3	19.17	1.5%	19.10	1.1%	19.03	0.7%	18.96	0.4%
Water PCM, DR4	19.33	2.3%	19.33	2.3%	19.33	2.3%	19.33	2.3%
Water PCM, DR5	19.32	2.3%	19.32	2.3%	19.32	2.3%	19.32	2.3%
Water PCM, DR6	19.32	2.3%	19.32	2.3%	19.32	2.3%	19.32	2.3%
Water PCM, DR7	19.24	1.9%	19.16	1.4%	19.08	1.0%	18.99	0.5%
Water PCM, DR8	19.07	0.9%	18.95	0.3%	18.83	-0.3%	18.70	-1.0%

Table 29

	FLAT, DR HE 2:00 & HE 3:00 PM, $0.5/kWh		FLAT, DR HE 2:00 & HE 3:00 PM, $0.10/kWh		FLAT, DR HE 2:00 & HE 3:00 PM, $0.15/kWh		FLAT, DR HE 2:00 & HE 3:00 PM, $0.2/kWh	
Control	24-h Cost	Diff. (%)	24-h Cost	Diff. (%)	24-h Cost	Diff. (%)	24-h Cost	Diff. (%)
Baseline	18.89	0.0%	18.89	0.0%	18.89	0.0%	18.89	0.0%
No PCM, DR1	18.68	-1.1%	18.60	-1.5%	18.52	-1.9%	18.45	-2.4%
No PCM, DR2	18.55	-1.8%	18.39	-2.6%	18.24	-3.5%	18.08	-4.3%
No PCM, DR3	18.60	-1.6%	18.48	-2.2%	18.36	-2.8%	18.24	-3.4%
No PCM, DR4	18.82	-0.4%	18.82	-0.4%	18.82	-0.4%	18.82	-0.4%
No PCM, DR5	18.81	-0.4%	18.81	-0.4%	18.81	-0.4%	18.81	-0.4%
No PCM, DR6	18.73	-0.8%	18.64	-1.3%	18.55	-1.8%	18.46	-2.3%
No PCM, DR7	18.76	-0.7%	18.69	-1.1%	18.62	-1.4%	18.56	-1.8%
No PCM, DR8	18.63	-1.4%	18.61	-1.5%	18.58	-1.7%	18.55	-1.8%
Water PCM, No DR	19.38	2.6%	19.38	2.6%	19.38	2.6%	19.38	2.6%
Water PCM, DR1	19.20	1.6%	19.13	1.3%	19.06	0.9%	18.98	0.5%
Water PCM, DR2	19.08	1.0%	18.94	0.2%	18.79	-0.5%	18.65	-1.3%
Water PCM, DR3	19.12	1.2%	19.01	0.6%	18.90	0.1%	18.79	-0.5%
Water PCM, DR4	19.33	2.3%	19.33	2.3%	19.33	2.3%	19.33	2.3%
Water PCM, DR5	19.32	2.3%	19.32	2.3%	19.32	2.3%	19.32	2.3%
Water PCM, DR6	19.24	1.8%	19.15	1.4%	19.06	0.9%	18.97	0.4%
Water PCM, DR7	19.26	2.0%	19.20	1.6%	19.14	1.3%	19.08	1.0%
Water PCM, DR8	19.06	0.9%	18.92	0.2%	18.78	-0.6%	18.65	-1.3%

Table 30

	FLAT, DR HE 3:00 & HE 4:00 PM, $0.05/kWh		FLAT, DR HE 3:00 & HE 4:00 PM, $0.10/kWh		FLAT, DR HE 3:00 & HE 4:00 PM, $0.15/kWh		FLAT, DR HE 3:00 & HE 4:00 PM, $0.20/kWh	
Control	24-h Cost	Diff. (%)	24-h Cost	Diff. (%)	24-h Cost	Diff. (%)	24-h Cost	Diff. (%)
Baseline	18.89	0.0%	18.89	0.0%	18.89	0.0%	18.89	0.0%
No PCM, DR1	18.70	-1.0%	18.64	-1.3%	18.58	-1.6%	18.53	-1.9%
No PCM, DR2	18.67	-1.1%	18.65	-1.3%	18.62	-1.5%	18.59	-1.6%
No PCM, DR3	18.65	-1.3%	18.58	-1.6%	18.52	-2.0%	18.45	-2.3%
No PCM, DR4	18.82	-0.4%	18.82	-0.4%	18.82	-0.4%	18.82	-0.4%
No PCM, DR5	18.73	-0.9%	18.65	-1.3%	18.56	-1.7%	18.48	-2.2%
No PCM, DR6	18.76	-0.7%	18.70	-1.0%	18.64	-1.4%	18.57	-1.7%
No PCM, DR7	18.86	-0.2%	18.90	0.0%	18.93	0.2%	18.97	0.4%
No PCM, DR8	18.76	-0.7%	18.86	-0.2%	18.96	0.4%	19.06	0.9%
Water PCM, No DR	19.38	2.6%	19.38	2.6%	19.38	2.6%	19.38	2.6%
Water PCM, DR1	19.22	1.7%	19.17	1.5%	19.11	1.2%	19.06	0.9%
Water PCM, DR2	19.20	1.6%	19.18	1.5%	19.15	1.4%	19.13	1.3%
Water PCM, DR3	19.18	1.5%	19.12	1.2%	19.06	0.9%	19.00	0.6%
Water PCM, DR4	19.33	2.3%	19.33	2.3%	19.33	2.3%	19.33	2.3%
Water PCM, DR5	19.24	1.8%	19.16	1.4%	19.08	1.0%	19.00	0.6%
Water PCM, DR6	19.27	2.0%	19.21	1.7%	19.15	1.4%	19.09	1.1%
Water PCM, DR7	19.36	2.5%	19.40	2.7%	19.43	2.9%	19.47	3.0%
Water PCM, DR8	19.17	1.5%	19.15	1.4%	19.12	1.2%	19.10	1.1%

Table 31

	FLAT, DR HE 4:00 & HE 5:00 PM, $0.05/kWh		FLAT, DR HE 4:00 & HE 5:00 PM, $0.10/kWh		FLAT, DR HE 4:00 & HE 5:00 PM, $0.15/kWh		FLAT, DR HE 4:00 & HE 5:00 PM, $0.20/kWh	
Control	24-h Cost	Diff. (%)	24-h Cost	Diff. (%)	24-h Cost	Diff. (%)	24-h Cost	Diff. (%)
Baseline	18.89	0.0%	18.89	0.0%	18.89	0.0%	18.89	0.0%
No PCM, DR1	18.75	-0.8%	18.74	-0.8%	18.72	-0.9%	18.71	-1.0%
No PCM, DR2	18.72	-0.9%	18.74	-0.8%	18.76	-0.7%	18.77	-0.6%
No PCM, DR3	18.70	-1.0%	18.68	-1.1%	18.66	-1.2%	18.64	-1.3%
No PCM, DR4	18.75	-0.8%	18.67	-1.2%	18.59	-1.6%	18.52	-2.0%
No PCM, DR5	18.75	-0.7%	18.69	-1.1%	18.63	-1.4%	18.57	-1.7%
No PCM, DR6	18.87	-0.1%	18.91	0.1%	18.95	0.3%	19.00	0.5%
No PCM, DR7	18.85	-0.2%	18.88	-0.1%	18.90	0.0%	18.92	0.2%
No PCM, DR8	18.79	-0.6%	18.91	0.1%	19.03	0.7%	19.15	1.4%
Water PCM, No DR	19.38	2.6%	19.38	2.6%	19.38	2.6%	19.38	2.6%
Water PCM, DR1	19.26	2.0%	19.25	1.9%	19.24	1.8%	19.23	1.8%
Water PCM, DR2	19.24	1.9%	19.26	2.0%	19.28	2.1%	19.30	2.2%
Water PCM, DR3	19.22	1.7%	19.20	1.7%	19.19	1.6%	19.17	1.5%
Water PCM, DR4	19.26	1.9%	19.19	1.6%	19.12	1.2%	19.05	0.8%
Water PCM, DR5	19.27	2.0%	19.21	1.7%	19.16	1.4%	19.10	1.1%
Water PCM, DR6	19.36	2.5%	19.41	2.7%	19.45	2.9%	19.49	3.2%
Water PCM, DR7	19.35	2.4%	19.37	2.5%	19.39	2.6%	19.41	2.8%
Water PCM, DR8	19.19	1.6%	19.20	1.6%	19.20	1.6%	19.20	1.6%

Table 32

	FLAT, DR HE 1:00 PM, $0.05/kWh		FLAT, DR HE 1:00 PM, $0.10/kWh		FLAT, DR HE 1:00 PM, $0.15/kWh		FLAT, DR HE 1:00 PM, $0.20/kWh	
Control	24-h Cost	Diff. (%)	24-h Cost	Diff. (%)	24-h Cost	Diff. (%)	24-h Cost	Diff. (%)
Baseline	18.89	0.0%	18.89	0.0%	18.89	0.0%	18.89	0.0%
No PCM, DR1	18.76	-0.7%	18.76	-0.7%	18.76	-0.7%	18.76	-0.7%
No PCM, DR2	18.70	-1.0%	18.70	-1.0%	18.70	-1.0%	18.70	-1.0%
No PCM, DR3	18.71	-0.9%	18.71	-0.9%	18.71	-1.0%	18.71	-1.0%
No PCM, DR4	18.82	-0.4%	18.82	-0.4%	18.82	-0.4%	18.82	-0.4%
No PCM, DR5	18.81	-0.4%	18.81	-0.4%	18.81	-0.4%	18.81	-0.4%
No PCM, DR6	18.82	-0.4%	18.82	-0.4%	18.82	-0.4%	18.82	-0.4%
No PCM, DR7	18.83	-0.4%	18.82	-0.4%	18.82	-0.4%	18.82	-0.4%
No PCM, DR8	18.68	-1.1%	18.69	-1.0%	18.71	-1.0%	18.72	-0.9%
Water PCM, No DR	19.38	2.6%	19.38	2.6%	19.38	2.6%	19.38	2.6%
Water PCM, DR1	19.27	2.0%	19.27	2.0%	19.27	2.0%	19.27	2.0%
Water PCM, DR2	19.22	1.8%	19.22	1.8%	19.22	1.8%	19.22	1.7%
Water PCM, DR3	19.23	1.8%	19.23	1.8%	19.23	1.8%	19.23	1.8%
Water PCM, DR4	19.33	2.3%	19.33	2.3%	19.33	2.3%	19.33	2.3%
Water PCM, DR5	19.32	2.3%	19.32	2.3%	19.32	2.3%	19.32	2.3%
Water PCM, DR6	19.32	2.3%	19.32	2.3%	19.32	2.3%	19.32	2.3%
Water PCM, DR7	19.32	2.3%	19.32	2.3%	19.32	2.3%	19.32	2.3%
Water PCM, DR8	19.19	1.6%	19.19	1.6%	19.19	1.6%	19.19	1.6%

Table 33

	FLAT, DR HE 2:00 PM, $0.05/kWh		FLAT, DR HE 2:00 PM, $0.10/kWh		FLAT, DR HE 2:00 PM, $0.15/kWh		FLAT, DR HE 2:00 PM, $0.20/kWh	
Control	24-h Cost	Diff. (%)	24-h Cost	Diff. (%)	24-h Cost	Diff. (%)	24-h Cost	Diff. (%)
Baseline	18.89	0.0%	18.89	0.0%	18.89	0.0%	18.89	0.0%
No PCM, DR1	18.71	-1.0%	18.65	-1.3%	18.60	-1.6%	18.54	-1.9%
No PCM, DR2	18.61	-1.5%	18.51	-2.0%	18.42	-2.5%	18.32	-3.0%
No PCM, DR3	18.64	-1.3%	18.57	-1.7%	18.50	-2.1%	18.42	-2.5%
No PCM, DR4	18.82	-0.4%	18.82	-0.4%	18.82	-0.4%	18.82	-0.4%
No PCM, DR5	18.81	-0.4%	18.81	-0.4%	18.81	-0.4%	18.81	-0.4%
No PCM, DR6	18.82	-0.4%	18.82	-0.4%	18.82	-0.4%	18.82	-0.4%
No PCM, DR7	18.74	-0.8%	18.65	-1.3%	18.56	-1.7%	18.48	-2.2%
No PCM, DR8	18.59	-1.6%	18.52	-2.0%	18.45	-2.3%	18.38	-2.7%
Water PCM, No DR	19.38	2.6%	19.38	2.6%	19.38	2.6%	19.38	2.6%
Water PCM, DR1	19.22	1.7%	19.17	1.5%	19.12	1.2%	19.06	0.9%
Water PCM, DR2	19.14	1.3%	19.05	0.8%	18.96	0.3%	18.87	-0.1%
Water PCM, DR3	19.17	1.5%	19.10	1.1%	19.03	0.7%	18.96	0.4%
Water PCM, DR4	19.33	2.3%	19.33	2.3%	19.33	2.3%	19.33	2.3%
Water PCM, DR5	19.32	2.3%	19.32	2.3%	19.32	2.3%	19.32	2.3%
Water PCM, DR6	19.32	2.3%	19.32	2.3%	19.32	2.3%	19.32	2.3%
Water PCM, DR7	19.24	1.9%	19.16	1.4%	19.08	1.0%	18.99	0.5%
Water PCM, DR8	19.07	1.0%	18.95	0.3%	18.83	-0.3%	18.71	-1.0%

Table 34

	FLAT, DR HE 5:00 PM, $0.05/kWh		FLAT, DR HE 3:00 PM, $0.10/kWh		FLAT, DR HE 3:00 PM, $0.15/kWh		FLAT, DR HE 3:00 PM, $0.20/kWh	
Control	24-h Cost	Diff. (%)	24-h Cost	Diff. (%)	24-h Cost	Diff. (%)	24-h Cost	Diff. (%)
Baseline	18.89	0.0%	18.89	0.0%	18.89	0.0%	18.89	0.0%
No PCM, DR1	18.74	-0.8%	18.71	-0.9%	18.69	-1.1%	18.67	-1.2%
No PCM, DR2	18.64	-1.3%	18.58	-1.6%	18.52	-2.0%	18.46	-2.3%
No PCM, DR3	18.67	-1.2%	18.62	-1.4%	18.58	-1.7%	18.53	-1.9%
No PCM, DR4	18.82	-0.4%	18.82	-0.4%	18.82	-0.4%	18.82	-0.4%
No PCM, DR5	18.81	-0.4%	18.81	-0.4%	18.81	-0.4%	18.81	-0.4%
No PCM, DR6	18.73	-0.8%	18.64	-1.3%	18.55	-1.8%	18.46	-2.3%
No PCM, DR7	18.85	-0.2%	18.87	-0.1%	18.89	0.0%	18.91	0.1%
No PCM, DR8	18.71	-1.0%	18.75	-0.8%	18.79	-0.5%	18.83	-0.3%
Water PCM, No DR	19.38	2.6%	19.38	2.6%	19.38	2.6%	19.38	2.6%
Water PCM, DR1	19.25	1.9%	19.23	1.8%	19.21	1.7%	19.19	1.6%
Water PCM, DR2	19.17	1.5%	19.12	1.2%	19.06	0.9%	19.01	0.6%
Water PCM, DR3	19.19	1.6%	19.15	1.4%	19.11	1.2%	19.07	0.9%
Water PCM, DR4	19.33	2.3%	19.33	2.3%	19.33	2.3%	19.33	2.3%
Water PCM, DR5	19.32	2.3%	19.32	2.3%	19.32	2.3%	19.32	2.3%
Water PCM, DR6	19.24	1.8%	19.15	1.4%	19.06	0.9%	18.97	0.4%
Water PCM, DR7	19.35	2.4%	19.37	2.5%	19.39	2.6%	19.41	2.7%
Water PCM, DR8	19.18	1.5%	19.16	1.4%	19.15	1.4%	19.13	1.3%

Table 35

	FLAT, DR HE 4:00 PM, $0.05/kWh		FLAT, DR HE 4:00 PM, $0.10/kWh		FLAT, DR HE 4:00 PM, $0.15/kWh		FLAT, DR HE 4:00 PM, $0.20/kWh	
Control	24-h Cost	Diff. (%)	24-h Cost	Diff. (%)	24-h Cost	Diff. (%)	24-h Cost	Diff. (%)
Baseline	18.89	0.0%	18.89	0.0%	18.89	0.0%	18.89	0.0%
No PCM, DR1	18.73	-0.9%	18.69	-1.1%	18.66	-1.3%	18.62	-1.4%
No PCM, DR2	18.74	-0.8%	18.77	-0.7%	18.80	-0.5%	18.83	-0.3%
No PCM, DR3	18.69	-1.1%	18.67	-1.2%	18.65	-1.3%	18.63	-1.4%
No PCM, DR4	18.82	-0.4%	18.82	-0.4%	18.82	-0.4%	18.82	-0.4%
No PCM, DR5	18.73	-0.9%	18.65	-1.3%	18.56	-1.7%	18.48	-2.2%
No PCM, DR6	18.85	-0.2%	18.88	-0.1%	18.91	0.1%	18.94	0.2%
No PCM, DR7	18.84	-0.3%	18.86	-0.2%	18.87	-0.1%	18.89	0.0%
No PCM, DR8	18.72	-0.9%	18.78	-0.6%	18.83	-0.3%	18.89	0.0%
Water PCM, No DR	19.38	2.6%	19.38	2.6%	19.38	2.6%	19.38	2.6%
Water PCM, DR1	19.24	1.8%	19.21	1.7%	19.17	1.5%	19.14	1.3%
Water PCM, DR2	19.25	1.9%	19.28	2.1%	19.31	2.2%	19.34	2.4%
Water PCM, DR3	19.22	1.7%	19.20	1.6%	19.18	1.5%	19.17	1.4%
Water PCM, DR4	19.33	2.3%	19.33	2.3%	19.33	2.3%	19.33	2.3%
Water PCM, DR5	19.24	1.8%	19.16	1.4%	19.08	1.0%	19.00	0.6%
Water PCM, DR6	19.35	2.4%	19.38	2.6%	19.41	2.7%	19.44	2.9%
Water PCM, DR7	19.34	2.4%	19.35	2.4%	19.37	2.5%	19.38	2.6%
Water PCM, DR8	19.19	1.6%	19.18	1.5%	19.17	1.5%	19.16	1.4%

Table 36

	FLAT, DR HE 5:00 PM, $0.05/kWh		FLAT, DR HE 5:00 PM, $0.10/kWh		FLAT, DR HE 5:00 PM, $0.15/kWh		FLAT, DR HE 5:00 PM, $0.20/kWh	
Control	24-h Cost	Diff. (%)	24-h Cost	Diff. (%)	24-h Cost	Diff. (%)	24-h Cost	Diff. (%)
Baseline	18.89	0.0%	18.89	0.0%	18.89	0.0%	18.89	0.0%
No PCM, DR1	18.78	-0.6%	18.81	-0.4%	18.83	-0.3%	18.85	-0.2%
No PCM, DR2	18.69	-1.1%	18.67	-1.2%	18.66	-1.2%	18.64	-1.3%
No PCM, DR3	18.72	-0.9%	18.72	-0.9%	18.72	-0.9%	18.72	-0.9%
No PCM, DR4	18.75	-0.8%	18.67	-1.2%	18.60	-1.6%	18.52	-2.0%
No PCM, DR5	18.84	-0.3%	18.86	-0.2%	18.88	0.0%	18.91	0.1%
No PCM, DR6	18.84	-0.3%	18.85	-0.2%	18.87	-0.1%	18.88	-0.1%
No PCM, DR7	18.83	-0.3%	18.84	-0.3%	18.85	-0.2%	18.86	-0.2%
No PCM, DR8	18.73	-0.9%	18.79	-0.5%	18.86	-0.2%	18.92	0.2%
Water PCM, No DR	19.38	2.6%	19.38	2.6%	19.38	2.6%	19.38	2.6%
Water PCM, DR1	19.30	2.1%	19.32	2.3%	19.34	2.4%	19.37	2.5%
Water PCM, DR2	19.21	1.7%	19.20	1.6%	19.19	1.6%	19.18	1.5%
Water PCM, DR3	19.24	1.8%	19.24	1.8%	19.24	1.8%	19.24	1.9%
Water PCM, DR4	19.26	1.9%	19.19	1.6%	19.12	1.2%	19.05	0.8%
Water PCM, DR5	19.34	2.4%	19.37	2.5%	19.39	2.6%	19.42	2.8%
Water PCM, DR6	19.34	2.4%	19.35	2.4%	19.36	2.5%	19.37	2.6%
Water PCM, DR7	19.33	2.3%	19.34	2.4%	19.35	2.4%	19.36	2.5%
Water PCM, DR8	19.20	1.6%	19.21	1.7%	19.22	1.7%	19.23	1.8%

Table 37

	GP-TOU DR HE 1:00 PM & HE 2:00 PM, $0.05/kWh		GP-TOU DR HE 1:00 PM & HE 2:00 PM, $0.10/kWh		GP-TOU DR HE 1:00 PM & HE 2:00 PM, $0.15/kWh		GP-TOU DR HE 1:00 PM & HE 2:00 PM, $0.20/kWh	
Control	24-h Cost	Diff. (%)	24-h Cost	Diff. (%)	24-h Cost	Diff. (%)	24-h Cost	Diff. (%)
Baseline	16.37	0.0%	16.37	0.0%	16.37	0.0%	16.37	0.0%
No PCM, DR1	15.98	-2.4%	15.92	-2.7%	15.87	-3.1%	15.81	-3.4%
No PCM, DR2	15.79	-3.6%	15.69	-4.1%	15.60	-4.7%	15.50	-5.3%
No PCM, DR3	15.82	-3.4%	15.75	-3.8%	15.67	-4.3%	15.60	-4.7%
No PCM, DR4	16.14	-1.4%	16.14	-1.4%	16.14	-1.4%	16.14	-1.4%
No PCM, DR5	16.15	-1.3%	16.15	-1.3%	16.15	-1.3%	16.15	-1.3%
No PCM, DR6	16.19	-1.1%	16.18	-1.1%	16.18	-1.1%	16.18	-1.1%
No PCM, DR7	16.11	-1.6%	16.03	-2.1%	15.94	-2.7%	15.85	-3.2%
No PCM, DR8	15.71	-4.1%	15.65	-4.4%	15.59	-4.7%	15.54	-5.1%
Water PCM, No DR	15.49	-5.4%	15.49	-5.4%	15.49	-5.4%	15.49	-5.4%
Water PCM, DR1	15.14	-7.5%	15.09	-7.8%	15.04	-8.2%	14.98	-8.5%
Water PCM, DR2	14.97	-8.6%	14.88	-9.1%	14.79	-9.7%	14.70	-10.2%
Water PCM, DR3	15.00	-8.4%	14.93	-8.8%	14.86	-9.2%	14.79	-9.6%
Water PCM, DR4	15.29	-6.6%	15.29	-6.6%	15.29	-6.6%	15.29	-6.6%
Water PCM, DR5	15.30	-6.5%	15.30	-6.5%	15.30	-6.5%	15.30	-6.5%
Water PCM, DR6	15.33	-6.4%	15.33	-6.4%	15.32	-6.4%	15.32	-6.4%
Water PCM, DR7	15.26	-6.8%	15.18	-7.3%	15.09	-7.8%	15.01	-8.3%
Water PCM, DR8	14.83	-9.4%	14.71	-10.2%	14.59	-10.9%	14.46	-11.7%

Table 38

	GP-TOU, DR HE 2:00 PM & HE 3:00 PM, $0.05/kWh		GP-TOU, DR HE 2:00 PM & HE 3:00 PM, $0.10/kWh		GP-TOU, DR HE 2:00 PM & HE 3:00 PM, $0.15/kWh		GP-TOU, DR HE 2:00 PM & HE 3:00 PM, $0.20/kWh	
Control	24-h Cost	Diff. (%)	24-h Cost	Diff. (%)	24-h Cost	Diff. (%)	24-h Cost	Diff. (%)
Baseline	16.37	0.0%	16.37	0.0%	16.37	0.0%	16.37	0.0%
No PCM, DR1	15.96	-2.5%	15.88	-3.0%	15.80	-3.5%	15.72	-4.0%
No PCM, DR2	15.73	-3.9%	15.57	-4.9%	15.42	-5.8%	15.26	-6.8%
No PCM, DR3	15.78	-3.6%	15.66	-4.4%	15.54	-5.1%	15.42	-5.8%
No PCM, DR4	16.14	-1.4%	16.14	-1.4%	16.14	-1.4%	16.14	-1.4%
No PCM, DR5	16.15	-1.3%	16.15	-1.3%	16.15	-1.4%	16.15	-1.4%
No PCM, DR6	16.09	-1.7%	16.00	-2.3%	15.91	-2.8%	15.82	-3.4%
No PCM, DR7	16.13	-1.4%	16.07	-1.9%	16.00	-2.3%	15.93	-2.7%
No PCM, DR8	15.73	-3.9%	15.70	-4.1%	15.68	-4.2%	15.65	-4.4%
Water PCM, No DR	15.49	-5.4%	15.49	-5.4%	15.49	-5.4%	15.49	-5.4%
Water PCM, DR1	15.12	-7.6%	15.05	-8.1%	14.98	-8.5%	14.91	-8.9%
Water PCM, DR2	14.92	-8.9%	14.77	-9.8%	14.63	-10.6%	14.49	-11.5%
Water PCM, DR3	14.96	-8.6%	14.85	-9.3%	14.74	-10.0%	14.63	-10.6%
Water PCM, DR4	15.29	-6.6%	15.29	-6.6%	15.29	-6.6%	15.29	-6.6%
Water PCM, DR5	15.30	-6.5%	15.30	-6.5%	15.30	-6.5%	15.30	-6.5%
Water PCM, DR6	15.24	-6.9%	15.15	-7.5%	15.06	-8.0%	14.98	-8.5%
Water PCM, DR7	15.28	-6.6%	15.22	-7.0%	15.16	-7.4%	15.10	-7.8%
Water PCM, DR8	14.82	-9.5%	14.68	-10.3%	14.54	-11.2%	14.41	-12.0%

Table 39

	GP-TOU, DR HE 3:00 PM & HE 4:00 PM, $0.05/kWh		GP-TOU, DR HE 3:00 PM & HE 4:00 PM, $0.10/kWh		GP-TOU, DR HE 3:00 PM & HE 4:00 PM, $0.15/kWh		GP-TOU, DR HE 3:00 PM & HE 4:00 PM, $0.20/kWh	
Control	24-h Cost	Diff. (%)	24-h Cost	Diff. (%)	24-h Cost	Diff. (%)	24-h Cost	Diff. (%)
Baseline	16.37	0.0%	16.37	0.0%	16.37	0.0%	16.37	0.0%
No PCM, DR1	15.98	-2.4%	15.92	-2.8%	15.86	-3.1%	15.80	-3.5%
No PCM, DR2	15.86	-3.1%	15.83	-3.3%	15.80	-3.5%	15.77	-3.7%
No PCM, DR3	15.83	-3.3%	15.76	-3.7%	15.70	-4.1%	15.63	-4.5%
No PCM, DR4	16.14	-1.4%	16.14	-1.4%	16.14	-1.4%	16.14	-1.4%
No PCM, DR5	16.07	-1.9%	15.98	-2.4%	15.90	-2.9%	15.81	-3.4%
No PCM, DR6	16.12	-1.5%	16.06	-1.9%	16.00	-2.3%	15.93	-2.7%
No PCM, DR7	16.24	-0.8%	16.27	-0.6%	16.31	-0.4%	16.35	-0.2%
No PCM, DR8	15.86	-3.1%	15.96	-2.5%	16.06	-1.9%	16.16	-1.3%
Water PCM, No DR	15.49	-5.4%	15.49	-5.4%	15.49	-5.4%	15.49	-5.4%
Water PCM, DR1	15.14	-7.5%	15.09	-7.8%	15.03	-8.2%	14.98	-8.5%
Water PCM, DR2	15.04	-8.2%	15.01	-8.3%	14.99	-8.4%	14.96	-8.6%
Water PCM, DR3	15.01	-8.3%	14.95	-8.7%	14.89	-9.0%	14.83	-9.4%
Water PCM, DR4	15.29	-6.6%	15.29	-6.6%	15.29	-6.6%	15.29	-6.6%
Water PCM, DR5	15.22	-7.0%	15.14	-7.5%	15.07	-8.0%	14.99	-8.5%
Water PCM, DR6	15.27	-6.7%	15.21	-7.1%	15.15	-7.4%	15.09	-7.8%
Water PCM, DR7	15.38	-6.1%	15.42	-5.8%	15.45	-5.6%	15.49	-5.4%
Water PCM, DR8	14.93	-8.8%	14.91	-8.9%	14.88	-9.1%	14.86	-9.2%

Table 40

	GP-TOU, DR HE 4:00 PM & HE 5:00 PM, $0.05/kWh		GP-TOU, DR HE 4:00 PM & HE 5:00 PM, $0.10/kWh		GP-TOU, DR HE 4:00 PM & HE 5:00 PM, $0.15/kWh		GP-TOU, DR HE 4:00 PM & HE 5:00 PM, $0.20/kWh	
Control	24-h Cost	Diff. (%)	24-h Cost	Diff. (%)	24-h Cost	Diff. (%)	24-h Cost	Diff. (%)
Baseline	16.37	0.0%	16.37	0.0%	16.37	0.0%	16.37	0.0%
No PCM, DR1	16.02	-2.1%	16.01	-2.2%	16.00	-2.3%	15.98	-2.4%
No PCM, DR2	15.90	-2.9%	15.92	-2.8%	15.94	-2.7%	15.95	-2.5%
No PCM, DR3	15.88	-3.0%	15.86	-3.1%	15.84	-3.3%	15.82	-3.4%
No PCM, DR4	16.06	-1.9%	15.99	-2.3%	15.91	-2.8%	15.84	-3.3%
No PCM, DR5	16.09	-1.7%	16.03	-2.1%	15.97	-2.5%	15.91	-2.8%
No PCM, DR6	16.23	-0.9%	16.27	-0.6%	16.31	-0.3%	16.36	-0.1%
No PCM, DR7	16.23	-0.9%	16.25	-0.7%	16.28	-0.6%	16.30	-0.4%
No PCM, DR8	15.88	-3.0%	16.01	-2.2%	16.13	-1.5%	16.25	-0.7%
Water PCM, No DR	15.49	-5.4%	15.49	-5.4%	15.49	-5.4%	15.49	-5.4%
Water PCM, DR1	15.19	-7.2%	15.17	-7.3%	15.16	-7.4%	15.15	-7.4%
Water PCM, DR2	15.08	-7.9%	15.10	-7.8%	15.12	-7.7%	15.13	-7.6%
Water PCM, DR3	15.05	-8.0%	15.04	-8.1%	15.02	-8.2%	15.01	-8.3%
Water PCM, DR4	15.22	-7.0%	15.15	-7.5%	15.08	-7.9%	15.01	-8.3%
Water PCM, DR5	15.25	-6.9%	15.19	-7.2%	15.14	-7.5%	15.08	-7.9%
Water PCM, DR6	15.37	-6.1%	15.41	-5.9%	15.45	-5.6%	15.49	-5.4%
Water PCM, DR7	15.37	-6.1%	15.39	-6.0%	15.41	-5.9%	15.43	-5.7%
Water PCM, DR8	14.95	-8.7%	14.96	-8.7%	14.96	-8.6%	14.96	-8.6%

Table 41

	GP-TOU, DR HE HE 1:00 PM, $0.05/kWh		GP-TOU, DR HE HE 1:00 PM, $0.10/kWh		GP-TOU, DR HE HE 1:00 PM, $0.15/kWh		GP-TOU, DR HE HE 1:00 PM, $0.20/kWh	
Control	24-h Cost	Diff. (%)	24-h Cost	Diff. (%)	24-h Cost	Diff. (%)	24-h Cost	Diff. (%)
Baseline	16.37	0.0%	16.37	0.0%	16.37	0.0%	16.37	0.0%
No PCM, DR1	16.03	-2.1%	16.03	-2.1%	16.03	-2.1%	16.03	-2.1%
No PCM, DR2	15.88	-3.0%	15.88	-3.0%	15.88	-3.0%	15.88	-3.0%
No PCM, DR3	15.89	-2.9%	15.89	-2.9%	15.89	-2.9%	15.89	-2.9%
No PCM, DR4	16.14	-1.4%	16.14	-1.4%	16.14	-1.4%	16.14	-1.4%
No PCM, DR5	16.15	-1.3%	16.15	-1.3%	16.15	-1.3%	16.15	-1.3%
No PCM, DR6	16.19	-1.1%	16.19	-1.1%	16.19	-1.1%	16.19	-1.1%
No PCM, DR7	16.20	-1.0%	16.20	-1.0%	16.20	-1.0%	16.20	-1.1%
No PCM, DR8	15.78	-3.6%	15.79	-3.5%	15.81	-3.4%	15.82	-3.3%
Water PCM, No DR	15.49	-5.4%	15.49	-5.4%	15.49	-5.4%	15.49	-5.4%
Water PCM, DR1	15.20	-7.2%	15.19	-7.2%	15.19	-7.2%	15.19	-7.2%
Water PCM, DR2	15.06	-8.0%	15.06	-8.0%	15.06	-8.0%	15.06	-8.0%
Water PCM, DR3	15.07	-8.0%	15.07	-8.0%	15.07	-8.0%	15.07	-8.0%
Water PCM, DR4	15.29	-6.6%	15.29	-6.6%	15.29	-6.6%	15.29	-6.6%
Water PCM, DR5	15.30	-6.5%	15.30	-6.5%	15.30	-6.5%	15.30	-6.5%
Water PCM, DR6	15.33	-6.4%	15.33	-6.4%	15.33	-6.4%	15.33	-6.4%
Water PCM, DR7	15.34	-6.3%	15.34	-6.3%	15.34	-6.3%	15.34	-6.3%
Water PCM, DR8	14.95	-8.7%	14.95	-8.7%	14.95	-8.7%	14.95	-8.7%

Table 42

	GP-TOU, DR HE HE 2:00 PM, $0.05/kWh		GP-TOU, DR HE HE 2:00 PM, $0.10/kWh		GP-TOU, DR HE HE 2:00 PM, $0.15/kWh		GP-TOU, DR HE HE 2:00 PM, $0.20/kWh	
Control	24-h Cost	Diff. (%)	24-h Cost	Diff. (%)	24-h Cost	Diff. (%)	24-h Cost	Diff. (%)
Baseline	16.37	0.0%	16.37	0.0%	16.37	0.0%	16.37	0.0%
No PCM, DR1	15.98	-2.4%	15.92	-2.7%	15.87	-3.1%	15.81	-3.4%
No PCM, DR2	15.79	-3.6%	15.70	-4.1%	15.60	-4.7%	15.51	-5.3%
No PCM, DR3	15.82	-3.4%	15.75	-3.8%	15.68	-4.2%	15.60	-4.7%
No PCM, DR4	16.14	-1.4%	16.14	-1.4%	16.14	-1.4%	16.14	-1.4%
No PCM, DR5	16.15	-1.3%	16.15	-1.3%	16.15	-1.3%	16.15	-1.3%
No PCM, DR6	16.19	-1.1%	16.19	-1.1%	16.19	-1.1%	16.18	-1.1%
No PCM, DR7	16.11	-1.6%	16.03	-2.1%	15.94	-2.6%	15.85	-3.2%
No PCM, DR8	15.69	-4.2%	15.62	-4.6%	15.55	-5.0%	15.48	-5.5%
Water PCM, No DR	15.49	-5.4%	15.49	-5.4%	15.49	-5.4%	15.49	-5.4%
Water PCM, DR1	15.14	-7.5%	15.09	-7.8%	15.04	-8.1%	14.99	-8.5%
Water PCM, DR2	14.97	-8.6%	14.88	-9.1%	14.79	-9.6%	14.70	-10.2%
Water PCM, DR3	15.00	-8.4%	14.93	-8.8%	14.86	-9.2%	14.80	-9.6%
Water PCM, DR4	15.29	-6.6%	15.29	-6.6%	15.29	-6.6%	15.29	-6.6%
Water PCM, DR5	15.30	-6.5%	15.30	-6.5%	15.30	-6.5%	15.30	-6.5%
Water PCM, DR6	15.33	-6.4%	15.33	-6.4%	15.33	-6.4%	15.33	-6.4%
Water PCM, DR7	15.26	-6.8%	15.18	-7.3%	15.10	-7.8%	15.01	-8.3%
Water PCM, DR8	14.83	-9.4%	14.71	-10.2%	14.59	-10.9%	14.47	-11.6%

Table 43

	GP-TOU, DR HE 3:00 PM, $0.05/kWh		GP-TOU, DR HE 3:00 PM, $0.10/kWh		GP-TOU, DR HE 3:00 PM, $0.15/kWh		GP-TOU, DR HE 3:00 PM, $0.20/kWh	
Control	24-h Cost	Diff. (%)	24-h Cost	Diff. (%)	24-h Cost	Diff. (%)	24-h Cost	Diff. (%)
Baseline	16.37	0.0%	16.37	0.0%	16.37	0.0%	16.37	0.0%
No PCM, DR1	16.01	-2.2%	15.99	-2.3%	15.96	-2.5%	15.94	-2.6%
No PCM, DR2	15.82	-3.3%	15.76	-3.7%	15.70	-4.1%	15.64	-4.5%
No PCM, DR3	15.85	-3.2%	15.80	-3.5%	15.76	-3.7%	15.71	-4.0%
No PCM, DR4	16.14	-1.4%	16.14	-1.4%	16.14	-1.4%	16.14	-1.4%
No PCM, DR5	16.15	-1.3%	16.15	-1.3%	16.15	-1.4%	16.15	-1.4%
No PCM, DR6	16.10	-1.7%	16.00	-2.2%	15.91	-2.8%	15.82	-3.4%
No PCM, DR7	16.22	-0.9%	16.24	-0.8%	16.26	-0.7%	16.28	-0.5%
No PCM, DR8	15.80	-3.5%	15.85	-3.2%	15.89	-2.9%	15.93	-2.7%
Water PCM, No DR	15.49	-5.4%	15.49	-5.4%	15.49	-5.4%	15.49	-5.4%
Water PCM, DR1	15.18	-7.3%	15.16	-7.4%	15.14	-7.5%	15.12	-7.7%
Water PCM, DR2	15.01	-8.3%	14.95	-8.7%	14.90	-9.0%	14.84	-9.3%
Water PCM, DR3	15.03	-8.2%	14.99	-8.5%	14.94	-8.7%	14.90	-9.0%
Water PCM, DR4	15.29	-6.6%	15.29	-6.6%	15.29	-6.6%	15.29	-6.6%
Water PCM, DR5	15.30	-6.5%	15.30	-6.5%	15.30	-6.5%	15.30	-6.5%
Water PCM, DR6	15.24	-6.9%	15.15	-7.4%	15.07	-8.0%	14.98	-8.5%
Water PCM, DR7	15.37	-6.1%	15.39	-6.0%	15.41	-5.9%	15.43	-5.7%
Water PCM, DR8	14.94	-8.8%	14.92	-8.8%	14.91	-8.9%	14.89	-9.0%

Table 44

	GP-TOU, DR HE HE 4:00 PM, $0.05/kWh		GP-TOU, DR HE HE 4:00 PM, $0.10/kWh		GP-TOU, DR HE HE 4:00 PM, $0.15/kWh		GP-TOU, DR HE HE 4:00 PM, $0.20/kWh	
Control	24-h Cost	Diff. (%)	24-h Cost	Diff. (%)	24-h Cost	Diff. (%)	24-h Cost	Diff. (%)
Baseline	16.37	0.0%	16.37	0.0%	16.37	0.0%	16.37	0.0%
No PCM, DR1	16.00	-2.3%	15.96	-2.5%	15.93	-2.7%	15.89	-2.9%
No PCM, DR2	15.92	-2.8%	15.95	-2.6%	15.98	-2.4%	16.01	-2.2%
No PCM, DR3	15.87	-3.0%	15.85	-3.2%	15.83	-3.3%	15.81	-3.4%
No PCM, DR4	16.14	-1.4%	16.14	-1.4%	16.14	-1.4%	16.14	-1.4%
No PCM, DR5	16.07	-1.9%	15.98	-2.4%	15.90	-2.9%	15.82	-3.4%
No PCM, DR6	16.22	-1.0%	16.24	-0.8%	16.27	-0.6%	16.30	-0.4%
No PCM, DR7	16.22	-0.9%	16.23	-0.8%	16.25	-0.7%	16.27	-0.6%
No PCM, DR8	15.82	-3.4%	15.88	-3.0%	15.93	-2.7%	15.99	-2.3%
Water PCM, No DR	15.49	-5.4%	15.49	-5.4%	15.49	-5.4%	15.49	-5.4%
Water PCM, DR1	15.16	-7.4%	15.13	-7.6%	15.09	-7.8%	15.06	-8.0%
Water PCM, DR2	15.09	-7.8%	15.12	-7.6%	15.15	-7.5%	15.18	-7.3%
Water PCM, DR3	15.05	-8.1%	15.04	-8.2%	15.02	-8.3%	15.00	-8.4%
Water PCM, DR4	15.29	-6.6%	15.29	-6.6%	15.29	-6.6%	15.29	-6.6%
Water PCM, DR5	15.22	-7.0%	15.15	-7.5%	15.07	-8.0%	14.99	-8.5%
Water PCM, DR6	15.36	-6.2%	15.38	-6.0%	15.41	-5.8%	15.44	-5.7%
Water PCM, DR7	15.36	-6.2%	15.37	-6.1%	15.39	-6.0%	15.40	-5.9%
Water PCM, DR8	14.94	-8.7%	14.94	-8.8%	14.93	-8.8%	14.92	-8.9%

Table 45

	GP-TOU, DR HE HE 5:00 PM, $0.05/kWh		GP-TOU, DR HE HE 5:00 PM, $0.10/kWh		GP-TOU, DR HE HE 5:00 PM, $0.15/kWh		GP-TOU, DR HE HE 5:00 PM, $0.20/kWh	
Control	24-h Cost	Diff. (%)	24-h Cost	Diff. (%)	24-h Cost	Diff. (%)	24-h Cost	Diff. (%)
Baseline	16.37	0.0%	16.37	0.0%	16.37	0.0%	16.37	0.0%
No PCM, DR1	16.06	-1.9%	16.08	-1.8%	16.10	-1.6%	16.13	-1.5%
No PCM, DR2	15.87	-3.1%	15.86	-3.2%	15.84	-3.2%	15.83	-3.3%
No PCM, DR3	15.90	-2.9%	15.90	-2.9%	15.90	-2.9%	15.90	-2.9%
No PCM, DR4	16.07	-1.9%	15.99	-2.3%	15.91	-2.8%	15.84	-3.3%
No PCM, DR5	16.17	-1.2%	16.20	-1.1%	16.22	-0.9%	16.24	-0.8%
No PCM, DR6	16.20	-1.0%	16.21	-1.0%	16.23	-0.9%	16.24	-0.8%
No PCM, DR7	16.21	-1.0%	16.22	-0.9%	16.23	-0.9%	16.24	-0.8%
No PCM, DR8	15.83	-3.3%	15.89	-2.9%	15.96	-2.5%	16.02	-2.1%
Water PCM, No DR	15.49	-5.4%	15.49	-5.4%	15.49	-5.4%	15.49	-5.4%
Water PCM, DR1	15.22	-7.0%	15.24	-6.9%	15.26	-6.8%	15.29	-6.6%
Water PCM, DR2	15.05	-8.1%	15.04	-8.1%	15.03	-8.2%	15.01	-8.3%
Water PCM, DR3	15.07	-7.9%	15.07	-7.9%	15.07	-7.9%	15.08	-7.9%
Water PCM, DR4	15.22	-7.0%	15.15	-7.4%	15.08	-7.9%	15.01	-8.3%
Water PCM, DR5	15.33	-6.4%	15.35	-6.2%	15.38	-6.1%	15.40	-5.9%
Water PCM, DR6	15.34	-6.3%	15.35	-6.2%	15.36	-6.1%	15.38	-6.1%
Water PCM, DR7	15.35	-6.2%	15.36	-6.2%	15.37	-6.1%	15.38	-6.1%
Water PCM, DR8	14.96	-8.6%	14.97	-8.6%	14.98	-8.5%	14.99	-8.4%

References

A.E. Kabeel, A. Khalil, M.M. Bassuoni, M.S. Raslan, Comparative experimental study of low GWP alternative for R134a in a walk-in cold room, In International Journal of Refrigeration, Volume 69, 2016, Pages 303-312, ISSN 0140-7007

Abdelaziz, O., J. Winkler, V. Aute, R. Radermacher. 2006. “Transient Simulation of a Transcritical Carbon Dioxide Refrigeration System System.” In Proceedings of the International Refrigeration and Air Conditioning Conference, Lafayette, IN, USA,

Albadi, M.H., and E.F. El-Saadany. 2008. “A Summary of Demand Response in Electricity Markets.” Electric Power Systems Research 78 (11): 1989–96.

Amendment to the Montreal Protocol on Substances that Deplete the Ozone Layer, Kigali 15 October 2016. C.N.872.2016.TREATIES-XXVII.2.f Available from: https://treaties.un.org/doc/Publication/CN/2016/CN.872.2016-Eng.pdf

ANSI/AHRI, 2015. “AHRI 540-2015 Performance Rating Of Positive Displacement Refrigerant Compressors and Compressor Units”.

Arteconi, A., N.J. Hewitt, and F. Polonara. 2012. “State of the Art of Thermal Storage for Demand-Side Management.” Applied Energy 93: 371–89.

Baek, J S, E A Groll, and P B Lawless. “Theoretical Performance of Transcritical Carbon Dioxide Cycle with Two-Stage Compression and Intercooling.” Proceedings of the Institution of Mechanical Engineers, Part E: Journal of Process Mechanical Engineering 219.2 (2005): 187-195.

Baxter, Van D. "Advances in supermarket refrigeration systems." Oak Ridge Natl. Lab., Oak Ridge, Tennessee 37 (2002): 831-6070.

Beshr, M., Bush, J., Aute, V. and Radermacher, R., 2016, August. Steady state testing and modeling of a CO2 two-stage refrigeration system with mechanical subcooler. In Proceedings of the 12th IIR Gustav Lorentzen Natural Working Fluids Conference (pp. 21-24).

Bingming, Wang, Wu Huagen, Li Jianfeng, and Xing Ziwen. 2009. “Experimental Investigation on the Performance of NH3/CO2 Cascade Refrigeration System with Twin-Screw Compressor.” International Journal of Refrigeration 32 (6). Elsevier Ltd and IIR: 1358–65.

Boccardi, G., F. Botticella, G. Lillo, R. Mastrullo, A.W. Mauro, and R. Trinchieri. 2017. “Experimental Investigation on the Performance of a Transcritical CO2 Heat Pump with Multi-Ejector Expansion System.” International Journal of Refrigeration 82. Elsevier Ltd: 389–400.

Bush, J, M. Beshr, V. Aute & R. Radermacher (2017) Experimental evaluation of transcritical CO2 refrigeration with mechanical subcooling, Science and Technology for the Built Environment

Bush, J, V. Aute & R. Radermacher. Transient Simulation of CO2 Booster Refrigeration System with Mechanical Subcooler in Demand Response Operation, Science and Technology for the Built Environment. Manuscript Accepted December, 2017

Bush, J., S. Mitchell. "Reaching Near-Zero GWP." ASHRAE Journal 59.2 (2017).

Cabrejas, C.P., 2006. “Parametric evaluation of a NH3/CO2 cascade system for supermarket refrigeration in laboratory environment.” Doctoral dissertation, M. Sc. thesis, Royal Institute of Technology, Stockholm.

California Air Resources Board. 2016. “Revised Proposed Short-Lived Climate Pollutant Reduction Strategy.”

Cavallini, A., Del Col, D., Doretti, L., Matkovic, M., Rossetto, L., Zilio, C., Censi, G., 2006. Condensation in horizontal smooth tubes: a new heat transfer model for heat exchanger design. Heat Tran. Eng. 27 (8), 31e38

Cecchinato, L., Corradi, M., Minetto, S., Chiesaro, P., 2007. An experimental analysis of a supermarket plant working with carbon dioxide as refrigerant. In: Proceedings of the 22nd IIR International Congress of Refrigeration; Beijing, China. 2007.

Chesi, A., Esposito, F., Ferrara, G. and Ferrari, L., 2014. Experimental analysis of R744 parallel compression cycle. Applied Energy, 135, pp.274-285.

Chieh, J.J., Lin, S.J. and Chen, S.L., 2004. Thermal performance of cold storage in thermal battery for air conditioning. International journal of refrigeration, 27(2), pp.120-128.

Aprea, C., Maiorino, A. and Mastrullo, R., 2011. Change in energy performance as a result of a R422D retrofit: An experimental analysis for a vapor compression refrigeration plant for a walk-in cooler. Applied energy, 88(12), pp.4742-4748.

da Silva, A., Bandarra Filho, E.P. and Antunes, A.H.P., 2012. Comparison of a R744 cascade refrigeration system with R404A and R22 conventional systems for supermarkets. Applied Thermal Engineering, 41, pp.30-35.

Dai, B., Liu, S., Zhu, K., Sun, Z. and Ma, Y., 2017. Thermodynamic performance evaluation of transcritical carbon dioxide refrigeration cycle integrated with thermoelectric subcooler and expander. Energy, 122, pp.787-800.

Dang, C., and E. Hihara. "Cooling heat transfer of supercritical carbon dioxide: a new correlation for heat transfer coefficient and effect of lubricant oil." Trans. JSRAE 120, no. 2 (2003): 175-183.

Deng, Jian-qiang, Pei-xue Jiang, Tao Lu, and Wei Lu. 2007. “Particular Characteristics of Transcritical CO2 Refrigeration Cycle with an Ejector.” Applied Thermal Engineering 27 (2): 381–88.

Dopazo, J.A. and Fernandez-Seara, J., 2011. Experimental evaluation of a cascade refrigeration system prototype with CO2 and NH3 for freezing process applications. international journal of refrigeration, 34(1), pp.257-267.

ENERGY STAR. “Supermarkets: An Overview of Energy Use and Energy Efficiency Opportunities”. Retrieved September 6, 2016 from https://www.energystar.gov/sites/default/files/buildings/tools/SPP%20Sales%20Flyer%20for%20Supermarkets%20and%20Grocery%20Stores.pdf

EPA. 2016 “Protection of stratospheric ozone: change of listing status for certain substitutes under the Significant New Alternatives Policy Program; Final Rule.” Federal Register 80(138):42870

EPA. 2018 “Heat Island Impacts”. Retrieved March 13, 2018 from https://www.epa.gov/heat-islands/heat-island-impacts

Faramarzi, Ramin T., Walker, D.H., 2004. Investigation of Secondary Loop Supermarket Refrigeration Systems. Consultant Report. Foster-Miller, Inc. California Energy Commission 500-04-0132004.

Fidorra, N., Minetto, S., Hafner, A., Banasiak, K. and Köhler, J., 2016. Analysis of Cold Thermal Energy Storage Concepts in CO2 Refrigeration Systems. In Gustav Lorentzen Natural Working Fluids Conference, Edinburgh.

Ge, Y. T., and S. A. Tassou. 2011. “Thermodynamic Analysis of Transcritical CO2 Booster Refrigeration Systems in Supermarket.” Energy Conversion and Management 52: 1868–75.

Ge, Y.T., and S.A. Tassou. 2014. “Control Optimizations for Heat Recovery from CO2 Refrigeration Systems in Supermarket.” Energy Conversion and Management 78 (February): 245–52.

Gullo, P., Elmegaard, B. and Cortella, G., 2016. Energy and environmental performance assessment of R744 booster supermarket refrigeration systems operating in warm climates. international journal of refrigeration, 64, pp.61-79.

Gullo, P., Tsamos, K., Hafner, A., Ge, Y. and Tassou, S.A., 2017. State-of-the-art technologies for transcritical R744 refrigeration systems–a theoretical assessment of energy advantages for European food retail industry. Energy Procedia, 123, pp.46-53.

Hafner, A., Försterling, S. and Banasiak, K., 2014. Multi-ejector concept for R-744 supermarket refrigeration. International Journal of Refrigeration, 43, pp.1-13.

Haida, M., Banasiak, K., Smolka, J., Hafner, A. and Eikevik, T.M., 2016. Experimental analysis of the R744 vapour compression rack equipped with the multi-ejector expansion work recovery module. international journal of refrigeration, 64, pp.93-107.

Hart, R., S Mangan, W Price. 2004. "Who Left the Lights On? Typical Load Profiles in the 21st Century." Proceedings of the ACEEE Summer Study on Energy Efficiency in Buildings

Hasnain, S.M. 1998. "Review on Sustainable Thermal Energy Storage Technologies, Part II: Cool Thermal Storage." Energy Conversion and Management 39 (11): 1139–53.

Heaney, M., Ian Doebber, I. and Adam Hirsch. 2015. Customer Baseline Load Modeling and Uncertainty Analysis for Quantifying Demand Response in Commercial Buildings. SR-5500- 65084. National Renewable Energy Laboratory (NREL), Golden, CO (US).

Heerup, C, and K Fredslund. 2016. "Calculated Versus Measured Performance for a Co 2 System." 12th IIR Gustav Lorentzen Natural Working Fluids Conference, Edinburgh, 2016.

Hirsch, A, J Clark, M Deru, K Trenbath, I Doebber, and D Studer. 2015. "Pilot Testing of Commercial Refrigeration-Based Demand Response."

Hou, Y., Ma, J., Liu, C., Cao, J., & Liu, X., 2014, Experimental Investigation on the Influence of EEV Opening on the Performance of Transcritical CO2 Refrigeration System. Applied Thermal Engineering 65, pp. 51-56.

Hovgaard, T.G., Larsen, L.F. and Jørgensen, J.B., 2011, December. Flexible and cost efficient power consumption using economic MPC a supermarket refrigeration benchmark. In Decision and Control and European Control Conference (CDC-ECC), 2011 50th IEEE Conference on (pp. 848-854). IEEE.

Huang, M.C., Chen, B.R., Hsiao, M.J. and Chen, S.L., 2007. Application of thermal battery in the ice storage air-conditioning system as a subcooler. International journal of refrigeration, 30(2), pp.245-253.

Jamali, S., Yari, M. and Mohammadkhani, F., 2017. Performance improvement of a transcritical CO2 refrigeration cycle using two-stage thermoelectric modules in sub-cooler and gas cooler. International Journal of Refrigeration, 74, pp.105-115.

Jiang, H., Aute, V. & Radermacher, R., 2006, CoilDesigner: A General-Purpose Simulation and Design Tool for Air-to-Refrigerant Heat Exchangers. International Journal of Refrigeration, 29(4), pp. 601-610.

Zubair, S.M., 2000. Design and rating of an integrated mechanical-subcooling vapor-compression refrigeration system. Energy Conversion and Management, 41(11), pp.1201-1222.

Kim, M., 2004, Fundamental Process and System Design Issues in CO2 Vapor Compression Systems. Progress in Energy and Combustion Science 30 (2), pp.119–74.

Klein, S. A., D. T. Reindl, and K. Brownell. "Refrigeration system performance using liquid-suction heat exchangers." International Journal of Refrigeration 23.8 (2000): 588-596.

Kondou, C. and Hrnjak, P., 2011. Heat rejection from R744 flow under uniform temperature cooling in a horizontal smooth tube around the critical point. international journal of refrigeration, 34(3), pp.719-731.

Lemmon, E.W., Huber, M.L., McLinden, M.O. NIST Standard Reference Database 23: Reference Fluid Thermodynamic and Transport Properties-REFPROP, Version 9.1, National Institute of Standards and Technology, Standard Reference Data Program, Gaithersburg, 2013.

Li, G., Hwang, Y. and Radermacher, R., 2012. Review of cold storage materials for air conditioning application. International journal of refrigeration, 35(8), pp.2053-2077.

Li, G., Hwang, Y., Radermacher, R. and Chun, H.H., 2013. Review of cold storage materials for subzero applications. Energy, 51, pp.1-17.

Llopis, R., Cabello, R., Sánchez, D. and Torrella, E., 2015. Energy improvements of CO2 transcritical refrigeration cycles using dedicated mechanical subcooling. International Journal of Refrigeration, 55, pp.129-141.

Llopis, R., Nebot-Andrés, L., Cabello, R., Sánchez, D. and Catalán-Gil, J., 2016. Experimental evaluation of a CO2 transcritical refrigeration plant with dedicated mechanical subcooling. International Journal of Refrigeration, 69, pp.361-368.

Llopis, R., Cabello, R., Sánchez, D. and Torrella, E., 2015. Energy improvements of CO2 transcritical refrigeration cycles using dedicated mechanical subcooling. International Journal of Refrigeration, 55, pp.129-141.

López-Navarro, A., Biosca-Taronger, J., Corberán, J.M., Peñalosa, C., Lázaro, A., Dolado, P. and Payá, J., 2014. Performance characterization of a PCM storage tank. Applied Energy, 119, pp.151-162.

Lorentzen, Gustav, and Jostein Pettersen. 1993. "A New , Efficient and Environmentally Benign System for Car Air Conditioning." International Journal of Refrigeration 16 (1): 4–12.

Lorentzen, Gustav. 1994. "Revival of Carbon Dioxide as a Refrigerant." International Journal of Refrigeration 17 (5). Elsevier: 292–301.

Mastrullo, R., Mauro, A.W. and Perrone, A., 2015. A model and simulations to investigate the effects of compressor and fans speeds on the performance of CO2 light commercial refrigerators. Applied Thermal Engineering, 84, pp.158-169.

Mazzola, D., Sheehan, J., Bortoluzzi, D., Smitt, G., Maurizio, O.. 2016. "Supermarket Application, Effects of Sub-Cooling on Real R744 Based Trans-Critical Plants in Warm and Hot Climate: Data Analysis" 12th IIR Gustav Lorentzen Natural Working Fluids Conference, Edinburgh, 2016.

Modelica Association. "Modelica specification, version 3.3." 2014. www.modelica.org.

Motegi, N., Piette, M.A., Watson, D.S., Kiliccote, S. and Xu, P., 2007. Introduction to commercial building control strategies and techniques for demand response. Lawrence Berkeley National Laboratory LBNL-59975."

Nebot-Andres, Laura, Rodrigo Llopis. Daniel Sanches, Jesus Catalan-Gil and Ramon Cabello 2017. "CO2 with Mechanical Subcooling vs. CO2 Cascade Cycles for Medium Temperature Commercial Refrigeration Applications Thermodynamic Analysis." Applied Sciences 7 (9)

Nebot-Andres, L., Llopis., R, Sanchez, D., Cabello, R. 2016. "Experimental Evaluation of a Dedicated Mechanical Subcooling System in a CO2 Transcritical Refrigeration Cycle." 12th IIR Gustav Lorentzen Natural Working Fluids Conference, Edinburgh, 2016.

Nekså, P., Rekstad, H., Zakeri, G.R. and Schiefloe, P.A., 1998. CO2-heat pump water heater: characteristics, system design and experimental results. International Journal of refrigeration, 21(3), pp.172-179.

O'Connell, N., Madsena, H., Delffa, P., Pinsonb, P. and O'Malleyc, M., 2014. Model Identification for Control of Display Units in Supermarket Refrigeration Systems. DTU Compute Technical Report, pp.1-17.

Oró, E., A. de Gracia, A. Castell, M.M. Farid, and L.F. Cabeza. 2012. "Review on Phase Change Materials (PCMs) for Cold Thermal Energy Storage Applications." Applied Energy 99: 513–33.

Pfafferott, Torge, and Gerhard Schmitz. 2004. "Modelling and Transient Simulation of CO2-Refrigeration Systems with Modelica." International Journal of Refrigeration 27 (1): 42–52.

Polzot, A, P D 'agaro, P Gullo, and G Cortella. 2015. "Water Storage To Improve the Efficiency of Co2 Commercial Refrigeration Systems." Proceedings of the 24th IIR International Congress of Refrigeration - ICR 2015, no. 1912.

Polzot, Alessio, Paola D'Agaro, and Giovanni Cortella. 2017. "Energy Analysis of a Transcritical CO2 Supermarket Refrigeration System with Heat Recovery." Energy Procedia 111 (September 2016). Elsevier B.V.: 648–57. doi:10.1016/j.egypro.2017.03.227.

Polzot, Alessio, Paola D'Agaro, Paride Gullo, and Giovanni Cortella. 2016. "Modelling Commercial Refrigeration Systems Coupled with Water Storage to Improve Energy Efficiency and Perform Heat Recovery." International Journal of Refrigeration 69: 313–23. doi:10.1016/j.ijrefrig.2016.06.012.

Purohit, N., Gullo, P. and Dasgupta, M.S., 2017. Comparative assessment of low-GWP based refrigerating plants operating in hot climates. Energy Procedia, 109, pp.138-145.

Qiao, H., Aute, V., Lee, H., Saleh, K., & Radermacher, R., 2013, A new model for plate heat exchangers with generalized flow configurations and phase change. International Journal of Refrigeration, 36(2), pp. 622-632.

Qiao, H., Aute, V. and Radermacher, R., 2015. Transient modeling of a flash tank vapor injection heat pump system–Part I: Model development. International journal of refrigeration, 49, pp.169-182.

Qiao, H. 2014, Transient Modeling of Two-Stage and Variable Refrigerant Flow Vapor Compression Systems with Frosting and Defrosting, Ph.D. Dissertation, University of Maryland, College Park, MD.

Qureshi, B.A. and Zubair, S.M., 2013. Mechanical sub-cooling vapor compression systems: Current status and future directions. International Journal of Refrigeration, 36(8), pp.2097-2110.

Rasmussen, L.B., Bacher, P., Madsen, H., Nielsen, H.A., Heerup, C. and Green, T., 2016. Load forecasting of supermarket refrigeration. Applied Energy, 163, pp.32-40.

Salazar, M., and F. Méndez. 2014. “PID Control for a Single-Stage Transcritical CO2 Refrigeration Cycle.” Applied Thermal Engineering 67 (1): 429–38.

Sanchez, D., Catalan-Gil, J., Llopis, R., Nebot-Andres, L., Cabello, R. and Torrella, E., 2016. Improvements in a CO2 Transcritical Plant Working with Two Different Subcooling Systems. In 12th IIR Gustav Lorentzen Natural Working Fluids Conference, Edinburgh.

Sánchez, D., R. Cabello, R. Llopis, and E. Torrella. 2012. “Development and Validation of a Finite Element Model for Water - CO2 Coaxial Gas-Coolers.” Applied Energy 93 (2012): 637–47.

Sarkar, J., 2013, Performance Optimization of Transcritical CO2 Refrigeration Cycle with Thermoelectric Subcooler. International Journal of Energy Research 37(2), pp. 121–28.

Sawalha, S., 2008, Theoretical Evaluation of Trans-Critical CO2 Systems in Supermarket Refrigeration. Part II: System Modifications and Comparisons of Different Solutions. International Journal of Refrigeration 31(3), pp. 525–34.

Sawalha, S., Karampour, M. and Rogstam, J., 2015. Field measurements of supermarket refrigeration systems. Part I: Analysis of CO2 trans-critical refrigeration systems. Applied Thermal Engineering, 87, pp.633-647.

Sawalha, S., Piscopiello, S., Karampour, M., Manickam, L. and Rogstam, J., 2017. Field measurements of supermarket refrigeration systems. Part II: Analysis of HFC refrigeration systems and comparison to CO2 trans-critical. Applied Thermal Engineering, 111, pp.170-182.

Schoenfeld, J.M., 2008. Integration of a thermoelectric subcooler into a carbon dioxide transcritical vapor compression cycle refrigeration system. University of Maryland, College Park.

Shafiei, S. Ehsan, Henrik Rasmussen, and Jakob Stoustrup. 2013. “Modeling Supermarket Refrigeration Systems for Demand-Side Management.” Energies 6 (2): 900–920.

Sharma, Atul, V.V. Tyagi, C.R. Chen, and D. Buddhi. 2009. “Review on Thermal Energy Storage with Phase Change Materials and Applications.” Renewable and Sustainable Energy Reviews 13 (2): 318–45.

Sharma, V, Fricke, B., Bansal, P., & Zha, S., 2015, Evaluation of a Transcritical CO2 Supermarket Refrigeration System for the USA Market. 6th IIR Conference: Ammonia and CO2 Refrigeration Technologies

Sharma, V., Fricke, B., & Bansal, P., 2014, Comparative Analysis of Various CO2 Configurations in Supermarket Refrigeration Systems. International Journal of Refrigeration, 46, pp. 86-99.

Shecco. "Global overview of natural refrigerants: Market Trends." ATMOsphere America Conference, San Diego, 2017.

Shecco. "GUIDE to Natural Refrigerants in Japan – State of the Industry 2016." Shecco Publications http://publication.shecco.com/publications/view/65#view

Shi, R.; Fu, D.; Feng, Y.; Fan, J.; Mijanovic, S. Dynamic Modeling of CO2 Supermarket Refrigeration System. In Proceedings of the International Refrigeration and Air Conditioning Conference, Lafayette, IN, USA, 12–15 July 2010.

Tay, N.H.S., Belusko, M. and Bruno, F., 2012. Experimental investigation of tubes in a phase change thermal energy storage system. Applied energy, 90(1), pp.288-297

Taylor B.N. and Kuyatt, C.E., Guidelines for Evaluating and Expressing the Uncertainty of NIST Measurement Results, National Institute of Standards and Technology Technical Note 1297, 1994

Tecumseh AE4430U-AA1ACK datasheet, Revised Feb. 2014

Tecumseh AJA7465YXDEC datasheet, Revised Aug. 2016

Tecumseh AJA7494ZXDXC datasheet, Revised Jan. 2014(a)

Torrella, E., D. Snchez, R. Llopis, and R. Cabello. 2011. "Energetic Evaluation of an Internal Heat Exchanger in a CO2 Transcritical Refrigeration Plant Using Experimental Data." International Journal of Refrigeration 34 (1): 40–49.

Torrella, Enrique, Rodrigo Llopis, Ramón Cabello, and Daniel Sánchez. 2009. "Experimental Energetic Analysis of the Subcooler System in a Two-Stage Refrigeration Facility Driven by a Compound Compressor." HVAC and R Research 15 (3): 583–96.

Trp, Anica. 2005. "An Experimental and Numerical Investigation of Heat Transfer during Technical Grade Paraffin Melting and Solidification in a Shell-and-Tube Latent Thermal Energy Storage Unit." Solar Energy 79 (6): 648–60.

Tsamos, K. M., Y. T. Ge, Idewa Santosa, S. A. Tassou, G. Bianchi, and Z. Mylona. 2017. "Energy Analysis of Alternative CO2 Refrigeration System Configurations for

Retail Food Applications in Moderate and Warm Climates." Energy Conversion and Management 150: 822–29.

Tsamos, Konstantinos M. 2016. "Performance Investigation & Optimisation of Co 2 Refrigeration Systems in Retail Food Stores," no. September.
U.S. EPA. "Prioritizing Leak Tightness During Commercial Refrigeration Retrofits." Retrieved September 6, 2016 from https://www.epa.gov/sites/production/files/documents/GChill_Retrofit.pdf

Ulmer, David. 2015. "Fundamentals of the Power Grid and Electricity Pricing". Retrieved March 13, 2018 from https://www.slideshare.net/EnergyCAP/catalyst-electricity-gridulmer

Vinther, K., Rasmussen, H., Izadi-Zamanabadi, R., Stoustrup, J. and Alleyne, A.G., 2015. Learning-based precool algorithms for exploiting foodstuff as thermal energy reserve. IEEE transactions on control systems technology, 23(2), pp.557-569

Wang, K., Eisele, M., Hwang, Y. and Radermacher, R., 2010. Review of secondary loop refrigeration systems. International Journal of Refrigeration, 33(2), pp.212-234.

Wang, S., Tuo, H., Cao, F., & Xing, Z., 2013, Experimental Investigation on Air-Source Transcritical CO2 Heat Pump Water Heater System at a Fixed Water Inlet Temperature. International Journal of Refrigeration 36 (3), pp. 701–16.

Waschull, Jörg, Roland Müller, Wolfgang Hernschier, and Ronny Künanz. 2014. "Cold Storage Devices for Smart Grid Integration." Energy Procedia 46. Elsevier: 48–57.

Wilcox, Stephen, and William Marion. Users manual for TMY3 data sets. Golden, CO: National Renewable Energy Laboratory, 2008.

Winkler, J., Aute, V., & Radermacher, R., 2008, Comprehensive Investigation of Numerical Methods in Simulating a Steady-State Vapor Compression System. International Journal of Refrigeration, 31(5), pp. 930-942.

Yang, L. and Zhang, C.L., 2011. On subcooler design for integrated two-temperature supermarket refrigeration system. Energy and Buildings, 43(1), pp.224-231.

Hwang, Y., Jin, D.H. and Radermacher, R., 2007. Comparison of R-290 and two HFC blends for walk-in refrigeration systems. International Journal of Refrigeration, 30(4), pp.633-641
Zhang, Z., Ma, Y., Li, M. and Zhao, L., 2013. Recent advances of energy recovery expanders in the transcritical CO2 refrigeration cycle. HVAC&R Research, 19(4), pp.376-384.

Zheng, Lixing, Jianqiang Deng, Yang He, and Peixue Jiang. 2015. “Dynamic Model of a Transcritical CO2 Ejector Expansion Refrigeration System.” International Journal of Refrigeration 60: 247–60.